I. The Electronic Structure of the Criegee Intermediate.

II. The Electronic Structure of Pyrazine.

III. Approximate Integral Methods and Correlated Wavefunctions.

Thesis by

Willard Rogers Wadt

In Partial Fulfillment of the Requirements

For the Degree of

Doctor of Philosophy

California Institute of Technology

Pasadena, California

1975

(Submitted August 30, 1974)

# ACKNOWLEDGMENTS

# ABSTRACTS

Part 1: The Electronic Structure of the Criegee Intermediate:
Ramifications for the Mechanism of Ozonolysis.

Generalized valence bond (GVB) and configuration interaction (CI) calculations using a double zeta basis set have been carried out on methylene peroxide ($H_2COO$), the reactive intermediate in the Criegee mechanism for ozonolysis of olefins. The ground state of methylene peroxide (using an open geometry) is shown to be a singlet biradical rather than a zwitterion. A strong analogy between methylene peroxide and its isoelectronic counterpart, ozone, is developed. The calculations also show that the ring state of methylene peroxide is 1 eV lower than the open form. Moreover, the ring state may reopen to give the dioxymethane biradical.

The ab initio results are combined with thermochemical data in order to analyze the stability of the Criegee intermediate as well as the possible modes of reaction in ozonolysis. With regard to ozonolysis in solution, the mechanism for epoxide formation is elucidated and the possible role of methylene peroxide rearrangement to dioxymethane is considered in interpreting the $^{18}O$ isotope experiments. With regard to ozonolysis in the gas phase, the production of many of the chemiluminescent species observed by Pitts and co-workers is explained. The production of reactive radicals such as OH and $HO_2$ in the course of ozonolysis, which may have important consequences for understanding the generation of photochemical air pollution, is also delineated.

## Part 2: The Electronic Structure of Pyrazine: A Valence Bond Model for Lone Pair Interaction.

A valence bond (VB) model is developed to describe the interaction of the lone pair excitations in pyrazine. Extensive ab initio minimal basis set (MBS) configuration interaction (CI) calculations show that the description of the n cations and $n\pi^*$ states of pyrazine afforded by the VB model is more accurate than that afforded by the molecular orbital (MO) model proffered by Hoffmann. The VB picture of the n cations and $n\pi^*$ states involves the interaction (resonance) of two equivalent, localized excitations. The resultant splitting is large (1 to 2 eV) because of a slight delocalization of the n orbitals induced by the Pauli principle. (The n orbitals are still 90% localized on the nitrogens.) The splitting of the $n\pi^*$ states is comparable to that of the n cations because the $\pi^*$ orbital is delocalized, even though the excitation process is localized on one nitrogen.

The MBS CI calculations indicate that the lowest ionization potential of pyrazine corresponds to the $^2A_g$ (n) state. Calculations on the lowest Rydberg states indicate that they involve excitations out of an n orbital rather than a $\pi$ orbital, in opposition to earlier spectroscopic assignments. Finally, the calculations show that the forbidden $1\ ^1B_{2g}$ ($n\pi^*$) states is 1 eV higher than the allowed $1\ ^1B_{3u}$ ($n\pi^*$) state, so that the perturbations observed in the absorption spectrum must be ascribed to another source.

## Part 3: Comparison of INDO and Ab Initio Methods for the Correlated Wavefunctions of the Ground and Excited States of Ozone.

The validity of using integral approximation schemes in conjunction with correlated wavefunctions has been tested by performing generalized valence bond (GVB) and extensive configuration interaction (CI) calculations with INDO approximate integrals on the ground and excited states of ozone. High quality ab initio calculations have previously shown correlation effects to be extremely important for describing ozone. We find that for the CI wavefunctions the INDO approximation leads to vertical excitation energies within about 30% [ from 0.8 eV too low to 0.6 eV too high with an RMS error of 0.5 eV], as compared with comparable ab initio calculations. We also found that the INDO GVB wavefunctions lead to bond angles in good agreement with experimental and ab initio calculations, but produced bond lengths that were too short. Most important was the discovery that INDO grossly favors closed geometries as opposed to open geometries, predicting the ground state of ozone to be an equilateral triangle state (even for correlated wavefunctions) with an energy 6 eV below the correct open state!

Part 4:   Comparison of INDO and Ab Initio Methods for Correlated
Wavefunctions of the Ground and Excited States of Methylene
and Ethylene.

The usefulness of the INDO integral approximation for corre-
lated wavefunctions was tested by carrying out GVB calculations on (1)
the three lowest states of methylene as a function of bond angle and (2)
the three lowest states of ethylene as a function of the dihedral twist
angle. The methylene potential curves obtained with INDO were in
good agreement (0.2 eV errors) with ab initio results, while the
ethylene curves were very poor (2 to 4 eV errors). Comparison with
ab initio calculations revealed two major problems in the INDO method
(1) the use of empirical values from atomic spectra for the one-center
exchange integrals and (2) the use of only one resonance or $\beta$ parameter
per atom.

Part 5: Approximate Integral Methods and Correlated Wavefunctions

Attempts to develop an approximate integral method that produces reliable results in conjunction with correlated wavefunctions are reported. Two basic lines of approach are pursued: (1) modification (or reparametrization) of INDO and (2) general investigation of truncated integral sets. The integral approximations were tested on the low-lying states of $H_2$, $H_3$, $C_2$, $O_2$, $C_2H_4$, $O_3$, and $C_6H_6$ using consistently correlated wavefunctions. No approximate method investigated gave satisfactory results on all the systems tested, with the $O_3$ and $C_2$ molecules presenting the greatest problems. However, good results, using approximate methods comparable in complexity with INDO, were obtained for describing the potential curves of the low-lying states of $H_2$, $H_3$, and $C_2H_4$. Finally, the calculations revealed two important guidelines for approximate integral methods. (1) Transformation to orthogonal atomic orbitals (especially the one-electron integrals) is necessary prior to any truncation of the integral set. Truncation of the standard nonorthogonal integral set leads to poor results, biasing the calculations toward short bond lengths and closed geometries. (2) Replacement of core electrons with local potentials rather than 2J-K potentials leads to better results, because the need to orthogonalize the valence orbitals to the core is obviated.

# TABLE OF CONTENTS

PART ONE:

The Electronic Structure of the Criegee Intermediate:

Ramifications for the Mechanism of Ozonolysis

I.   INTRODUCTION

The reaction of ozone and olefins (in solution) with its puzzling set of products has intrigued chemists for years.[1-3] More recently, the gas phase analogue has come under scrutiny as an important link in the chain of photochemical smog production.[4] The isolation in solution of 1, 2, 4-trioxolanes rather than 1, 2, 3-trioxolanes from ozone-olefin reaction mixtures and the incorporation of foreign aldehydes in the 1, 2, 4-trioxolanes led Criegee[5] 25 years ago to propose the following mechanism,
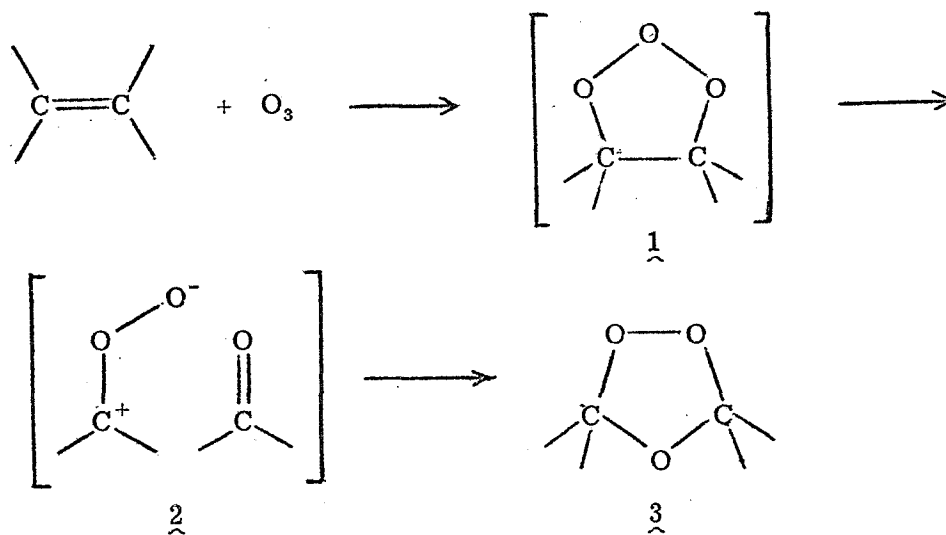


Since then a great deal of experimental work has substantiated the Criegee mechanism as either the predominant or at least a major pathway for ozonolysis in solution.[2, 3, 6-8] However, no definitive mechanistic studies have as yet been performed on gas phase ozonolysis.

Recent extensive ab initio calculations[9, 10] have shown that ground state ozone is basically a singlet biradical (4)
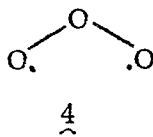
rather than the resonance of two VB zwitterions (5)



5
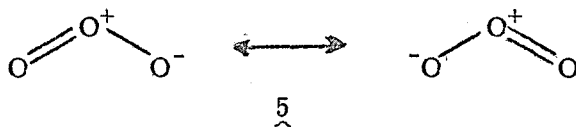
as often proposed. In fact, the state that corresponds most closely to 5 is actually 4-5 eV higher than the ground state![9a,b] Since the Criegee intermediate, methylene peroxide (2), is isoelectronic to ozone, we expected it to have an analogous ground state and hence to correspond essentially to a singlet biradical (6)



6
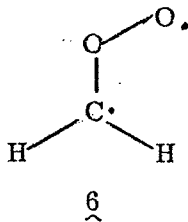
rather than a zwitterion (2) as is normally assumed. In this paper we report the results of extensive generalized valence bond (GVB) and configuration interaction (CI) studies on the low-lying states of methylene peroxide (6).

## II.   THE QUALITATIVE GVB DESCRIPTION OF $H_2COO$

We have found that a good picture of the ground and low-lying excited states for a molecule can be obtained prior to any calculations by building up the molecule from its component atoms in their ground atomic configuration.[10] Higher lying states may be found by considering excited atomic configurations.  The basic idea here is that the energy involved in the atomic excitation carries over to the molecular system.

Methylene peroxide may be formed by bonding a ground state methylene ($^3B_1$) to a ground state oxygen ($^3\Sigma_g^-$) molecule.  Previous work on methylene[11] and oxygen[12] has shown that constructing their respective ground states from ground state atoms leads to the following representation (GVB diagram)



$$CH_2(^3B_1) \qquad\qquad O_2(^3\Sigma_g^-)$$
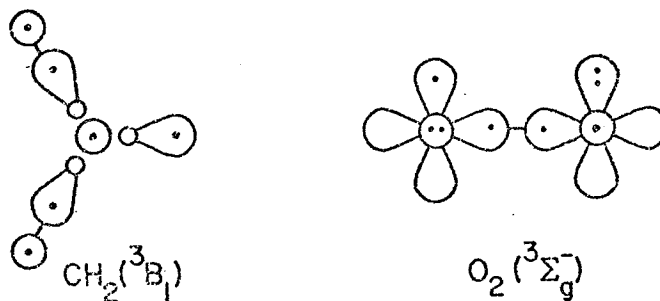
Here, we have ignored the core orbitals, 1s for carbon, 1s and 2s for oxygen, which are tightly bound and remain relatively unchanged for all the low-lying states.  The hydrogen 1s orbitals are represented by $\bigcirc$, the carbon and oxygen 2p orbitals are     represented by $\infty$ if in the plane of the paper and by $\bigcirc$ if perpendicular to the plane of the paper, and the carbon sp hybrids are represented by $\infty\bigcirc$.  Dots indicate the number of electrons in each orbital and tie lines indicate the coupling of two singly-occupied orbitals into a bonding pair.  We will often simplify our diagrams by using lines to represent bonds, e.g.,

in order to emphasize the orbitals involved in interactions between two molecular units.

Before forming methylene peroxide, a few comments about the $\pi$ system of the oxygen molecule are warranted. GVB calculations on $O_2(^3\Sigma_g^-)$ have shown that the two sets of three-electron pi bonds contribute a total of $\sim 60$ kcal to the $O_2$ bond.[9,10] The origin of the bonding may be understood in terms of two effects that occur as the two atoms are brought together. Because of the Pauli principle, the singly-occupied $p_\pi$ orbital on one center must become orthogonal to the doubly-occupied $p_\pi$ orbital on the other center. This leads to antibonding character in the singly-occupied orbital.



AO            GVB
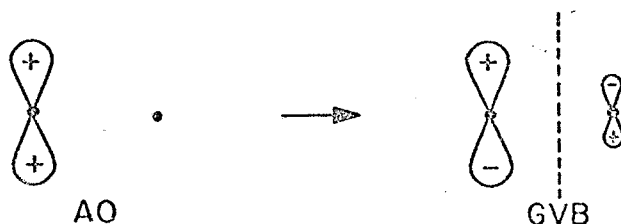
However, the doubly-occupied orbital may delocalize onto the other center leading to a significant bonding effect.



AO            GVB
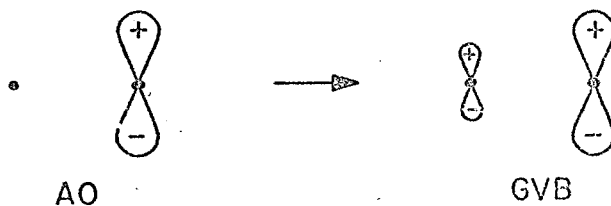
The result of delocalization of these two orbitals would normally introduce ionic character into the wavefunction; however, the doubly-occupied $\pi$ orbitals in the x and y planes delocalize in opposite directions so that the total wavefunction remains neutral. The three-electron $\pi$ bond becomes

much weaker ($\sim 13$ kcal/mole instead of 30 kcal/mole) when one of the counterbalancing delocalizations is stopped, e.g., when $O_2$ is bonded to an H or $CH_3$ to form a peroxy radical.[13]

The two reasonable geometries for bonding $CH_2$ ($^3B_1$) to $O_2$ ($^3\Sigma_g^-$) have the $CH_2$ and COO planes either perpendicular or coplanar



planar        perpendicular

In the perpendicular form, there is a bad interaction between the central oxygen $\pi$ pair and the CH bonds. In the planar form, the central $\pi$ pair may delocalize onto the carbon, while the carbon $p_\pi$ orbital becomes orthogonal to the $\pi$ pair (building in antibonding character). Such delocalization of the $\pi$ pair was found to be quite important for bonding in ozone.[9c,10] However, in methylene peroxide the delocalization onto the carbon will be much less because of its lower electronegativity. Nevertheless, one would expect the planar form to be more favorable than the perpendicular.

The planar structure for methylene peroxide (7)



7

gives rise to both a singlet and a triplet state. The relative energy of the singlet and triplet states is governed by the size of the overlap (S) of the

two singly-occupied $\pi$ orbitals.[14] For atomic $\pi$ orbitals the overlap is quite small (S ~ 0.01), so that the singlet and triplet states should be nearly degenerate. However, because of the (bonding) delocalization of the $\pi_c$ pair and the concomitant (antibonding) delocalization of the $\pi_\ell$ and $\pi_r$ orbitals, the overlap between the $\pi_\ell$ and $\pi_r$ orbitals is much higher (S = 0.25). Consequently, the singlet state is expected to be significantly lower than the triplet. In ozone, the corresponding overlap is S = 0.28 and the comparable singlet-triplet splitting is 1.47 eV.[9b, c, 10] The splitting in methylene peroxide should be smaller than in ozone (we find $\Delta E$ = 0.84 eV), since the central oxygen $\pi$ pair will not delocalize as much onto the less electronegative carbon. As a result, the overlap of the terminal $p_\pi$ orbitals is smaller and, hence, the splitting energy.

To facilitate the discussion of the various methylene peroxide states, we will label each state according to the number of $\pi$ electrons. For example, the states obtained from 7 are $^1A'(4\pi)$ and $^3A'(4\pi)$.

Other low-lying states that are formed from ground atomic configurations may be found by rotating either end of methylene peroxide by 90° giving rise to 8 and 9.



8                    9
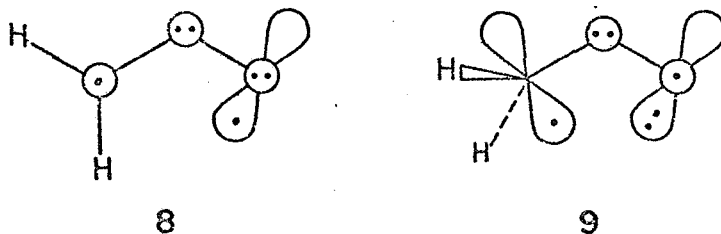
Configurations 8 and 9 lead to $^{1,3}A''(5\pi)$ and $^{1,3}A''(3\pi)$ states, respectively. For 8 and 9 the triplet states are expected to be slightly lower in energy since the singly-occupied orbitals are orthogonal. The analogous singlet and triplet states in ozone are ~2 eV above the ground state.[9,10] Since the $\pi$ bonds in methylene peroxide are weaker than in ozone, one would expect energies of the A'' $3\pi$ and $5\pi$ ——————————————————|

states to be significantly less than 2 eV. Moreover, the $3\pi$ states should

be lower than the $5\pi$ states, since the CO $\pi$ bond is weaker than the OO $\pi$

bond. Also, the oxygen $\pi$ pair-oxygen $\pi$ pair interaction (of 8) is worse

than the oxygen $\pi$ pair-CH bond interaction (of 9), since the CH bonds are

bent back away from the $\pi$ pair.

Finally, rotation of both terminal groups by 90° leads to 10
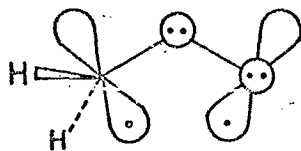


10

and two more higher-lying states, $^{1,3}A'(4\pi)$. Since the two singly-occupied

orbitals have small overlap, the singlet state is expected to be slightly

lower than the triplet. The analogous states in ozone appear near 4 eV.[9,10]

To distinguish the $^{1,3}A'$ $(4\pi)$ states obtained from 7 and 10, we denote them

as planar (7) or perpendicular (10) according to the orientation of the

hydrogens with respect to the COO plane. The perpendicular $^{1}A'(4\pi)$ state

is particularly interesting in that it should lead to a ring-like equilibrium

geometry.
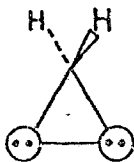


11

(All other states discussed above involve repulsive interactions between

the terminal atoms and should have equilibrium bond angles > 100°.) In

ozone, the ring state is calculated to lie 1.5 eV above the ground state.[9,10]

The ring state in methylene peroxide is even more interesting from a

mechanistic point of view than its ozone counterpart since it may reopen

by breaking the OO $\sigma$ bond to give the dioxymethane biradical
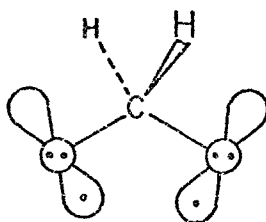
12

Depending on the energetics of this rearrangement, this pathway may have important implications for the isotope ($^{18}$O) studies of ozonolysis (vide infra).

Configuration 12 leads to $^{1,3}A_1$ ($4\pi$) states [the molecular symmetry is now $C_{2v}$ instead of $C_s$], the singlet is expected to be slightly lower in energy. Rotating either of the oxygens by $90°$ leads to $^{1,3}A_2$ ($3\pi$) and $^{1,3}B_1$ ($3\pi$) states, the triplets being lower in energy. Rotating both the oxygens leads to $^{1,3}A_1'$ ($2\pi$) states, the singlet expected to be only slightly lower, since the singly-occupied orbitals have small overlap. The central CH bond will not delocalize as the central oxygen $\pi$ pair did in methylene peroxide.

All of these states are covalent in character; none correspond to the zwitterionic structure (2) normally used for the Criegee intermediate. For ozone the lowest ionic states arise from charge transfer of a $\pi$ electron from the central to the terminal oxygen.[9,10,15]
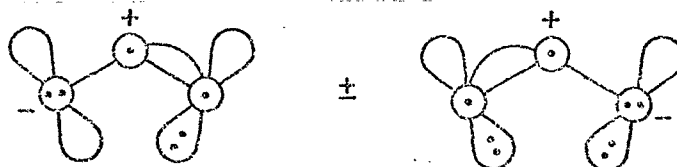


13

The minus combination leads to the lower state ($1\ ^1B_2$), which is the upper state of the well-known Hartley band at 4-6 eV.[16] Note that these configurations (13) are just VB zwitterionic structures (5) often written for the ozone ground state. The zwitterionic structures actually describe an excited

state 4-6 eV above the ground state.

One would expect the lowest ionic structures for the methylene per-
oxide to be analogous to those of ozone, i.e.,



14



15
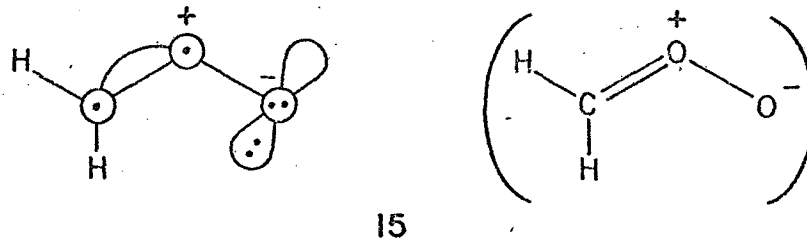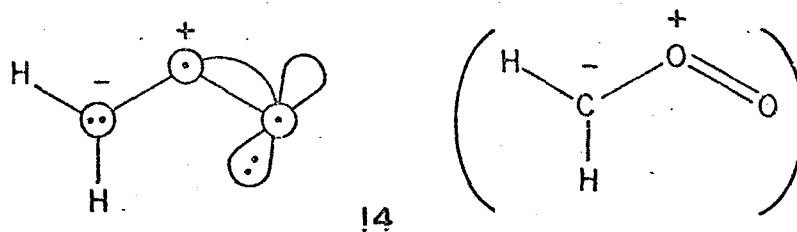
Using simple electronegativity arguments, 15 is expected to be lower in
energy than 14. In fact, the Criegee intermediate is often written as 15,
but it still should be 3-4 eV above the singlet biradical configuration (7).
The structure (2) usually given for the Criegee intermediate corresponds
to 16



16                                    2
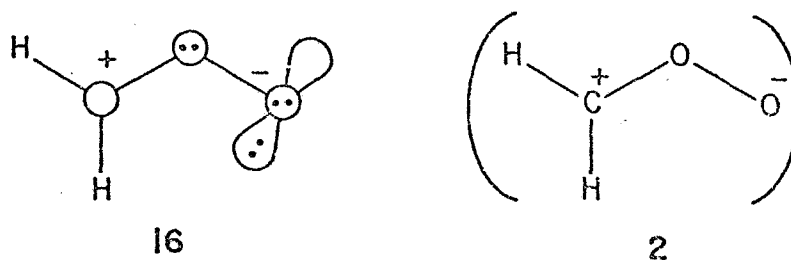
and is actually just a poor representation of the state that is well described
by 15. The very bad pair-pair interaction between the doubly-occupied

oxygen $p_\pi$ orbitals will cause the central $\pi$ pair to delocalize onto carbon, giving rise to 15. Therefore, even before any calculations it is evident that 2 is an incorrect representation of the Criegee intermediate. Moreover, the foregoing argument demonstrates the importance of associating electrons with orbitals, when thinking about molecules. Structure 2 may appear reasonable, but 16 certainly does not!

["

## III.  CALCULATIONAL DETAILS

### A.  Geometries

In this initial investigation of the Criegee intermediate, calculations were performed at the equilibrium geometries for the states of interest. (More extensive potential curves will be generated later.) Since the Criegee intermediate is a highly reactive species, experimental geometries are not available.  Nevertheless, very reasonable geometries may be developed by referring to experimental and theoretical results on related systems.

The various geometric parameters employed in this study are listed in Table I.  In every case, the CH bond distance was assumed to be 1.08 Å and the HCH bond angle to be 120°.  A slightly smaller bond angle (113°- 116°) may be more appropriate for the configurations in which the carbon is bonded to both oxygens.[17-19]  The effect of using a slightly larger bond angle, however, should be negligible.

Configurations 7-10 involve either three or four $\pi$ electrons on the oxygens.  The OO bond distance is expected to be shorter for the states with three oxygen $\pi$ electrons.  In fact, experimental results on the hydroperoxyl radical, HOO, suggest an OO bond distance of 1.34 Å



$3\pi$                    $4\pi$
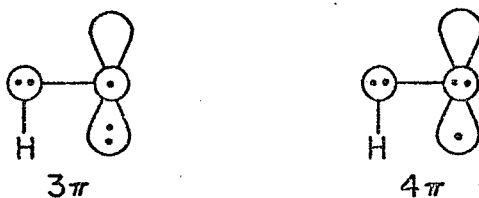
for the $3\pi$ states and 1.40 Å for the $4\pi$ states.[20,21]  In order not to bias the geometry in favor of either the states with three oxygen $\pi$ electrons or those with four, we took the OO bond distance to be 1.37 Å for configurations 7-10.  It should be mentioned that one would expect the OO bond distance in methylene peroxide to be on the average larger than that in the

TABLE I.  Geometries

| Configuration | $R_{OO}$ | $R_{CO}$ | $\angle$ COO |
|---|---|---|---|
| 7, 8 | 1.37 Å | 1.35 Å | 103° |
| 9, 10 | 1.37 | 1.41 | 103° |
| | | | $\angle$ OCO |
| 11 | 1.45 | 1.436 | 60.6° |
| 12 | -- | 1.41 | 106° |

hydroperoxyl radical, because of the repulsive interactions with the larger methylene group.

The COO bond angle was taken to be 103° for configurations 7-10. This bond angle is intermediate with respect to the experimental COO angle of 105° in dimethyl peroxide and the experimental HOO angle of 100° in hydrogen peroxide.[22] The COO angle in 1, 2, 4-trioxolane is 99.2°.[19] Using the same reasoning for the OO bond distance, the CO bond distance is expected to be shorter for the planar configuration than for the perpendicular. For the perpendicular configurations (9 and 10), the CO bond distance was assumed to be the same as in dimethyl ether, namely, 1.41Å.[16] This is a normal length for a CO single bond. The CO bond distance in the planar configurations (7 and 8) is expected to be shorter than 1.41 Å but longer than the CO bond distances in the $^3n\pi*$ (1.31 Å) and the $^1n\pi*$ (1.32 Å) states of formaldehyde.[16]



$H_2CO(n\pi^*)$
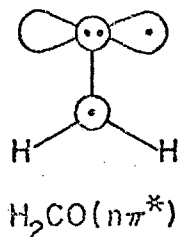
Therefore, we took the CO bond distance to be 1.35 Å. The reduction of 0.06 Å in bond length for a three-electron $\pi$ bond is the same as found in the hydroperoxyl radical.

The reason why we took into account the effect of the three-electron CO $\pi$ bond and not the three-electron OO $\pi$ bond when determining geometries is that describing the perpendicular states necessitated a geometry change relative to the planar case, while the number of oxygen $\pi$ electrons did not.

For the ring state (11), the CO bond distance was assumed to be 1.436 Å as in ethylene oxide[18] and the OO bond distance to be 1.45 Å as in the analogous ring state of ozone.[9b] Finally, for the dioxymethane biradical (12), the CO bond distance was assumed to be 1.41 Å, while the OCO bond angle was chosen to be 106° in analogy to 1,2,4-trioxolane. A slightly shorter CO bond distance would be more appropriate for the dioxymethane $3\pi$ and $2\pi$ states.

## B. Basis Set and Wavefunctions

All the calculations were performed with the Dunning[23] double-zeta [4s, 2p/2s] contraction of the Huzinaga[24] (9s, 5p/4s) set of primitive gaussian basis functions. The hydrogen exponents were scaled to 1.2

Earlier calculations on ozone have shown that the Hartree-Fock (HF) wavefunction provides a very poor description of many of the low-lying states, leading for example, to a triplet ground state![10c] A much better description is obtained with the GVB wavefunction,[12,25] which allows singlet-paired orbitals to be singly-occupied and overlapping rather than forcing the orbitals to be doubly-occupied or orthogonal as in HF. Specifically, the doubly-occupied HF orbitals are replaced in the GVB wavefunction by a pair of nonorthogonal singlet-coupled orbitals.

$$\text{HF:} \quad \frac{1}{\sqrt{2}} \, \varphi(1) \, \varphi(2) \, [\alpha(1)\beta(2) - \beta(1)\alpha(2)]$$

$$\text{GVB:} \quad \frac{1}{\sqrt{2}} [\varphi_a(1) \, \varphi_b(2) + \varphi_b(1) \, \varphi_a(2)][\alpha(1)\beta(2) - \beta(1)\alpha(2)] .$$

Splitting an HF doubly-occupied orbital into a GVB pair increases in importance as the overlap of $\varphi_a$ and $\varphi_b$ decreases. For example, the ground state of $H_2$ is fairly well described by an HF wavefunction near the equilibrium bond distance, but as the molecule is pulled apart the description

becomes increasingly worse.[10, 25, 26] The electrons are not allowed to localize on the separating atoms. Ionic character is introduced and the HF wavefunction does not dissociate properly.

Turning to the planar $^1A'$ ($4\pi$) state of methylene peroxide (7), it should be recalled that the $\pi$ orbitals on the outer carbon and oxygen have relatively low overlap and will not be well described by an HF wavefunction. In fact, for the analogous state of ozone forcing these electrons into the same orbital introduces an error of $> 3$ eV.[9c] As a consequence in the HF description the $^3B_2$ ($4\pi$) state of ozone is 2.2 eV lower than the $^1A_1$ ($4\pi$) state.[9c] We will want to consider the dissociation of the Criegee intermediate into $CH_2 + O_2$ or $CH_2O + O$. At the dissociation limits the orbitals involved in the CO or OO bonds are singly-occupied. Therefore, to obtain a consistent description the CO and OO bonding orbitals are split into GVB pairs. The remaining orbitals are doubly-occupied at both the equilibrium geometry and the dissociation limits. These orbitals will not be split, since there are no significant differential effects to describe.

Therefore, a wavefunction with three GVB pairs will be employed for the planar $^1A'$ ($4\pi$) state. To simplify the solution for this wavefunction, two approximations are made[12]: (1) orbitals from different pairs are taken to be orthogonal (strong orthogonality) and (2) the orbitals in each pair are assumed to be singlet-coupled (perfect pairing).[27] The resulting wavefunction, designated GVB(3/PP) has the form

$$\Psi = \mathcal{A}[\, \phi_1^2 \cdots \phi_n^2 (\phi_a \phi_b + \phi_b \phi_a)(\phi_c \phi_d + \phi_d \phi_c)(\phi_e \phi_f + \phi_f \phi_e)\alpha\beta \ldots \alpha\beta].$$

When solving for the wavefunction, the equivalent representation of the GVB pairs in terms of two natural orbitals is used.[28]

$$\phi_a \phi_b + \phi_b \phi_a = c_1 \phi_1^2 - c_2 \phi_2^2 \,.$$

For the corresponding planar $^3A'(4\pi)$ state, the same GVB(3/PP) wavefunction is employed except that the terminal $\pi$ orbitals are triplet coupled and are taken to be orthogonal. (For triplet-paired orbitals, orthogonalization is not a restriction on the wavefunction.) Similarly, GVB(3/PP) wavefunctions are employed for the planar $^{1,3}A''(5\pi)$ and perpendicular $^{1,3}A''(3\pi)$ states ($\underset{\sim}{8}$ and $\underset{\sim}{9}$), taking the orthogonal singly-occupied orbitals on the terminal atoms to be singlet- or triplet-coupled. In the GVB(3/PP) wavefunction for the perpendicular $^1A'(4\pi)$ state, the singly-occupied orbitals on the terminal atoms form a nonorthogonal GVB pair, while for the perpendicular $^3A'(4\pi)$ state they are taken to be orthogonal. The GVB(3/PP) wavefunction correctly describes the forming of the ring state ($\underset{\sim}{11}$) and the reopening to give $\underset{\sim}{12}$. GVB(3/PP) wavefunctions were used for both the $^1A_1(4\pi)$ and $^1A_1(2\pi)$ states arising from $\underset{\sim}{12}$.

Earlier we mentioned two restrictions imposed on the GVB(3/PP) wavefunction, namely, strong orthogonality and perfect pairing. Past experience has shown that these restrictions, in general, do not alter the qualitative orbital picture of the system in question.[9-12] However, to obtain quantitatively accurate excitation energies ($\sim 0.1$ eV) relaxation of these restrictions is necessary. The restrictions are removed by performing CI calculations allowing excitations among the six GVB orbitals (in addition we allowed excitations from the lone pairs on the oxygen).

Three types of CI wavefunctions were employed:

1.    GVB(3): a limited intrapair CI involving the six GVB orbitals to relax the perfect pairing spin coupling restriction.

2.    GVB-CI: a limited CI involving the six GVB orbitals and the two oxygen lone pairs that relaxes both the perfect pairing and strong orthogonality restrictions. (This calculation provides the best

energies for quantitative use.)

3.    SD-CI: all single and double excitations from the dominant config-
      uration(s) within the valence space (8 orbitals = 6 GVB + 2 lone pairs).
      There are two dominant configurations for the planar and perpendic-
      ular $^1A'$ ($4\pi$) states as well as for the $^1A_1$ ($2\pi$) and $^1A_1$ ($4\pi$) states of
      1̰3̰. The remaining states have only one dominant configuration.

      Previous calculations have shown that the ionic charge transfer states
of ozone are not well described by CI calculations within the GVB space.[9b]
The calculated vertical excitation energies are 1-2 eV too high. This result
is not at all surprising since ionic charge transfer states are known to involve
diffuse orbitals.[29] We have performed a more extensive CI calculation to
remedy this problem.

4.    $\pi$ POL(2) CI: the GVB-CI configurations plus all single and double
      excitations from the dominant configuration(s) [within an 11 (8 valence
      plus $3\pi$ virtual) orbital space], with the restriction that only single
      excitations were allowed into the three double-zeta (DZ) virtual $\pi$ orbitals.

      We performed $\pi$ POL(2) CI calculations on the ionic planar $4\pi$ and
$5\pi$ states as well as on the ionic perpendicular $3\pi$ states of methylene per-
oxide. To check the description of the ionic charge transfer states provided
by the DZ basis set, the basis was augmented with one diffuse $p_\pi$ primitive
gaussian on each oxygen and the carbon. The exponents (0.028 for oxygen
and 0.021 for carbon) were optimized to describe 3p Rydberg states for the
respective atoms.[30] Using the augmented basis set, we performed more
extensive POL(2) CI calculations on the ionic planar $4\pi$ states.

5.    R($\pi$) POL(2) CI: same as the $\pi$ POL(2) CI except single excitations
      are allowed into the larger six orbital (DZ + R) virtual $\pi$ space.

## IV. RESULTS

The results of the GVB(3/PP) and CI calculations are shown in Table II. In general, the CI calculations were based on the GVB(3/PP) wavefunction optimized for the state in question except for the higher roots [e.g., planar $2\,^1A'(4\pi)$], the $1\,^3A_1(4\pi)$ state [$1\,^1A_1(4\pi)$ vectors used] and the $1\,^3A_1(2\pi)$, $1\,^{1,3}A_2(3\pi)$, and $1\,^{1,3}B_1(3\pi)$ states [$1\,^1A_1\,(2\pi)$ vectors used]. In Table III, we compare the energies of the planar $4\pi$ and $5\pi$ states with their ozone analogues. The parallel between the spectrum of states for the Criegee intermediate and ozone is manifest.

The basic ordering of states turns out to be in excellent agreement with what we predicted from the qualitative GVB description. The $^1A'(4\pi)$ state is the lowest in energy for planar methylene peroxide. However, the ring state is calculated to be $\sim 1$ eV lower than the planar $^1A'(4\pi)$ state. The interpretation and ramifications of this result will be discussed later.

Comparing the GVB(3/PP) energies with the various CI calculations, it is clear that relaxation of the spin-coupling [GVB(3)] and relaxation of the strong orthogonality between the GVB pairs and the oxygen lone pairs [GVB-CI] are both very important. As in ozone, the GVB(3/PP) wavefunction underestimates the strength of the $\pi$ bonds in the planar $^1A'(4\pi)$ state, leading to excitation energies that are too small. Relaxing the spin-coupling, in general, decreases the energy of the planar $^1A'(4\pi)$ state 0.2 eV relative to the other states. Relaxing the strong orthogonality restriction is even more important, lowering the energy of the planar $^1A'(4\pi)$ state 0.4 to 0.1 eV relative to the other states. Finally, we see that the SD-CI and the GVB-CI involve approximately the same number of spin eigenfunctions (SEF's) and lead to qualitatively similar results.

TABLE II. CI results for methylene peroxide and dioxymethane (in eV).

| State | GVB(3/PP) | GVB(3) | SD-CI | GVB-CI | $\pi$ POL(2) CI |
|---|---|---|---|---|---|
| A) Open Planar COO | | | | | |
| $4\pi$ 1 $^1$A$'$ | 0.0$^a$ [8]$^b$ | 0.0$^a$ [37]$^b$ | 0.0$^a$ [119]$^b$ | 0.0$^a$ [180] | 0.0$^a$ [475]$^b$ |
| 1 $^3$A$'$ | 0.21 [4] | 0.45 [39] | 0.78 [148] | 0.84 [234] | 0.80 [673] |
| 2 $^1$A$'$ | | 5.87 [37] | 5.18 [119] | 4.60 [180] | 3.66 [475] |
| 2 $^3$A$'$ | | 12.25 [39] | 8.47 [148] | 7.96 [234] | 7.64 [673] |
| 3 $^1$A$'$ | | 13.10 [37] | | 9.46 [180] | 8.68 [475] |
| 3 $^3$A$'$ | | 14.23 [39] | | 11.09 [234] | |
| $5\pi$ 1 $^3$A$''$ | 0.60 [4] | 0.83 [25] | 1.33 [145] | 1.43 [135] | 1.24 [627] |
| 1 $^1$A$''$ | 0.65 [4] | 0.88 [17] | 1.40 [109] | 1.50 [99] | 1.30 [423] |
| 2 $^3$A$''$ | | 12.78 [25] | | 8.68 [135] | 8.20 [627] |
| 2 $^1$A$''$ | | 14.90 [17] | 10.29 [109] | 9.47 [99] | 9.11 [423] |
| B) Open Perpendicular COO | | | | | |
| $3\pi$ 1 $^3$A$''$ | 0.13 [4] | 0.31 [25] | 0.60 [161] | 0.71 [216] | 0.64 [750] |
| 1 $^1$A$''$ | 0.22 [4] | 0.44 [17] | 0.74 [117] | 0.83 [150] | 0.76 [503] |
| 2 $^3$A$''$ | | 13.16 [25] | 7.88 [161] | 7.47 [216] | 6.68 [750] |
| 2 $^1$A$''$ | | 15.08 [17] | 8.01 [117] | 7.53 [150] | 6.76 [503] |
| $4\pi$ 1 $^1$A$'$ | 0.35 [8] | 0.43 [37] | 1.14 [169] | 1.39 [37] | |
| 1 $^3$A$'$ | 0.65 [4] | 0.81 [39] | 1.42 [207] | 1.78 [39] | |
| 2 $^1$A$'$ | | 7.58 [37] | 6.67 [169] | 8.54 [37] | |
| 2 $^3$A$'$ | | 13.20 [39] | 10.31 [207] | 14.17 [39] | |
| C) Ring | | | | | |
| $4\pi$ $^1$A$'$ | -1.59 [8] | -1.88 [37] | -1.12 [169] | -0.91 [37] | |

TABLE II. (continued)

| State | GVB(3/PP) | GVB(3) | SD-CI | GVB-CI | $\pi$ POL(2) CI |
|---|---|---|---|---|---|
| D) Open Perpendicular OCO | | | | | |
| $4\pi$ 1 $^1A_1$ | -1.67 [8] | -1.34 [37] | -0.61 [169] | -0.37 [ 37] | |
| 1 $^3A_1$ | | -1.20 [39] | -0.58 [207] | -0.24 [39] | |
| $3\pi$ 1 $^3A_2$ | | -1.03 [100] | -0.18 [220] | -0.65 [432] | |
| 1 $^1A_2$ | | -0.97 [ 68] | 0.02 [ 160] | -0.48 [300] | |
| 1 $^3B_1$ | | -0.88 [100] | 0.19 [220] | -0.52 [432] | |
| 1 $^1B_1$ | | -0.78 [ 68] | 0.38 [160] | -0.31 [300] | |
| $2\pi$ 1 $^1A_1$ | -2.14 [8] | -1.79 [37] | -1.06 [120] | -0.96 [180] | |
| 1 $^3B_2$ | | -1.76 [34] | -1.03 [158] | -0.93 [234] | |

[a] Energies for the 1 $^1A'$ state are -188.59319, -188.61073, -188.64223, -188.64617, and -188.67240 for columns 1-5, respectively (energies in hartrees).

[b] Number of spin eigenfunctions used in CI listed in brackets.

TABLE III. Comparison of ozone and planar methylene peroxide energies.

| Methylene Peroxide | $\Delta E$ | Ozone | $\Delta E$ |
|---|---|---|---|
| $1\,^1A'\,(4\pi)$ | 0.0 | $1\,^1A_1\,(4\pi)$ | $0.0^a$ |
| $1\,^3A'\,(4\pi)$ | 0.84 | $1\,^3B_2\,(4\pi)$ | $1.47^a$ |
| $1\,^3A''\,(5\pi)$ | 1.43 | $1\,^3B_1\,(5\pi)$ | $(1.45)^b$ |
| | | $1\,^3A_2\,(5\pi)$ | $(1.73)^b$ |
| $1\,^1A''\,(5\pi)$ | 1.50 | $1\,^1B_1\,(5\pi)$ | $1.98^a$ |
| | | $1\,^1A_2\,(5\pi)$ | $2.06^a$ |

[a] Reference 9b.

[b] Reference 63.

However, the GVB-CI should be quantitatively more reliable and will be used as the basis for a discussion of the Criegee intermediate and its role in ozonolysis.

From Table II we see that performing the $\pi$ POL(2) CI, which allows the ionic states to become more diffuse, lowers the excitation energies by $\sim 0.6$ eV on the average. This is in agreement with the results on the analogous ionic states of ozone.[9b] In Table IV, we compare the $\pi$ POL(2) CI results for the planar $^1A'(4\pi)$ states with and without the diffuse functions. Augmenting the DZ basis set with diffuse functions lowers the excitation energies by $\leq 0.03$ eV. Therefore, we may conclude that introduction of diffuse functions is not necessary.

In Table IV we also list the calculated dipole moments for the three $^1A'(4\pi)$ states as well as the transition moments and oscillator strengths for the excitations $1\,^1A'(4\pi) \rightarrow 2\,^1A'(4\pi)$ and $1\,^1A'(4\pi) \rightarrow 3\,^1A'(4\pi)$. The dipole moment of the $1\,^1A'(4\pi)$ state (3.03 Debye) is much greater than that for ground state ozone (0.58 Debye[31]). The significant increase in the dipole moment is a manifestation of the polarization of the CO bond toward the oxygen, as is evident from the direction of the dipole moment vector (cf. Table IV.B). The size and direction of the dipole and transition moments for the $2\,^1A'(4\pi)$ and $3\,^1A'(4\pi)$ are in agreement with our simple picture that these states involve charge transfer from the central oxygen $\pi$ pair to the terminal oxygen [$2\,^1A'(4\pi)$] or the carbon [$3\,^1A'(4\pi)$]. Both charge transfer transitions are strong with calculated oscillator strengths of 0.100 and 0.058 for the $2\,^1A'(4\pi)$ and $3\,^1A'(4\pi)$ states, respectively. These oscillator strengths are comparable to that for the analogous transition in the Hartley band of ozone (f = 0.085).[9c] Since the $1\,^1A'(4\pi) \rightarrow 2\,^1A'(4\pi)$ transition is strong and relatively low-lying (the

TABLE IV. $^1$A' $(4\pi)$ ionic states of methylene peroxide.

A)  Vertical excitation energies (in eV)

| | $\pi$ POL(2) CI | |
|---|---|---|
| | DZ$(\pi)^a$ | DZ$(\pi)$ + R$(\pi)^b$ |
| 1 $^1$A' $(4\pi)$ → 2 $^1$A' $(4\pi)$ | 3.66 (0.100)$^c$ | 3.64 |
| 1 $^1$A' $(4\pi)$ → 3 $^1$A' $(4\pi)$ | 8.68 (0.058) | 8.65 |

B)  Dipole moments (in Debye)$^d$

| | $\mu_i$ |
|---|---|
| 1 $^1$A' $(4\pi)$ | 3.03 |
| 2 $^1$A' $(4\pi)$ | 4.84 |
| 3 $^1$A' $(4\pi)$ | 3.02 |
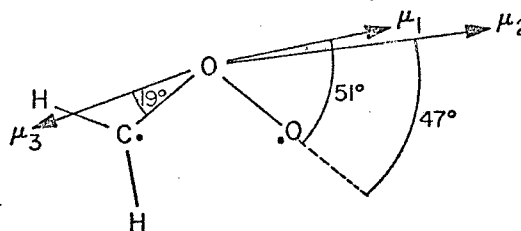


C)  Transition moments (in atomic units)$^d$

| | $|M_{ij}|$ |
|---|---|
| 1 $^1$A' $(4\pi)$ → 2 $^1$A' $(4\pi)$ | 1.06 |
| 1 $^1$A' $(4\pi)$ → 3 $^1$A' $(4\pi)$ | 0.52 |
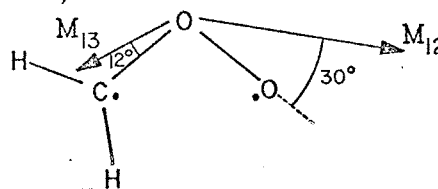


$^a$475 spin-eigenfunctions.

$^b$ 697 spin-eigenfunctions.

$^c$ Oscillator strength.

$^d$ Calculated using DZ $(\pi)$ POL (2) CI wavefunction.  The central oxygen was used as the origin.

band maximum should be at 3.64 eV or 3410 Å), it may be seen in spectro-scopic experiments on olefin ozonolyses if methylene peroxide is present in reasonable quantities.

Before discussing the implications of our results, we should compare our results with the only previous ab initio calculations on methylene peroxide. Ha et al.[32] employed a closed shell HF wavefunction with a DZ basis. A modest geometry search was carried out with the conclusion that the ring state is lower than the open planar form, in agreement with our results. However, the poor description of planar $^1A'$ ($4\pi$) states provided by the HF wavefunctions vitiates the quantitative aspects of their geometry optimization.

## V.   THE QUANTITATIVE GVB DESCRIPTION OF $H_2COO$

### A.   Planar Methylene Peroxide

As expected, the ground state of the planar Criegee intermediate is a singlet biradical. The overlap of the terminal $\pi$ orbitals is 0.25, slightly smaller in magnitude than the overlap in ozone (0.28).[9c,10] This indicates that there is still significant delocalization of the central oxygen $\pi$ pair onto the outer atoms with the concomitant (Pauli-principle-induced) increase in the antibonding character of the terminal $\pi$ orbitals.

Contour plots for the six GVB orbitals and two oxygen lone pairs from the planar $^1A'$ $(4\pi)$ state are given in Figure 1, while plots of the analogous orbitals for the ground state of ozone are given in Figure 2. The (bonding) delocalization of the central $\pi$ pair onto the outer oxygen in $H_2COO$ is comparable to that in $O_3$, but the delocalization onto the less electronegative carbon is much less, as expected. Consequently, the three-electron CO $\pi$ bond is much weaker than the three-electron OO $\pi$ bond. Also, we note that the (antibonding) delocalization of the carbon singly-occupied orbital is much greater than that of the oxygen singly-occupied orbital.

The OO $\sigma$ bonding orbitals in $H_2COO$ are nearly identical to those in $O_3$. However, for the CO $\sigma$ bond, the oxygen 2p orbital is much less delocalized than for the OO $\sigma$ bond, while the carbon sp hybrid is significantly delocalized onto the oxygen. Again this is what one would expect from simple electronegativity arguments. Finally, the oxygen lone pair in $H_2COO$ possesses a significant amount of the CH bond character. This delocalization is not physically meaningful, since the oxygen lone pair orbital is not uniquely defined as the other plotted orbitals are.[33]

Fig. 1. Contour plots of the planar methylene peroxide $^1A'$ ($4\pi$) GVB(3/PP) orbitals. The contour increment is 0.05 a.u.
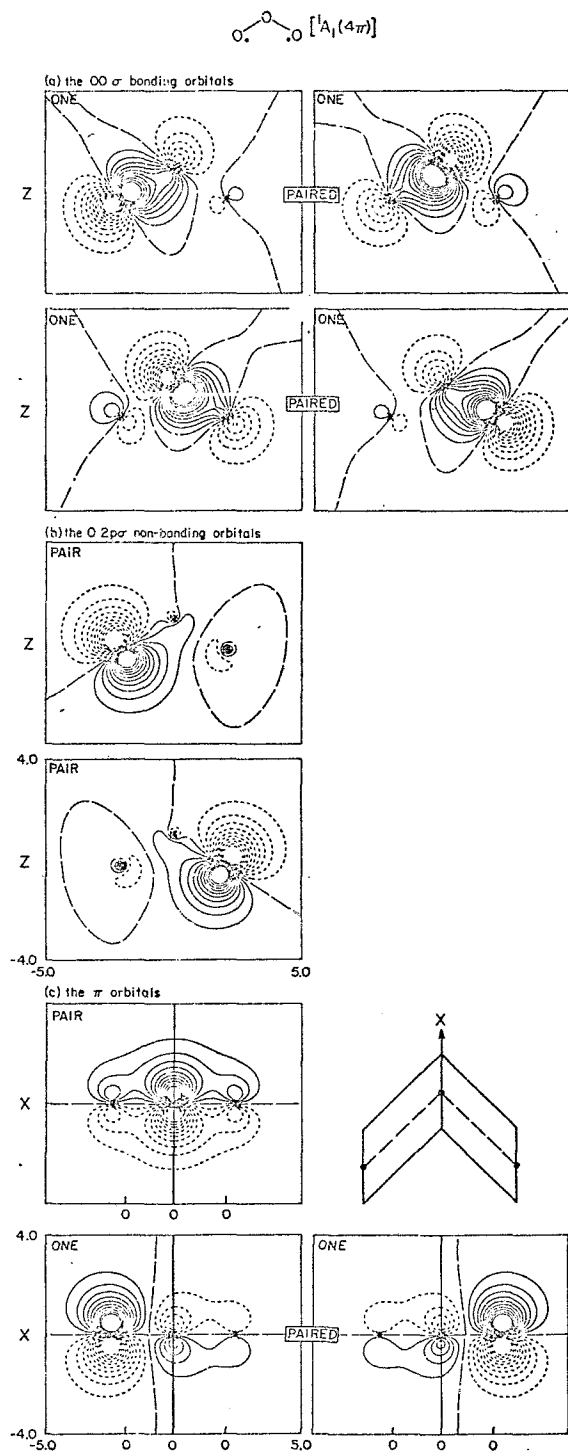
Fig. 2. Contour plots of the ozone $^1A_1(4\pi)$ GVB(3/PP) orbitals.
The contour increment is 0.05 a.u.

The plots in Figures 1 and 2 substantiate the qualitative GVB description of $H_2COO$ and $O_3$ obtained by building these molecules from ground state atoms. The atomic character of all the orbitals plotted is manifest. It is interesting to note that the $\sigma$ orbitals on each oxygen are basically 2p orbitals set at an atomic angle of 90°, so that the 2p orbitals do not, in general, point towards the atom to which they are bonded.

The splitting of the planar $^{1,3}A'$ ($4\pi$) states (0.84 eV) is 40% smaller than the comparable splitting in ozone (1.47 eV). This is a manifestation of the weaker $\pi$ bonds in the Criegee intermediate. Similarly, the excitation energies to the planar $^{1,3}A''$ ($5\pi$) states are 40% smaller than the analogous excitation energies in ozone.

Except for minor differences in the singly-occupied $\pi$ orbitals, the orbital plots for the $^3A'$ ($4\pi$) state are superimposable on those for the $^1A'$ ($4\pi$) state. Plots for the three $\pi$ orbitals and the singly-occupied $\sigma$ orbital from the $^1A''$ ($5\pi$) state are given in Figure 3. [ The plots for the $^3A''$ ($5\pi$) are superimposable.] The $\sigma$ bonding orbitals in the $^1A''$ ($5\pi$) have barely changed from the $^1A'$ ($4\pi$) state.

Comparing the $\pi$ orbitals in Figures 1 and 3, we see that the central oxygen $\pi$ pair delocalizes more onto the carbon for the $5\pi$ states, since it cannot delocalize in a bonding fashion onto the outer oxygen. Therefore, the three-electron CO $\pi$ bond is expected to be slightly stronger in the $5\pi$ states. The central $\pi$ pair also builds in antibonding character to become orthogonal to the pair localized on the outer oxygen. Finally, we see that the singly-occupied nonbonding orbital, now uniquely defined, is localized on the outer oxygen. This reinforces the conclusion that the delocalization of the nonbonding orbital in the $^1A'$ ($4\pi$) state was solely an artifact of the computational method.

Fig. 3. Contour plots of the planar methylene peroxide $^1A''(5\pi)$
GVB(3/PP) orbitals. The contour increment is 0.05 a.u.

Before going on to the perpendicular states, the $4\pi$ and $5\pi$ ionic states will be discussed. Analysis of the CI wavefunctions for the $2\ ^{1,3}A'\ (4\pi)$, $3\ ^{1,3}A'\ (4\pi)$, and $2\ ^{1,3}A''(5\pi)$ allows one to conclude that these states are ionic. Moreover, the $2\ A'\ (4\pi)$ states correspond to charge transfer of a $\pi$ electron from the central oxygen to the terminal oxygen [configuration 15], while the $3\ A'\ (4\pi)$ states involve charge transfer to the carbon [configuration 14]. Referring to the $\pi$ POL(2) CI results we see that the lower electronegativity of the carbon leads to a splitting of 5 eV between the two types of charge transfer states. As expected from the analogy to ozone, the configuration (15) usually written for the Criegee intermediate is 3.64 eV [vertical excitation] above the true singlet biradical ground state!

Finally, the ionic $5\pi$ states correspond to configuration 17.

17
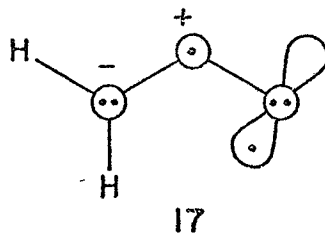
The outer $\pi$ pair on the oxygen delocalizes onto the central oxygen, so that the ionic $5\pi$ states are expected to occur at energies comparable to the $3\ A''(5\pi)$ states. The results in Table II confirm this.

B.    Perpendicular Methylene Peroxide

The excitation energies to the perpendicular $^{1,3}A''\ (3\pi)$ states are one-half the energies to the planar $^{1,3}A''(5\pi)$. This is to be expected for two reasons: (1) as discussed previously, the CO $\pi$ bond is weaker than the OO $\pi$ bond and, thus, easier to break, and (2) the interaction of the central $\pi$ pair with the CH bonding pair is not as bad as with the terminal oxygen $\pi$ pair, since the CH pairs are bent away from the central oxygen.

However, it should be pointed out that the difference in the energies of the $3\pi$ and $5\pi$ states is exaggerated, since the CO bond length was allowed to increase in the (perpendicular) $3\pi$ states, while the OO bond length in the planar $5\pi$ states was forced to be the same as in the $4\pi$ states.

Plots of the $\pi$ orbitals and $\sigma$ nonbonding orbitals for the $^1A''$ ($3\pi$) state are given in Figure 4. [ The plots for the $^3A''$ ($3\pi$) are superimposable.] As expected, the central $\pi$ pair delocalizes onto the outer oxygen even more than in the planar $^1A'$ ($4\pi$) state. The singly-occupied carbon $\sigma$ nonbonding orbital builds in antibonding character to become orthogonal to the oxygen lone pair. The other $\sigma$ bonding orbitals are nearly identical to those of the $^1A'$ ($4\pi$) state. We point out here that the carbon 2p orbital is more diffuse than the oxygen 2p orbital, as expected.

When both ends of the Criegee intermediate are rotated to give the perpendicular $^1A'$ ($4\pi$) state, there is a significant amount of bonding between the singly-occupied orbitals on the terminal carbon and oxygen even with the bond angle of 103°! The presence of this bonding is manifest in that the perpendicular $^3A'$ ($4\pi$) state is 0.39 eV= 9.0 kcal/mole higher than the singlet. (The singlet and triplet states would be nearly degenerate in the absence of the 1-3 bonding effect.) This is very similar to the situation encountered in the trimethylene biradical (with a bonding of 5 kcal/mole for a CCC angle of 112°[34]).

The six GVB $\sigma$ bonding orbitals for the $^1A'$ ($4\pi$) state are plotted in Figure 5. One can really see that the terminal carbon and oxygen 2p orbitals are already beginning to overlap one another. The calculated overlap is 0.23.
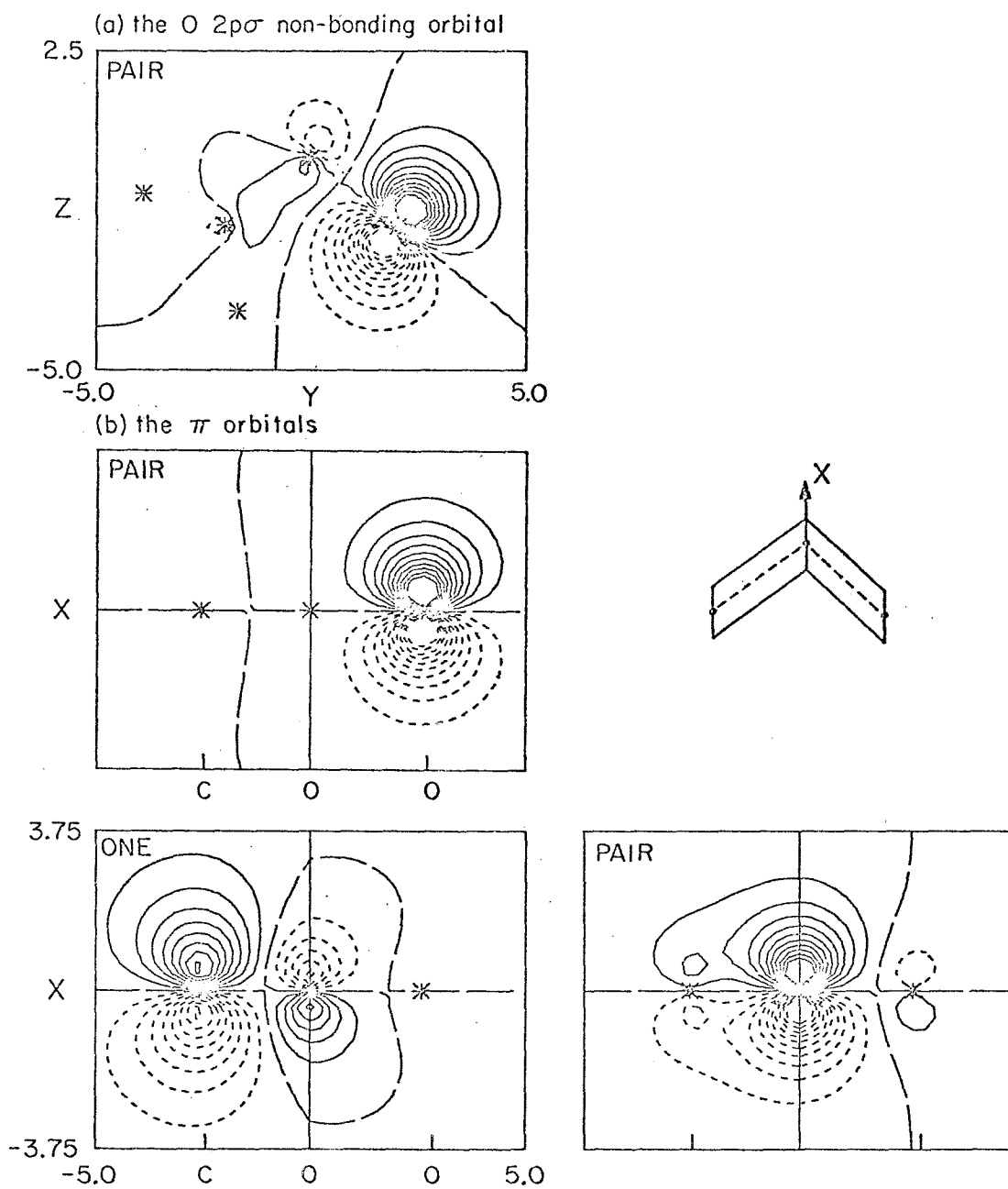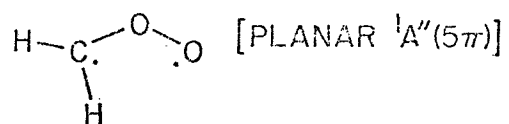
33
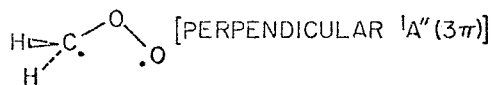


Fig. 4. Contour plots of the perpendicular methylene peroxide $^1A''(3\pi)$ GVB(3/PP) orbitals. The contour increment is 0.05 a. u.
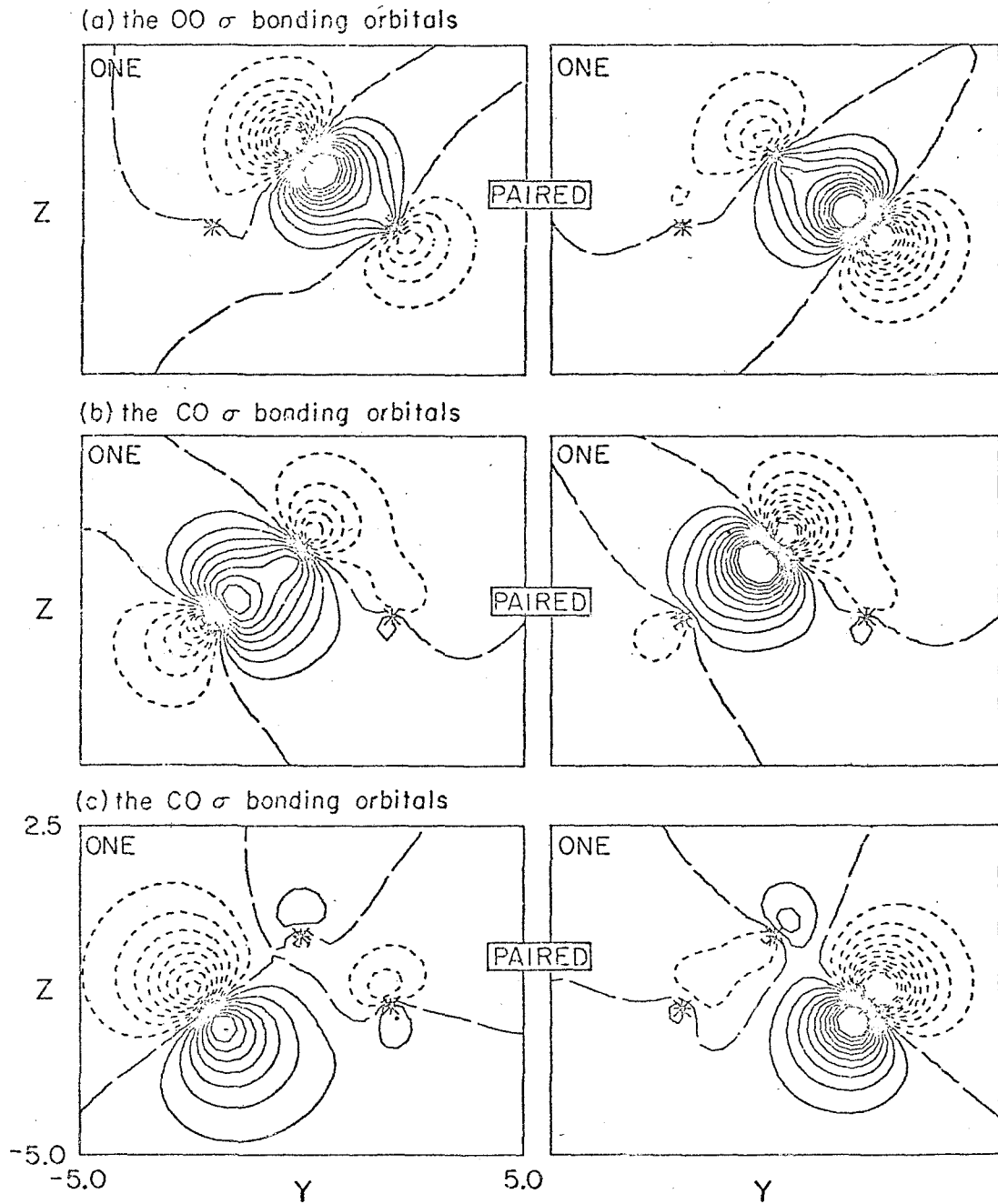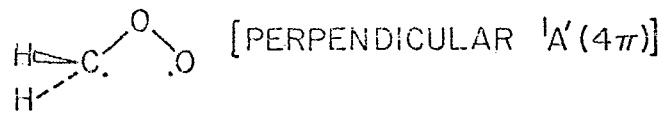
34



Fig. 5.    Contour plots of the perpendicular methylene peroxide $^1A'$ $(4\pi)$
GVB(3/PP) orbitals.    The contour increment is 0.05 a.u.

C.     The Ring State

Closing the COO bond angle to obtain the ring state lowers the energy of the perpendicular $^1A'$ ($4\pi$) state by 2.30 eV. Thus, the ring state in methylene peroxide is 0.9 eV lower than planar $^1A'$ ($4\pi$) state, while in ozone the ring state is 1.5 eV higher than the ground state.[9] The difference in the two cases (2.4 eV) is too large to be accounted for solely by the weaker CO $\pi$ bond in methylene peroxide. This judgment is supported by the fact that the $1\,^1A_1$ ($2\pi$) state of the dioxymethane biradical (vide infra) is slightly lower in energy than the ring state. The $\pi$ bond in the $1\,^1A_1$ ($2\pi$) state is negligible since the $1\,^3A_1$ ($2\pi$) state is only 0.03 eV higher. Therefore, we conclude that losing the $\pi$ bond is responsible for reducing the splitting of the ring and the open biradical state by 1.5 eV from what it was in ozone. This is reasonable since the singlet-triplet splitting of the open biradical in ozone was also 1.5 eV.[9] Similarly, the splitting of the $^{1,3}A'$ ($4\pi$) states in methylene peroxide is 0.8 eV, so that the weaker $\pi$ bond can account for only $1.5 - 0.8 = 0.7$ eV of the destabilization of the planar state relative to the ring state.

The remaining 1.7 eV of destabilization must arise from the $\sigma$ system. Here we note that the OO $\sigma$ bond formed in the ozone ring state is worth $\sim 12$ kcal/mole, while the CO $\sigma$ bond formed in the methylene peroxide ring state is worth $\sim 56$ kcal/mole (vide infra). The differential effect, 44 kcal/mole = 1.9 eV, nicely accounts for the stability of the methylene peroxide ring state.

Plots of the six GVB $\sigma$ bonding orbitals for the methylene peroxide ring state are given in Figure 6. The orbitals still retain their basic atomic character and so are not directed towards the atom with which they form a bond. As before, the carbon orbitals delocalize more than the oxygen orbitals.
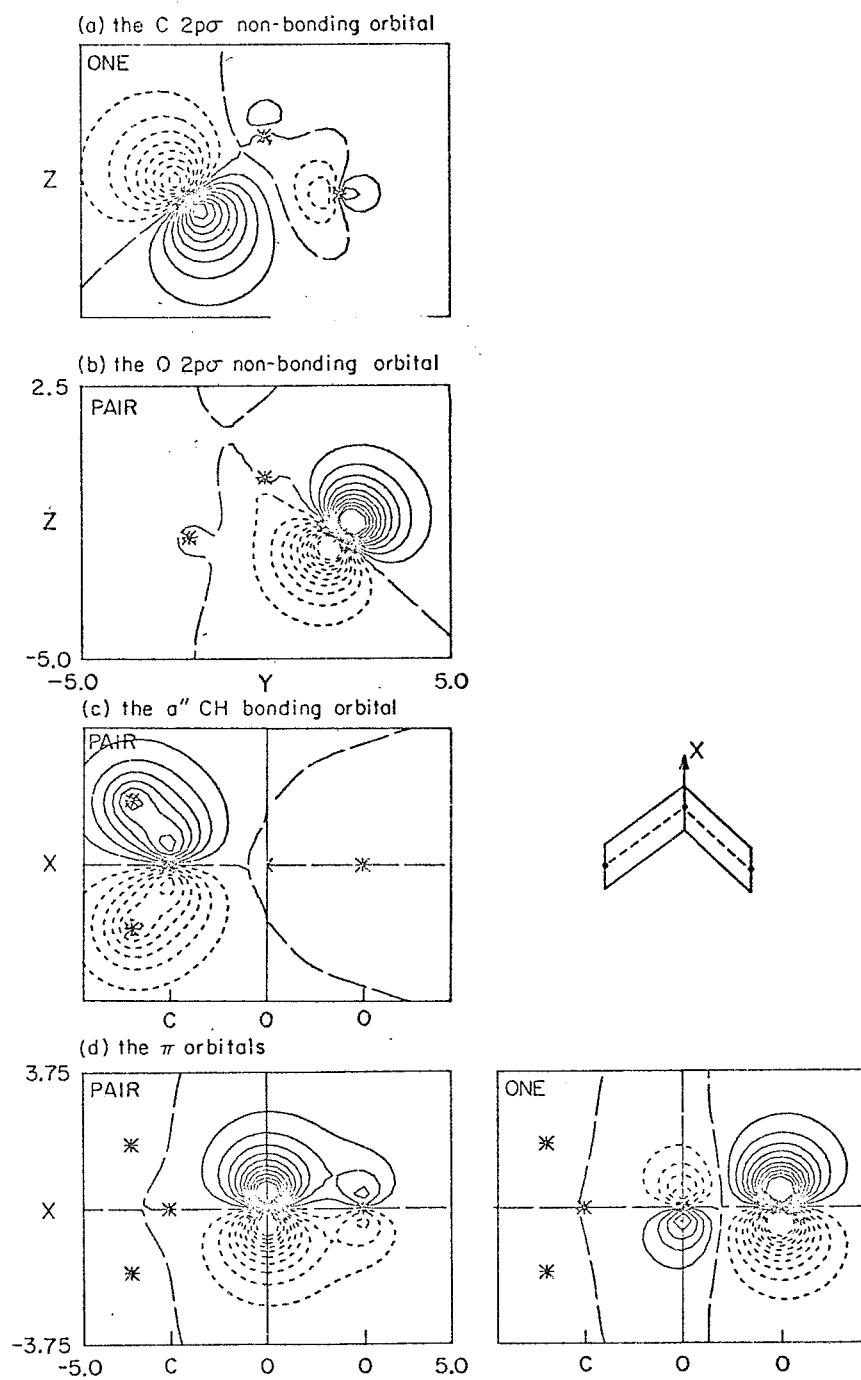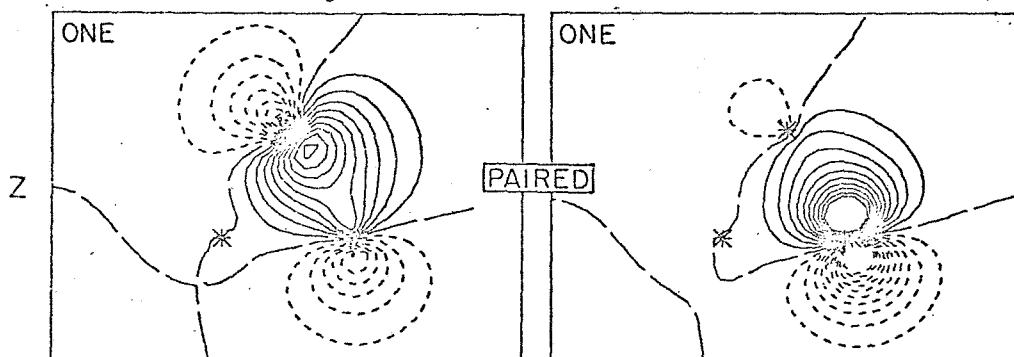
Fig. 6. Contour plots of the ring methylene peroxide $^1A_1(4\pi)$ GVB(3/PP) orbitals. The contour increment is 0.05 a.u.

D.    Dioxymethane

Comparing the low-lying states of the dioxymethane biradical with their counterparts in ozone, we see that the width of the spectrum has been drastically decreased. The smaller excitation energies in dioxymethane demonstrate the loss of bonding in the $\pi$ system. The central CH bonds cannot delocalize as the central oxygen $\pi$ pair did in ozone or methylene peroxide. The excitations to the $3\pi$ states (analogous to the $5\pi$ states of ozone) occur in the range 0.3-0.6 eV instead of 1.8-2.1 eV.[9]

In Figure 7 the plots of the six GVB $\sigma$ bonding orbitals for the $^1A'(4\pi)$ state of dioxymethane are given. They are exactly what one would expect to get upon opening the ring state by breaking the OO $\sigma$ bond. In Figure 8 the $\pi$ and oxygen long pairs for the $^1A'(2\pi)$ state are plotted. As mentioned above, the CH bond does not delocalize significantly and the singly-occupied orbitals are localized on the oxygens. The overlap of the singly-occupied $\pi$ orbitals is 0.05 instead of 0.25 as in methylene peroxide.

38



Fig. 7. Contour plots of the dioxymethane $^1A_1(4\pi)$ GVB(3/PP) orbitals. The contour increment is 0.05 a.u.

[PERPENDICULAR $^1A_1(2\pi)$]
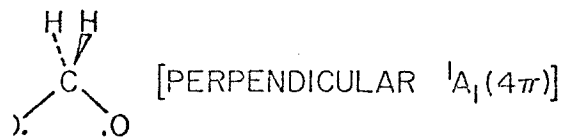
(a) the CO $\sigma$ bonding orbital
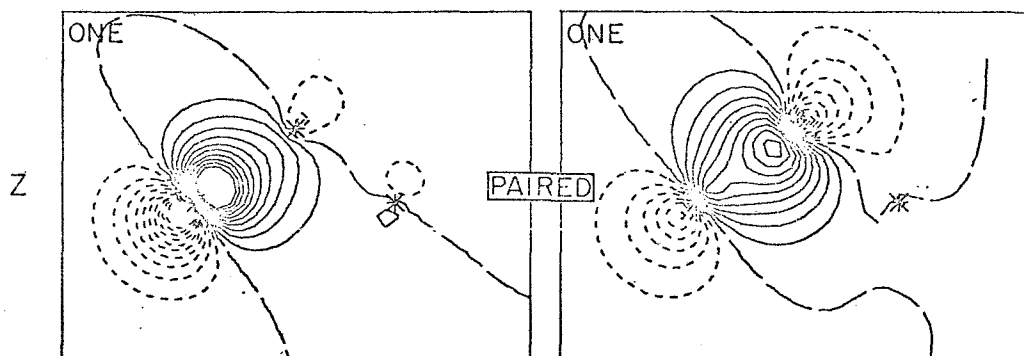
(b) the CO $\sigma$ bonding orbitals

(c) the O $2p\sigma$ non-bonding orbitals

(d) the $a''$ CH bonding orbitals

(e) the $\pi$ orbitals

Fig. 8.  Contour plots of the dioxymethane $^1A_1(2\pi)$ GVB (3/PP) orbitals. The contour increment is 0.05 a.u.

## VI.  STABILITY OF THE CRIEGEE INTERMEDIATE

### A.  GVB Calculations

For methylene peroxide to play an important role as an intermediate in the ozonolysis mechanism it must have a reasonable lifetime. One might imagine that methylene peroxide, if formed, would rapidly fall apart into $CH_2 + O_2$ or $H_2CO + O$. This possibility can be checked by calculating the dissociation energies of the states of methylene peroxide.

### 1.  Planar Methylene Peroxide

First consider the planar $^1A'(4\pi)$ state [or $^3A'(4\pi)$]. Breaking the CO bond leads to $CH_2(^3B_1) + O_2(^3\Sigma_g^-)$
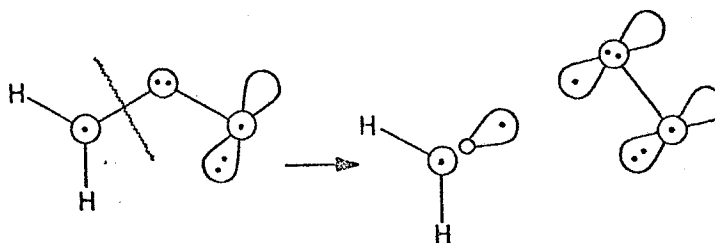


while breaking the OO bond leads to $H_2CO(^3A'') + O(^3P)$
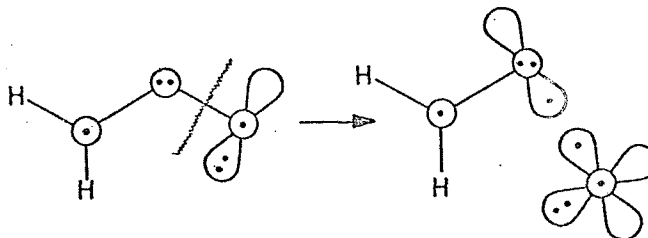


The calculated dissociation energies using consistent GVB-CI wavefunctions are listed in Tables V and VI. The OO and CO bond strengths are calculated to be 43.5 and 55.9 kcal/mole, respectively, so that the planar $^1A'(4\pi)$ state is stable with respect to dissociation.[35] The planar $^3A'(4\pi)$ state is only 19.4 kcal/mole above the $^1A'(4\pi)$ state and so it is also bound with respect to dissociation. Even the planar $^3A''(5\pi)$ and $^1A''(5\pi)$ states are bound states as they are 33.0 and 34.6 kcal/mole above the $^1A'(4\pi)$ state.[36]

TABLE V. Bond strengths of methylene peroxide (kcal/mole)

|  | GVB-CI |
| --- | --- |
| $H_2COO$ [ Plan 1 $^1A'$ ($4\pi$)] $\rightarrow$ $H_2CO$ ($^3A''$) + $O(^3P)$ | 43.5 |
| $H_2COO$ [ Plan 1 $^1A'$ ($4\pi$)] $\rightarrow$ $CH_2(^3B_1)$ + $O_2(^3\Sigma_g^-)$ | 55.9 |
| $H_2COO$ [ Perp 1 $^3A''$ ($4\pi$)] $\rightarrow$ $H_2CO(^1A_1)$ + $O(^3P)$ | -53.8 |
| $H_2COO$ [ Perp 1 $^3A''$ ($4\pi$)] $\rightarrow$ $CH_2(^3B_1)$ + $O_2(^3\Sigma_g^-)$ | 39.7 |

|  | GVB(PP) | GVB-CI |
| --- | --- | --- |
| $H_2COO$ [ Plan 1 $^1A'$ ($4\pi$)] | -188.59319 a.u. | -188.64617 a.u. |
| $H_2COO$ [ Perp 1 $^3A''$ ($3\pi$)] | -188.58844 | -188.62025 |
| $H_2CO$ ($^3A''$) | -113.77798[a] | -113.77798[a] |
| $H_2CO$ ($^1A_1$) | -113.88504[a] | -113.90722[a] |
| $O$ ($^3P$) | -74.79884[b] | -74.79884[b] |
| $CH_2$ ($^3B_1$) | -38.9119[c] | -38.9119[c] |
| $O_2$ ($^3\Sigma_g^-$) | -149.60125[d] | -149.64510[d] |

[a] Reference 64.

[b] Reference 23.

[c] Reference 11a.

[d] Reference 65.

TABLE VI. Dissociation energies (kcal/mole).

| State | Geometry | Dissociation Products | $\Delta E$ |
|---|---|---|---|
| $1\ ^1A'\ (4\pi)$ | COO Plan | $H_2CO(^3A'') + O(^3P)$ | -43.5 |
| $1\ ^3A'\ (4\pi)$ | COO Plan | $H_2CO(^3A'') + O(^3P)$ | -24.1 |
| $1\ ^3A''(5\pi)$ | COO Plan | $H_2CO(^3A'') + O(^3P)$ | -10.5 |
| $1\ ^1A''(5\pi)$ | COO Plan | $H_2CO(^3A'') + O(^3P)$ | -8.9 |
| $1\ ^3A''(3\pi)$ | COO Perp | $H_2CO(^1A_1) + O(^3P)$ | 53.8 |
| $1\ ^1A''(3\pi)$ | COO Perp | $H_2CO(^1A_1) + O(^1D)$ | 5.6 |
| $1\ ^1A'\ (4\pi)$ | COO Perp | $H_2CO(^1A_1) + O(^1D)$ | 24.1 |
| $1\ ^3A'\ (4\pi)$ | COO Perp | $H_2CO(^1A_1) + O(^3P)$ | 78.5 |
| $1\ ^1A_1\ (4\pi)$ | Ring | $H_2CO(^1A_1) + O(^3P)$ [spin change] | 16.5 |
| $1\ ^1A_1(4\pi)$ | OCO Perp | $H_2CO(^1A_1) + O(^3P)$ [spin change] | 28.9 |
| $1\ ^3A_1(4\pi)$ | OCO Perp | $H_2CO(^1A_1) + O(^3P)$ | 31.9 |
| $1\ ^3A_2\ (3\pi)$ | OCO Perp | $H_2CO(^1A_1) + O(^3P)$ | 22.4 |
| $1\ ^1A_2(3\pi)$ | OCO Perp | $H_2CO(^1A_1) + O(^3P)$ [spin change] | 26.4 |
| $1\ ^3B_1(3\pi)$ | OCO Perp | $H_2CO(^1A_1) + O(^3P)$ | 26.4 |
| $1\ ^1B_1\ (3\pi)$ | OCO Perp | $H_2CO(^1A_1) + O(^3P)$ [spin change] | 30.3 |
| $1\ ^1A_1\ (2\pi)$ | OCO Perp | $H_2CO(^3A'') + O(^3P)$ | -65.6 |
| $1\ ^3B_2\ (2\pi)$ | OCO Perp | $H_2CO(^3A'') + O(^3P)$ | -64.9 |

Breaking the CO bond in the 5π states leads to $CH_2(^3B_1) + O_2(^1\Delta_g)$
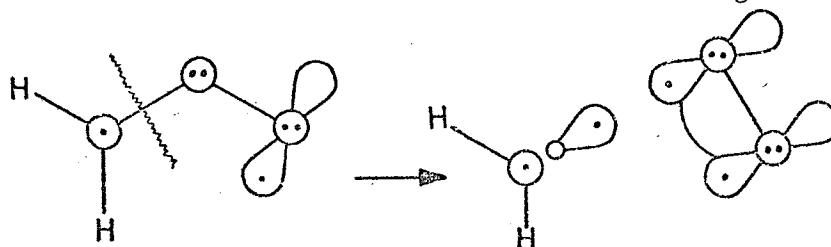


for the triplet state and $CH_2(^1B_1) + O_2(^1\Delta_g)$ for the singlet state. Since $O_2(^1\Delta_g)$ is 22.5 kcal/mole above $O_2(^3\Sigma_g^-)$[37] and $CH_2(^1B_1)$ is 44.7 kcal/mole above $CH_2(^3B_1)$,[11a] the CO bond strength in the 5π states is 45.4 kcal/mole for the triplet and 88.5 kcal/mole for the singlet.

The utility of GVB diagrams is evident, since without them one might naively assume that planar methylene peroxide would dissociate into ground state $H_2CO$, rather than the nπ* state. The nπ* state of $H_2CO$ is about 3 eV or 70 kcal/mole above the ground state,[16] so that methylene peroxide is actually higher in energy than $H_2CO(^1A_1) + O(^3P)$. Therefore, one could have been mislead concerning the stability of planar methylene peroxide.

## 2.  Perpendicular Methylene Peroxide

Turning to the perpendicular form of methylene peroxide, we find a totally different situation. For the perpendicular $^3A''$ (3π) state breaking the CO bond leads to $CH_2(^3B_1) + O_2(^3\Sigma_g^-)$
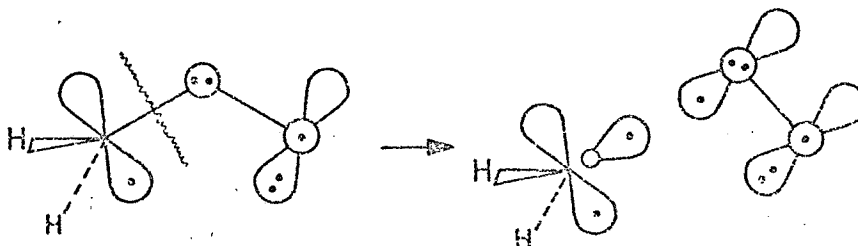


and a calculated bond strength of 39.7 kcal/mole. However, breaking the OO bond leads to $H_2CO(^1A_1) + O(^3P)$
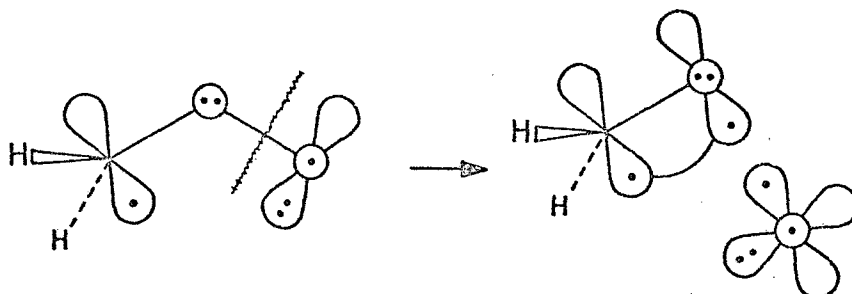
and a calculated bond strength of -53.8 kcal/mole, i.e., the perpendicular $^3A''$ ($3\pi$) state will fall apart. Breaking the OO bond in the $^1A''$ ($3\pi$) state leads to $H_2CO(^1A_1) + O(^1D)$. Since $O(^1D)$ is 45.4 kcal/mole above $O(^3P)$ [38] and the $^1A''$ ($3\pi$) state is 2.8 kcal/mole above the $^3A''(3\pi)$ state, the $^1A''$ ($3\pi$) state is unbound by only 5.6 kcal/mole. Dissociation to $H_2CO(^1A_1) + O(^3P)$ is 45.4 kcal/mole further downhill, but is a much slower process as it requires a change in multiplicity, i.e., intersystem crossing. Finally, the perpendicular $^3A'$ ($4\pi$) state will fall apart into $H_2CO(^1A_1) + O(^3P)$ [downhill by 78.5 kcal/mole], while the perpendicular $^1A'$ ($4\pi$) state will collapse into the ring state [downhill by 53.0 kcal/mole]. The $^1A'$ ($4\pi$) state is unbound with respect to $H_2CO(^1A_1) + O(^1D)$, but this is downhill by only 24.1 kcal/mole.

The $3\pi$ and $4\pi$ triplet states of dioxymethane readily dissociate into $H_2CO(^1A_1) + O(^3P)$. The $3\pi$ and $4\pi$ singlet states, however, are bound by 15-20 kcal/mole with respect to dissociation into $H_2CO(^1A_1) + O(^1D)$, but may dissociate slowly by intersystem crossing into $H_2CO(^1A_1) + O(^3P)$. The singlet and triplet $2\pi$ states dissociate into $H_2CO(^3A'') + O(^3P)$ and so have CO bond strengths on the order of 65 kcal/mole.

B.    Thermochemical Calculations

   1.    Methylene Peroxide

As a check of our quantum mechanical dissociation energies, we recalculated them using a thermochemical argument.[39] The experimental heats of formation for the various dissociation products were obtained for the most part from Benson.[39-41] The heat of formation of methylene per- oxide is, of course, not known  experimentally, so it must be estimated by constructing it up from related molecules for which there are experimental data.

Methylene peroxide may be formed from methyl peroxide by pulling off one of the hydrogens.
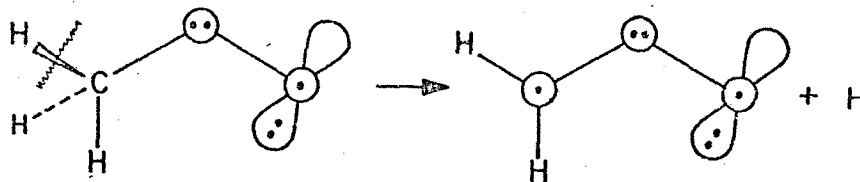
so that $\Delta H_f^0(\dot{C}H_2OO\cdot) = D(H-CH_2OO)$ - $\Delta H_f^0(H) + \Delta H_f^0(CH_3OO\cdot)$. The CH bond strength in methyl peroxide should be comparable to that in methanol,
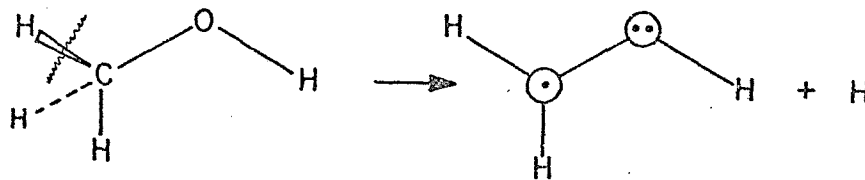
$D(H - CH_2OH) = 94$ kcal/mole,[39,42,43] since in both cases the resulting state is stabilized by a three-electron CO $\pi$ bond. Moreover, since $D(H - CH_2CH_3) = 98$ kcal/mole, the three-electron CO $\pi$ bond is worth

4 kcal/mole. By analogy, $D(H-CH_2OO)$ is assumed to be 94 kcal/mole.

To estimate $\Delta H_f^0(CH_3OO\cdot)$, we use

$$\Delta H_f^0(CH_3OO\cdot) = \Delta H_f^0(CH_3O) + \Delta H_f^0(O) - D(CH_3O - O)$$

$$= 3.5 + 59.6 - D(CH_3O - O) = 63.1 - D(CH_3O - O)$$

inserting the experimental values for $\Delta H_f^0(CH_3O)$ and $\Delta H_f^0(O)$. To estimate $D(CH_3O - O)$, we consider

$$D(HO - O) = \Delta H_f^0(OH) + \Delta H_f^0(O) - \Delta H_f^0(HOO\cdot) = 9.4 + 59.6 - 5 = 64.$$

In addition, it is know experimentally that $D(HO - OH) = 51.3$ kcal/mole, while $D(RO - OR) = 38$ kcal/mole. From this, we conclude that each R group destabilizes an OO $\sigma$ band by 7 kcal/mole through repulsive interactions with the oxygen lone pairs. Therefore, we assume $D(CH_3O-O) = 64 - 7 = 57$, so that $\Delta H_f^0(CH_3OO\cdot) = 63.1 - 57 = 6$ kcal/mole (in agreement with the tentative experimental value of 6.7 kcal/mole). Finally, we obtain

$$\Delta H_f^0(\overset{\bullet}{C}H_2OO\cdot) = 94 - 52.1 + 6 = 48 \text{ kcal/mole}.$$

Using this value, we find

$$D(CH_2O-O) = \Delta H_f^0(CH_2O^*) + \Delta H_f^0(O) - \Delta H_f^0(\overset{\bullet}{C}H_2OO\cdot)$$

$$= 46 + 59.6 - 48 = 57\tfrac{1}{2} \text{ kcal/mole}.$$

This result    is in excellent agreement with our previous estimate, $D(O-OR) = 57$ kcal/mole. Therefore, we will assume $\Delta H_f^0(\overset{\bullet}{C}H_2OO\cdot) = 48$ kcal/mole. Using this value, we calculate the OO and CO bond strengths to be

$$D(CH_2O-O) = 46 + 59.6 - 48 \cong 57\tfrac{1}{2} \text{ kcal/mole}$$

$$D(CH_2-O) = \Delta H_f(CH_2) + \Delta H_f(O_2) - \Delta H_f^0(CH_2OO)$$

$$= 93 + 0 - 48 = 45 \text{ kcal/mole.}$$

Comparing with the ab initio results, we see that there is a discrepancy of

~ 10 kcal/mole in each bond strength. Since both the thermochemical and ab initio results are expected to have errors of ± 5 kcal/mole, the agreement between the two approaches is reasonable.

## 2.   Dioxymethane

Thermochemical estimates of the heat of formation for dioxymethane are also readily made. Dioxymethane is formed by breaking both OH bonds in dihydroxymethane

$$H_2C \overset{O-H}{\underset{O-H}{<}} \longrightarrow H_2C \overset{\dot{O}}{\underset{\dot{O}}{<}} + 2H$$
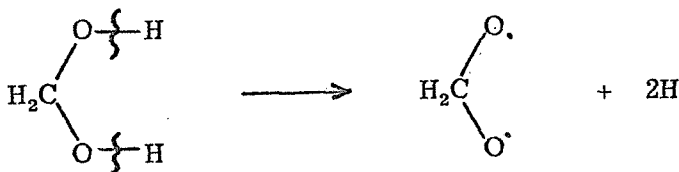
or $\Delta H_f(CH_2\dot{O}_2) = D(H_2C(OH)O-H) + D(H_2C(\dot{O})O-H) + \Delta H_f^0(H_2C(OH)_2) - 2\Delta H_f^0(H)$. Experiment gives $D(RO-H) = 104$ kcal/mole so that

$$\Delta H_f(CH_2\dot{O}_2) = 104 + 104 + \Delta H_f^0(H_2C(OH)_2) - 2(52) = 104 + \Delta H_f^0(H_2C(OH)_2).$$

To estimate $\Delta H_f^0(H_2C(OH)_2)$, we consider

$$\Delta H_f^0(H_2C(OH)_2) = \Delta H_f(OH) + \Delta H_f(H_2\dot{C}OH) - D(H_2C(OH)-OH)$$

$$= 9.4 - 6 - D(H_2C(OH)-OH) = 3.4 - D(H_2C(OH)-OH).$$

But, from our previous calculations we would expect

$$D(H_2C(OH)-OH) = D(R-OH) - (\text{Stabilization of three-electron } CO\,\pi \text{ bond})$$

$$= 92 - 4 = 88.$$

Therefore, we have $\Delta H_f^0(H_2C(OH)_2) = -84.5$ kcal/mole. The experimental value for $\Delta H_f^0(H_2C(OH)_2) = -93.5$ kcal/mole is probably in error as it leads to $D(H_2C(OH)-OH) = 97$, an unrealistically large value.

Using $\Delta H_f^0(H_2C(OH)_2) = 84.5$, we have $\Delta H_f^0(H_2C\dot{O}_2) = 19.5$ kcal/mole. It is important to note that the heat of formation assumes there is no

interaction between the two radical electrons. There are in fact three possible configurations ($2\pi, 3\pi$, and $4\pi$), each leading to both singlet and triplet states, some of which show significant interactions. Thus it does not correspond to a specific state of dioxymethane. One can get a better reference point to compare with the ab initio results by forming the ring state.
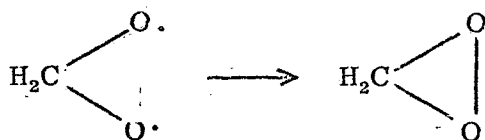


The energy drops by just the strength on the new OO $\sigma$ bond. Normally, $D(RO-OR) = 38$, but a correction must be made for strain. Using Benson's[39] estimate of 26 kcal/mole strain energy for a three-membered ring, the heat of formation of the ring state becomes 7.5 kcal/mole.

As a check of our previous estimate of $\Delta H_f(\dot{C}H_2OO\cdot)$, we recalculate it using the heat of formation of the ring state. Breaking one of the CO $\sigma$ bonds in the ring state costs $D(R-OR) - 26 = 82 - 26 = 56$ kcal/mole, so that the heat of formation for the perpendicular $A'(4\pi)$ state with no interaction between the radical electrons is 63.5 kcal/mole. Rotating both terminal groups and forming three-electron CO and OO $\pi$ bonds gives the planar $^1A'(4\pi)$ state. As before, the three-electron CO $\pi$ bond is worth 4 kcal/mole, while the OO $\pi$ bond is worth 13 kcal/mole. The latter result was obtained from heats of formation of HOO$\cdot$ and ROO$\cdot$. Therefore, the calculated heat of formation of the planar $^1A'(4\pi)$ state is 46.5 kcal/mole, which is in good agreement with our previous result of 48 kcal/mole.

## C. Comparison of GVB and Thermochemical Calculations

In Table VII we compare the relative energies of the ring state with the open methylene peroxide and dioxymethane states as calculated by thermochemical and ab initio techniques. The thermochemical energies for the perpendicular biradical species assume no interaction between the radical electrons. In order to get appropriate ab initio energies for comparison, the corresponding perpendicular singlet and triplet $(4\pi)$ state energies were averaged. For these cases, reference to spin multiplicity in the state designation is dropped.

The agreement between the thermochemical and ab initio results for the perpendicular states is better than the expected errors. However, the relative energies of the planar and perpendicular states appear to be underestimated by the GVB calculations. There are two apparent reasons for this discrepancy. (1) The GVB-CI may be biased in favor of the planar state as many more configurations or spin eigenfunctions are used for the planar state. In this case, the SD-CI provides a more consistent description of the planar and perpendicular states, reducing the discrepancies with the thermochemical results by $\sim 5$ kcal/mole. Note, however, that the relative energies of the perpendicular states are the same in both CI calculations, reaffirming that the smaller GVB-CI has all the important configurations required for a consistent description. (2) The energies of the perpendicular states are too high relative to the planar state because of the chosen geometry and basis set. Double-zeta bases are known to favor states with open geometries versus those with ring geometries. Introduction of polarization functions (d basis functions) leads to a more consistent

TABLE VII. Relative adiabatic energies (kcal/mole).

| | Thermo-chemical | GVB-CI | SD-CI |
|---|---|---|---|
| [ Plan $^1A'$ (4$\pi$)] - [ Ring $^1A_1$ (4$\pi$)] | 39 | 21.0 | 25.8 |
| [ Plan $^1A'$ (4$\pi$)] - [ Perp $A'$ (4$\pi$)] | -17 | -36.5 | -29.5 |
| [ Perp $^1A'$(4$\pi$)] - [ Perp $A'$ (4$\pi$)] | 56 | 57.5 | 55.3 |
| [ Perp $A_1$ (4$\pi$)] - [ Ring $^1A_1$ (4$\pi$)] | 12 | 13.9 | 12.1 |
| [ Perp $A'$ (4$\pi$)] - [ Perp $A_1$ (4$\pi$)] | 44 | 43.6 | 43.2 |

description.                    Finally, the geometry employed for the perpendicular $^{1,3}A'(4\pi)$ states is not optimal. As mentioned previously, a longer OO bond should have been used to account for the repulsive interaction of the oxygen $\pi$ pairs.

One important conclusion that may be drawn from the data in Table VII is that Benson's[39] estimate of 26 kcal/mole for the strain energy of a three-membered ring is consistent with our ab initio calculations.

## VII. IMPLICATIONS FOR THE MECHANISM OF OZONOLYSIS

### A. Solution Phase

#### 1. Formation of the Primary Ozonide

Figure 9 shows an energy level diagram for the ozonolysis of ethylene.[44] The overall pathway assumed by the Criegee mechanism, shown by the dotted line in Figure 9, is certainly feasible from a thermochemical standpoint. However, interesting facets of ozonolysis will become evident if we pursue the Criegee mechanism step by step.

Ozonolysis of ethylene is known to have a very low activation energy (4-5 kcal/mole).[45-48] Nonconcerted addition of ozone to ethylene would lead to an activation energy of > 10 kcal/mole (cf. Figure 9), so that the primary ozonide must be formed in a concerted manner. Bailey[48] has proposed a loosely bound $\pi$-complex (18) between the ozone and olefin as a precursor to the primary ozonide.



18
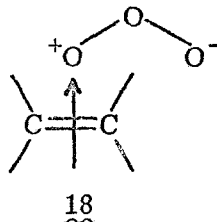
Since we now know that the ozone is a singlet biradical rather than a zwitterion, the possibility of a $\pi$-complex as envisioned by Bailey becomes very remote. The only experimental evidence for a $\pi$ complex relates to complexes (presumably charge transfer in nature) between ozone and aromatic $\pi$ systems.[6,49]

There is some experimental evidence that the primary ozonide is not always formed. The production of epoxides and concomitant evolution of
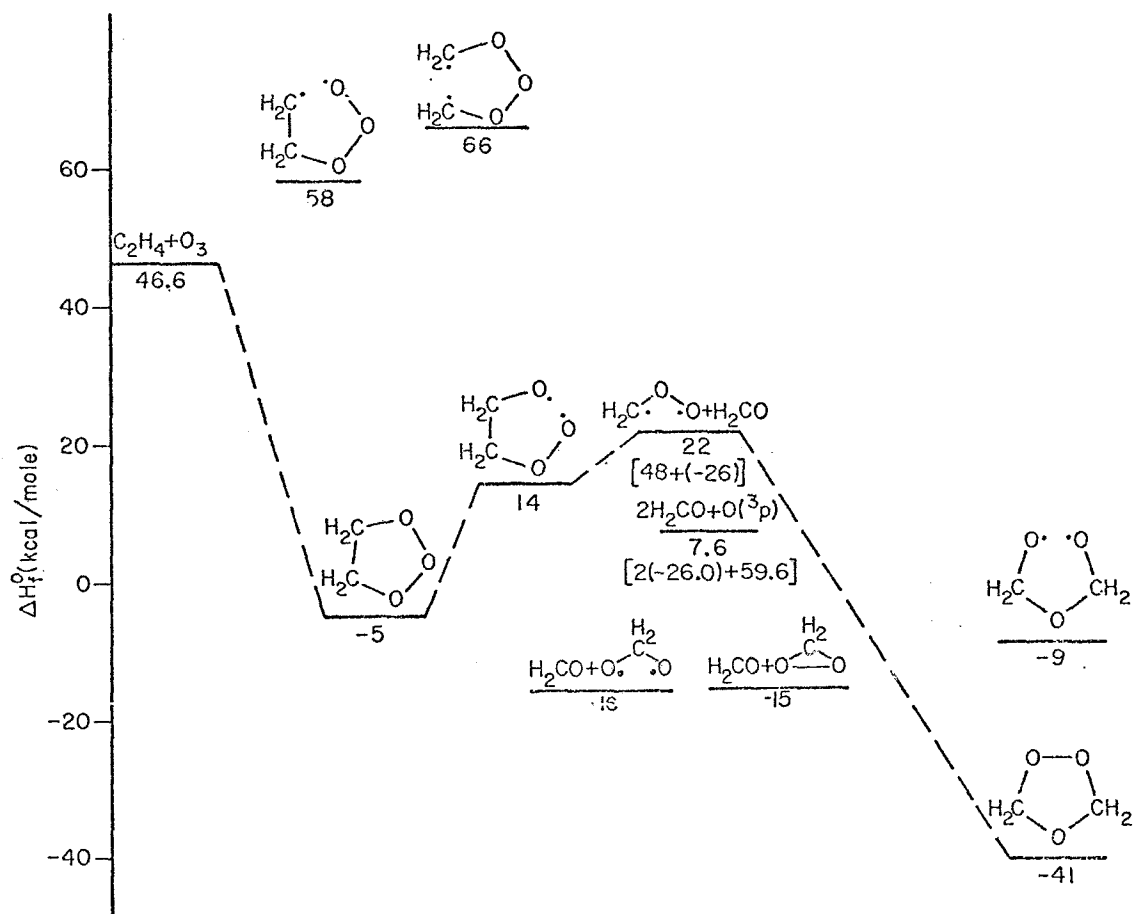
Figure 9. The thermochemistry of ozonolysis. The calculated heats of formation are shown below each molecule or set of molecules.

$O_2$ in certain systems rather than production of secondary ozonides has been interpreted as evidence for a $\sigma$ complex (19).[50]



19
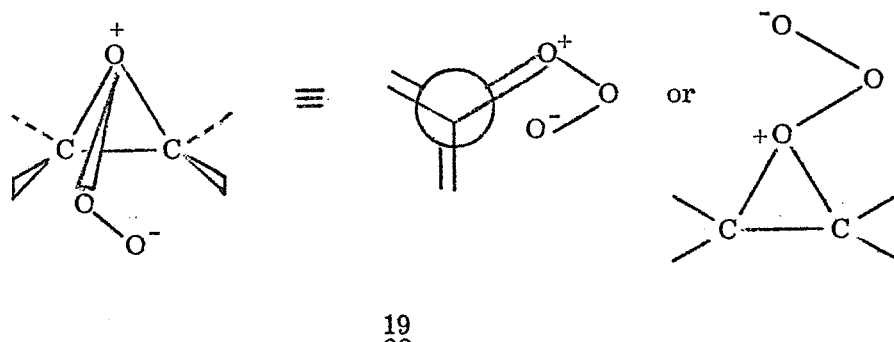
It is easy to see how 19 can lose $O_2$ to form an epoxide or proceed directly to a secondary ozonide. However, 19 is shown to be an unreasonable structure when the analogous GVB diagram is drawn (20).



20
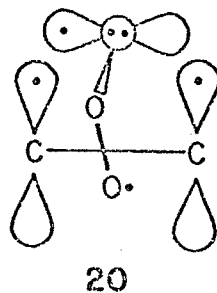
Too many electrons are being crammed in the same region of space.

The production of epoxides is greatest in 1-olefins with the 1 position disubstituted with bulky groups (21).[48]



21
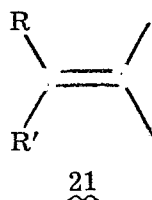
Bailey has performed extensive studies on 21 varying R and R′ with the conclusion that the production of epoxides and evolution of $O_2$ is directly

correlated with steric hindrance.[48] To explain these results, Bailey proposed that the ozone addition was not concerted but rather proceeded through an open $\sigma$ complex (22), which could give off $O_2$ and close to the expoxide.[5b,51]

22
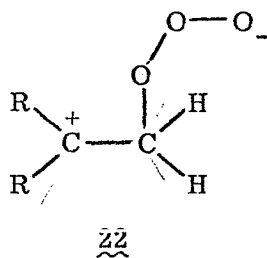
This approach is much more reasonable although 22 is a poor representation of the intermediate. The appropriate GVB diagram is given by 23

23
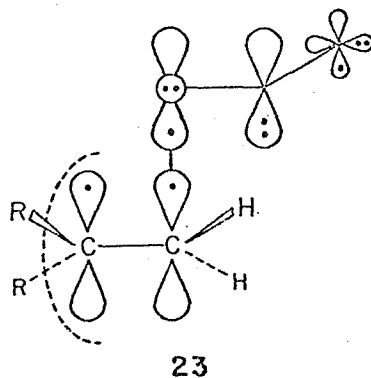
The dotted line in 23 crudely represents the space excluded by the bulky R groups. A bidentate attack by the ozone is just not possible. Moreover, we see that as the OO $\sigma$ bond starts to break to give off $O_2$ ($^3\Sigma_g^-$) the remaining O is in perfect position to close to the epoxide.
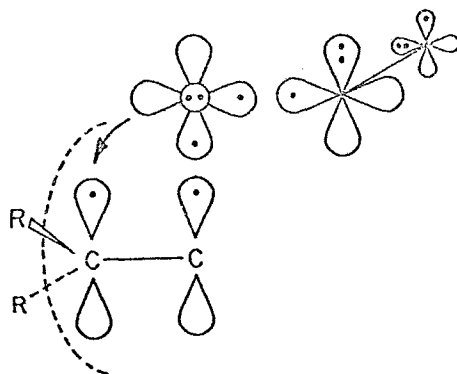
## 2. Decomposition of the Primary Ozonide

Decomposition of the primary ozonide into methylene peroxide and formaldehyde is likely to proceed via the biradical intermediate shown in Figure 9, in which only a weak OO $\sigma$ bond is broken. Formation of the Criegee intermediate from the equilibrium conformation of either the primary ozonide or the higher energy intermediate leads preferentially to the perpendicular $^1A''$ ($3\pi$) state. Use of molecular models is necessary to see this result for the concerted reaction, while the state produced by the biradical intermediate may be seen as follows:
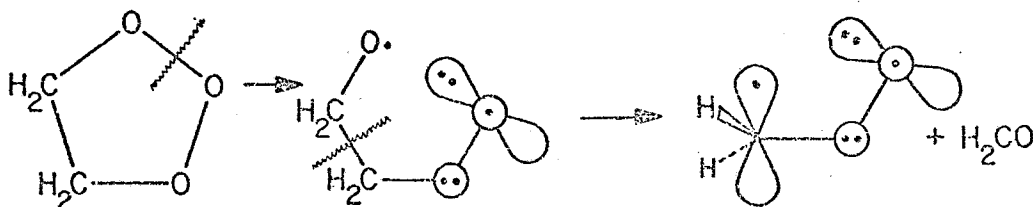


The orientation of the oxygens to give a three-electron $\pi$ bond in the intermediate determines the state of methylene peroxide that is produced. Since the energy of the perpendicular $^1A''$ ($3\pi$) state is 19.1 kcal/mole above that of the planar $^1A'$ ($4\pi$) state assumed in Figure 2, formation of this state of methylene peroxide is downhill from $O_3$ + $C_2H_4$ by only 3.5 kcal/mole. Consequently, the decomposition of the primary ozonide may be slow enough so that the low-energy planar $^1A'$ ($4\pi$) state is formed. In fact, formation of the $^1A''$($4\pi$) state is expected to be the primary decomposition pathway in solution, where the quenching rates of the primary ozonide are high relative to the gas phase.

At this point it seems obvious that decomposition of the primary ozonide leads to a singlet biradical state of methylene peroxide. How then did the Criegee zwitterion gain such a broad acceptance among chemists? As previously stated, simple VB structures indicated that ozone was a zwitterion and hence it was natural to conclude that methylene peroxide was also. Moreover, Criegee[5b] carried out an ozonolysis of styrene which did not produce any detectable amounts of polystyrene. From this result, he concluded that no radicals were present, confirming the postulate that methylene peroxide was zwitterion.

We now know that both ozone and methylene peroxide are singlet biradicals. The key conceptual problem that led to the misinterpretation of the styrene experiment was the failure to recognize that singlet biradicals may behave very differently from simple radicals. The persistence of this misconception is evident in the analysis of some very illuminating mechanistic work on ozonolysis by Murray and Suzui.[8] They photolyzed diazo compounds in the presence of $O_2$ and aldehyde. Secondary ozonides were produced, which were interpreted as confirmation of the Criegee zwitterion as an intermediate in ozonide formation. The following reaction scheme was proposed[8]

$$(C_6H_5)_2CN_2 \xrightarrow{h\nu} (C_6H_5)_2C: \xrightarrow{O_2} (C_6H_5)_2\overset{.}{C}-O-O\cdot$$

$$(C_6H_5)_2\overset{.}{C}-O-O\cdot \longrightarrow \begin{cases} \text{radical reactions} \\ (C_6H_5)_2C=\overset{+}{O}\diagup^{O^-} \end{cases}$$

$$(C_6H_5)_2C=\overset{+}{O}\diagup^{O^-} \xrightarrow{RCHO} \underset{C_6H_5}{\overset{C_6H_5}{>}}\!\!\!\!\!\times\!\!\underset{O}{\overset{O-O}{<}}\!\!\!\!\!\times\!\!\underset{H}{\overset{R}{<}}$$
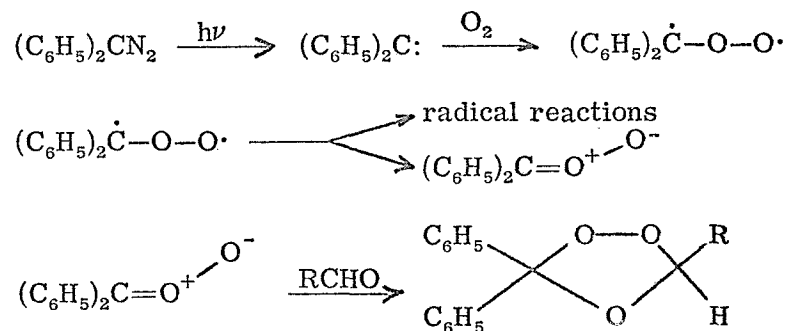
The diphenyl methylene peroxide is assumed to lead to reactions

characteristic of free-radicals and that only the zwitterionic form can produce the secondary ozonides.[52]

The intermediacy of the zwitterion in forming secondary ozonides is not only unnecessary, as shown in Figure 9, but it is also incorrect since the zwitterionic state is too energetic ($\sim 75$ kcal/mole) to be populated. Therefore, replacing the zwitterion model with the biradical model will not cause any major conflict with experiment, although it should have important consequences for interpretation of experiment.

### 3. The Role of Dioxymethane

The planar $^1A'$ ($4\pi$) state produced by the decomposition of the primary ozonide should have enough excess energy to deform into the more stable ring state. The ring state in turn may reopen and attack either an aldehyde to give the secondary ozonide or an olefin to give a 1,3-dioxolane
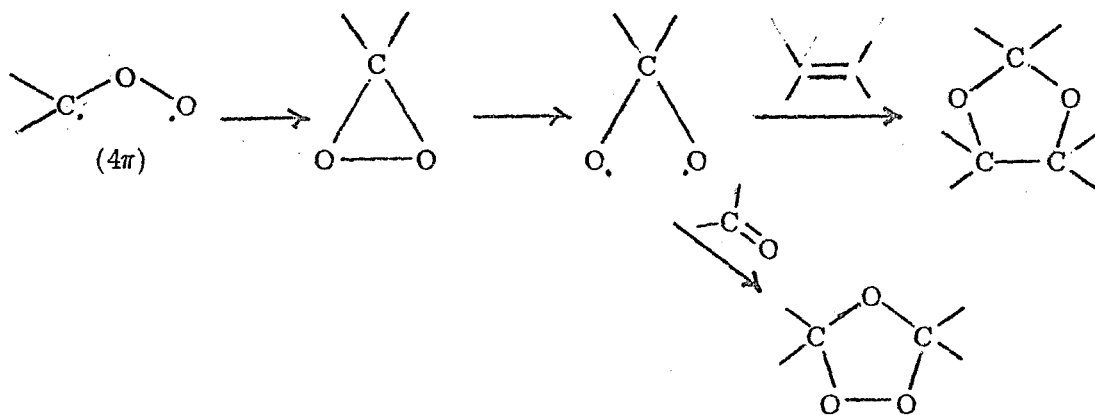


The reaction of dioxymethane with formaldehyde is downhill by some 35 kcal/mole, while the reaction with ethylene is downhill nearly 100 kcal/mole! However, there is no experimental evidence for production of 1,3-dioxolanes and trapping experiments were interpreted to rule out the possibility of dioxymethane as an intermediate.[53]

A few comments about the latter experiments are in order. It is clear that formation of dioxymethane would have important ramifications for the oxygen isotope labeling work. Attack of aldehyde labeled with $^{18}O$ by dioxymethane would lead to a statistical distribution of the labeled oxygen in the secondary ozonide. Attack of labeled aldehyde, on the other hand, by methylene peroxide would lead to secondary ozonide with the labeled oxygen exclusively in the ether position. This fact stirred Fliszar and co-workers[53] to investigate the possibility of dioxymethane as an intermediate. They ran ozonolyses in the presence of alcohols in order to trap the Criegee intermediate. Trapping of methylene peroxide with alcohol was assumed to lead exclusively to alkoxyhydroperoxides, which is in agreement with the thermochemistry of the reaction.



$$\Delta H = -54 \text{ kcal/mole}$$

$$\Delta H = -8 \text{ kcal/mole.}$$
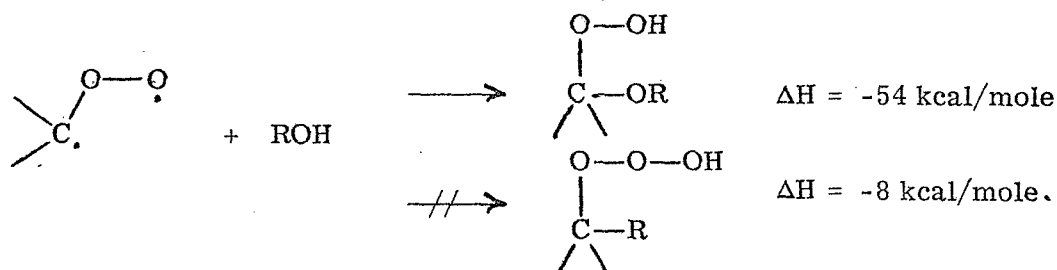
Trapping of dioxymethane with alcohol was assumed to lead exclusively to hydroxyperoxides, which is not actually supported by the thermochemistry



$$\Delta H = -35 \text{ kcal/mole}$$

$$\Delta H = -38 \text{ kcal/mole.}$$
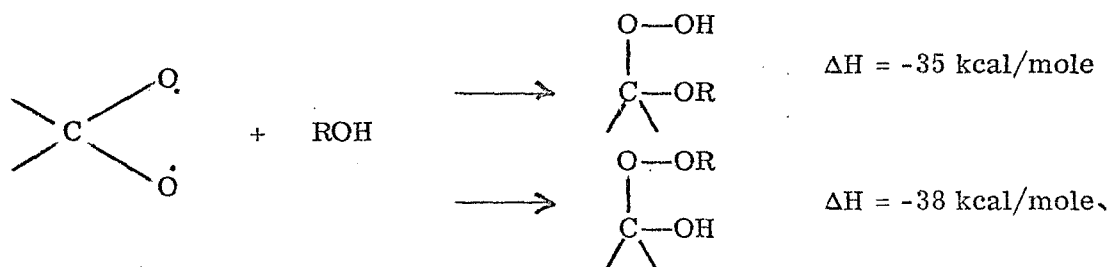
More dynamic data are necessary to be able to distinguish between these

two reaction pathways. In any case, Fliszar[53] could not detect any hydroxy-peroxides. However, this result is not conclusive proof against dioxy-methane, as previously thought.

B.   Gas Phase

    1.   Decomposition of the Primary Ozonide

The thermochemistry scheme for ozonolysis outlined in Figure 9, of course, applies in the gas phase, but the solvent is no longer present to soak up excess energy rapidly. Production of highly excited and/or reactive species ensues. Some of these may be important in carrying the chain reactions that occur in atmospheric air pollution.

As intimated in Section IV.A.1, the perpendicular $^1A''$ ($3\pi$) state of methylene peroxide is formed preferentially in the decomposition of the primary ozonide. If the perpendicular $^1A''$ ($3\pi$) state is produced, then according to Table VI it should decompose into $H_2CO(^1A_1) + O(^1D)$. The $O(^1D)$ will react rapidly with almost anything that is around, e.g.,[54]

    (1)   $O(^1D) + O_3 \rightarrow 2 O_2(^1\Sigma_g^+)$

    (2)   $O(^1D) + C_2H_4 \rightarrow OH + C_2H_3$

    (3)   $O(^1D) + H_2CO \rightarrow OH + HCO$
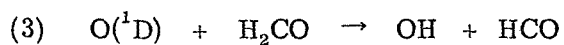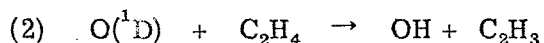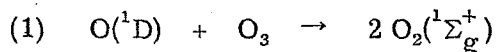
The production of hydroxyl radicals is important not only because of their role in smog production,[55] but also because Pitts and co-workers[4] have seen chemiluminescence assigned to $OH(^2\Sigma^+)$ from low pressure (2 Torr) ozonolysis of olefins (ethylene, cis-2-butene and isobutene). However, formation of $OH(^2\Sigma^+)$ is endothermic by 48 kcal/mole in reaction 2 and by 29 kcal/mole in reaction 3. Therefore, only ground state $OH(^2\Pi)$ will be produced.

The perpendicular $^1A''$ ($3\pi$) state may also dissociate into HCO + OH



$$\rightarrow \quad HCO \quad + \quad OH \qquad \Delta H = -51 \text{ kcal/mole}$$
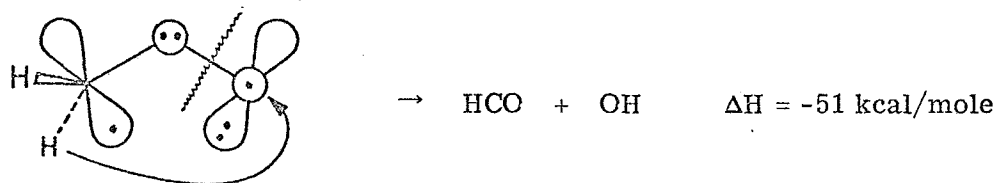
This is not the appropriate place to pursue the myriad of reactions possible for reactive species such as the formyl and hydroxyl radicals. However, to show what is involved, consider just the reactions of the formyl radical expected in the presence of $O_3$ or $O_2$.

$$HCO + O_2 \rightarrow HO_2 + CO \qquad \Delta H = -28.5 \text{ kcal/mole}$$

$$HCO + O_2 \rightarrow \overset{\displaystyle O}{\overset{\displaystyle \|}{HCOO}} \qquad \Delta H = -43 \text{ kcal/mole}$$

$$HCO + O_3 \rightarrow \overset{\displaystyle O}{\overset{\displaystyle \|}{HCO}} + O_2 \qquad \Delta H = -77 \text{ kcal/mole}$$

$$HCO + O_3 \rightarrow CO + OH + O_2 \qquad \Delta H = -58 \text{ kcal/mole}$$
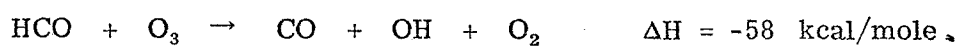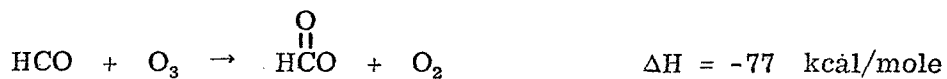
If any methylene peroxide in the planar $^1A''$ ($4\pi$) state is formed by the decomposition of the primary ozonide, one would expect it to react with $H_2CO$ (to give the secondary ozonide), $O_3$ (vide infra), or with $O_2$, if present.[56]



$\Delta H = -24 \text{ kcal/mole}$

$\Delta H = -18 \text{ kcal/mole}$

$\Delta H = -6 \text{ kcal/mole}$
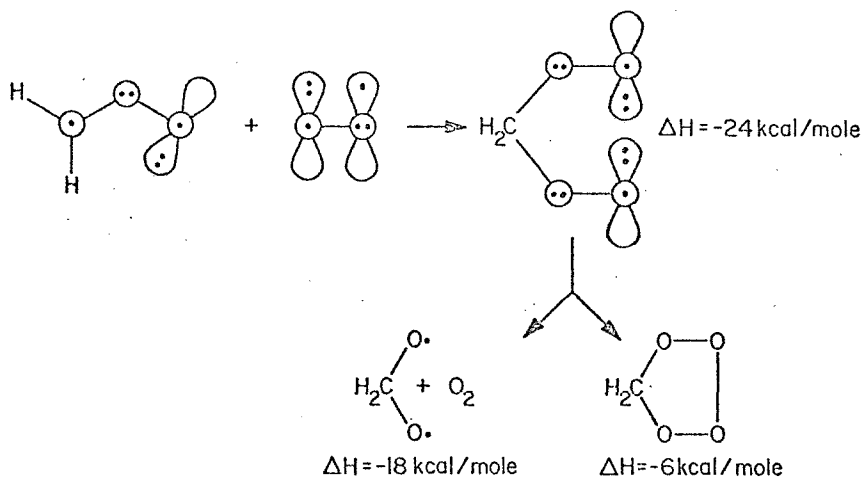
The diperoxy compound should lose oxygen to give dioxymethane.

Dioxymethane may also be formed directly by rearrangement of methylene peroxide as discussed earlier. In either case, our calculations show that the most stable form of dioxymethane is the $^1A_1(2\pi)$ state (lower than even the ring state). Examining the GVB diagram for the $^1A_1(2\pi)$ state shows that it is in a perfect conformation for a simple H migration, leading to formic acid. This process is downhill by 95 kcal/mole!



$$\rightarrow \quad HC\!\!-\!\!OH \qquad \Delta H \cong -95 \text{ kcal/mole.}$$
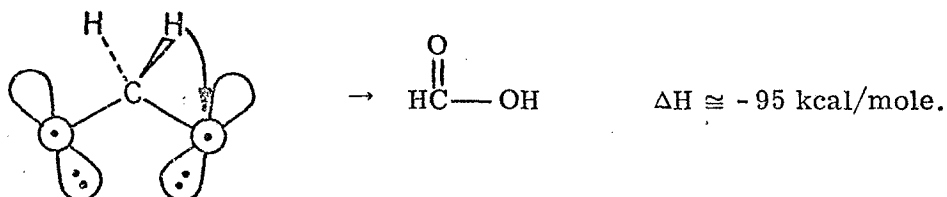
Formic acid is one of the products found in the gas phase ozonolyses.[4,57,58]

The CH bond strength in formic acid is 92.5 kcal/mole, so that it may decompose producing an H atom

$$\text{(4)} \quad H\overset{O}{\overset{\|}{C}}OH \quad \rightarrow \quad \cdot\overset{O}{\overset{\|}{C}}OH \quad + \quad H$$
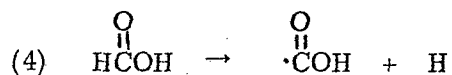
The H atom would be expected to react as follows[57]

$$H + O_3 \rightarrow HO + O_2 \qquad \Delta H = -76.5 \text{ kcal/mole}$$

$$H + C_2H_4 \rightarrow C_2H_5 \qquad \Delta H = -38.5 \text{ kcal/mole}$$

and if $O_2$ if present,

$$H + O_2 \xrightarrow{M} HO_2 \qquad \Delta H = -47 \text{ kcal/mole.}$$

We see that the most favorable reaction is with ozone, leading to highly vibrationally excited products. In fact, previous work of the $H + O_3$ reaction shows that up to the $\nu = 9$ vibrational level of OH will be populated (all the

exothermicity in the newly formed OH bond).[59] Subsequent chemilumines-
cence emission from the nine lowest vibrational levels, the Meinel bands,[60]
has been seen by Pitts and co-workers[4,61] in low-pressure ozonolysis
studies. However, they see the same emission for ozonolysis of tetramethyl-
ethylene so that (as they pointed out) there must be another pathway for pro-
duction of H or excited OH.

The ·C(O)OH radical from (4) would be expected to react with $O_2$ or
$O_3$ to give

$$\underset{\displaystyle \cdot COH}{\overset{\displaystyle O}{\|}} + O_3 \rightarrow \underset{\displaystyle \overset{\displaystyle C}{\cdot}-\underset{\displaystyle \cdot}{O}}{\overset{\displaystyle O}{\|}} + O_2 + OH \qquad \Delta H = -34 \text{ kcal/mole}$$

$$\searrow CO_2 \qquad \Delta H = -51 \text{ kcal/mole.}$$

In addition, the dioxymethane may itself react with $O_3$ or $O_2$

$$\underset{\displaystyle H_2C}{\overset{\displaystyle /O\cdot}{\diagdown}}_{\displaystyle O\cdot} + O_2 \rightarrow \underset{\displaystyle HCO\cdot}{\overset{\displaystyle O}{\|}} + HO_2 \qquad \Delta H = -39 \text{ kcal/mole}$$

$$+ O_3 \rightarrow \underset{\displaystyle HCO\cdot}{\overset{\displaystyle O}{\|}} + OH + O_2 \quad \Delta H = -69 \text{ kcal/mole.}$$

Subsequent reaction of $HCO_2$ with $O_2$ or $O_3$ gives

$$HCO_2 + O_2 \rightarrow \underset{\displaystyle \overset{\displaystyle C}{\cdot}-\underset{\displaystyle \cdot}{O}}{\overset{\displaystyle O}{\|}} + HO_2 \qquad \Delta H = -12 \text{ kcal/mole}$$

$$HCO_2 + O_3 \rightarrow \underset{\displaystyle \overset{\displaystyle C}{\cdot}-\underset{\displaystyle \cdot}{O}}{\overset{\displaystyle O}{\|}} + OH + O_2 \qquad \Delta H = -32 \text{ kcal/mole.}$$

The reactions of OH (and $HO_2$) expected for low pressure gas phase
ozonolyses have previously been outlined by Pitts.[4]

## 2. Chemiluminescent Products

Although reasonable reaction pathways exist for forming almost every possible combination of H, C, and O atoms, there are still certain important experimental results that have not yet been explained with our calculations. First, chemiluminescence has been detected from $H_2CO(^1A'')$ and $OH(^2\Sigma^+)$.[4,61] The planar $^1A'$ (4$\pi$) state of methylene peroxide dissociates to $H_2CO(^3A'')$ + $O(^3P)$, but both ab initio and thermochemical calculations indicate that the reaction of $O_3$ + $C_2H_4$ is not exothermic enough to provide the $^1A'$ (4$\pi$) state with enough vibrational energy to dissociate. The most likely mechanism for production of $H_2CO(^1A'')$ is attack by ozone on the planar $^1A'$ (4$\pi$) state of methylene peroxide.



$$\Delta H = -27 \text{ kcal/mole}$$
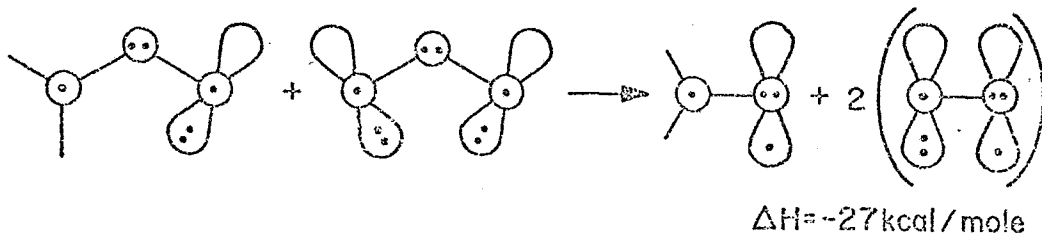
Although both the $^3A''$ and $^1A''$ states of formaldehyde may be produced by this reaction, emission is seen from the $^1A''$ state since the $^3A''$ state is known not to emit.[62] Pitts has also seen chemiluminescent emission from glyoxal[4] and biacetyl[61] (presumably formed by dimerization of the formyl and acetyl radicals, respectively). The excited states are assumed to arise from energy transfer with $H_2CO$ ($^1A''$ or $^3A''$).[61]

Formation of $OH(^2\Sigma^+)$ is not as easy to rationalize. Energy transfer from $H_2CO$ ($^1A''$ or $^3A''$) is not possible since the electronic excitation energy in OH is ~ 1 eV greater than in $H_2CO$.[16,37] Earlier, we showed that the perpendicular $^1A''(3\pi)$ state of methylene peroxide decomposed into

$H_2CO$ ($^1A_1$) + O($^1D$). However, the subsequent reaction of O($^1D$) + $H_2CO(^1A_1$) to give HCO + OH($^2\Sigma^+$) was endothermic by 29 kcal/mole. Therefore, formation of OH($^2\Sigma^+$) is not understood.

Chemiluminescence from vibrationally excited OH($^2\Pi$), the Meinel bands, has also been seen in low pressure ozonolysis of a variety of methylated ethylenes.[4,61] The emission from OH corresponds closely to that produced by the reaction H + $O_3 \rightarrow OH^*_{\nu \leqslant 9}$ + $O_2$, which is exothermic by 77 kcal/mole. For ozonolysis of ethylene, we outlined one mechanism for production of H atoms and, thence, the Meinel band, namely,

$$H_2C\overset{O\cdot}{\underset{O\cdot}{<}} \quad \rightarrow \quad \overset{O}{\overset{\|}{HC}}-OH \quad \rightarrow \quad H + \cdot\overset{O}{\overset{\|}{C}}OH$$
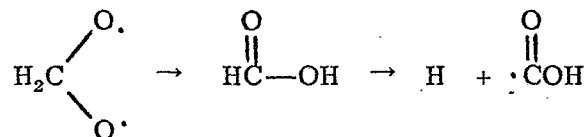
Another mechanism for producing H atoms is decomposition of the vibrationally excited $H_2CO(^1A_1)$, $H_2CO(^1A'')$, or $H_2CO(^3A'')$ into H + HCO, requiring 85, 13, and 4 kcal/mole of vibrational energy, respectively. The needed vibrational energy is supplied by the reaction of methylene peroxide with $O_3$, e.g.,

$$\text{(structure)} \quad + 2 O_2 \qquad \Delta H = -127 \text{ kcal/mole}$$

$$+ 2O(^3P) + O_2 \qquad \Delta H = -8 \text{ kcal/mole.}$$
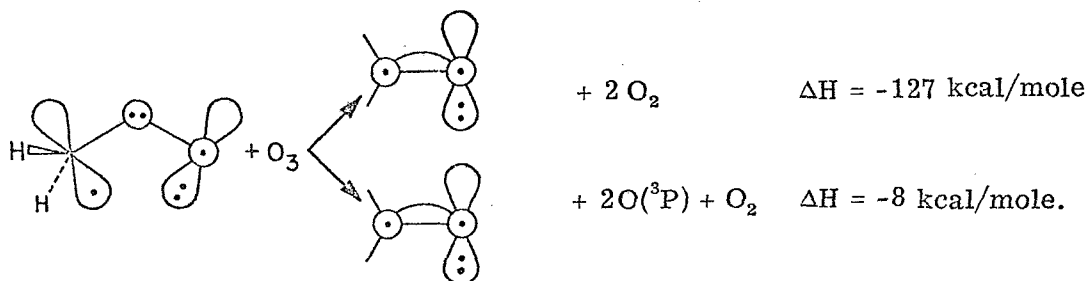
Therefore, the observation of the Meinel bands from the ozonolysis of ethylene is reasonable. On the other hand, the Meinel bands are also seen when tetramethylethylene reacts with ozone.

Ozonolysis of tetramethylethene should lead to dimethylmethylene peroxide, which might undergo a hydrogen migration to form an $\alpha$-unsatu-rated hydroperoxide.



$$\Delta H = -52 \, kcal \, / \, mole$$
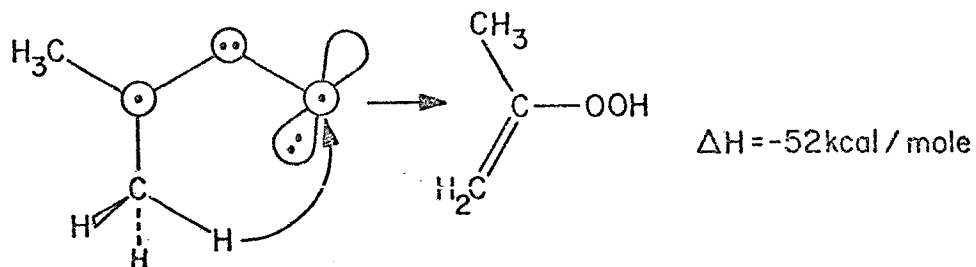
The hydroperoxide may decompose losing an OH group or be attacked by $O_3$. Subsequent decomposition of the resulting adduct might lead to production of H atoms. This scheme is very cumbersome and tenuous. However, it is evident how multiple reactions with ozone may break the tetramethylethylene into molecules similar to those obtained in ethylene ozonolysis and, hence, some of the same chemiluminescent species may be produced.

## VIII. CONCLUSION

By performing high quality ab initio calculations we have shown that
the ground state of methylene peroxide (the Criegee intermediate) is a
singlet biradical rather than a zwitterion. The zwitterionic description in
actuality corresponds to a state $3\frac{1}{2}$ eV above the singlet biradical ground
state. A strong analogy between the ground and low-lying excited states of
methylene peroxide and its isoelectronic counterpart, ozone, was demon-
strated. The excitation energies in methylene peroxide were, in general,
smaller than the comparable energies in ozone. This was reasonable in
light of the weaker $\pi$ bonds expected for methylene peroxide. The ring
state of methylene peroxide was found to lie nearly 1 eV lower than the
planar open state, while the analogous ring state in ozone is 1.5 eV higher
than the open ground state.[9] The ring state can reopen, breaking the weak
OO bond, to form dioxymethane. The $^{1}A_{1}$ $(2\pi)$ state of dioxymethane was
found to be lower than even the ring state.

Combining our ab initio results with thermochemical data, we ana-
lyzed the stability of the Criegee intermediate as well as the possible
modes of reaction in ozonolysis. We were able to explain the production
of many of the chemiluminescent species observed by Pitts and co-workers[4,61]
in their low pressure ozonolysis studies. However, the mechanism for
formation of $OH(^{2}\Sigma^{+})$ was not evident in our scheme. Our calculations also
predict the production of reactive radicals such as OH and $HO_2$ in the course
of ozonolysis, which may have important consequences for understanding
the generation of photochemical air pollution. Further calculations and
experiments are warranted in this area.

With regard to ozonolysis in solution, the mechanism whereby epoxides are produced by ozonolysis of 1-olefins disubstituted at the 1 position with bulky groups was elucidated. Also, the possible role of methylene peroxide rearrangement to dioxymethane in interpreting the $^{18}$O isotope experiments was reexamined and shown to be plausible.

Finally, it is clear that more calculations are needed on the initial phases of ozonolysis, the formation of the primary ozonide and its subsequent decomposition. As indicated by the gas phase work, the decomposition of the primary ozonide into an aldehyde and the Criegee intermediate may only be telling part of the story.

## REFERENCES

1. Schoenbein reported the first ozonolysis (of ethylene) in 1855!

   C. F. Schoenbein, J. Prakt. Chem., 66, 282 (1855). References 2 and 3 provide reviews of more recent work.

2. P. S. Bailey, Chem. Rev., 58, 925 (1958).

3. R. W. Murray, Accts. Chem. Res., 1, 313 (1968).

4. R. Atkinson, B. J. Finlayson, and J. N. Pitts, J. Amer. Chem. Soc., 95, 7592 (1973); and references cited therein.

5. (a) R. Criegee and G. Weiner, Justus Liebigs Ann. Chem., 546, 9 (1949); (b) R. Criegee, Rec. Chem. Progr., 18, 111 (1957).

6. L. A. Hall, I. C. Hisatsune, and J. Heicklen, J. Amer. Chem. Soc., 94, 4856 (1972); and references cited therein.

7. C. W. Gillies and R. L. Kuczkowski, ibid., 94, 7609 (1972).

8. R. W. Murray and A. Suzui, ibid., 95, 3343 (1973).

9. (a) P. J. Hay and W. A. Goddard III, Chem. Phys. Lett., 14, 46 (1972); (b) P. J. Hay, T. H. Dunning, Jr., and W. A. Goddard III, ibid., 23, 457 (1973); (c) W. A. Goddard III, P. J. Hay, and T. H. Dunning, Jr., J. Amer. Chem. Soc. (to be published).

10. W. A. Goddard III, T. H. Dunning, Jr., W. J. Hunt, and P. J. Hay, Accts. Chem. Res., 6, 368 (1973).

11. (a) P. J. Hay, W. J. Hunt, and W. A. Goddard III, Chem. Phys. Lett., 13, 30 (1972); (b) idem, J. Amer. Chem. Soc., 94, 8293 (1972).

12. W. J. Hunt, P. J. Hay, and W. A. Goddard III, J. Chem. Phys., 57, 738 (1972).

13. T. H. Dunning, Jr., and W. A. Goddard III (unpublished results).

14. The wavefunctions for the singlet (S) and triplet (T) states are

$$\psi_S = \mathcal{A}[(\text{core})(\pi_\ell \pi_r + \pi_r \pi_\ell)\alpha\beta\ldots\alpha\beta]$$

$$\psi_T = \mathcal{A}[(\text{core})(\pi_\ell \pi_r - \pi_r \pi_\ell)\alpha\beta\ldots\alpha\beta] .$$

Using the same orbitals for both states, the energies are

$$\psi_S = E_{\text{core}} + \frac{E_0 + E_x}{1 + S^2}$$

$$\psi_T = E_{\text{core}} + \frac{E_0 - E_x}{1 - S^2}$$

where

$$E_0 = \langle \pi_\ell \pi_r | \mathcal{H}(1,2) | \pi_\ell \pi_r \rangle$$

$$E_x = \langle \pi_\ell \pi_r | \mathcal{H} | \pi_r \pi_\ell \rangle = 2 \langle \pi_\ell | \pi_r \rangle \langle \pi_\ell | h | \pi_r \rangle + \langle \pi_\ell \pi_r | 1/r_{12} | \pi_r \pi_\ell \rangle$$

$$= 2S\, h_{\ell r} + K_{\ell r} .$$

Thus if $E_x > 0$, the triplet state is lower and if $E_x < 0$, the singlet state is lower. Since

$$S \geqslant 0$$

$$K_{\ell r} \geqslant 0$$

$$h_{\ell r} \leqslant 0$$

and normally $S|h_{\ell r}| > K_{\ell r}$, we see that the singlet state is usually lower when the orbitals are nonorthogonal, while the triplet state is always lower when the orbitals are orthogonal.

15. Note how the ionic structures involve excited atomic configurations, namely a mixture of $O(^1D)$ and $O(^1S)$
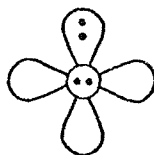
16. G. Herzberg, <u>Molecular Spectra and Molecular Structure</u> (Van Nostrand, Princeton, N.J., 1967), Vol. 3.

17. The HCH bond angle is 116° in methylene oxide[18] and 113° in 1, 2, 4-trioxolane.[19]

18. G. L. Cunningham, A. W. Boyd, R. J. Myers, W. D. Gwinn, and W. I. Le Van, J. Chem. Phys., 19, 676 (1951).

19. C. W. Gillies and R. L. Kuczkowski, J. Amer. Chem. Soc., 94, 6337 (1972).

20. H. E. Hunziker and H. R. Wendt, J. Chem. Phys., 60, 4622 (1974). The OO bond lengths were calculated using Badger's rule.[21]

21. R. M. Badger, <u>ibid.</u>, 3, 710 (1935).

22. L. E. Sutton, <u>Tables of Interatomic Distances</u> (The Chemical Society, London, 1958).

23. T. H. Dunning, Jr., J. Chem. Phys., 53, 2823 (1970).

24. S. Huzinaga, <u>ibid.</u>, 42, 1293 (1965).

25. (a) R. C. Ladner and W. A. Goddard III, ibid., 51, 1073 (1969); (b) W. A. Goddard III and R. C. Ladner, J. Amer. Chem. Soc., 93, 6750 (1971).

26. W. A. Goddard III, Phys. Rev., 157, 81 (1967).

27. There are four other independent ways of coupling six electrons into a singlet. For example, one could couple the orbitals in each of two pairs into a triplet and then couple the two resultant triplet pairs into a singlet. These couplings are included in the CI calculations. They lead to minor energy corrections.

28. A. C. Hurley, J. E. Lennard-Jones, and J. A. Pople, Proc. Roy. Soc. (London), A220, 446 (1953).

29. T. H. Dunning, Jr., W. J. Hunt, and W. A. Goddard III, Chem.

Phys. Lett., $\underset{\sim}{4}$, 147 (1969).

30. T. H. Dunning, Jr. (unpublished results).

31. R. Trambarulo, S. N. Ghosh, C. A. Burrus, Jr., and W. Gordy, J. Chem. Phys., $\underset{\sim}{21}$, 851 (1953); R. H. Hughes, ibid., $\underset{\sim}{24}$, 131 (1956).

32. T.-K. Ha, H. Kühne, S. Vaccani, and Hs.H. Günthard, Chem. Phys. Lett., $\underset{\sim}{24}$, 172 (1974).

33. The CH bonds and the oxygen lone pairs in $H_2COO$ are described by doubly-occupied orbitals in the GVB(3/PP) wavefunctions. Therefore, as in the HF description, mixing of these orbitals does not change the energy and so application of the variational principle does not uniquely define these orbitals. The standard procedure for choosing one set of doubly-occupied orbitals rather than another leads to delocalized orbitals. Therefore, the delocalization is purely an artifact of the method. Finally, the oxygen lone pairs in $O_3$ are also not uniquely defined. In fact, the GVB(3/PP) wavefunction leads to symmetric and antisymmetric combinations of the orbitals actually plotted in Figure 2.

34. P. J. Hay, W. J. Hunt, and W. A. Goddard III, J. Amer. Chem. Soc., $\underset{\sim}{94}$, 638 (1972).

35. Since we do not have extensive potential surfaces, but rather energies at a few key geometries, we cannot consider the most general pathways for dissociation. However, the GVB diagrams are very useful as a guide for considering more complicated dissociation mechanisms.

36. The binding energies of the $5\pi$ states will be underestimated because of the nonoptimal OO bond length employed in the calculations.

37. Reference 16, Vol. 1.

38. C. E. Moore, <u>Atomic Energy Levels,</u> National Bureau of Standards (U.S.), Circular No. 467 (1949).

39. S. W. Benson, <u>Thermochemical Kinetics: Methods for the Estimation of Thermochemical Data and Rate Parameters</u> (Wiley, New York, 1968).

40. The heat of formation for $CH_2(^3B_1)$ was obtained from Chupka,[41] while heats of formation for the excited states were calculated using the experimental adiabatic excitation energies.[16,37,38]

41. W. A. Chupka and C. Lifshitz, J. Chem. Phys., 48, 1109 (1968).

42. Experimental heats of formation were taken from Benson.[39,43]

43. S. W. Benson, F. R. Cruickshank, D. M. Golden, G. R. Haugen, H. E. O'Neal, A. S. Rodgers, R. Shaw, and R. Walsh, Chem. Rev., 68, 279 (1968).

44. The various heats of formation employed in Figure 9 are based either on experiment or on thermochemical calculations analogous to those presented earlier in this Section VI.

45. Gas phase measurements of the activation energy lead to 4.7 ± 0.2 kcal/mole[46] and 4.2 ± 0.4 kcal/mole[47] in good agreement with one another.

46. W. B. De More, Int. J. Chem. Kinet., 1, 209 (1969).

47. J. J. Bufalini and A. P. Altshuller, Can. J. Chem., 43, 2243 (1965).

48. P. S. Bailey and A. G. Lane, J. Amer. Chem. Soc., 89, 4473 (1967).

49. P. S. Bailey, J. W. Ward, and R. E. Hornish, ibid., 93, 3552 (1971).

50. R. W. Murray, R. D. Youssefyeh, and P. R. Story, ibid., 89, 2429 (1967).

51.  Criegee[5b] had proposed earlier a similar mechanism for epoxide production.

52.  Quoting from Ref. 8: "Presumably, a portion of the diradical carbonyl oxide then populates the dipolar form which reacts with aldehyde to give ozonide. The low ozonide yields are presumably due to leakage of the carbonyl oxide into free-radical processes at the diradical state."

53.  G. Klutsch, J. Grignon, J. Renard, and S. Fliszar, Can. J. Chem., $\underline{48}$, 1598 (1970).

54.  K. L. Demerjian, J. A. Kerr, and J. G. Calvert, Advan. Environ. Sci. Technol., $\underline{4}$, 1 (1973).

55.  H. Niki, E. E. Daby, and B. Weinstock, Advan. Chem. Ser., $\underline{113}$, 16 (1972).

56.  Many of the gas phase ozonolyses are carried out in the presence of relatively large amounts of $O_2$.

57.  W. E. Scott, E. R. Stephens, P. L. Hanst, and R. C. Doerr, Proc. Amer. Petrol. Inst., $\underline{3}$ (37), 171 (1957).

58.  T. Vrbaski and R. J. Cvetanovic, Can. J. Chem., $\underline{38}$, 1053, 1063 (1960).

59.  (a) K. G. Anlauf, R. G. MacDonald, and J. C. Polanyi, Chem. Phys. Lett., $\underline{1}$, 619 (1968); (b) P. E. Charters, R. G. MacDonald, and J. C. Polanyi, Appl. Opt., $\underline{10}$, 1747 (1971).

60.  A. B. Meinel, Astrophys. J., $\underline{111}$, 555 (1950).

61.  B. J. Finlayson, J. N. Pitts, and H. Akimoto, Chem. Phys. Lett., $\underline{12}$, 495 (1972).

62.  J. G. Calvert and J. N. Pitts, Jr., Photochemistry (Wiley, New York, 1966), p. 371.

63.    T. H. Dunning, Jr. (unpublished results).

64.    L. A. Harding and W. A. Goddard III, manuscript in preparation.

65.    W. A. Goddard III and W. R. Wadt (unpublished results).

PART TWO:

The Electronic Structure of Pyrazine:

A Valence Bond Model for Lone Pair Interactions

## I.  Introduction

The nature of the excited states of pyrazine has been of great interest among spectroscopists and theoreticians for many years.[1] In addition to the $\pi \to \pi^*$ transitions, analogous to those of benzene, one expects new $n \to \pi^*$ transitions involving the non-bonding (or lone pair) orbitals on the nitrogen. Since there are two nitrogens in pyrazine, the question arises as to how the states involving excitations from the two different nitrogens interact with one another. With the advent of photo-electron spectroscopy,[2] the question has been extended to the interaction of the two possible n cations.

Two models for the interaction of the lone pairs have been previously developed, namely, the exciton model of El-Sayed and Robinson[3] and the molecular orbital (MO) model of Hoffmann.[4] The MO model has had good success in elucidating the photoelectron spectra (vide infra). In this paper we present an alternative model based on valence bond (VB) ideas. Ab initio minimal basis set (MBS) calculations have been carried out to test the usefulness of the VB model. In these calculations, emphasis has been placed on describing the $n\pi^*$ excited states and the n cations. More extensive calculations using a double zeta basis will be reported elsewhere.[5]

## II. Qualitative VB Model

### A) n Cations

To begin with, the VB view of the lone pairs in the ground state of pyrazine is represented by 1a and 1b [6]



The non-bonding orbitals are represented by ◁◯ and the electrons by dots. In the VB model the lone pairs are localized and equivalent, so that the ground state wavefunction is

$$\Phi = \mathcal{A}(\Phi_{core} n_\ell^2 n_r^2 \alpha\beta \ldots \alpha\beta) ,$$

where $\Phi_{core}$ represents the remaining electrons.

Now consider ionization of one of the lone pair electrons. One can remove the electron from either the left or right lone pair. These equivalent ion states are combined (resonance) to form two n cation states, $^2A_g$ and $^2B_{1u}$
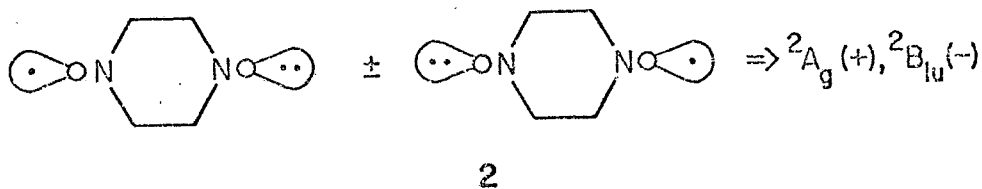


The wavefunctions in this approximation are [7]

$$\Psi(^2A_g) = (\Psi_L + \Psi_R)/\sqrt{2(1+S)} \tag{1}$$

$$\Psi(^2B_{1u}) = (\Psi_L - \Psi_R)/\sqrt{2(1-S)} , \tag{2}$$

where[8]

$$\Psi_L = \mathcal{A}[(\Phi_{core})n_r^2 n_\ell \, \alpha\beta \ldots \alpha\beta\alpha] \tag{3}$$

$$\Psi_R = \mathcal{A}[(\Phi_{core})n_\ell^2 n_r \, \alpha\beta \ldots \alpha\beta\alpha] \tag{4}$$

and[9]

$$S = \langle \Psi_L | \Psi_R \rangle = -\langle n_\ell | n_r \rangle . \tag{5}$$

The splitting energy of the n cations is

$$\Delta E = E(^2A_g) - E(^2B_{1u})$$

$$= \frac{1}{2(1+S)} \langle \Psi_L + \Psi_R \, | \, \mathcal{H} \, | \Psi_L + \Psi_R \rangle - \frac{1}{2(1-S)} \langle \Psi_L - \Psi_R \, | \mathcal{H} | \, \Psi_L - \Psi_R \rangle .$$

By symmetry

$$\langle \Psi_L | \mathcal{H} | \Psi_L \rangle = \langle \Psi_R | \mathcal{H} | \Psi_R \rangle \quad \text{and} \quad \langle \Psi_L | \mathcal{H} | \Psi_R \rangle = \langle \Psi_R | \mathcal{H} | \Psi_L \rangle$$

so that we obtain

$$\Delta E = \left( \frac{1}{1+S} - \frac{1}{1-S} \right) \langle \Psi_L | \mathcal{H} | \Psi_L \rangle + \left( \frac{1}{1+S} + \frac{1}{1-S} \right) \langle \Psi_L | \mathcal{H} | \Psi_R \rangle$$

$$= \frac{-2S}{1-S^2} \langle \Psi_L | \mathcal{H} | \Psi_L \rangle + \frac{2}{1-S^2} \langle \Psi_L | \mathcal{H} | \Psi_R \rangle$$

$$\Delta E = 2 \langle \Psi_L | \mathcal{H} | \Psi_R \rangle - 2S \langle \Psi_L | \mathcal{H} | \Psi_L \rangle + \mathcal{O}(S^2). \tag{6}$$

Since $\Phi_{core}$ is taken to be the same in $\Psi_L$ and $\Psi_R$,[7] we need only consider the non-bonding orbitals $n_\ell$ and $n_r$ in evaluating (6). Moreover, the one-electron terms dominate the two-electron terms[10] so that (6) becomes [using $S = -S_{\ell r}$ from (5)]

$$\Delta E \cong 2 \langle \Psi_L | h | \Psi_R \rangle + 2 S_{\ell r} \langle \Psi_L | h | \Psi_L \rangle$$

$$= 2[ -S_{\ell r} (h_{\ell\ell} + h_{rr}) - h_{\ell r} ] + 2 S_{\ell r} (2 h_{rr} + h_{\ell\ell})$$

$$\Delta E = 2 (S_{\ell r} h_{rr} - h_{\ell r}) , \tag{7}$$

where

$$S_{\ell r} = <n_\ell | n_r>$$

$$h_{\ell r} = <n_\ell | h | n_r>$$

$$h_{\ell \ell} = <n_\ell | h | n_\ell>$$

$$h_{rr} = <n_r | h | n_r> \quad .$$

Equation (7) has the same form as the one-electron exchange energy in $H_2$, which is dominated by $S_{\ell r} t_{rr}$, where $t$ represents the kinetic energy operator.[11] Since $t_{rr}$ is positive, we have

$$\Delta E \propto S_{\ell r} \quad . \tag{8}$$

Thus, we arrive at the very simple and intuitively reasonable result that the splitting energy is proportional to the overlap of the non-bonding orbitals.

Since the nitrogens are well separated (2.79 Å), one would expect the overlap of the atomic hybrid non-bonding orbitals to be quite small and positive; hence, considering only the n orbitals one would expect $\Delta E$ to be quite small and positive (that is, $^2B_{1u}$ lower). However, the effect on the atomic n orbitals of the other $\sigma$ and $\pi$ electrons present in pyrazine must be taken into account. Towards this end, we solve for the optimal wavefunctions, [designated generalized valence bond (GVB)] of the form given in (1) and (2). Some rehybridization and scaling of n orbitals is expected, but the most important effect is induced by the Pauli principle.

Because of the Pauli principle, no more than two electrons can be symmetrically coupled or "paired up". As a result electrons become partitioned into singlet (symmetric) pairs, e.g., CC, CH, CN$\sigma$ bonds, $\pi$ bonds, 1s pairs and lone pairs. The interaction between the singlet-coupled pairs is

repulsive, so that the orbitals in different pairs tend to become orthogonal to one another. In the case of the non-bonding orbitals (singly- or doubly-occupied) nodal planes are expected to develop as shown in 3 in order to make the n orbital orthogonal (Pauli principle) to the $\sigma_{CC}$ and $\sigma_{CN}$ bonding pairs.



**3**

Note that the nodal patterns of the n orbitals favor a negative overlap. Thus, the effect of the Pauli induced orthogonalization is to decrease $S_{\ell r}$ (algebraically) and it could make $S_{\ell r}$ negative. In fact, we find that the overlap is 0.0156 prior to orthogonalization and -0.106 after orthogonalization. Using (8), the Pauli orthogonalization reverses the predicted state ordering, leading to the $^2A_g$ state below the $^2B_{1u}$.

B) $n\pi^*$ States

Now we turn to the $n\pi^*$ states. In 4 we show the ground state of pyrazine again except that the $\pi$ electrons are included (represented by circles, indicating 2p orbitals perpendicular to the plane of the paper) and are shown coupled into the two VB Kekulé structures
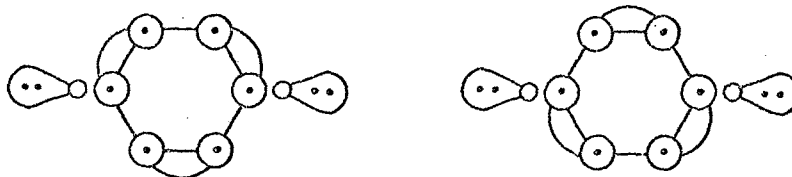


**4**

The tie lines indicate a pair of orbitals singlet-coupled into a $\pi$ bond. The simplest VB model for the $n \rightarrow \pi^*$ excitation involves promotion of an electron

from a non-bonding orbital to the $p_\pi$ orbital on the same nitrogen. In this manner electroneutrality of all the atoms is maintained. There are three ways to pair the $\pi$ orbitals into bonds in this case.



5a          5b          5c
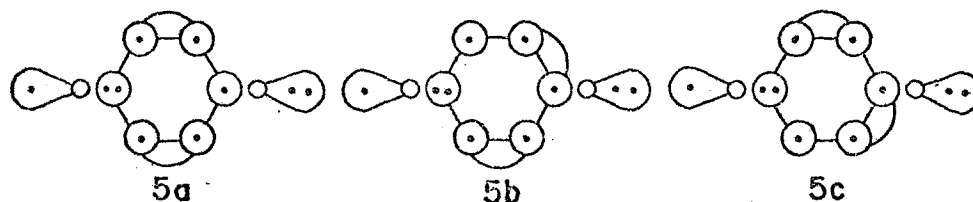
Note that although the electron promotion is assumed to be localized on one nitrogen, the resulting unpaired $\pi^*$ orbital is on either the ortho carbons or on the para nitrogen.

Exciting a lone pair electron from the right nitrogen leads to a comparable set of $n\pi^*$ configurations which must be combined (resonance) with those in 5 to get states of the correct total symmetry



$$\Rightarrow B_{3u}(+), B_{2g}(-)$$

6
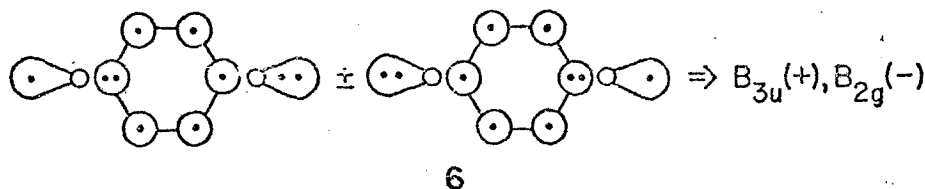
Using the same arguments as before, the splitting of the $n\pi^*$ states is expected to be proportional to the product of the lone pair and $\pi^*$ orbital overlaps,

$$\Delta E = E(B_{3u}) - E(B_{2g}) \propto S_{n_\ell n_r} S_{\pi_\ell^* \pi_r^*} \qquad (9)$$

Since the $\pi^*$ orbitals are quite delocalized, the splitting energy of the $n\pi^*$ states is expected to be only slightly smaller than that of the n cations.

Determining the sign of $S_{\pi_\ell^* \pi_r^*}$ and, hence, $\Delta E$ requires examination of the three couplings of the $\pi$ orbitals. In 7 we show the approximate

position of the nodal planes that will be induced by the Pauli principle to make the $\pi^*$ orbital orthogonal to three pairs of $\pi$ electrons. (The $\sigma$ structure is suppressed).
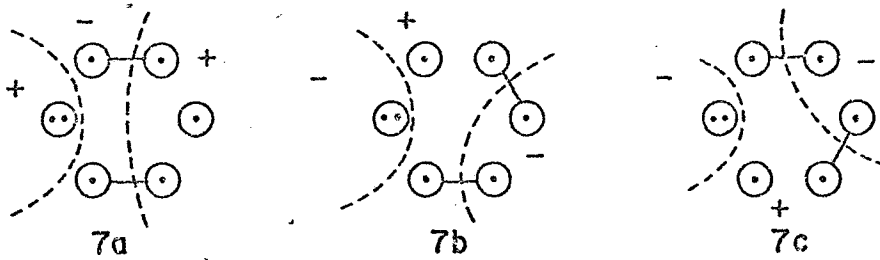


Making the phases of the three structures consistent, we see that the $\pi^*$ orbital will have the form



8
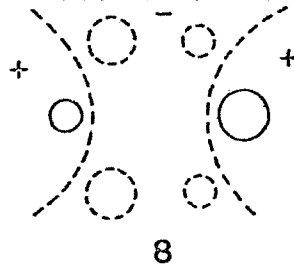
so that the overlap, $S_{\pi^*_\ell \, \pi^*_r}$, will be positive and

$$\Delta E = E(B_{3u}) - E(B_{2g}) < 0$$

or

$$E(B_{3u}) < E(B_{2g}) \ .$$

The $B_{3u}$ $n\pi^*$ states are stabilized with respect to the $B_{2g}$.

Finally, unpaired $n$ and $\pi^*$ orbitals may be singlet- or triplet-coupled, giving rise to $^1n\pi^*$ and $^3n\pi^*$ states. The energies of these are given by

$$E\,(^1n\pi^*) = E_0 + K$$

$$E\,(^3n\pi^*) = E_0 - K \quad ,$$

where $K = \langle n\pi^* | n\pi^* \rangle$ is the two-electron exchange integral between the unpaired $n$ and $\pi^*$ orbitals. Since $K$ is positive, the triplet is lower than the singlet.

We will later consider self-consistent adjustments of the VB orbitals (i.e., GVB). Since -K is negative for the triplet state, we expect the orbitals for the triplet to readjust so as to increase K, while those for the singlet state should readjust so as to decrease K. Thus configurations 5b and 5c with the $\pi^*$ orbital on the ortho carbon are favored for the triplet, while 5c with the $\pi^*$ orbital on the para nitrogen is favored for the singlet. In fact, to increase further the value of K for the $^3n\pi^*$ state, the following ionic configurations are expected to come into play.



9a                    9b
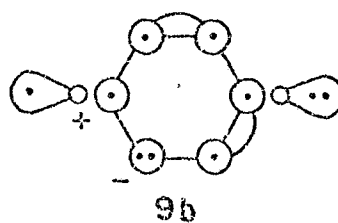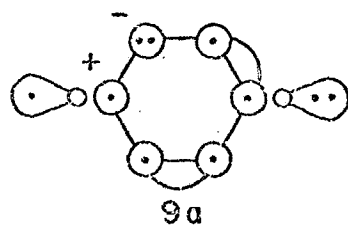
III. Qualitative MO Model

We present a brief description of the MO model for lone pair inter-action developed by Hoffmann[4] in order to compare it with the VB model. To begin with, symmetry orbitals, $n_+$ and $n_-$, are formed from the localized (VB type) non-bonding orbitals, $n_\ell$ and $n_r$

$$n_+ = (n_\ell + n_r)/\sqrt{1+S_{\ell r}}$$

$$n_- = (n_\ell - n_r)/\sqrt{1-S_{\ell r}} \quad ,$$
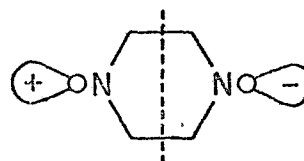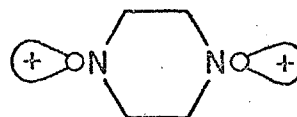
where $S_{\ell r} = \langle n_\ell | n_r \rangle$. The separation of the orbital energies, $\Delta \epsilon$, for $n_+$ and $n_-$ is

$$\Delta \epsilon = \epsilon(n_+) - \epsilon(n_-) = \langle n_+ | \mathcal{H} | n_+ \rangle - \langle n_- | \mathcal{H} | n_- \rangle$$

$$= \frac{2}{1-S_{\ell r}^2} \langle n_\ell | \mathcal{H} | n_r \rangle - \frac{2S_{\ell r}}{1-S_{\ell r}^2} \langle n_\ell | \mathcal{H} | n_\ell \rangle$$

or by arguments similar to those used before

$$\Delta \epsilon \propto -S_{\ell r} \quad .$$

The splitting of the orbital energies is proportional to minus the overlap of the lone pairs. Since for localized n orbitals $S_{\ell r}$ is small and positive, we have

$$\Delta \epsilon = \epsilon(n_+) - \epsilon(n_-) < 0$$

or as expected

$$\epsilon(n_+) < \epsilon(n_-) \quad .$$

This corresponds to what Hoffmann[4] calls "through space" interaction.

Now, we must consider the effects of the other $\sigma$ and $\pi$ electrons by performing a simple Hartree-Fock (HF) calculation. Hoffmann[4] found that the key interactions are between the n orbitals and the $\sigma$ orbitals associated with the $\sigma_{CC}$ bond. Since the interaction of two orbitals with different symmetry vanishes, the $n_+$ orbital interacts only with the $\sigma_{CC}$ orbitals, while the $n_-$ orbital interacts only with the $\sigma_{CC}^*$ orbital. Simple perturbation arguments show that these interactions tend to stabilize $n_+$ with respect to $n_-$ as shown in the diagram below.
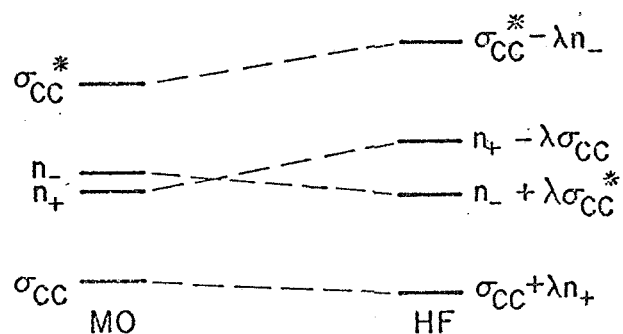


Hoffmann[4] refers to the resultant splitting of $n_+$ and $n_-$ as "through bond" interaction.

Using Koopmans' theorem[12] to equate the vertical ionization potential to negative the orbital energy, the "through bond" interaction leads to the following ordering of the n cations: $E(^2A_g) < E(^2B_{1u})$, i.e., an electron in the $n_+$ orbital is easier to ionize than one in the $n_-$ orbital. This result is in agreement with the conclusion of the VB model.

The MO model for the $n \to \pi^*$ excitations assumes that the lowest transitions will be to the lowest unoccupied $\pi^*$ MO, namely, the $2b_{3u}$ shown in $\underset{\sim\sim}{10}$

$2b_{3u}$

10
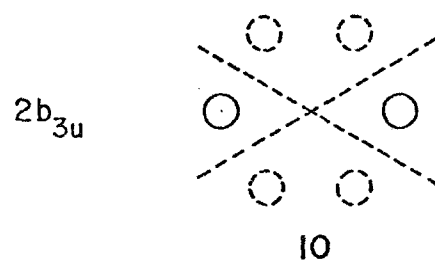
Therefore, the lowest $n\pi^*$ state is expected to arise from the excitation

$n_+ \rightarrow 2b_{3u}$, giving the $B_{3u}$ $n\pi^*$ state. The excitation $n_- \rightarrow 2b_{3u}$ leads to the

$B_{2g}$ $n\pi^*$ state at a higher energy, again in agreement with the VB model.

The splitting of the $B_{3u}$ and $B_{2g}$ $n\pi^*$ states is predicted to be comparable

to that of the n cations.

## IV. Qualitative Comparison of the VB and MO Models

At one level the VB and MO models for lone pair interaction seem
quite similar. Both begin by considering atomic-like lone pairs which have
small overlap and, hence, a small splitting. Then the rest of the pyrazine
molecule is taken into account. Upon optimization for the molecule, the
orbitals delocalize, leading to large changes in the overlap and splitting
energy. Moreover, the delocalization effects are such that the splitting
energy changes sign relative to the small atomic lone pair interaction.
Finally, the $\pi^*$ orbital is delocalized in both cases.

On the other hand, the methods by which the interactions are
explained and evaluated are radically different. In the VB model the splitting
energies arise from the interaction (resonance) of two many-electron wave-
functions (configurations) that describe two equivalent excitation processes.
In the MO model the splittings arise from the interaction of ground state
orbitals (one-electron wavefunctions). As a result, the ground state lone
pair orbitals are localized and equivalent in VB but delocalized and inequiva-
lent in MO. Furthermore, the excitation process giving rise to the n cations
or $n\pi^*$ states is localized on one nitrogen in VB but delocalized over both
nitrogens in MO.

We believe that the VB model provides a picture that is closer to the
results of more exact wavefunctions than the MO model. Support for this
contention may be found prior to any calculations. For example, in VB
only the total wavefunction reflects the full symmetry of the molecule. The
component configurations are allowed to have a lower symmetry ($C_{2v}$ instead
of $D_{2h}$). This freedom allows the excitation to be localized on one nitrogen
as well as allowing the remaining occupied orbitals to adjust or polarize

in response to the excitation as was evident in the difference of the $\pi^*$ orbitals for the $^1n\pi^*$ and $^3n\pi^*$ states. On the other hand, in MO (or HF) the individual orbitals are <u>forced</u> to be symmetry functions, and hence, delocalized.

Trying to describe excited states in terms of a one-electron promotion between two delocalized orbitals can lead to problems. For instance, consider the $n\pi^*$ states described by $n_+ \to \pi^*$ in the MO model. Recalling that the $\pi^*$ orbital $(2b_{3u})$ on the nitrogens is given by $\pi_\ell + \pi_r$, we have

$$n_+ \pi^* = (n_\ell + n_r)(\pi_\ell + \pi_r)$$

$$= (n_\ell \pi_\ell + n_r \pi_r) + (n_\ell \pi_r + n_r \pi_\ell)$$

$$\text{covalent} \qquad \text{ionic}$$

so that significant ionic character is <u>necessarily</u> introduced into the wavefunction. The result is excitation energies that are much too high.

The difficulties of using symmetry orbitals are not as apparent in the case of the n cations. Consider the MO wavefunction for the $^2A_g$ state

$$\psi^{MO}(^2A_g) = \mathcal{A}[\, (\Phi_{core})\, n_-^2 n_+\, \alpha\beta \ldots \alpha\beta\alpha\,]$$

$$= \mathcal{A}[\, (\Phi_{core})\, (n_\ell - n_r)^2 (n_\ell + n_r)\, \alpha\beta \ldots \alpha\beta\alpha\,]$$

$$= \mathcal{A}[\, (\Phi_{core})(n_\ell^2 n_r + n_r^2 n_\ell)\, \alpha\beta \ldots \alpha\beta\alpha] = (\psi_L + \psi_R)/\sqrt{1+S}\, ,$$

which is equivalent to the simple VB wavefunction. However, when solving for the $^2A_g$ state variationally, $\Phi_{core}$ is forced to be symmetric in the HF wavefunction but is allowed to polarize appropriately for $\psi_L$ and $\psi_R$ in the GVB wavefunction.

Finally, although the MO model for lone pair interaction is based on the ground state orbitals, these orbitals are not uniquely defined. One can apply an arbitrary unitary transformation to the space of occupied HF orbitals without changing the energy. This fact adds a note of uncertainty to the MO model. How are the orbitals produced by an HF calculation defined? The answer is Koopmans' theorem.[12]

Previously we mentioned that Koopmans' theorem allows one to equate vertical ionization potentials with negative the orbital energies. There is actually more to it. For an HF wavefunction the energy of the ground (N electron) state may be related to the various cation (N-1 electron) state energies via the orbital energy, i.e.,

$$E_{N+1} = E_N - \epsilon \ .$$

However, since the orbitals and orbital energies are not uniquely defined by the HF calculation, one is faced with an infinity of choices for the cation energy. Koopmans[12] concluded that the best choice of $\epsilon$ would lead to the lowest energy for $E_{N-1}$. Consequently, the value of $\epsilon$ is maximized and the resulting orbital becomes well defined. Therefore, we see that the ground state orbitals reflect the nature of the various cations. This explains how the two ground state lone pair orbitals $n_+$ and $n_-$ are calculated to be inequivalent by HF. The inequivalence actually arises only in the n cations or $n\pi^*$ states as shown in the VB model.

## V. Calculational Details

The goal of these calculations is to test some of the current concepts concerning the excited states of pyrazine, particularly those proffered in the VB model. To do this it is important to allow the orbitals to delocalize and readjust in the presence of other electrons. For example, the orbitals of the n cation (in $\psi_L$ and $\psi_R$) are expected to polarize in response to the n ionization as shown in $\underset{\sim\sim}{11}$



$\underset{}{11}$
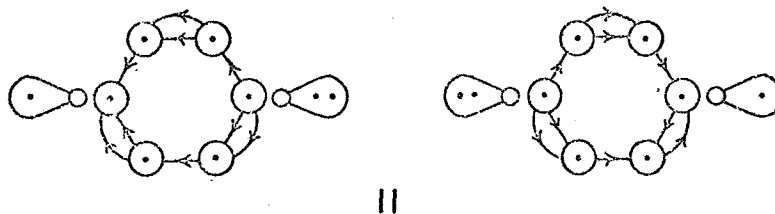
The method of calculating these effects is the generalized valence bond (GVB) method.[13] However, because the orbitals in $\psi_L$ and $\psi_R$ are, in general, non-orthogonal, evaluating expressions such as $<\psi_L |\mathcal{K} |\psi_R>$ involves $\sim 21!$ or $22!$ terms and is not currently feasible. Therefore, we designed a configuration interaction (CI) calculation that would mimic the GVB wavefunction.

### A) Localized n Orbitals

The brute force method would be to take the ground state $(^1A_g)$ HF vectors and perform a large scale CI among the 28 valence orbitals. Because of the large number of orbitals, this procedure is cumbersome and the results are not easy to interpret in terms of simple concepts. The major problem with using HF ground state vectors is that the orbitals are not uniquely partitioned into orbitals of different character (lone pair,

92

the singly occupied non-bonding orbital
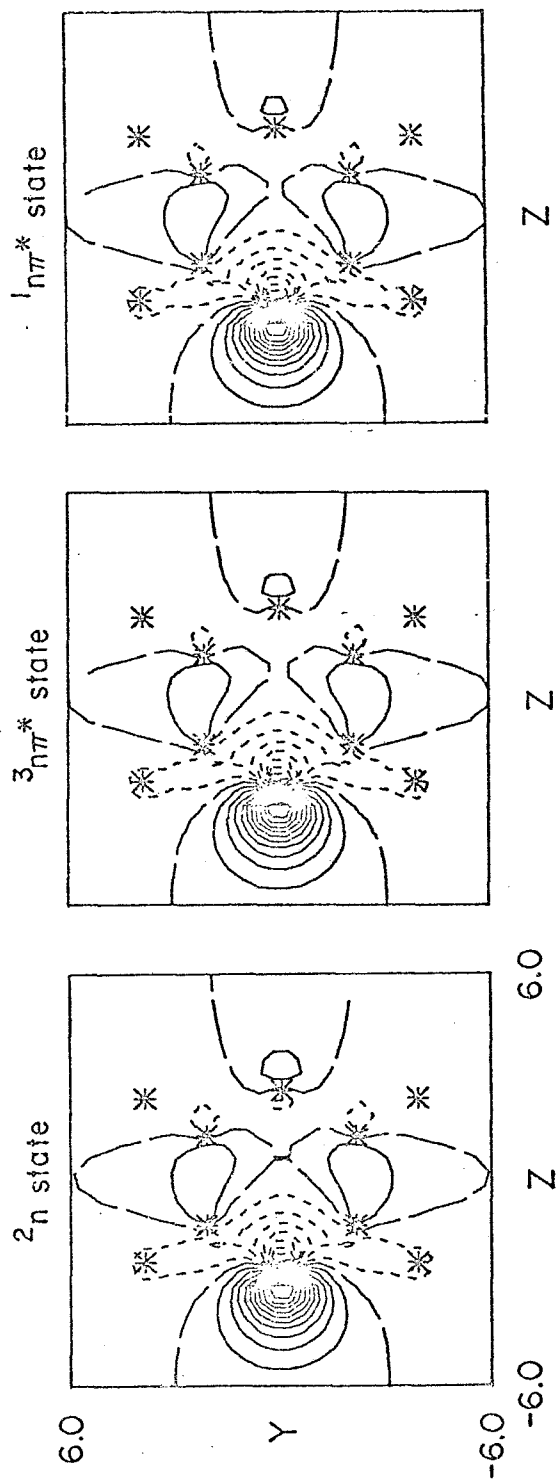


Fig. 1. Contour plots of the singly-occupied n orbital from the $^2$n, $^3$n$\pi$*, and $^1$n$\pi$* SCF wavefunctions. The contour increment is 0.05 a. u.

TABLE I. Mulliken populations for the singly-occupied n orbital.

| | | | $^2n$ | $^1n\pi*$ | $^3n\pi*$ |
|---|---|---|---|---|---|
| excited | N | s | 0.163 | 0.155 | 0.172 |
| | | z | 0.719 | 0.735 | 0.722 |
| | | Total | 0.882 | 0.890 | 0.894 |
| ortho | C | | 0.037 | 0.036 | 0.035 |
| ortho | H | | 0.020 | 0.019 | 0.019 |
| meta | H | | 0.008 | 0.008 | 0.007 |
| para | N | | 0.011 | 0.006 | 0.009 |

HF ($^1A_g$)                    Symmetrized GVB
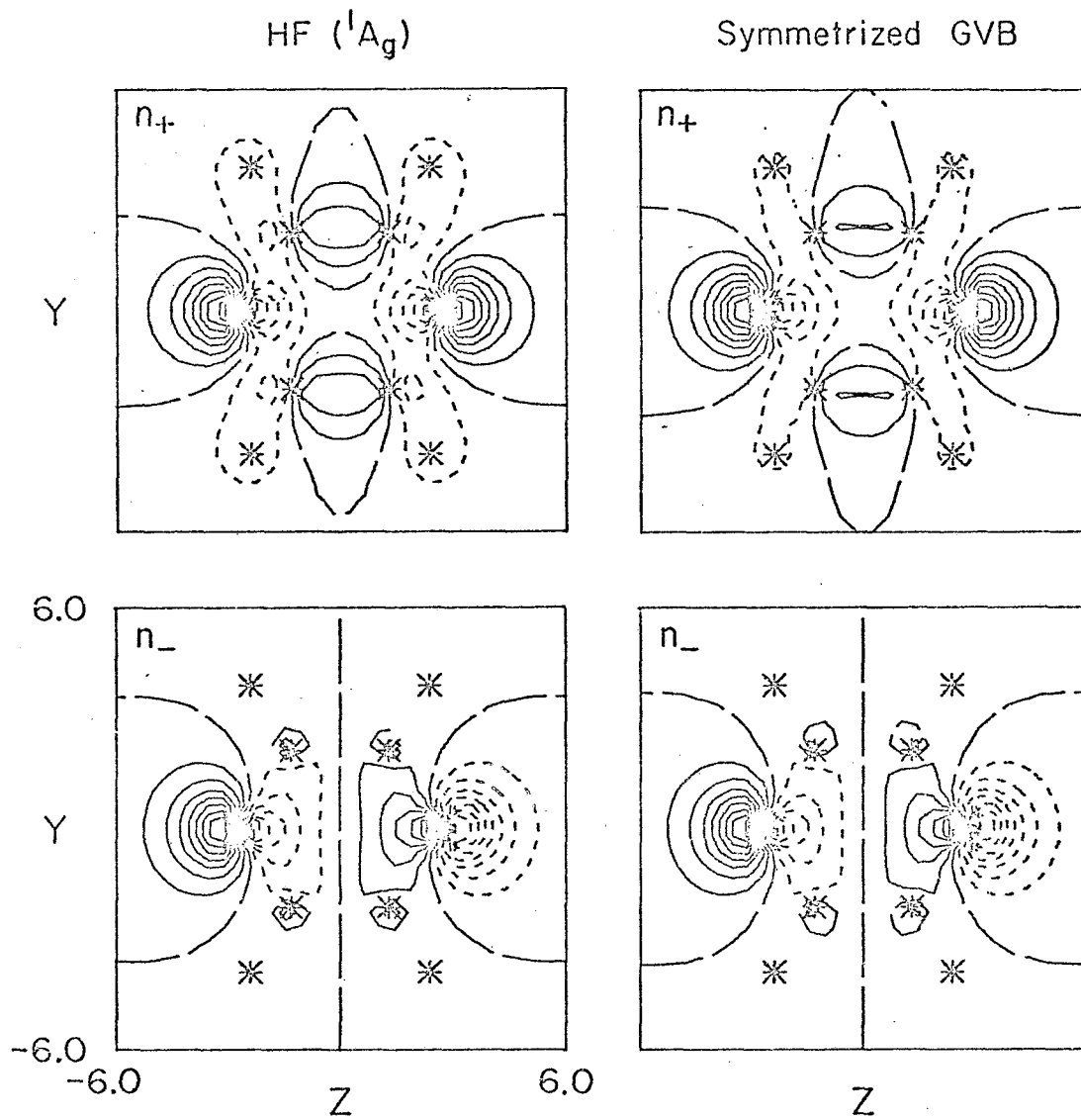


Fig. 2.  Contour plots of the HF 1 $^1A_g$ and symmetrized GVB $n_+$ and $n_-$ orbitals.  The contour increment is 0.05 a.u.

TABLE II.  Mulliken populations for the n symmetry orbitals from the $^1A_g$, $^2A_g$, and $^2B_{1u}$ states.

| | | | $n_+$ | | $n_-$ | |
|---|---|---|---|---|---|---|
| | | | GVB | HF | GVB | HF |
| $^1A_g$ | N | z | 0.171 | 0.120 | 0.185 | 0.176 |
| | | | 0.678 | 0.566 | 0.760 | 0.759 |
| | | Total | 0.849 | 0.686 | 0.945 | 0.935 |
| | C | | 0.098 | 0.216 | 0.049 | 0.054 |
| | H | | 0.053 | 0.097 | 0.006 | 0.010 |
| $^2A_g$ | N | z | 0.166 | 0.129 | 0.188 | 0.181 |
| | | | 0.696 | 0.628 | 0.749 | 0.738 |
| | | Total | 0.862 | 0.757 | 0.937 | 0.919 |
| | C | | 0.097 | 0.179 | 0.058 | 0.067 |
| | H | | 0.041 | 0.063 | 0.005 | 0.014 |
| $^2B_{1u}$ | N | s | 0.175 | 0.133 | 0.186 | 0.180 |
| | | z | 0.675 | 0.588 | 0.768 | 0.773 |
| | | Total | 0.850 | 0.721 | 0.954 | 0.953 |
| | C | | 0.102 | 0.195 | 0.041 | 0.043 |
| | H | | 0.047 | 0.083 | 0.005 | 0.004 |

CC bonding, CH bonding, etc.). In order to obtain unique non-bonding orbitals for the CI calculations, we performed open shell HF calculations with a fully convergent SCF program[14] on the $^2$n, $^1$n$\pi$, and $^3$n$\pi$ states allowing the symmetry to be reduced to $C_{2v}$. In other words, in each case we solved for one of the resonant configurations. The singly-occupied non-bonding orbital is uniquely defined in the three wavefunctions. As shown by the contours plots in Figure 1 and the Mulliken populations in Table I, the non-bonding orbital is in each case quite localized on one nitrogen (88-90%). Since all three non-bonding orbitals are so similar, we chose one, the $^3$n$\pi$* orbital, to partition the HF space into n and $\sigma$ orbitals.

Taking the localized n orbital, symmetry functions, $n_+$ and $n_-$, were formed and projected onto the occupied HF orbitals for the $^1A_g$, $^2A_g$ and $^2B_{1u}$ states.[15] The remaining $\sigma$ orbitals were orthognalized to the n orbitals. In this manner, we partitioned the HF occupied space into n and $\sigma$ orbitals, greatly facilitating the CI calculations. The fact that the simple HF calculation on the ground state mixes extra $\sigma$ character into the n orbitals (especially $n_+$) is shown in Figure 2 and Table II, where contour plots and Mulliken populations are presented for the HF and the symmetized GVB n orbitals, respectively. Note how the $n_-$ orbital is naturally more localized than the $n_+$ because of the node through the CC bond.

Before describing the CI calculations, we should state that SCF calculations were performed using Huzinaga's[16] (7s, 3p/3s) set of primitive gaussian basis functions contracted to a MBS [2s, 1p/1s] by Dunning.[17] All calculations were carried out at the experimental equilibrium geometry for pyrazine.[1]

B) n $-\pi$ CI

In all the CI calculations, the $^2A_g$ and $^2B_{1u}$ vectors were used for the respective n cations, while the $^1A_g$ vectors were employed for all the states of the neutral species as well as for the $\pi$ cations. Eight different types of CI calculations were performed:

(1) HF-CI: only the HF configuration was included,

(2) S-CI: the HF configuration plus single excitations into the $\pi$ space (6 orbitals),

(3) $\pi$ CI: the HF configuration plus a full CI within the $\pi$ space (6 orbitals),

(4) n-$\pi$ CI: the HF configuration plus a full CI within the n + $\pi$ space (8 orbitals).

C) Relaxation of the $\sigma$ Core

In the above four CI calculations the same doubly-occupied $\sigma$ orbitals are used for all states. In order to test the importance of the polarization of the CN, CC, and CH bonds, two more CI calculations were designed. It was not feasible to include the entire valence $\sigma$ space (20 orbitals) along with the 2 n and 6 $\pi$ orbitals.[18] Therefore, we partitioned the $\sigma$ space into the 12 $\sigma_{CC}$ and $\sigma_{CN}$ orbitals and the 8 $\sigma_{CH}$ orbitals. This partition has the added advantage in that the $\sigma_{CC}$ and especially the $\sigma_{CN}$ orbitals are expected to polarize more than the $\sigma_{CH}$ orbitals in the n cations and n$\pi$* states.

The $\sigma$ orbitals were partitioned by taking the two $\sigma$ or $\sigma$* orbitals for each symmetry type that had the greatest CH character and combining them in such a way that the p function on the carbon was directed toward the hydrogen. The success of this simple partitioning is shown in Table III

TABLE III.   H atom Mulliken populations for the $\sigma_{CH}$ orbitals.

| State | $\sigma_{CH}$ | Total H$\sigma$ | $\sigma^*_{CH}$ | Total H$\sigma^*$ |
|-------|------|------|------|------|
| $^1A_g$ | 0.684 | 0.732 | 1.152 | 1.268 |
| $^2A_g$ | 0.594 | 0.645 | 1.169 | 1.355 |
| $^2B_{1u}$ | 0.608 | 0.653 | 1.164 | 1.347 |

where the H atom Mulliken populations in the $\sigma_{CH}$ and $\sigma^*_{CH}$ orbitals are compared with the total H populations. We see that the $\sigma_{CH}$ orbitals constructed in this manner account for about 90% of the total CH space.

The two CI's allowing relaxation in the $\sigma$ orbitals are denoted as

(5) $\sigma_{CC/CN}$ POL(1) CI and

(6) $\sigma_{CH}$ POL(1) CI.

Both CI's include all the configurations in the n-$\pi$ CI plus single excitations in the $\sigma_{CC}/\sigma_{CN}$ or $\sigma_{CH}$ space from two basic configurations. One of the two basic configurations is the HF configuration, while the other allows the lone pair excitation to localize on one nitrogen. For example, the HF configuration of the $^2A_g$ state is

$$\mathcal{A}[\,(\Phi_{core})\,n_-^{\,2}\,n_+\,\alpha\beta\ldots\alpha\beta\alpha]\quad,$$

while the second basic configuration is

$$\mathcal{A}[\,(\Phi_{core})n_+^{\,2}\,n_-\,\alpha\beta\ldots\alpha\beta\alpha]\;.$$

Taking + and − combinations of the above configurations gives

$$\mathcal{A}[(\Phi_{core})n_\ell^{\,2}\,n_r\,\alpha\beta\ldots\alpha\beta\alpha]$$

$$\mathcal{A}[\,(\Phi_{core})n_r^{\,2}\,n_\ell\,\alpha\beta\ldots\alpha\beta\alpha]\;,$$

so that we are actually allowing relaxation of the $\sigma$ orbitals in response to the localized excitation.

D) <u>Further Relaxation of the $\pi$ Space</u>

A final set of CI calculations was performed using a slightly extended basis. The MBS was augmented by the most diffuse $p_x$ primitive

in Huzinaga's[16] (3p) set. This basis set is designated MBS + DZ($\pi$).

Two CI calculations were performed allowing relaxation of the $\pi$ orbitals with the added six "double zeta" $\pi$ virtuals,

(7) $\pi$ POL(2) CI and

(8) $\pi$ POL(3) CI.

In the $\pi$ POL(2) CI all the configurations in the n-$\pi$ CI were included plus all those arising from single and double excitations from the ground state HF configuration [within a 14 (2n, 12$\pi$) orbital space] with the restriction that only single excitations are allowed in the "double zeta" $\pi$ space. The $\pi$ POL(3) CI is the same as the $\pi$ POL(2) CI except that up to triple excitations are allowed from the ground HF configuration

### E) Rydberg States

Simple calculations were also made to locate the position of the lowest singlet Rydberg states arising from excitations out of the two most loosely bound orbitals $6a_g(n_+)$ and $1b_{1g}(\pi)$. In order to describe the diffuse Rydberg states two augmented basis sets were employed.

(9) MBS + R($\sigma$): MBS augmented with two diffuse s, $p_y$, and $p_z$ functions centered at the CC bond midpoints and at the nitrogens. The carbon exponents were 0.060 and 0.020, while the nitrogen exponents were 0.075 and 0.025.

(10) MBS + R($\pi$): MBS augmented with two diffuse $p_x$ functions centered at each of the four carbons and two nitrogens. The exponents were the same as for MBS + R($\sigma$).

The Rydberg states were calculated using the improved virtual orbital (IVO) method.[19] In this method the SCF occupied orbitals from the ground state (or excited state) are used and the correct excited state

hamiltonian for the virtual orbitals (without self-terms) is solved, yield-
ing a whole spectrum of excited states from one calculation. IVO calcu-
lations on $H_2O$[19,20] and $O_2$[21] have led to good agreement with experiment.
In general, the calculations on pyrazine used ground state orbitals,
although a few runs were made with the appropriate cation orbitals.

## VI. Results: Ramifications for the VB Model

### A) n Cations

The various SCF and CI results for the n cations are listed in Table IV. First we see that in every case the $^2A_g$ state is lower than the $^2B_{1u}$ state as predicted by both the VB and MO models. However, even the simple SCF results point to important differences in the two models. When the lone pair ionization is allowed to localize on one nitrogen as in the VB model, the energy drops significantly (0.8 eV relative to the $^2A_g$ state). Therefore, we may conclude that the description of the n cations in terms of resonant and antiresonant combinations of localized excitations (VB) is more correct than the description in terms of interactions of symmetry orbitals (MO).

Correlating the $\pi$ system ($\pi$ CI) lowers the absolute energies of the $^2A_g$ and $^2B_{1u}$ states by 2.4 eV, but the excitation energies are unchanged. That is, the $\pi$ correlation energy of the ground state and n cations are comparable. In the $\pi$ CI, the ionization is still forced to arise from a delocalized symmetry orbital. On the other hand, as soon as the CI calculation includes configurations that allow a localized description of the excitation, as in the n-$\pi$ CI, the energies of the n cations drop dramatically relative to the ground state.[22] The excitation energy to the $^2A_g$ state drops 1.2 eV, while that to the $^2B_{1u}$ state drops 1.6 eV.

Analysis of the CI wavefunctions reinforces the VB model of localized excitations. For example, after the HF configuration (CI coefficient $= 0.90$) the most important configuration (CI coefficient $= 0.25$) in the n-$\pi$ CI wavefunction for the $^2A_g$ state is a double excitation with respect to the HF configuration, namely $5b_{1u}$ $(n_-) \rightarrow 6a_g$ $(n_+)$, $1b_{2g}(\pi) \rightarrow 2b_{3u}(\pi^*)$. The effect

TABLE IV. SCF and CI results for the n cations (in eV).

| | Vertical Ionization Potentials | | Splitting Energies | CI Energy Lowerings | |
|---|---|---|---|---|---|
| | $^2A_g$ | $^2B_{1u}$ | $\Delta E$ | $^2A_g$ | $^2B_{1u}$ |
| Nonlocalized wavefunctions | | | | | |
| MO Level | | | | | |
|   Koopmans' theorem | 12.03 | 14.70 | 2.67 | -0.71 | -1.15 |
|   SCF | 11.32 | 13.55 | 2.23 | 0.0 | 0.0 |
|   S-CI | 11.51 | 13.37 | 1.86 | -0.40 | -0.02 |
| CI Level | | | | | |
|   $\pi$-CI | 11.48 | 13.36 | 1.88 | 2.04 | 2.39 |
| Localized wavefunctions | | | | | |
| MO Level | | | | | |
|   SCF | 10.52 | | -- | -- | -- |
| CI Level - no $\sigma$ readjustment | | | | | |
|   n-$\pi$ CI | 10.27 | 11.70 | 1.43 | 3.32 | 4.12 |
|   $\pi$ POL(2)CI | 10.01 | 11.51 | 1.48 | 3.92 | 4.66 |
| CI Level - $\sigma$ readjustment | | | | | |
|   $\sigma_{CH}$ POL(1)CI | 10.24 | 11.72 | 1.48 | 3.42 | 4.17 |
|   $\sigma_{CC/CN}$ POL(1) CI | 9.81 | 11.45 | 1.64 | 3.88 | 4.48 |
|   POL-CI[a] | 9.52 | 11.28 | 1.76 | 4.58 | 5.07 |

[a] POL-CI: Results of the three POL CI's are combined assuming pairwise additivity.

of this configuration may be revealed by considering just the four

orbitals $5b_{1u}(n_-)$, $6a_g(n_+)$, $1b_{2g}(\pi)$, $2b_{3u}(\pi^*)$ represented by $(n_\ell - n_r)$,

$(n_\ell + n_r)$, $(\pi_\ell - \pi_r)$ and $(\pi_\ell + \pi_r)$, respectively. Then, the HF configuration

is

$$n_-^2 n_+ \pi^2 = (n_\ell - n_r)^2 (n_\ell + n_r)(\pi_\ell - \pi_r)^2$$

$$= (n_\ell^2 n_r + n_r^2 n_\ell)(\pi_\ell^2 - \pi_\ell \pi_r - \pi_r \pi_\ell + \pi_r^2) \ ,$$

and the second dominant configuration is[23]

$$n_+^2 n_- (\pi\pi^* + \pi^*\pi) = (n_\ell + n_r)^2 (n_\ell - n_r)[ (\pi_\ell - \pi_r)(\pi_\ell + \pi_r) + (\pi_\ell + \pi_r)(\pi_\ell - \pi_r)]$$

$$= (n_r^2 n_\ell - n_\ell^2 n_r)(\pi_\ell^2 - \pi_r^2) \ .$$

Adding the two configurations leads to configurations of the form

$$n_r^2 n_\ell \pi_\ell^2$$

$$n_\ell^2 n_r \pi_r^2 \ ,$$

which clearly represent the polarization of the $\pi$ system toward the

ionized nitrogen.

Since polarization of the $\pi$ system is important in the n cations, one

would expect polarization of the $\sigma$ system to be significant. We found that

relaxation of the $\sigma_{CC}$ and $\sigma_{CN}$ orbitals lowers the energy by 0.4 - 0.5 eV,

while relaxation of the $\sigma_{CH}$ orbitals lowers the energy by 0.05 - 0.1 eV.

These results are in accord with our conjecture that the CH bonds (further

removed from the excited nitrogen) polarize much less than the $\sigma_{CN}$ bonds

adjacent to the excited nitrogen.

Finally, the fact that the $\pi$ POL(2) CI leads to an absolute energy

lowering of $\sim 0.6$ eV and a decrease in the ionization potentials of $\sim 0.2$ eV

indicates that the atomic scaling of the $p_x(\pi)$ orbitals is not appropriate

for either the ground state or n cations. Similar results may hold true

for the $\sigma$ system, indicating a need to perform double zeta calculations.[5]

Since the configurations added to the n-$\pi$ CI in the three POL CI's

are mutually exclusive (exactly in a mathematical sense and roughly in a

physical sense), one can sum the respective CI lowerings to get a reasonable

estimate of the CI energies to be obtained if the POL CI's are carried out

simultaneously. The vertical ionization potentials for the $^2A_g$ and $^2B_{1u}$

states are predicted at 9.53 eV and 11.27 eV. Comparison with photo-

electron spectra will be made in Section VII.

B) n$\pi$* States

The various SCF and CI results for $^3$n$\pi$* and $^1$n$\pi$* states are listed

in Table V and Table VI, respectively. Just as for the n cations, HF

calculations enforcing $D_{2h}$ symmetry lead to much larger excitation energies

than when the orbitals are allowed to localize (the S-CI results of Tables

V and VI are essentially equivalent to those of self-consistent HF calculations

using symmetry orbitals). Thus, the VB model of localized excitations is

more appropriate than the delocalized model.

As discussed previously using $D_{2h}$ symmetry orbitals not only forces

the excitation to be delocalized, but introduces significant ionic character

into the wavefunction. Neither of these effects are removed by correlating

the $\pi$ system. In fact, the excitation energies to the n$\pi$* states increase

by 1 eV since there is 1 eV more correlation in the ground state six-electron

$\pi$ system than in the seven-electron $\pi$ system of the n$\pi$* states.[24]

The CI results for the n$\pi$* states are very similar to those for the

n cation. Allowing the excitation to localize as in the n-$\pi$ CI decreases

the n$\pi$* excitation energies by 1.5 to 2.75 eV! The splitting energies are

also reduced by 0.8 eV. The most important configurations apart from

TABLE V. SCF and CI results for the $^3n\pi^*$ states (in eV).

| | Vertical Excitation Energies | | Splitting Energies | CI Energy Lowerings | |
|---|---|---|---|---|---|
| | $^3B_{3u}$ | $^3B_{2g}$ | $\Delta E$ | $^3B_{3u}$ | $^3B_{2g}$ |
| Nonlocalized wavefunctions | | | | | |
| MO Level | | | | | |
| S-CI | 3.97 | 5.71 | 1.74 | 0.0 | 0.0 |
| CI Level | | | | | |
| $\pi$-CI | 4.95 | 6.72 | 1.77 | 1.44 | 1.41 |
| Localized wavefunctions | | | | | |
| MO Level | | | | | |
| SCF | 3.41 | | -- | -- | -- |
| CI Level - no $\sigma$ readjustment | | | | | |
| n-$\pi$ CI | 3.39 | 4.53 | 1.14 | 3.06 | 3.66 |
| $\pi$ POL(2)CI | 3.07 | 4.32 | 1.25 | 3.72 | 4.22 |
| CI Level - $\sigma$ readjustment | | | | | |
| $\sigma_{CH}$ POL(1)CI | 3.37 | 4.53 | 1.16 | 3.15 | 3.73 |
| $\sigma_{CC/CN}$ POL(1)CI | 2.94 | 4.31 | 1.37 | 3.52 | 4.05 |
| POL-CI[a] | 2.60 | 4.03 | 1.43 | 4.26 | 4.68 |

[a] POL-CI: Results of the three POL CI's are combined assuming pairwise additivity.

TABLE VI.  SCF and CI results for the $^1n\pi^*$ states (in eV).

| | Vertical Excitation Energies | | Splitting Energies | CI Energy Lowerings | |
|---|---|---|---|---|---|
| | $^1B_{3u}$ | $^1B_{2g}$ | $\Delta E$ | $^1B_{3u}$ | $^1B_{2g}$ |
| Nonlocalized wavefunctions | | | | | |
| MO Level | | | | | |
| S-CI | 5.17 | 7.04 | 1.87 | 0.0 | 0.0 |
| CI Level | | | | | |
| $\pi$-CI | 6.12 | 8.00 | 1.88 | 1.45 | 1.45 |
| Localized wavefunctions | | | | | |
| MO Level | | | | | |
| SCF | 4.09 | | -- | -- | -- |
| CI Level - no $\sigma$ readjustment | | | | | |
| n-$\pi$ CI | 4.19 | 5.25 | 1.06 | 3.46 | 4.27 |
| $\pi$ POL(2)CI | 3.90 | 5.08 | 1.18 | 4.09 | 4.78 |
| CI Level - $\sigma$ readjustment | | | | | |
| $\sigma_{CH}$ POL(1) CI | 4.17 | 5.26 | 1.09 | 3.55 | 4.33 |
| $\sigma_{CC/CN}$ POL(1)CI | 3.75 | 5.05 | 1.30 | 3.89 | 4.63 |
| POL-CI[a] | 3.44 | 4.89 | 1.45 | 4.61 | 5.20 |

[a] POL-CI:  Results of the three POL CI's are combined assuming pairwise addivity.

from the HF configuration are the double excitations $n_+ \rightarrow n_-, \pi \rightarrow \pi^*$ or $n_- \rightarrow n_+, \pi \rightarrow \pi^*$

that allow the excitation to localize. For example, in the $^1B_{3u}$ state the HF

configuration has a coefficient of 0.87, while the next most important

configuration arises from the double excitation $5b_{1u}$ $(n_-) \rightarrow 6a_g(n_+)$,

$1b_{2g}(\pi) \rightarrow 2b_{3u}(\pi^*)$ with coefficient 0.31. In this case the HF configuration

is

$$n_-^2 n_+ \pi^2 \pi^* = (n_\ell - n_r)^2 (n_\ell + n_r)(\pi_\ell - \pi_r)^2(\pi_\ell + \pi_r)$$

$$= (n_\ell^2 n_r + n_r^2 n_\ell)(\pi_\ell^2 \pi_r - \pi_r \pi_\ell^2 + \pi_r^2 \pi_\ell - \pi_\ell \pi_r^2) ,$$

and the second configuration

$$n_+^2 n_- \pi \pi^{*2} = (n_\ell + n_r)^2(n_\ell - n_r)(\pi_\ell - \pi_r)(\pi_\ell + \pi_r)^2$$

$$= (n_r^2 n_\ell - n_\ell^2 n_r)(\pi_\ell^2 \pi_r - \pi_r \pi_\ell^2 - \pi_r^2 \pi_\ell + \pi_\ell \pi_r^2) .$$

Adding these two leads to

$$n_\ell^2 n_r(\pi_r^2 \pi_\ell - \pi_\ell \pi_r^2) + n_r^2 n_\ell (\pi_\ell^2 \pi_r - \pi_r \pi_\ell^2)$$

or

$$n_\ell^2 n_r \pi_r(\pi_r \pi_\ell + \pi_\ell \pi_r) + n_r^2 n_\ell \pi_\ell(\pi_\ell \pi_r + \pi_r \pi_\ell) ,$$

the appropriate localized excitation.

As in the case of the n cation, relaxation of the $\sigma_{CN}$ and $\sigma_{CC}$ orbitals

is much more important than relaxing the $\sigma_{CH}$ orbitals. Again, the $\pi$ POL(2)

CI indicates that double zeta calculations are warranted to optimize the scale

of the orbitals. The POL CI's tend to increase the splitting energies of the

$n\pi^*$ states as well as the n cations. However, the splitting energies are

still smaller than those predicted by the MO model (S-CI or $\pi$ CI).

Finally, we consider the differences in the $^1n\pi^*$ and $^3n\pi^*$ states.

Plots of the $\pi^*$ orbitals from the open shell HF calculations on the $^1n\pi^*$ and

$^3n\pi^*$ states are shown in Figure 3. As expected from considerations of the

the singly occupied $\pi^*$ orbital
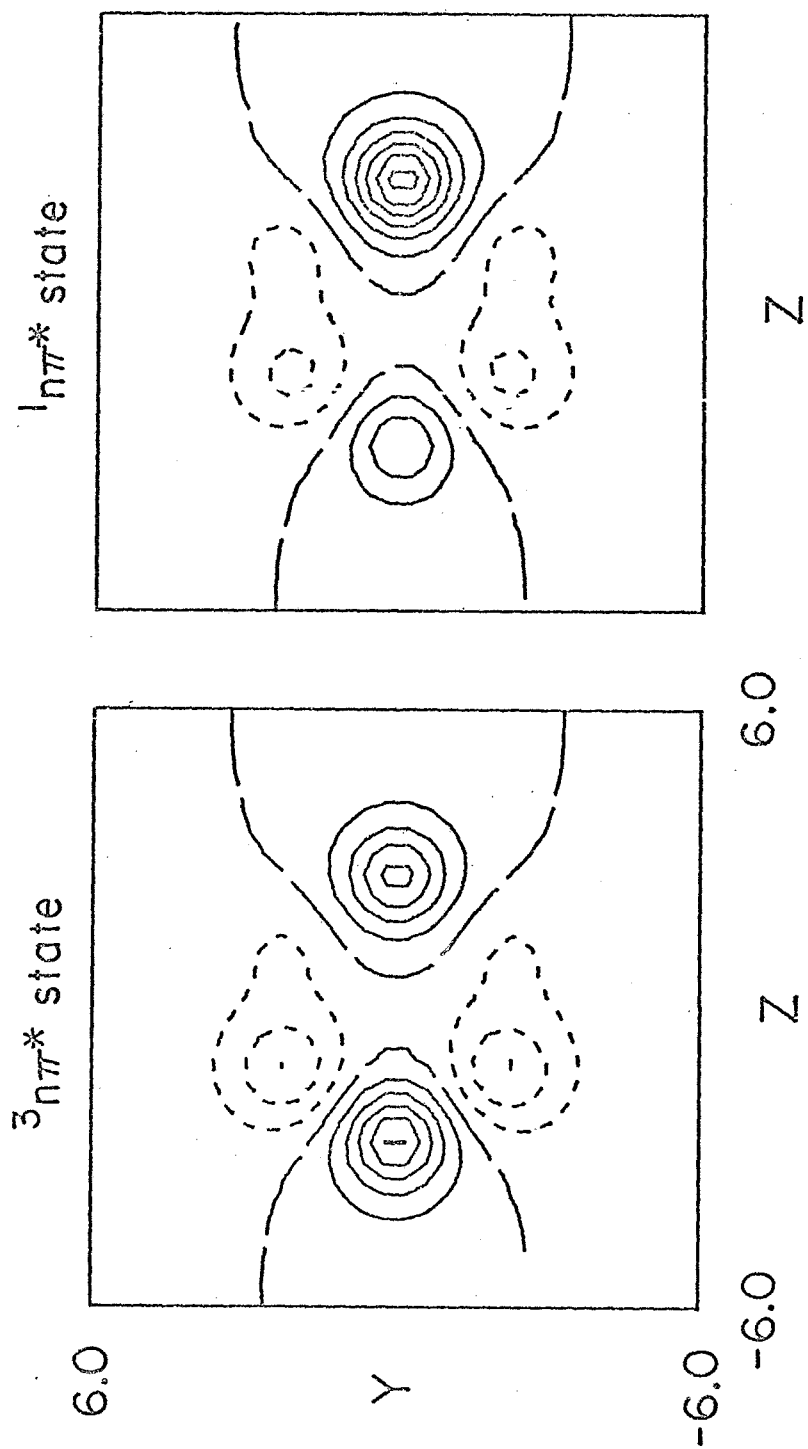


Fig. 3. Contour plots of the singly-occupied $\pi^*$ orbital from the $^3n\pi^*$ and $^1n\pi^*$ SCF wavefunctions. The contour increment is 0.05 a.u.

---

110

exchange integrals (cf. Section II.B) the $\pi^*$ orbital in the $^1n\pi^*$ state localizes more on the para nitrogen, while the $\pi^*$ orbital in the $^3n\pi$ state has more density on the excited nitrogen and the ortho carbons. The conclusions drawn from the plots are confirmed by the Mulliken populations shown in Table VII.

Since the $\pi^*$ orbital is more localized for the $^1n\pi^*$ state, the splitting energy (between the $B_{3u}$ and $B_{2g}$ states) is expected to be smaller than that for the $^3n\pi^*$ states. The CI calculations bear out this expectation, although the difference in splitting energies is only 0.07 eV. Note that the MO model calculations (S-CI) predict the $^1n\pi^*$ splitting energy to be larger ($\sim 0.12$ eV) than for $^3n\pi^*$, in direct contradiction to the VB model.

C) VB Model: Final Comments

The calculations have shown conclusively that the VB model provides a more accurate description of the interaction of the n cation and $n\pi^*$ excited states. The excitations from the lone pairs are localized, although the nature of the pyrazine $\pi$ system leads to a delocalized $\pi^*$ orbital. The relatively large splitting of the n cations is explained by the slight delocalization of the non-bonding orbitals that allows them to become orthogonal to the $\sigma$ bonding orbitals (Pauli principle). We use the word slight, since Mulliken populations show that the non-bonding orbitals are still 90% localized on one nitrogen. The large splitting of the n cations is only slightly diminished in the $n\pi^*$ states because of the delocalized nature of the $\pi^*$ orbital.

In Section II.A we stated that the Pauli-principle-induced delocalization of the non-bonding orbitals leads to a negative overlap of $n_\ell$ and $n_r$.

TABLE VII.   Mulliken populations for the $\pi^*$ orbitals.

| State | excited N | ortho C | meta C | para N |
|---|---|---|---|---|
| $^3n\pi^*$ | 0.333 | 0.170 | 0.024 | 0.279 |
| $^1n\pi^*$ | 0.100 | 0.110 | 0.026 | 0.628 |

Consequently, the $^2A_g$ and $^{1,3}B_{3u}$ states are stabilized relative to the $^2B_{1u}$ and $^{1,3}B_{2g}$, respectively. However, perusal of the plots in Figure 1 for the non-bonding orbitals from the $^2n$, $^1n\pi^*$ and $^3n\pi^*$ states reveals that the overlap of $n_\ell$ and $n_r$ is positive! At first, this appears to contradict both the VB model and the CI results. The real problem is that in the simple VB model we assumed that the $\sigma$ and $\pi$ electrons did not polarize in response to the lone pair excitation. This assumption allowed us to reduce the interaction of the two configurations $\Psi_L$ and $\Psi_R$ to a three- (or four-) electron problem and to show that the splitting energy was proportional to the overlap of $n_\ell$ and $n_r$. The $\sigma$ and $\pi$ electrons do polarize in the $^2n$, $^1n\pi^*$ and $^3n\pi^*$ cases, so that one must consider the entire many-electron wavefunction for $\Psi_L$ and $\Psi_R$. Moreover, the overlap of $\Psi_L$ and $\Psi_R$ does not reduce to the overlap $n_\ell$ and $n_r$. Thus, $<n_\ell | n_r>$ may be positive, while $<\Psi_L | \Psi_R>$ is negative. The calculations prove that $<\Psi_L | \Psi_R>$ is, in fact, negative.

We still have not shown that orthogonalization of the non-bonding orbitals to a symmetric $\sigma$ core will lead to the negative overlap assumed in the VB model. To check, we took the $n_+$ and $n_-$ orbitals used in the CI calculations and completely localized them by taking + and - combinations and zeroing all the coefficients for basis functions not on the left of right nitrogen, respectively. These localized "atomic like" lone pairs were orthogonalized to the symmetric $\sigma$ core. The resulting orbitals are plotted in Figure 4. Although it is difficult to tell from the plots, the actual overlap of $n_\ell$ and $n_r$ is -0.106 in agreement with the expectations of the VB model. The Mulliken populations for these orbitals are shown in Table VIII.

We may conclude that the assumption of a symmetric core in the VB model, although not rigorously correct, does not lead to incorrect conclusions. This is very gratifying since the assumption allows one to draw simple pictures and perform back-of-the-envelope calculations.

113

the non-bonding orbitals orthogonalized to symmetric σ core
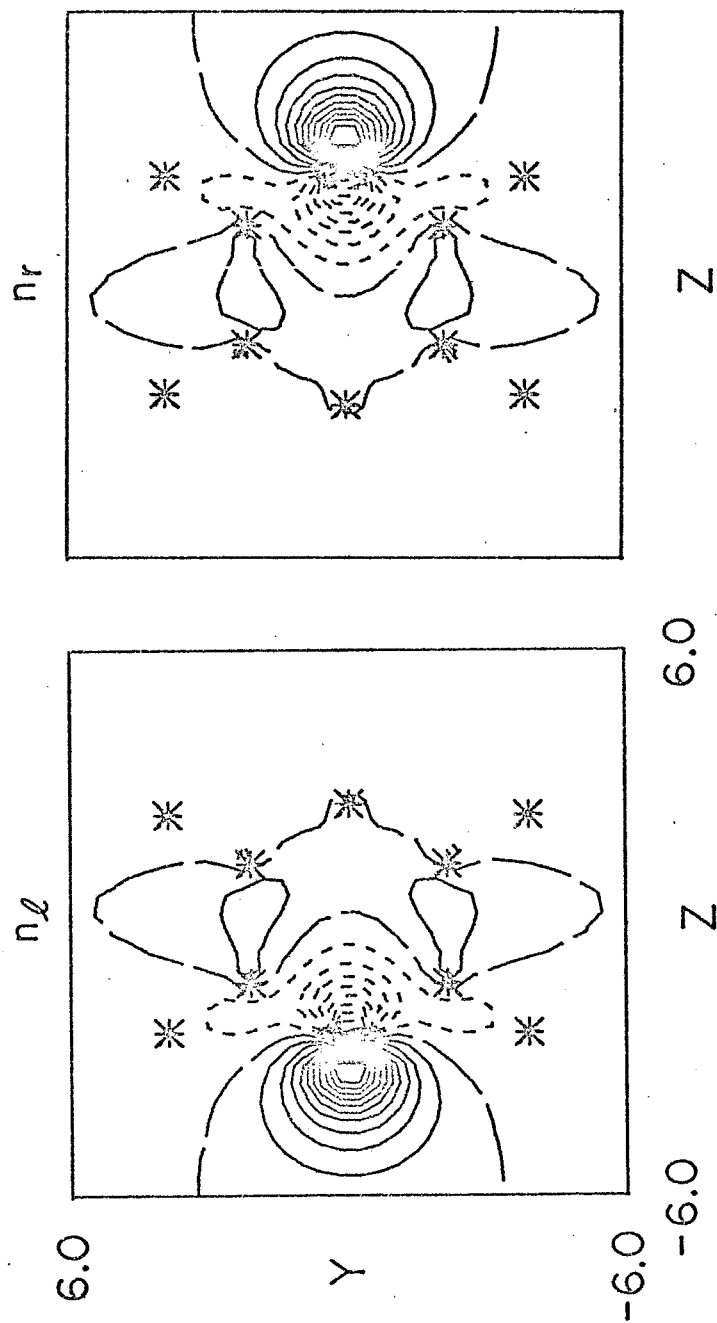


Fig. 4. Contour plots of the $n_\ell$ and $n_r$ orbitals orthogonalized to a symmetric σ core. The contour increment is 0.05 a. u.

TABLE VIII. Mulliken populations of the $n_\ell$ and $n_r$ orthogonalized to a symmetric $\sigma$ core.

| | | $n_\ell$ or $n_r$ |
|---|---|---|
| excited N | s | 0.117 |
| | z | 0.832 |
| | Total | 0.949 |
| ortho C | | 0.011 |
| ortho H | | 0.008 |
| meta C | | 0.025 |
| meta H | | 0.001 |
| para N | | 0.005 |

## VII. Results: Comparison with Experiment and Previous Calculations

### A) n Cations

As mentioned in the introduction, the MO model was very useful in interpreting the photoelectron spectrum of pyrazine. There are four bands below 12 eV in the photoelectron spectrum which are expected to correspond to the two n cations and the two lowest $\pi$ cations. The vertical ionization potentials occur at 9.63, 10.18, 11.35 and 11.77 eV.[25] Prior to the appearance of Hoffmann's[4] MO model, in which he predicted a large splitting (1-2 eV) of the n cations and that the $^2A_g$ state should be lower, these results would have been quite puzzling.

Nevertheless, the first four bands have been assigned in various ways: $\pi\pi nn$,[2] $\pi nn\pi$,[2] $n\pi n\pi$,[25,29] $\pi n$,[26] $n\pi\pi n$,[27] $n\pi\sigma\pi$[28] (in increasing energy). Of these, the most reasonable is that of Gleiter, Heilbronner and Hornung,[25] who assign the bands in increasing energy to $^2A_g(n)$, $^2B_{1g}(\pi)$, $^2B_{1u}(n)$, $^2B_{2g}(\pi)$. Their assignment is based on band shapes and is also supported by recent angular photoelectron work.[29] The first and third bands are peaked near the middle and resemble closely the two n cation bands in diazabicyclooctane (12).[30]
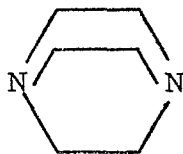


12

The second and fourth bands are peaked at low energy, i.e., the vertical and adiabatic ionization energies coincide, and resemble the $\pi$ cation bands in benzene.[2] This assignment implies that the $\pi$ cations retain the ground

state geometry, while the n cations change significantly.

Our results are the first ab initio calculations on the pyrazine cation. Previous theoretical estimates of the ionization potentials had been obtained using Koopmans' theorem in conjunction with semi-empirical[4,25,31-33] or MBS ab initio[34-36] ground state HF wavefunctions. The results in Table IV show that Koopmans' theorem leads to ionization potentials for the n cations that are 2 to 3 eV too high and exaggerates the splitting by 1 eV. Therefore, none of the previous calculations of ionization potentials are reliable.

In Table IX, we list our results for both the n cations and the two lowest $\pi$ cations, $^2B_{1g}$ and $^2B_{2g}$. Although the CI results for the n cations appear to support the $n\pi n\pi$ assignment,[25] especially when the $\sigma_{CC/CN}$POL(1) CI results are considered, cf. Table IV, the calculated ionization potentials for the $\pi$ cations are high by 1.5 to 2.0 eV. Since high quality CI wavefunctions are being employed, the only explanation for such a large error is the inflexible MBS employed. The high ionization energies indicate that the MBS exponents are too diffuse. As a result, the $\pi$ electrons are not properly shielded by the $\sigma$ core and so are too tightly bound. This problem has been corrected by using a double zeta basis and the resulting $\pi$ ionization potentials are in good agreement with experiments.[5]

### B) $n\pi^*$ Excited States

The uv absorption, excitation, fluorescence and phosphorescence spectra of pyrazine have been studied extensively.[1] Over the years the lowest energy singlet-singlet band system has often been analyzed in terms of a strong (allowed) $n \to \pi^*$ transition to the $^1B_{3u}$ state and a weak (forbidden) $n \to \pi^*$ transition usually thought to be the $^1B_{2g}$ state. The evidence for the second $^1n\pi^*$ state has ranged from direct observation,[3,37-40] to indirect manifestations in the $^1B_{3u}$ bands such as vibronic line broadening[41] or

TABLE IX. Vertical ionization potentials (in eV).

| State | K.T.[a] | SCF | GVB CI[b] | $\pi$ POL(2)CI | Expt[c] |
|---|---|---|---|---|---|
| $^2A_g$ (n) | 12.03 | 11.32 | 10.27 | 10.01 | 9.63 |
| $^2B_{1g}$ ($\pi$) | 12.14 | 11.68 | 12.48 | 12.31 | 10.18 |
| $^2B_{1u}$ (n) | 14.70 | 13.55 | 11.70 | 11.51 | 11.35 |
| $^2B_{2g}$ ($\pi$) | 13.39 | -- | 13.36 | 13.16 | 11.77 |

[a] Koopmans' Theorem.

[b] GVB CI: n $\pi$ CI for the n cations and $\pi$ CI for the $\pi$ cations.

[c] Reference 21.

electronic Coriolis interactions observed in the rotational structure.[42] The most recent spectroscopic studies show that the $^1B_{2g}$ state is higher than the $^1B_{3u}$.[43,44] Finally, none of the work on the $^3n\pi^*$ states indicates the presence the $^3B_{2g}$ state near the $^3B_{3u}$ state.[43-45]

From Tables V and VI we see that our calculations indicate that the $^{1,3}B_{2g}$ states are at least 1eV higher than the $^{1,3}B_{3u}$ states. Therefore, if there is another state near the $^1B_{3u}$, it is not the $^1B_{2g}$. The experimental excitation energies of the $^1B_{3u}$ and $^3B_{3u}$ states are 3.2-3.3 and 3.8-3.9 eV, respectively.[1,46] Our n-$\pi$ CI excitation energies are in reasonable agreement with experiment, being high by 0.1-0.3 eV, while the POL CI's lead to excitation energies that are too low by 0.1-0.3 eV. The singlet-triplet splitting is overestimated by 0.2 eV.

## C. Comparison with previous theoretical calculations

The only previous ab initio study of the excited states of pyrazine was that of Hackmeyer and Whitten (HW).[36] They employed a basis set comparable to our MBS+DZ($\pi$) and the same geometry except that the CH bond lengths were taken as 1.05 Å[47] instead of 1.09 Å[48] as in our work. After performing an HF calculation on the ground state, they carried out CI calculations using the two lone pair orbitals, three occupied $\pi$ orbitals and six $\pi^*$ orbitals (two $b_{3u}$ and $a_u$, one $b_{2g}$ and $b_{1g}$) determined by IVO-type calculations (the $b_{1g}$ is determined by symmetry). The configurations were chosen by performing single and double excitations from one to three basic configurations, subjecting the generated configurations to an energy-lowering criterion and repeating this process with the larger set of basic configurations. This procedure produces a set of configurations comparable

to our $\pi$ POL(3) CI.

In Table X, we list the number of configurations employed in the GVB CI,[49] $\pi$ POL(2) CI, and $\pi$ POL(3) CI as well as the energy lowerings for the $^1A_g$ and $^1B_{3u}$ states to contrast with the CI calculation of HW. We note that the smaller GVB CI leads to energy lowerings comparable to those of HW. Accordingly the $\pi$ POL CI energy lowerings are significantly better than HW, although they involve a comparable number of configurations. Finally, we note that including the non-bonding orbitals in the CI calcula- tions on the $^1A_g$ state decreases the energy by only 0.07 eV, while the number of configurations approximately doubles. This result supports the use of just the $\pi$ space in the CI calculations on the $\pi\pi^*$ states.

In Table XI we compare our CI results with those of HW and with experiment. Comparing the $\pi$ POL(3) CI results with HW, we see that the $n\pi^*$ excitation energies are, in general, 0.3 to 0.6 eV lower in the $\pi$ POL(3) CI. The $B_{3u}/B_{2g}$ and $A_u/B_{1g}$ $n\pi^*$ state splitting energies are 0.1 to 0.3 eV smaller in the $\pi$ POL(3) CI. The smaller splitting and excitation energies for the $n\pi^*$ states in the $\pi$ POL(3) CI derive from the use by HW of the ground state HF $n_+$ and $n_-$ orbitals, which have $\sigma$ character mixed in artificially. Except for the $\pi\pi^*$ states $>8$ eV, the calculated excitations from HW and $\pi$ POL(3) CI agree to $\pm 0.05$ eV for the $\pi\pi^*$ states, as expected.

In both HW and the present work the excitation energies to the $1\,^1B_{1u}$ and $2\,^1B_{2u}$ $\pi\pi^*$ states are overestimated by $2\frac{1}{2}$ to 3 eV. Extensive CI calculations by Hay and Shavitt[50] have shown that the analogous states in benzene have significant ionic character and, hence, are more diffuse than the normal valence excited states. Consequently, these states cannot be well described by a MBS+DZ($\pi$) basis set.

TABLE X. Size of the CI calculations.

| State | | GVB-CI | $\pi$ POL(2) CI | $\pi$ POL(3) CI | HW[a] |
|---|---|---|---|---|---|
| $^1A_g$ | Configs.[b] | 75 | 176 | 324 | 255 |
| | $\Delta E$[c] | 2.49 | 2.83 | 2.88 | 2.44 |
| $^1A_g$ ($\pi$ only)[d] | Configs. | 42 | 75 | 139 | 255 |
| | $\Delta E$ | 2.42 | 2.76 | 2.81 | 2.44 |
| $^1B_{3u}$ | Configs. | 96 | 128 | 260 | 216 |
| | $\Delta E$ | 3.73 | 4.23 | 4.44 | 3.44 |

[a] Reference 32.

[b] Spatial configurations. Each configuration yields one to six spin eigenfunctions and one to 20 determinants.

[c] $\Delta E$ is the CI energy lowering relative to the single HF configuration (in eV).

[d] Excitations are allowed only within the $\pi$ space.

TABLE XI.  CI results (in eV).

| State | HF CI | S-CI | GVB CI | $\pi$ POL(2)CI | $\pi$ POL(3)CI | Expt.[b] | HW |
|---|---|---|---|---|---|---|---|
| $1\,^1A_g$ (G.S.) | $0.0^a$ | $0.0^a$ | $0.0^a$ | $0.0^a$ | $0.0^a$ | | $0.0^a$ |
| $1\,^3B_{3u}$ ($n\pi^*$) | 4.64 | 3.96 | 3.45 | 3.25 | 3.10 | 3.2-3.3 | 3.56 |
| $1\,^3B_{3u}$ ($n\pi^*$) | 5.47 | 4.94 | 4.23 | 4.07 | 3.91 | 3.8-3.9 | 4.22 |
| $1\,^3B_{1u}$ ($\pi\pi^*$) | 5.17 | 4.02 | 4.14 | 4.08 | 4.07 | 3.4-3.5$^c$ | 4.11 |
| $1\,^3B_{2g}$ ($n\pi^*$) | 6.64 | 5.83 | 4.70 | 4.56 | 4.41 | | 4.99 |
| $1\,^3A_u$ ($n\pi^*$) | 6.62 | 5.79 | 5.34 | 5.10 | 4.88 | | 5.14 |
| $1\,^1A_u$ ($n\pi^*$) | 6.76 | 5.79 | 5.37 | 5.12 | 4.90 | | 5.22 |
| $1\,^1B_{2g}$ ($n\pi^*$) | 7.75 | 7.09 | 5.38 | 5.30 | 5.12 | | 5.65 |
| $1\,^1B_{2u}$ ($\pi\pi^*$) | 8.68 | 6.49 | 5.41 | 5.34 | 5.26 | 4.8-4.9 | 5.29 |
| $1\,^3B_{2u}$ ($\pi\pi^*$) | 6.02 | 5.47 | 5.59 | 5.46 | 5.36 | | 5.39 |
| $2\,^3B_{1u}$ ($\pi\pi^*$) | 5.46 | 4.62 | 5.58 | 5.49 | 5.41 | | 5.41 |
| $1\,^3B_{1g}$ ($n\pi^*$) | 9.55 | 8.24 | 6.68 | 6.51 | 6.27 | | 6.89 |
| $1\,^1B_{1g}$ ($n\pi^*$) | 9.73 | 8.23 | 6.83 | 6.65 | 6.41 | | 7.04 |
| $2\,^1A_g$ ($n\pi^*$)$^d$ | | | 6.97 | 7.03 | 6.54 | | 7.33 |
| $3\,^3B_{1u}$ ($n\pi^*$)$^d$ | | | 7.33 | 7.41 | 6.93 | | 7.73 |
| $1\,^3A_g$ ($\pi\pi^*$) | 10.53 | 9.98 | 7.80 | 7.80 | 7.67 | | 7.64 |
| $1\,^3B_{3g}$ ($\pi\pi^*$) | 11.19 | 10.90 | 7.88 | 7.85 | 7.73 | | 7.79 |
| $2\,^3B_{2g}$ ($n\pi^*$) | | | 8.33 | 8.27 | 7.93 | | 8.31 |
| $2\,^1B_{2g}$ ($n\pi^*$) | | | 8.47 | 8.42 | 8.09 | | 8.47 |
| $2\,^3B_{2u}$ ($\pi\pi^*$) | 7.45 | 6.92 | 9.20 | 8.72 | 8.62 | | 8.38 |
| $3\,^1A_g$ ($\pi\pi^*$) | 13.55 | 13.18 | 9.04 | 9.04 | 8.85 | | |
| $1\,^1B_{3g}$ ($\pi\pi^*$) | 13.55 | 12.70 | 9.04 | 9.01 | 8.90 | | |
| $2\,^3B_{3g}$ ($\pi\pi^*$) | | | 9.44 | 9.42 | 9.11 | | |
| $1\,^1B_{1u}$ ($\pi\pi^*$) | 9.69 | 9.48 | 9.87 | 9.41 | 9.31 | 6.5-6.6 | 9.10 |
| $2\,^1B_{3u}$ ($n\pi^*$) | | | 9.64 | 9.65 | 9.34 | | |
| $2\,^1B_{2u}$ ($\pi\pi^*$) | 10.05 | 7.94 | 10.93 | 10.52 | 10.36 | 7.6-7.7 | 9.95 |

$^a$ The ground state energies (in a.u.) from left to right are -261.95270, -261.95270,
-262.04408  (-262.04180),  -262.05674 (-262.05421),  -262.05872 (-262.05613),
-262.3579.  The CI energies in which only the $\pi$ space was used are listed
parenthetically.

$^b$ References 1 and 42.

$^c$ Reference 37.

$^d$ Dominant configurations involve a double excitation, $n \to \pi^*$, $n \to \pi^*$.

Our $\pi$ POL(3) CI calculations are in good agreement with experiment for both the 1 $^1B_{3u}$ and 1 $^3B_{3u}$ excitation energies. However, the excitation energies to the 1 $^3B_{1u}$ and 1 $^1B_{2u}$ $\pi\pi^*$ states are high by 0.6 and 0.4 eV, respectively. This may again be a manifestation of the inflexibility of the MBS that we saw more dramatically in the case of the $\pi$ cations.

Finally, we have the question of the mystery state tentatively observed in the vicinity of the $^1B_{3u}$ $n\pi^*$ state. Our calculations show only one state proximate to the $^1B_{3u}$, namely the $^3B_{1u}$ $\pi\pi^*$ state. Although the adiabatic energy of the $^3B_{1u}$ is known to be 0.5 eV lower, it is possible that $^3B_{1u}$ and $^1B_{3u}$ potential surfaces may cross or be very close to one another for the ground state geometry (at energies near 4 eV). Although the interaction of the states is spin-forbidden, a strong spin-orbit interaction is expected between the two states.[51] Therefore, in the advent of near degeneracy of the $^1B_{3u}$ and $^3B_{1u}$ potential surfaces, the $^3B_{1u}$ state is a plausible origin of the perturbations observed in the $^1B_{3u}$ bands.

## D. Rydberg States

### 1. Excitation Energies

In the previous section, we ruled out the possibility of another $^1n\pi^*$ or $^1\pi\pi^*$ state being in the vicinity of the $^1B_{3u}$ state. However, there is a possibility that the lowest Rydberg singlet state, namely the $^1A_g$ (n $\rightarrow$ 3s) state, is near the $^1B_{3u}$ state. At first, this sounds preposterous in light of the vacuum uv work of Parkin and Innes (PI)[52] and Scheps, Florida, and Rice (SFR)[53] who observed the lowest allowed Rydberg singlet (presumably n$\rightarrow$3p) at $6\frac{3}{4}$ eV. However, in water the $^1B_1(\pi\rightarrow3s)$ Rydberg state is 2.5 eV lower than the $^1B_1(\pi\rightarrow3p_z)$ state. The large separation arises from the

fact that the OH bonds in water are strongly polarized toward the oxygen so that the electron in the 3s orbital "sees" the protons; the 3s orbital tightens and lowers the energy.[16,17] Therefore, we set out to calculate the energies of the lowest Rydberg states in pyrazine using the IVO method,[16] which was successfully applied to water.[16,17] Singlet excitation energies were calculated for the lowest Rydberg states arising from excitation of an electron from either a non-bonding orbital or the most loosely bound $\pi$ orbital. The excitation energies were calculated by subtracting the stability of the Rydberg orbital from the experimental adiabatic ionization potential[16] (9.28 eV for n and 10.11 for $\pi$).[2] This procedure assumes that the potential surfaces of the Rydberg state and appropriate cation are similar, so that the difference in the adiabatic and vertical excitation energies are the same.

The results of the IVO calculations are given in Table XII. Two sets of calculations were made, one using a ground state core and the other using the appropriate cation core ($^2$n and $^2B_{1g}$). The calculated stabilities of the Rydberg orbitals are seen to be relatively insensitive to the type of core. This is a manifestation of the inflexibility of the MBS in that the cation orbitals cannot contract relative to the neutral orbitals. Using the $^2$n core instead of the $^1A_g$ core for the n Rydberg states is more correct in that the excitation is then described as being localized. Although the Rydberg orbitals are shifted toward the excited nitrogen when the $^2$n cation is used, the actual stability of each orbital is only slightly affected.

Analyzing the /vacuum uv spectrum of pyrazine, SFR[53] interpreted the bands in terms of two Rydberg series, one weak and one strong, both converging to 9.28 eV. The electronic origins for the lowest members of the series

124

TABLE XII. Adiabatic singlet Rydberg excitation energies (in eV).

| State | | ${}^1A_g$ core | ${}^2n$ core | ${}^2B_{1g}$ core | Expt. | $f_{calc}$ |
|---|---|---|---|---|---|---|
| ${}^1A_g$ $n_+(a_g)$ | → 3s | 6.60 | 6.58 | | | |
| ${}^1B_{2u}$ | → $3p_y$ | 7.23 | 7.13 | | 6.84 | $7.33 \times 10^{-3}$ |
| ${}^1B_{3u}$ | → $3p_x$ | 7.32 | 7.33 | | | $1.98 \times 10^{-5}$ |
| ${}^1B_{1u}$ | → $3p_z$ | 7.38 | 7.41 | | 6.75 | $9.22 \times 10^{-4}$ |
| ${}^1A_g$ | → $3d_{y^2}{}^b$ | 7.72 | 7.74 | | | |
| ${}^1B_{3g}$ | → $3d_{yz}$ | 7.93 | 7.92 | | | |
| ${}^1B_{2g}$ | → $3d_{xz}$ | 8.06 | 8.11 | | | |
| ${}^1B_{1g}$ | → $3d_{xy}$ | 8.08 | 8.06 | | | |
| ${}^1A_g$ | → $3d_{z^2}{}^b$ | 8.17 | 8.23 | | | |
| ${}^1B_{1g}$ $\pi(b_{1g})$ | → 3s | 7.27 | | 7.39 | | |
| ${}^1B_{3u}$ | → $3p_y$ | 7.87 | | 7.88 | | $5.52 \times 10^{-3}$ |
| ${}^1B_{2u}$ | → $3p_x$ | 8.13 | | 8.24 | | $7.57 \times 10^{-3}$ |
| ${}^1A_u$ | → $3p_z$ | 8.30 | | 8.31 | | |
| ${}^1B_{1g}$ | → $3d_{y^2}{}^b$ | 8.39 | | 8.46 | | |
| ${}^1B_{2g}$ | → $3d_{yz}$ | 8.76 | | 8.75 | | |
| ${}^1A_g$ | → $3d_{xy}$ | 8.82 | | 8.84 | | |
| ${}^1B_{3g}$ | → $3d_{xy}$ | 8.92 | | 8.95 | | |
| ${}^1B_{1g}$ | → $3d_{z^2}{}^b$ | 9.15 | | 9.18 | | |

[a] $f_{calc}$ = oscillator strength calculated using ${}^1A_g$ core IVO's.

[b] The $3d_{2z^2 - x^2 - y^2}$ and $3d_{x^2 - y^2}$ orbitals cannot be properly described since the diffuse functions are partitioned into $\sigma$ and $\pi$ sets.

were observed at 6.75 eV (weak) and 6.84 eV (strong). SFR assigned the
weak band to the $^1B_{3u}[\pi(b_{1g}) \to 3p_y]$ state and the strong band to the
$^1B_{2u}[\pi(b_{1g}) \to 3p_x]$ state. Their assignment was based on the fact that one
would expect three allowed transitions from the $n_+(a_g)$ orbital, namely
$n_+(a_g) \to 3p_x$ (weak), $n_+(a_g) \to 3p_y$ (weak) and $n_+(a_g) \to 3p_z$ (strong). Moreover,
their assignment of the strong band to the $^1B_{2u}$ state is supported by the
rotational contour analysis of PI.[52]

Therefore, the Rydberg state assignments indicate that the lowest
ionization in pyrazine involves a $\pi$ electron in agreement with the
photoionization work,[54] but in conflict with the photoelectron work.[25, 29]
Since our n cation calculations[55] are in agreement with the photoelectron
results, we have assumed in calculating the energies in Table XI that
the lowest ionization involves the n cation. Support for this assumption
may be found in the Rydberg spectra. SFR observed that the pyrazine
Rydberg series has much richer vibrational structure than the Rydberg
series in benzene. This indicates that there is a substantial change in the
geometry of pyrazine between the ground state and the Rydberg states,
while there is little change in benzene.[53] This difference is consistent
with the idea that the pyrazine Rydberg states involve an excitation out
of an n orbital, while the benzene Rydberg states involve an excitation out
of a $\pi$ orbital.

The IVO calculations predict the three $n \to 3p$ transitions to be within
0.15 eV of one another, in qualitative agreement with SFR.[53] However,
the calculated oscillator strengths are very different from our initial
expectations. The $n_+ \to 3p_z$ is not the strongest transition, but rather the
$n_+ \to 3p_y$. The relative intensities of the $n_+ \to 3p_y$, $n_+ \to 3p_z$ and $n_+ \to 3p_x$ are
calculated to be 370:47:1. There are two important ramifications of this

result. (1) The strongest observed transition, $n \to 3p_y$, is y-polarized in agreement with the rotational contour analysis of PI.[52] (2) The $n \to 3p_x$ transition is so weak that it would be very difficult to observe. Therefore, the observation of only two transitions by SFR[53] is understandable.

SFR[53] observed the electronic origin of the weak band $(n \to 3p_z)$ 0.09 eV below that of the strong band $(n \to 3p_y)$, while the IVO calculations lead to the $n \to 3p_z$ transition 0.15 eV higher than the $n \to 3p_y$. However, the calculated excitation energies are all too high by 0.5 eV, probably because of the inflexibility of the MBS description of the core. Therefore, errors in the calculated excitation energies of 0.24 eV are not unreasonable. On the other hand, it is possible that the origin of the weak $n_+ \to 3p_z$ transition was misassigned.

Finally, our calculations indicate that the relatively strong $\pi(b_{1g}) \to 3p_x$ and $\pi(b_{1g}) \to 3p_y$ transitions should be observed 0.6 to 0.8 eV above the set of $n \to 3p$ transitions, i.e., near 7.5 eV. However, the very strong $\pi \to \pi^*$ transition to the $2^1 B_{2u}$ state occurs in this region and so it would be difficult to abstract the Rydberg transitions from the spectrum.

### 2. Nature of Rydberg Orbitals

The $\sigma$ Rydberg orbitals[56] excited from the $n_+(a_g)$ and $\pi(b_{1g})$ orbitals are plotted (in the molecular plane) in Figure 5.

For the $\pi$ Rydberg orbitals[56] (Figure 6) plots are made 1 bohr and 6 bohr above the molecular plane. Comparing the Rydberg orbitals from the $n_+$ and $\pi$ orbitals, we see that they are quite similar, except that there is greater electron density near the nitrogens for $\sigma$ Rydbergs from the $n_+$ orbital. The greater density is a manifestation that the Rydberg orbital has to get orthogonal (Pauli principle) to only one nitrogen lone pair instead of two.

the 3σ Rydberg orbitals of pyrazine



Fig. 5.  Contour plots of the pyrazine 3σ Rydberg orbitals excited from the 6 a$_g$ (n$_+$) and 1 b$_{1g}$ (π) orbitals.  The contours are:  0.0,  ± 0.01,  ± 0.02154,  and ± 0.04641.

the 3π Rydberg orbitals of pyrazine
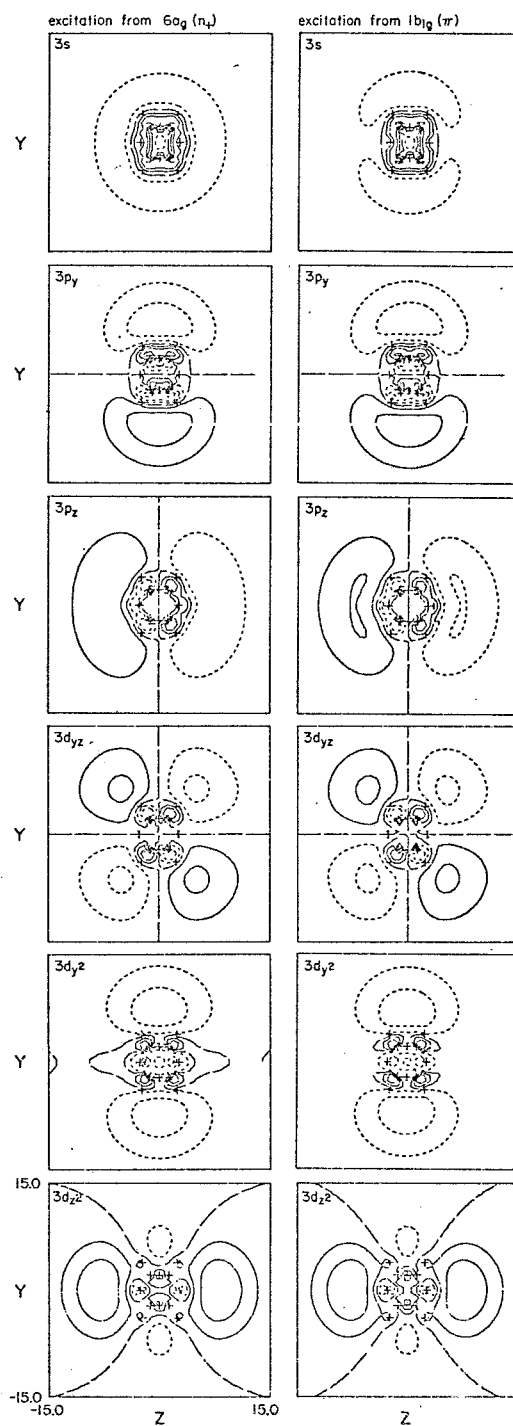


Fig. 6. Contour plots of the pyrazine $3\pi$ Rydberg orbitals
excited from the $6\,a_g$ $(n_+)$ and $1\,b_{1g}$ $(\pi)$ orbitals. The
contours are: $0.0$, $\pm 0.01$, $\pm 0.02154$, and $\pm 0.04641$.

We have been labeling these Rydberg states with a principal quantum number of 3. However, this designation is not consistent with the atomic concept that n=3 orbitals have two nodes. The Rydberg orbitals must get orthogonal to the core orbitals (Pauli principle). For the $\sigma$ Rydberg orbitals two spherical nodal planes (diagramed below) are required for orthogonality to the $\sigma$ core.
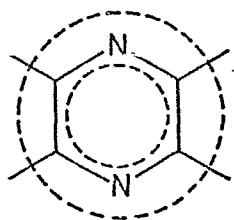


As is apparent from the plots, these nodal planes are always present whether the orbital is an s, p, or d. Thus, the s orbital has two nodal planes, the $p_\sigma$ three and the $d_\sigma$ four. Consequently, assigning principal quantum numbers according to the number of nodal planes would not indicate the basic character of these orbitals. A better scheme is to group the orbitals according to size. In Table XIII we compare the sizes of the pyrazine Rydberg orbitals with the n=3 and n=4 Rydberg orbitals of water,[17] using the expectation values $<x^2>$, $<y^2>$ and $<z^2>$ to measure size. Plots of the 3s and $3p_z$ orbitals for $H_2O$ [excited from either the $n(a_1)$ or $\pi(b_1)$ orbital] are also shown in Figure 7 for comparison. The pyrazine orbitals are clearly comparable in size to the n=3 water orbitals.

In passing, we note that the $\pi$ Rydberg orbitals in pyrazine require only one nodal plane to become orthogonal to the core.

TABLE XIII. Size of pyrazine and water Rydberg orbitals.

| Orbital From / To | Pyrazine $n_+$ $(a_g)$ | | | Pyrazine $\pi$ $(b_{1g})$ | | | Water $\pi$ $(1b_1)$ | | |
|---|---|---|---|---|---|---|---|---|---|
| | $\langle x^2\rangle$ | $\langle y^2\rangle$ | $\langle z^2\rangle$ | $\langle x^2\rangle$ | $\langle y^2\rangle$ | $\langle z^2\rangle$ | $\langle x^2\rangle$ | $\langle y^2\rangle$ | $\langle z^2\rangle$ |
| 3s | 21.713 | 20.242 | 18.013 | 21.874 | 21.146 | 12.940 | 5.079 | 7.578 | 8.548 |
| $3p_x$ | 44.325 | 18.828 | 13.929 | 44.738 | 18.947 | 14.186 | 42.959 | 14.320 | 15.372 |
| $3p_y$ | 13.055 | 56.546 | 14.081 | 12.828 | 54.067 | 12.396 | 5.230 | 16.549 | 6.996 |
| $3p_z$ | 15.830 | 23.696 | 51.020 | 16.955 | 27.335 | 47.481 | 14.850 | 15.443 | 28.148 |
| $3d_{xy}$ | 39.079 | 41.358 | 13.876 | 39.114 | 41.376 | 13.887 | | | |
| $3d_{xz}$ | 42.909 | 20.746 | 40.095 | 45.219 | 22.249 | 41.671 | 56.508 | 18.836 | 52.843 |
| $3d_{yz}$ | 14.839 | 49.539 | 40.529 | 15.009 | 51.050 | 39.720 | 19.466 | 58.504 | 24.847 |
| $3d_{y^2}$ | 17.827 | 51.327 | 10.449 | 17.929 | 46.766 | 9.940 | 29.149 | 71.700 | 20.334 |
| $3d_{z^2}$ | 15.131 | 13.764 | 51.865 | 12.199 | 13.185 | 60.712 | 39.382 | 19.725 | 68.460 |
| 4s | | | | | | | 48.006 | 36.288 | 60.571 |
| $4p_x$ | | | | | | | 254.068 | 89.689 | 86.209 |
| $4p_y$ | | | | | | | 30.259 | 90.321 | 59.605 |
| $4p_z$ | | | | | | | 81.665 | 80.579 | 184.486 |
| $4d_{xy}$ | | | | | | | | | |
| $4d_{xz}$ | | | | | | | 79.908 | 239.756 | 87.682 |
| $4d_{yz}$ | | | | | | | | | |
| $4d_{y^2}$ | | | | | | | | | |
| $4d_{z^2}$ | | | | | | | | | |

the 3σ Rydberg orbitals of water

excitation from 3a₁ (n)

excitation from 1b₁ (π)



Fig. 7. Contour plots of the water 3s and 3p_z Rydberg orbitals excited from the 3a (n), and 1 b₁ (π) orbitals. The contours are: 0.0, ± 0.01, ± 0.02154, ± 0.04641, and ± 0.1.

## E. Relationship of the $n\pi^*$ and $\pi\pi^*$ states

In Figure 8, we compare the spectra of $n\pi^*$ and $\pi\pi^*$ excited states for pyrazine. Previously we considered the lowest $n\pi^*$ states, namely $1^{1,3}B_{3u}$ and $1^{1,3}B_{2g}$. In these states, the $\pi^*$ orbital has $b_1$ symmetry (for the $C_{2v}$ group) as is evident from the plots in Figures 3 and 4. Another higher lying set of $n\pi^*$ states ($A_u$ and $B_{1g}$) is obtained in which the $\pi^*$ orbital is of $a_2$ symmetry, i.e., with a node through the nitrogens. The $b_1\pi^*$ and $a_2\pi^*$ orbitals of pyrazine correspond to the $e_u\pi^*$ orbital of benzene. In contradistinction to the case of the $b_1\pi^*$ orbital, the $a_2\pi^*$ orbital cannot localize on the excited nitrogen to maximize the favorable exchange interaction in the triplet (nor localize on the para nitrogen to minimize the bad exchange interaction in the singlet). As a result the singlet-triplet splittings in the $A_u$ and $B_{1g}$ states are ~0.1 eV compared to ~0.75 eV for the $B_{3u}$ and $B_{2g}$ states.

The third set of $n\pi^*$ states involves the second $b_1$ $\pi^*$ orbital (corresponding to $a_{2g}\pi^*$ of benzene), but the ordering of the $B_{2g}$ and $B_{3u}$ states is reversed, with the $B_{2g}$ lower. The reversal in state ordering arises from the fact that the second $b_1$ $\pi_r^*$ and $\pi_\ell^*$ orbitals have a negative overlap (induced by the Pauli principle), while the opposite was true for the lowest b, $\pi^*$ and $\pi_\ell^*$ orbitals (cf. Section II.B).

Finally, there are two $n\pi^*$ states ($^1A_g$ and $^3B_{1u}$) that involve a double excitation. The VB picture for these states is shown below



13
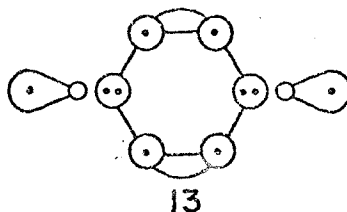
Figure 8. Energy level diagram for the $n\pi^*$ and $\pi\pi^*$ states of pyrazine.
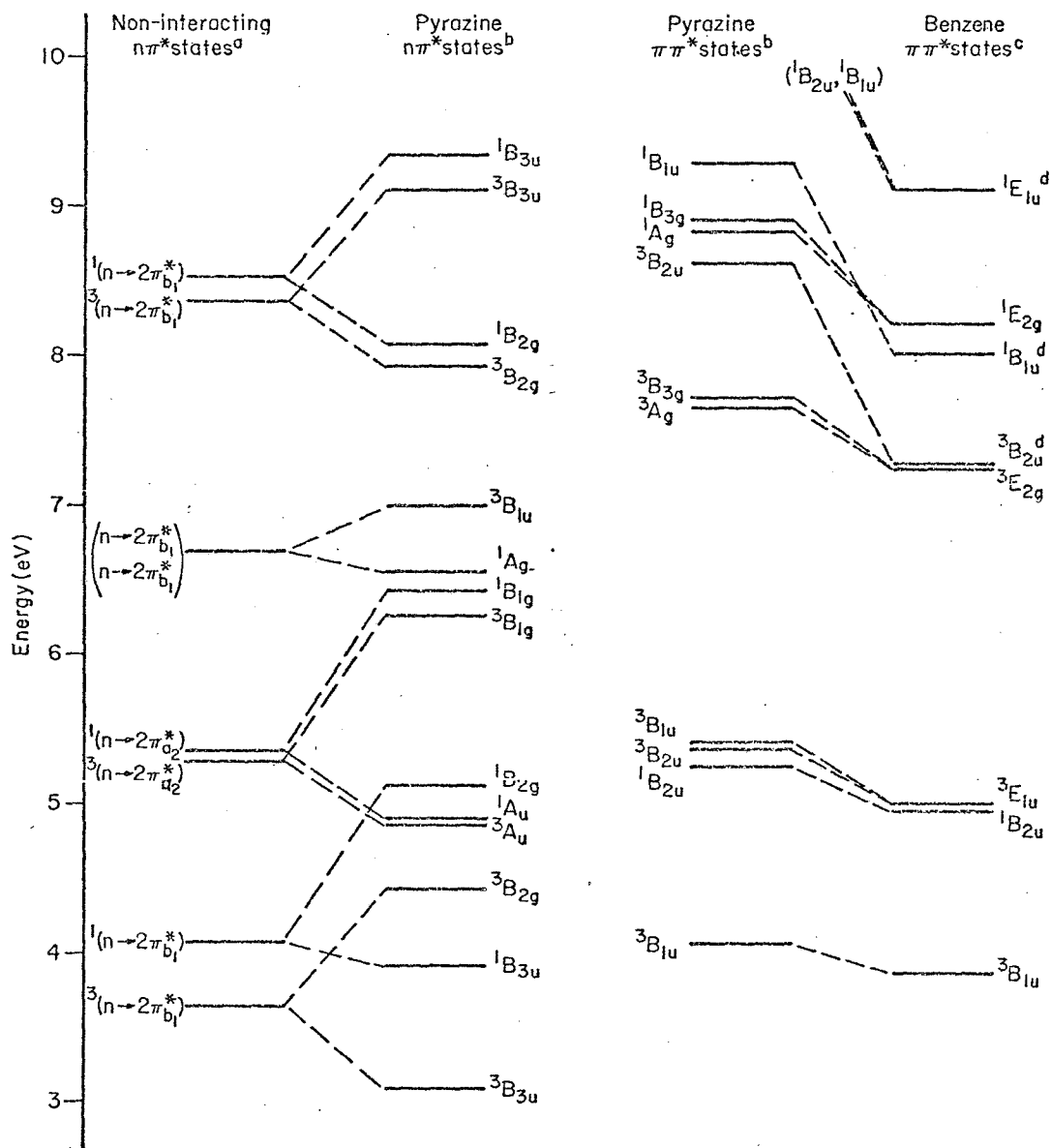


(a) SCF calculations with relaxed symmetry ($C_{2v}$). Only the lowest two levels are based on actual calculations. The other levels represent educated guesses.

(b) $\pi$ POL(3) CI energies.

(c) $\pi$ POL(3) CI energies from Reference 57.

(d) These states are ionic in character and may not be well described by a double zeta basis.[50]

The two unpaired n orbitals can be singlet or tripled coupled leading to $^1A_g$ and $^3B_{1u}$ states, respectively. Because of the Pauli-induced coupling of the $n_\ell$ and $n_r$ orbitals, the singlet state should be lower; the calculated singlet-triplet splitting is 0.30 eV. The excitation energies to the $^1A_g$ and $^3B_{1u}$ states are approximately twice that for the $1^{1,3}B_{3u}$, as would be expected from 13.

For the $\pi\pi^*$ states we have compared the excitation energies to those of benzene (using comparable CI calculations, that is, POL(3) CI with a valence double zeta basis for the $\pi$ system).[57] The calculations on benzene employed a double zeta basis for the $\sigma$ core, so that the description of the benzene $\sigma$ core is much more accurate than the MBS description of the pryazine $\sigma$ core. Consequently, all the benzene $\pi\pi^*$ states are calculated at lower energies and it is difficult to make any quantitative statements concerning the effect of the nitrogens. However, it is interesting to note that the doubly-degenerate $^3E_{1u}$, $^3E_{2g}$ and $^1E_{2g}$ states of benzene are split by only 0.1 eV or less in pyrazine.

## VIII. Summary

We have proposed a VB model for describing the n cations and

$n\pi^*$ states of pyrazine. The n cations and $n\pi^*$ states are described by

a resonant (or antiresonant) combination of two equivalent configurations

which describe either an n ionization or an n to $\pi$ promotion localized on

one of the nitrogens. The splitting energy of the resonant and antiresonant

wavefunctions is proportional to the overlap (or product of overlaps) of

the singly-occupied orbitals. i. e. , $\Delta E \propto \langle n_\ell | n_r \rangle$ for the n cations and

$\Delta E \propto \langle n_\ell | n_r \rangle \langle \pi_\ell^* | \pi_r^* \rangle$ for the $n\pi^*$ states. The orthogonalization of the

n orbitals to the $\sigma$ core mandated by the Pauli principle leads to a negative

overlap for $n_\ell$ and $n_r$, but a positive overlap for $\pi_\ell^*$ and $\pi_r^*$. Consequently,

the $^2A_g$ and $^{1,3}B_{3u}$ states are stabilized with respect to the $^2B_{1u}$ and $^{1,3}B_{2g}$

states, respectively. Finally, although the $n \rightarrow \pi$ promotion is localized

on one nitrogen, the resulting $\pi^*$ orbital is delocalized because of the nature

of the benzene-like $\pi$ system. Thus, the splitting energy of the $n\pi^*$ states

is predicted to be only slightly smaller ($\sim 2/3$ the size) than the n cation

splitting.

Ab inito MBS CI calculations show that the VB model affords a

more accurate description of the n cations and $n\pi^*$ states than the MO

model,[4] which leads to errors of $1\frac{1}{2}$ to 2 eV. The non-bonding orbitals

are actually quite localized (90% on one nitrogen), in contradistinction to

the delocalized symmetry orbitals of the MO model.

Comparison of our results on the n cations with experiment confirm

the photoelectron assignments of Gleiter, Heilbronner and Hornung,[25]

namely $^2A_g(n)$, $^2B_{1g}(\pi)$, $^2B_{1u}(n)$, $^2B_{2g}(\pi)$ in order of increasing energy.

The calculated splitting of the n cations is 1.64 eV; the experimental value

is 1.72 eV. We found that an MBS leads to a poor description of the $\pi$ cations.

Finally, the assignment of the lowest ionization potential to the n orbital implies that the previous assignments of the Rydberg series[52,53] in terms of $\pi(b_{1g}) \rightarrow$ np excitations are incorrect. Assuming that the lowest ionization is from an n orbital, our IVO[16] Rydberg calculations show that the strong transition observed at 6.84 eV corresponds to $n_+ \rightarrow 3p_y$ ($^1B_{2u}$), while the weak transition observed at 6.75 eV corresponds to $n_+ \rightarrow 3p_z$ ($^1B_{1u}$). The $n_+ \rightarrow 3p_x$ ($^1B_{3u}$) transition is calculated to be $\sim 50$ times weaker than the $n_+ \rightarrow 3p_z$ and, thus, the observation of only one weak band, which was used to assign the Rydberg transitions as $\pi(b_{2g}) \rightarrow 3p$,[53] is not surprising, although a search for the other weak band is warranted.

Analysis of the pyrazine Rydberg orbitals reveals that they should be classified as to principal quantum number according to their size rather than the number of nodal planes. We find that two spherical nodal planes are required for $\sigma$ Rydberg orbitals to be orthogonal to the core, while only one node is required for $\pi$ Rydberg orbitals.

# REFERENCES

1. K. K. Innes, J. P. Byrne, and I. G. Ross, J. Mol. Spectrosc., 22, 125 (1967), and references cited therein.

2. D. W. Turner, C. Baker, A. D. Baker, and C. R. Brundle, Molecular Photoelectron Spectroscopy (Interscience, New York, 1970).

3. M. A. El-Sayed and G. W. Robinson, Mol. Phys. 4, 273 (1961).

4. (a) R. Hoffmann, A. Imamura, and W. J. Hehre, J. Amer. Chem. Soc., 90, 1499 (1968); (b) R. Hoffmann, Accts. Chem. Res., 4, 1 (1971).

5. W. R. Wadt, W. A. Goddard III, and T. H. Dunning, Jr. (to be published).

6. The $\pi$ electrons have been suppressed for the moment, while the hydrogens will be suppressed throughout the paper.

7. The self-consistent wavefunctions for the $\Psi(^2A_g)$ or $\Psi(^2B_{1u})$ states lead to doubly-occupied $\sigma$ and $\pi$ orbitals that are polarized toward the singly-occupied non-bonding orbital. (See the section on Calculational Details.) Therefore, $\Phi_{core}$ is not the same for both $\Psi_L$ and $\Psi_R$ and $S = \langle \Psi_L | \Psi_R \rangle \neq \langle n_\ell | n_r \rangle$. Also, the singly-occupied non-bonding orbital will be contracted relative to the doubly-occupied lone pair. The upshot of all this is that equation (5) cannot be reduced to (6). The splitting energy cannot be analyzed in terms of a simple three-electron problem or shown to be proportional to overlap of $n_\ell$ and $n_r$. However, the results indicate that our simple VB model is in accord with more accurate but much more involved descriptions.

8.     $\Psi_L$ and $\Psi_R$ are not actually normalized since

$$\langle \Psi_L | \Psi_L \rangle = \langle \mathcal{A} [ (\Phi_{core}) n_r^2 n_\ell \, \alpha\beta \ldots \alpha\beta\alpha] \, | \, \mathcal{A} [ (\Phi_{core}) n_r^2 n_\ell \, \alpha\beta \ldots \alpha\beta\alpha] \rangle .$$

All the orbitals in $\hat{\Phi}_{core}$ are orthogonal to one another and to $n_r$ and $n_\ell$ , so that

$$\langle \Psi_L | \Psi_L \rangle = \langle \mathcal{A} (n_r^2 n_\ell \, \alpha\beta\alpha) | \mathcal{A} (n_r^2 n_\ell \, \alpha\beta\alpha) \rangle .$$

All the terms vanish by spin orthogonality except those involving

interchange of electrons 1 and 3 or no interchange at all, so that

$$\langle \Psi_L | \Psi_L \rangle = 1 - \langle n_\ell | n_r \rangle^2 \equiv 1 - S_{\ell r}^2 .$$

Therefore, we assume that the normalization factor of $1 / \sqrt{1 - S_{\ell r}^2}$

is included in the antisymmetrizer.

9.     Substituting (3) and (4) into $S = \langle \Psi_L | \Psi_R \rangle$ gives

$$\langle \Psi_L | \Psi_R \rangle = [1/(1 - S_{\ell r}^2)] \langle \mathcal{A} (n_r^2 n_\ell \, \alpha\beta\alpha) | \mathcal{A} (n_\ell^2 n_r \, \alpha\beta\alpha) \rangle .$$

As in Ref. 8, all the terms vanish except those involving inter-

change of electrons 1 or 3 or no interchange at all, so that

$$\langle \Psi_L | \Psi_R \rangle = [1/(1 - S_{\ell r}^2)] (S_{\ell r}^3 - S_{\ell r})$$

or

$$\langle \Psi_L | \Psi_R \rangle = - S_{\ell r} .$$

10.     Evaluating the two-electron part of (6) gives

$$\Delta E(2e^-) = 2(3 S_{\ell r} K_{\ell r} - S_{\ell r} J_{\ell r}) + 2 S_{\ell r} (J_{\ell \ell} + 2 J_{\ell r} - K_{\ell r})$$

$$= 2 S_{\ell r} (J_{\ell \ell} + J_{\ell r} + 2 K_{\ell r}) .$$

The $S_{\ell r} J_{\ell \ell}$ term is the largest but is obviously dominated by $S_{\ell r} h_{\ell \ell}$

which appears in the one-electron part of (6).

11. (a) C. W. Wilson, Jr., and W. A. Goddard III, Chem. Phys. Lett., 5, 45 (1970); (b) idem, Theor. Chim. Acta, 26, 195, 211 (1972).

12. T. Koopmans, Physica, 1, 104 (1934).

13. (a) S. L. Guberman and W. A. Goddard III, Chem. Phys. Lett., 14, 460 (1972); (b) D. L. Huestis and W. A. Goddard III, ibid., 16, 157 (1972); (c) W. A. Goddard III, T. H. Dunning, Jr., W. J. Hunt, and P. J. Hay, Accts. Chem. Res., 6, 368 (1973).

14. W. J. Hunt, W. A. Goddard III, and T. H. Dunning, Jr., Chem. Phys. Lett., 6, 147 (1970).

15. The CI calculations reported in Section V employed unprojected $n_+$ and $n_-$ orbitals. The effect of projection is relatively minor (excitation energies change by at most 0.2 eV), but, in general, projection leads to lower absolute energies in the CI calculations by 3 to 8 millihartrees.

16. S. Huzinaga, D. McWilliams, and B. Dansky, J. Chem. Phys., 54, 2283 (1971).

17. T. H. Dunning, Jr. (private communication). The 7s primitives were contracted 5s, 3s.

18. The six 1s core orbitals were always forced to be doubly-occupied and were taken from the HF calculation on the ground state.

19. W. J. Hunt and W. A. Goddard III, Chem. Phys. Lett., 3, 414 (1969).

20. W. A. Goddard III and W. J. Hunt, ibid., 24, 464 (1974).

21. D. C. Cartwright, W. J. Hunt, W. Williams, S. Trajmar, and W. A. Goddard III, Phys. Rev. A, 8, 2436 (1973).

22. The absolute energy of the $^1A_g$ state in the n-$\pi$ CI decreases by only 0.07 eV relative to the $\pi$ CI.

23. There is another independent spin eigenfunction that can be found from this configuration. However, we consider just the one that

makes the largest contribution to the CI wavefunction.

24. The decrease in $\pi$ correlation energy when a seventh electron is added may at first seem unreasonable. However, in the seven-electron $\pi$ system, one of the $p_\pi$ orbitals is doubly-occupied (cf. 5) so that there are only five singly-occupied $p_\pi$ orbitals. Since the correlation energy of the singly-occupied $p_\pi$ orbitals is much greater than that of the doubly-occupied $p_\pi$ orbital, the ground state with six singly-occupied $p_\pi$ orbitals is expected to have a larger $\pi$ correlation energy.

25. R. Gleiter, E. Heilbronner, and V. Hornung, Angew. Chem., 82, 878 (1970); Helv. Chim. Acta, 55, 255 (1972).

26. M. J. S. Dewar and S. D. Worley, J. Chem. Phys., 51, 263 (1969).

27. K. A. Muszkat and J. Schäublein, Chem. Phys. Lett., 13, 301 (1972).

28. C. Fridh, L. Åsbrink, B. O. Jonsson, and E. Lindholm, Int. J. Mass Spec. Ion Physics, 8, 101 (1972).

29. D. L. Ames, J. P. Maier, F. Watt, and D. W. Turner, Faraday Disc. Chem. Soc., 54, 277 (1972).

30. E. Heilbronner and K. A. Muszkat, J. Amer. Chem. Soc., 92, 3818 (1970).

31. (a) T. Yonezawa, H. Yamabe, and H. Kato, Bull. Chem. Soc. Japan, 42, 76 (1969); (b) T. Yonezawa, H. Kato, and H. Kato, Theor. Chim. Acta, 13, 125 (1969).

32. M. Sundboom, Acta Chem. Scand., 25, 487 (1971).

33. R. L. Ellis, G. Kuehnlenz, and H. H. Jaffe, Theor. Chim. Acta, 26, 131 (1972).

34. E. Clementi, J. Chem. Phys., 46, 4737 (1967).

35. J. D. Petke, J. L. Whitten, and J. A. Ryan, ibid., 48, 953 (1968).

36. M. Hackmeyer and J. L. Whitten, ibid., 54, 3739 (1971).

37. M. Ito, R. Shimada, T. Kuraishi, and W. Mizushima, J. Chem. Phys., 26, 1508 (1957).

38. M. A. El-Sayed and G. W. Robinson, ibid., 34, 1840 (1961); 35, 1896 (1961).

39. The vapor spectrum of 2,6-dimethylpyrazine was interpreted in terms of a second forbidden $n\pi^*$ state.[40]

40. W. R. Moomaw, M. R. DeCamp, and P. C. Podore, Chem. Phys. Lett., 14, 255 (1972).

41. R. M. Hochstrasser and C. Marzzacco, J. Chem. Phys., 49, 971 (1968).

42. K. K. Innes, A. H. Kalantar, A. Y. Khan, and T. J. Durnick, J. Mol. Spectrosc., 43, 477 (1972).

43. C. J. Marzzacco and E. F. Zalewski, J. Mol. Spectrosc., 43, 239 (1972).

44. H.-K. Hong and G. W. Robinson, ibid., 52, 1 (1974).

45. W. R. Moomaw and M. A. El-Sayed, J. Chem. Phys., 45, 3890 (1966); 48, 2502 (1968).

46. M. N. Pisanias, L. G. Christophorou, J. G. Carter, and D. L. McCorkle, J. Chem. Phys., 58, 2110 (1973).

47. P. J. Wheatley, Acta Cryst., 10, 182 (1957).

48. V. Schomaker and L. Pauling, J. Amer. Chem. Soc., 61, 1769 (1939).

49. GVB-CI designates an $n-\pi$ CI for the $n\pi^*$ states and a $\pi$ CI for the $\pi\pi^*$ states.

50. P. J. Hay and I. Shavitt, Chem. Phys. Lett., 22, 33 (1973); J. Chem. Phys., 60, 2865 (1974).

51. (a) M. A. El-Sayed, J. Chem. Phys., 38, 2834 (1963); (b) idem, Accts. Chem. Res., 1, 8 (1968).

52. J. E. Parkin and K. K. Innes, J. Mol. Spectrosc., 15, 407 (1965).

53. R. Scheps, D. Florida, and S. A. Rice, ibid., 44, 1 (1972).

54. A. J. Yencha and M. A. El-Sayed, J. Chem. Phys., 48, 3469 (1968).

55. The double zeta calculations[5] verify that the photoelectron assignments are correct.

56. By $\sigma$ Rydberg orbitals we mean the Rydberg orbitals symmetric with respect to reflection in the molecular plane, i.e., 3s, $3p_y$, $3p_z$, $3d_{yz}$, $3d_{y^2}$, and $3d_{z^2}$. Similarly the $\pi$ Rydberg orbitals are $3p_x$, $3d_{xy}$, and $3d_{xz}$.

57. W. A. Goddard III (unpublished results).

PART THREE:

Comparison of INDO and Ab Initio Methods for the

Correlated Wavefunctions of the Ground and Excited States of Ozone

## I. Introduction

In recent years significant progress has been made in developing efficient procedures for carrying out high quality ab initio calculations.[1-4] Extensive configuration interaction (CI) calculations with large basis sets have been reported for the ground and excited states of molecules such as $C_2H_4$,[5] $C_4H_6$,[6,7] $C_6H_6$,[8] $O_3$,[9] $CO_2$[10] etc., and for ground state potential surfaces of reactions such as[11,12,13]

$$LiH + H \rightarrow Li + H_2$$
$$H_2 + F \rightarrow H + HF$$
$$F_2 + H \rightarrow F + HF .$$
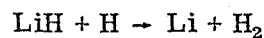
Despite this progress, we have a long way to go before such ab initio methods will be efficient enough (in both computer time and people time) for thorough mechanistic investigations of chemically interesting reactions (involving, perhaps, hundreds or thousands of geometries).

To circumvent the feasibility restrictions of ab initio procedures, a number of approximate methods for calculating wavefunctions have been developed. Most of these approximations involve some empiricism, i.e., parametric fitting of experiment. Moreover, essentially all the semiempirical methods are based upon closed-shell Hartree-Fock (HF) wavefunctions, including:

(i) Non-interative approaches such as extended Hückel theory (EHT).[14]

(ii) Self-consistent charge generalizations of EHT.[15]

    (iii)  CNDO.[16]

    (iv)  INDO[17] and MINDO.[18]

    (v)  NDDO.[19]

    (vi)  Non-iterative simple pseudopotential approaches (commonly used for solids).[20]

    (vii)  X$\alpha$-type approaches (commonly used for solids).[21]

(The CNDO, INDO, and X$\alpha$ methods have also been used with unrestricted HF wavefunctions, which allows the lowest state of each spin to be treated approximately). It is well known that simple HF wavefunctions (even when carried out exactly) generally lead to poor descriptions of the relative ordering of molecular excited states. For example, the ground states of $C_2$ and $O_3$ are known[22,23] to be singlet states, but in each case the HF wavefunction leads to a triplet ground state.[9b,24-28] Even worse are the descriptions HF wavefunctions usually give for potential surfaces involving bond formation or breakage.[29,30] This is unfortunate since it is just in the study of such excited states and reactions that reliable theoretical wavefunctions are so greatly needed. Consequently, in studying such systems we must expect to use wavefunctions which contain the electron correlation or many-body effects responsible for the improper behavior of the HF wavefunctions.

Since semiempirical methods have been developed and used only in conjunction with HF wavefunctions, there is little information on the appropriateness of approximate methods for correlated wavefunctions. To elucidate this situation we have used the INDO approximation of molecular integrals to calculate correlated wavefunctions for the excited states of ozone and have compared these results with those from

comparable ab initio calculations. INDO appeared to be the most suitable semiempirical approach to test as it was designed and parameterized to fit minimal basis set ab initio HF wavefunctions. In addition, INDO is one of the most popular and successful of the approximate methods, but more important is that INDO often distinguishes correctly between singlet and triplet states and generally yields reasonably good geometries for closed-shell molecules.[31] For example, INDO yields the proper ordering and separation between the $^1A_1$ and $^3B_1$ states of $CH_2$ and leads to good values for the bond angles.[32]

Ozone was selected, as the test case, since recent ab initio calculations[9] have shown it to be particularly poorly treated by HF wavefunctions, i.e., the many-body corrections are large. A summary of the ab initio results on ozone is presented in the next section for convenience of discussion.

## II.  Preliminaries

A.  Summary of Ab Initio Results for Ozone.  Ab initio calculations have been performed on the excited states of ozone using the Hartree-Fock (HF), generalized valence bond (GVB), and configuration interaction (CI) methods in conjunction with both minimal basis sets[9a] (MBS) and extended basis sets [9b, 9c] [specifically, double zeta (DZ) basis sets[33]].  Nine low-lying states ($<7$ eV for the ground state equilibrium geometry) were found.  Of these, the first eight states (all $<4$ eV) involve essentially covalently bonded wavefunctions that can be well described by taking three ground state oxygen atoms and pairing the atomic orbitals in various ways to form bonds.  These states, in

turn, can be grouped into three types of configurations according to the number of $\pi$ electrons, i.e., the number of electrons in orbitals anti-symmetric to the molecular plane.[34]

$$4\pi: \ ^1A_1 \text{ (ground state), } ^3B_2$$
$$5\pi: \ ^3A_2, \ ^1A_2, \ ^3B_1, \ ^1B_1$$
$$6\pi: \ 2^1A_1, \ 2^3B_2$$

The remaining low-lying state, $^1B_2(4\pi)$, has a large amount of ionic character. The calculated vertical excitation energies for these states are listed in Table I.

The ab initio calculations[9] showed that the $^1A_1(6\pi)$ state of ozone has an equilibrium bond angle of $60°$. Using the DZ basis, this ring state was found[9c] to be about 1.5 eV above the $^1A_1(4\pi)$ ground state. However, with the MBS, the ring state, $^1A_1(6\pi)$, was found to be nearly degenerate with the $^1A_1(4\pi)$ state.[9a]

Finally, ab initio HF calculations[9b] lead to a triplet ground state with the singlet state 2.2 eV higher (vertical excitation energy)! The CI calculations, on the other hand, lead to a singlet ground state with the first triplet state at 1.11 and 1.47 eV (vertical excitation energy) for MBS and DZ, respectively. Thus, the correlation errors in the HF description are quite large (3 eV for the $1a_2$ pair) and differ greatly from state to state. This makes ozone an excellent case for testing the validity of the INDO approximation for correlated wavefunctions.

B. GVB and CI Calculations. The major weakness of the re-stricted HF wavefunction is that the orbitals are forced to be doubly-occupied. This restriction is reasonable for inner core orbitals,

Table I. Vertical Excitation Energies of Ozone (Electron Volts)[a]

| | HF | | GVB(1) | | | MBS CI[b] | | | | DZ CI[c] | EXPER[j] |
|---|---|---|---|---|---|---|---|---|---|---|---|
| | INDO MBS | ab initio DZ[d] | INDO MBS | ab initio MBS[e] | DZ[d] | No. of DET | No. of SEF | INDO | ab initio[e] | ab initio | |
| $^1A_1(4\pi)$ | 0.00 | 0.00 | 0.00 | 0.00 | 0.00 | 197 | 92 | 0.00 | 0.00 | 0.00 | |
| $^3B_2(4\pi)$ | -2.24 | -2.16 | 0.51 | 0.51 | 0.68 | 155 | 114 | 0.89 | 1.11 | 1.47 | |
| $^3B_1(5\pi)$ | --- | 0.58 | 0.88[f] | 1.04[f] | 1.23[f] | 247 | 186 | 2.66 | 2.02 | 1.74 | |
| $^3A_2(5\pi)$ | 0.94 | 0.79 | | | | 247 | 186 | 2.37 | 1.79 | 1.80 | |
| $^1A_2(5\pi)$ | --- | 1.25 | 0.95[f] | 1.15[f] | 1.34[f] | 382 | 135 | 2.54 | 1.96 | 1.98 | |
| $^1B_1(5\pi)$ | --- | 1.42 | | | | 382 | 135 | 2.83 | 2.24 | 2.06 | 2.05-2.15 |
| $^3B_2(6\pi)$ | -1.09 | -0.52 | 1.66 | 2.09 | 2.33 | 138 | 106 | 2.47 | 3.20 | 3.86 | |
| $^1A_1(6\pi)$ | 4.54 | 3.72 | 1.80 | 2.26 | 2.51 | 191 | 92 | 2.67 | 3.50 | 4.18 | |
| $^1B_2(4\pi)$ | 4.37 | 3.85 | 7.12 | 8.05 | 6.70 | 366 | 122 | 7.88 | 6.70 | 5.60 | 4.86 |
| RING $^1A_1(6\pi)$ | -6.08[g] | 0.36[h] | -6.74[g] | 0.15[i] | 1.50[h] | | | | | 1.57 | |

[a] Ground state experimental geometry employed unless otherwise noted.

[b] All single and double excitations [within the GVB(3/PP) space] from dominant configurations. [Two configurations except for $^3B_2(4\pi)$ and $^3B_2(6\pi)$].

[c] DZ (double zeta basis) CI results from Hay, Dunning and Goddard (ref. 9c). A brief description is included in section II(b). N. B. Excitations were allowed from 2s-like orbitals.

[d] DZ ab initio results from Goddard, Hay and Dunning, ref. 9b.

[e] MBS (minimum basis set) results from Hay and Goddard, ref. 9a.

[f] Symmetry was not imposed in these calculations, since a lower energy is obtained for unsymmetric wavefunctions.

[g] Bond angle = 60°. Bond length = 1.255 Å [optimal bond length for INDO GVB(1)].

[h] Bond angle = 60°. Bond length = 1.458 Å [optimal bond length for DZ GVB(1)].

[i] Bond angle = 60°. Bond length = 1.433 Å [optimal bond length for MBS GVB(1)].

j Ref. 43

but usually not for the orbitals involved in bonds (vide infra). In the GVB method, the double-occupancy restriction is relaxed, replacing the doubly-occupied orbital with a pair of singly-occupied non-orthogonal singlet-coupled orbitals.

$$\text{HF: } [\phi^{HF}(1)\,\phi^{HF}(2)] \tag{1a}$$

$$\text{GVB: } [\phi_a^{GVB}(1)\,\phi_b^{GVB}(2) + \phi_b^{GVB}(1)\,\phi_a^{GVB}(2)] \tag{1b}$$

For purposes of calculation and comparison, these GVB orbitals, $\phi_a$ and $\phi_b$, are expressed in terms of natural orbitals, $\phi_1$ and $\phi_2$, so that (1b) becomes

$$\phi_a(1)\,\phi_b(2) + \phi_b(1)\,\phi_a(2) = C_1^2\,\phi_1(1)\,\phi_1(2) - C_2^2\,\phi_2(1)\,\phi_2(2) \tag{2}$$

Generally, the first natural orbital, $\phi_1$, corresponds closely to the HF orbital, $\phi^{HF}$ (or to a linear combination of HF orbitals).

The simplest form of the GVB wavefunction consists of an antisymmetrized product of singlet pairs [as in (2)] with the appropriate product of spin functions

$$\mathcal{A}[(\phi_a\phi_b + \phi_b\phi_a)(\phi_c\phi_d + \phi_d\phi_c)\cdots \alpha\beta\alpha\beta\cdots] \tag{3}$$

This is referred to as the perfect pairing GVB wavefunction[36] and is denoted by GVB(PP) to distinguish it from the more general GVB wavefunction in which the spin function in (3) is allowed to be completely general (i.e., optimized).[37, 38] Since double excitations are well known to be the most important in correlating HF wavefunctions, we see from (2) and (3) that the GVB(PP) wavefunction includes the most crucial of these (along with important higher order terms). The more general spin

coupling the GVB wavefunction allows certain correlation terms (including some double excitations) that are important in some states of ozone.

The 1s orbitals of the oxygen atom hardly change upon bond formation. As a result, the correlation errors in the 1s pair are expected to be independent of geometry and the same for all (low-lying) excited states. In such cases, the pairs in (3) are not correlated, but rather are taken as in (1a) instead of (1b). For ozone, the only three pairs that are important to correlate are those that dissociate to singly-occupied oxygen atom orbitals as the molecule is pulled apart. Such a wavefunction is denoted as GVB(3), indicating that all orbitals are doubly-occupied except for three pairs (referred to as the GVB split pairs). Of course, all orbitals are solved for self-consistently.

After solving for the GVB(3/PP) wavefunction, we carried out CI calculations using the GVB orbitals (in natural orbital form) just as in the ab initio studies. Orbitals from the GVB(3/PP) wavefunction of the ground state, $^1A_1(4\pi)$, were employed for the $4\pi$ and $5\pi$ states, while orbitals from the GVB(3/PP) wavefunction of the $^1A_1(6\pi)$ state were employed for the $6\pi$ states. In these calculations the experimental geometry was used ($R_{OO}$ =1.278Å, $\theta$ = 116.8°[43]). The CI consisted of all single and double excitations from the dominant configurations [two configurations except for the $^3B_2(4\pi)$ and $^3B_2(6\pi)$ states, each of which has only one dominant configuration], but restricting the 1s-like and 2s-like orbitals to remain doubly-occupied.

In comparing the results of ab initio and INDO MBS calculations, it is relevant to compare both results with the exact answers in order to determine how important the INDO errors are relative to the error

intrinsic to the use of minimum basis sets. Unfortunately, experimental vertical excitation energies are known for only two of the eight transitions under consideration. Consequently, we must use the results of much more extensive calculations as reference standards. Using a DZ basis, Hay, Dunning, and Goddard[9c] have carried out extensive CI calculations on each of the nine states of interest here. Their approach was to (i) solve for the GVB(3/PP) wavefunction for the ground state; (ii) include all single and double excitations from the dominant configurations with the restrictions that (iii) the 1s-like orbitals were kept doubly occupied and (iv) configurations involving two non-GVB orbitals were deleted. Such calculations are expected to yield vertical excitation energies to within 0.1 or 0.2 eV for valence excited states. (See, for example, the results of Winter et al.[10] on $CO_2$.)

Since the GVB orbitals are optimized in terms of their ability to include correlation effects, moderate size CI wavefunctions are equivalent to performing a nearly complete CI in the usual HF basis of occupied and virtual orbitals. [As an example, for the $^1A_1(4\pi)$ state the CI involved 92 spin eigenfunctions (SEF) or 197 determinants; a full CI would involve 207,025 determinants.] This GVB-CI wavefunction is similar to what would be obtained by using Bender and Schaefer's iterative natural orbital first-order CI wavefunction method.[44]

Two of the GVB split pairs correspond to $OO\sigma$ bonding pairs and are found to be similar for all nine lower states. The third pair, however, changes drastically from state to state. Consequently, a good qualitative description of the excited states is obtained with the GVB(1) wavefunction. We have also compared the results of ab initio and INDO approximations

using this simpler description.

In this case we find that the $^1A_1(4\pi)$ state involves splitting of the $1a_2(\pi)$ orbital of the HF wavefunction with the $2b_1(\pi)$ orbital. Similarly the $^1A_1(6\pi)$ state involves splitting of the $4a_1(n$ or $\sigma)$ orbital with the $3b_2(n$ or $\sigma)$ orbital. (N.B. The orbitals arising from 1s basis functions were not included in numbering the orbitals). The INDO HF open shell states were calculated using the open shell methods of Hunt, Goddard, and Dunning,[41, 42] designed to ensure full convergence.

III. Results

A. Vertical Excitation Energies. The vertical excitation energies for ozone (using the experimental geometry) are shown in Table I. We see that for both the GVB(1) and the CI calculations the ab initio MBS results are in good agreement with the ab initio DZ results for the first eight states. The INDO calculations give somewhat poorer results. Comparing the INDO and ab initio MBS-GVB(1) results, the $^1A_1(4\pi) \rightarrow {}^3B_2(4\pi)$ excitation energy is reproduced exactly, while INDO appears to under-estimate each n $\rightarrow \pi$ excitation by $\sim 0.2$ eV or 10%. However, the fairly good agreement may be fortuitous, since the use of the optimum theoretical geometries rather than the experimental geometries leads to INDO transition energies (vertical: 1.17 eV; adiabatic: 1.05 eV) much larger than the ab initio values (vertical: 0.24 eV; adiabatic: 0.22 eV).

Comparing INDO and ab initio MBS CI results, we see that the agreement is not as good as for GVB(1) calculations. For INDO the $^3B_2(4\pi) - {}^1A_1(4\pi)$ separation is low by 0.22 eV or 20%, the four $5\pi$ states

are all high by about 0.6 eV or 30%, and the $6\pi$ states are too high by

0.73 and 0.83 eV or about 20%. The $^1B_2(4\pi)$ state in INDO is also high

by 1.18 eV or about 15%, but this ionic state is not well described by

the MBS ab initio wavefunction, either.

  B. Geometries. The calculated geometries for the $^1A_1(4\pi)$ and

$^3B_2(4\pi)$ states using GVB(1) are listed in Table II. The bond angles from

INDO and ab initio MBS calculations are in good agreement with each

other and with experiment [for $^1A_1(4\pi)$]. The bond lengths, on the other

hand, differ greatly, INDO giving bond lengths that are too short by

0.17 Å. In passing, we note that it is important to use equivalent bases

and wavefunctions for these comparisons, since systematic errors in

bond lengths are expected.[45,46] The short OO bonds obtained with INDO

for ozone are to be expected since for open shell HF calculations on

ground state $O_2(^3\Sigma_g^-)$, INDO gives R = 1.140Å,[31] while ab initio MBS

calculations give R = 1.217Å[46] (experimental R = 1.207Å[31]).

Moreover, INDO calculations using a closed shell HF wavefunction

yielded a ground state bond length for ozone too short by 0.11Å[46] and

for $H_2O_2$ an OO bond length too short by 0.255Å.[31,49]

  Despite the good agreement on bond angles described above for

INDO and ab initio MBS calculations, decreasing the bond angle below

90° leads to disastrous results with INDO. The four $5\pi$ and two $6\pi$ states

all drop significantly in energy as the bond angle decreases, whereas

all but one of these states should increase in energy. Moreover, the

energy of the $^1A_1(6\pi)$ ring state (60°) is 6.74 eV below the energy of the

open $^1A_1(4\pi)$ state (the real ground state)! In the ab initio MBS descrip-

tion[9a] this ring state is nearly degenerate with the $^1A_1(4\pi)$ state. Hence,

INDO gives a ring energy too low by about 6.7 eV.

Table II. Optimum Geometries for Ozone

|  |  | $^1A_1(4\pi)$ | | | $^3B_2(4\pi)$ | | |
|---|---|---|---|---|---|---|---|
|  |  | INDØ | Ab Initio | | INDØ | Ab Initio | |
|  |  | MBS | MBS | DZ | MBS | MBS | DZ |
| GVB(1) | R(Å) | 1.19 | 1.35 | 1.38 | 1.21 | 1.38 | 1.45 |
|  | $\theta$ | 118° | 113° | --- | 111° | 110° | --- |
| Experiment | R(Å) |  | 1.278 |  |  | --- |  |
|  | $\theta$ |  | 116.8° |  |  | --- |  |

For the four $5\pi$ and the $^3B_2(6\pi)$ states ab initio MBS calculations lead to strictly repulsive potential curves as the bond angle is decreased below 90°. INDO calculations on these states, however, lead to potential curves with a double minimum, the correct one at large angles (100 - 130°) and a spurious one at small angles (60°). However, the error in the INDO description of the $5\pi$ states is less than that for the $6\pi$ states. INDO GVB(1) calculations lead to a vertical excitation energy (at 60°) from the $^1A_1(6\pi)$ to the $5\pi$ states of about 6.5 eV which is only ~2.5 eV greater than the comparable ab initio MBS value (~4 eV[47]). Thus, the INDO energies of the $5\pi$ states are about 3 to 4 eV too low for small angles.[50] As a result, while the ab initio calculations lead to $5\pi$ states at 60° with energies about 3 eV above the comparable states at 117°, the INDO calculations lead to $5\pi$ states at 60° with energies about 0 to 1 eV below the comparable states at 117°.

## IV. Discussion

The most grevious fault of INDO apparent in our calculations on ozone is the strong bias towards closed geometries,[51] even when unfavorable electron interactions should make small bond angles strictly repulsive, e.g., for the $^1A_1(5\pi)$, $^3A_2(5\pi)$, $^1B_1(5\pi)$, $^3B_1(5\pi)$, and $^3B_2(6\pi)$ states. Similar problems with INDO have been found previously.[48] It appears as if INDO does not properly represent the repulsion involved when triplet-coupled electrons are forced into close proximity. In addition it appears that INDO gives rise to $\pi$ bonds that are far too strong. The latter explanation would be consistent with the short bond lengths observed for $^1A_1(4\pi)$ and the large transition energies observed for the $4\pi \rightarrow 5\pi$ and $4\pi \rightarrow 6\pi$ transitions (at the calculated equilibrium geometry). Consequently, the use of INDO for calculating equilibrium geometries as in conformational

studies or reaction pathways is very risky, even if correlation effects are included.

Our calculations show that INDO treats the electron correlations involved in the GVB(1) wavefunction fairly well, so that using such correlated wavefunctions will cure some of the gross errors encountered when INDO is used with the HF method. However, introduction of CI need not improve the energy spectrum obtained with INDO and, in fact, may make it worse. (See, for example, the reordering of the $5\pi$ and $6\pi$ states after CI). Nevertheless, despite certain significant errors in describing the overall energy spectrum, INDO does reproduce many of the energy separations properly, e.g., the singlet-triplet splittings of states arising from the same configurations. This indicates to us that it may be possible to develop a method on the order of INDO in complexity that would yield reliable results (comparable at least to ab initio MBS calculations). Work is in progress along these lines.

# REFERENCES

(1)    H. F. Schaefer III, "The Electronic Structure of Atoms and Molecules: A Survey of Rigorous Quantum Mechanical Results," (Addison-Wesley, Reading, Massachusetts, 1972).

(2)    W. J. Hunt, P. J. Hay, and W. A. Goddard II, J. Chem. Phys., 57, 738 (1972).

(3)    P. J. Hay, J. Chem. Phys., 59, 2468 (1973).

(4)    R. C. Raffenetti, J. Chem. Phys., 59, 5936 (1973).

(5)    C. F. Bender, T. H. Dunning, Jr., H. F. Schaefer III, W. A. Goddard III, and W. J. Hunt, Chem. Phys. Lett., 15, 171 (1972).

(6)    T. H. Dunning, Jr., R. P. Hosteny, and I. Shavitt, J. Amer. Chem. Soc., 95 5067 (1973).

(7)    G. Levin and W. A. Goddard III (to be published).

(8)    P. J. Hay and I. Shavitt, Chem. Phys. Lett., submitted for publication.

(9)    (a) P. J. Hay and W. A. Goddard III, Chem. Phys. Lett., 14, 46 (1972); (b) W. A. Goddard III, P. J. Hay, and T. H. Dunning, Jr., J. Amer. Chem. Soc., submitted for publication. (c) P. J. Hay, T. H. Dunning, Jr. and W. A. Goddard III, Chem. Phys. Lett., in press.

(10)   N. W. Winter, C. F. Bender, and W. A. Goddard III, Chem. Phys. Lett., 20 489 (1973).

(11)   R. C. Ladner and W. A. Goddard III, Theoret. Chim. Acta, in press.

(12)   (a) C. F. Bender, P. K. Pearson, S. V. O'Neill, and H. F. Schaefer III, J. Chem. Phys., 56, 4626 (1972); (b) Science, 176, 1412 (1972).

158

(13) S. V. O'Neill, P. K. Pearson, H. F. Schaefer III, _J. Chem. Phys._, 58, 1126 (1973).

(14) R. Hoffmann, _J. Chem. Phys._, 39, 1397 (1963).

(15) (a) L. G. Cusachs and J. W. Reynolds, _J. Chem. Phys._, 43, 5160 (1965); (b) R. Rein, N. Fukuda, H. Win, G. A. Clarke, and F. E. Harris, _J. Chem. Phys._, 45, 4743 (1966); (c) F. E. Harris, _J. Chem. Phys._, 48, 4027 (1968).

(16) (a) J. A. Pople and G. A. Segal, _J. Chem. Phys._, 43, 5136 (1965); (b) J. A. Pople and G. A. Segal, _J. Chem. Phys._, 44, 3289 (1966).

(17) J. A. Pople, D. L. Beveridge, and P. A. Dobosh, _J. Chem. Phys._, 47, 2026 (1967).

(18) (a) N. C. Baird and M. J. S. Dewar, _J. Chem. Phys._, 50, 1262 (1969); (b) M. J. S. Dewar and E. Haselbach, _J. Amer. Chem. Soc._, 92, 590 (1970).

(19) J. A. Pople, D. P. Santry, and G. A. Segal, _J. Chem. Phys._, 43, 5129 (1965).

(20) J. C. Phillips and L. Kleinman, _Phys. Rev._, 116, 287 (1959).

(21) J. C. Slater and J. H. Wood, _Intern. J. Quantum Chem._, 45, 3 (1971).

(22) E. A. Ballik and D. A. Ramsey, _Astrophys. J._, 137, 84 (1963).

(23) O. R. Wulf, Proc. _Nat. Acad. Sci._, 13, 744 (1927).

(24) G. Verhaegen, W. G. Richards, and C. M. Moser, _J. Chem. Phys._, 46, 160 (1967).

(25) The HF wavefunction also leads to a triplet ground state for BeO,[26] while good CI calculations lead to a singlet state.[27] Although there is no definitive experimental evidence for a ground singlet state,[28]

159

correlations between theoretical calculations and the available
experiments point strongly toward a ground singlet state.

(26)     W. M. Huo, K. J. Freed, and W. Klemperer, J. Chem. Phys.,
         46, 3556 (1967).

(27)     (a) H. F. Schaefer III, J. Chem. Phys., 55, 176 (1971); (b) S. V.
         O'Neill, P. K. Pearson, and H. F. Schaefer III, Chem. Phys. Lett.,
         10, 404 (1971).

(28)     A. Lagerquist, "Investigations of the Band-Spectrum of Beryllium
         Oxide," Thesis, University of Stockholm, 1948.

(29)     W. A. Goddard III, Phys. Rev., 157, 81 (1967).

(30)     These problems of the HF wavefunction do not depend on whether an
         ab initio or an approximate method is employed.

(31)     J. A. Pople and D. L. Beveridge, "Approximate Molecular Orbital
         Theory," (McGraw-Hill, New York, 1970).

(32)     W. R. Wadt and W. A. Goddard III (to be published).

(33)     T. H. Dunning, Jr., J. Chem. Phys., 53, 2823 (1970).

(34)     The GVB description of the $5\pi$ states involves two degenerate con-
         figurations corresponding essentially to $n \rightarrow \pi$ promotions, i.e.,
         an excitation from a $2p\sigma$ lone pair to a $\pi$ orbital, on the left or right
         terminal oxygen atoms. This wavefunction has $C_s$ rather than $C_{2v}$
         symmetry. Expressing the GVB orbitals in terms of symmetry
         orbitals leads to four dominant configurations, two of $A_2$ symmetry
         and two of $B_1$ symmetry. These are just the dominant configurations
         in the CI wavefunction. However, in the HF description, only one
         such $C_{2v}$ configuration is used. As a result the HF energy of the
         $5\pi$ states is high by about 2.75 eV.

(35) A. C. Hurley, J. E. Lennard-Jones and J. A. Pople, Proc. Roy. Soc., Ser. A., 220, 446 (1953).

(36) The methods used to calculate the GVB(PP) wavefunction (discussed in reference 4) impose orthogonality between orbitals of different pairs. This restriction, known as strong orthogonality, is not important in ozone.

(37) The spin function may be optimized simultaneously with the orbitals, as in the SOGI method[38] (where strong orthogonality is not imposed), or after the orbitals have been optimized, by performing a limited CI on the space spanned by the GVB(PP) orbitals, using just those configurations that will optimize spin. The latter method was employed in the ab initio DZ calculations on ozone.[9b]

(38) (a) R. C. Ladner and W. A. Goddard III, J. Chem. Phys., 51, 1073 (1969); (b) W. A. Goddard III and R. C. Ladner, J. Amer. Chem. Soc., 93, 6750 (1971).

(39) In the DZ basis, there is enough flexibility to split the lone pair orbitals on the outer oxygens. Splitting the $2p\sigma$ lone pair orbitals would lead to a more consistent description (with respect to electron correlation) of the vertical excitation energies to the $5\pi$ states, as they involve an $n \rightarrow \pi$ promotion. Since the lone pair orbitals in a DZ basis are very similar to simple oxygen 2p orbitals, one would expect the correlation energy of the two orbitals to be about the same. DZ GVB(2/PP) calculations on oxygen atoms give an energy lowering of 0.24 eV when the doubly-occupied 2p orbital is split.[40] Hence, the tabulated ab initio DZ vertical transition energies to $5\pi$ states are probably too small by about the same.

(40)  T. H. Dunning, Jr., (private communication).

(41)  W. J. Hunt, W. A. Goddard III, and T. H. Dunning, Jr., Chem. Phys. Lett., 6, 147 (1970).

(42)  The CNINDO program[32] from QCPE handles open shell states via the unrestricted HF(UHF) method. The program can only calculate one state for each spin. More importantly, one cannot be sure that the state obtained is the lowest in energy for that spin, since the trial guess is taken from an EHT calculation and may lead to the wrong state. For example, in ozone the CNINDO program leads to the $^3A_2(5\pi)$ state instead of the $^3B_2(4\pi)$ state. Moreover, the energy of the $^3A_2(5\pi)$ state calculated by CNINDO is not reliable for two reasons. First, the CNINDO program assumes that the HF orbitals will have $C_{2v}$ symmetry. In fact, the optimum orbitals are asymmetric; forcing them to be symmetric, as in the CNINDO program, increases the energy by 2.75.[34] Second, this program uses the unrestricted Hartree-Fock (UHF) wavefunction, which is a Slater determinant (just as in HF) but with up spin orbitals allowed to be different than down spin orbitals. Generally, the UHF wavefunction leads to similar energies as HF, but for the $^3A_2$ state of ozone we find the UHF energy to be 0.63 eV lower (for orbitals of $C_{2v}$ symmetry). The use of UHF for open shell states and HF for closed shell states can lead to inconsistent descriptions with respect to correlation energy. Using general open shell techniques,[41] we avoided these problems.

(43)  G. Herzberg, Molecular Spectra and Molecular Structure, Vol. 3 (Van Nostrand, Princeton, N.J., 1967).

(44)    (a) C. F. Bender and E. R. Davidson, J. Phys. Chem., 70, 2675
(1966); (b) C. F. Bender and E. R. Davidson, J. Chem. Phys.,
47, 360 (1967); (c) H. F. Schaefer III and C. F. Bender, J. Chem.
Phys., 55, 1720 (1971).

(45)    Ab initio MBS wavefunctions generally overestimate bond lengths,
since a MBS does not have enough flexibility to describe the con-
traction of the wavefunction that occurs upon bond formation. On
the other hand, ab initio HF wavefunctions generally underestimate
bond lengths, because the wavefunction dissociates improperly.
Consequently, the use of HF with MBS leads to a cancellation of
errors and, as a result, often gives good bond lengths. (See, for
example, the extensive studies by Pople[46] and coworkers.)

(46)    M. D. Newton, W. A. Lathan, W. J. Hehre, and J. A. Pople,
J. Chem. Phys., 52, 4064 (1970).

(47)    P. J. Hay (private communication). The $5\pi$ states ($^{1,3}A_2$, $^{1,3}B_1$) at
60° may be viewed as excited states relative to the $^1A_1(6\pi)$ state,
arising from a $\pi \rightarrow \sigma^*$ promotion.

(48)    M. Froimowitz and P. J. Gans, J. Amer. Chem. Soc., 94, 8020
(1972); see also T. Morton, Ph.D. thesis, California Institute of
Technology (1972).

(49)    M.S. Gordon and J.A. Pople, J. Chem. Phys., 49 4643 (1968).

(50)    Although ab initio results on the $4\pi$ states are not available at 60°
for comparison, the absence of a double-minimum in the INDO
potential curves indicates (along the results on the $5\pi$ states) that
the preference for small angles in the INDO description of the states
of ozone is proportional to the number of $\pi$ electrons.

(51) Subsequent to submission of this paper, A. K. Q. Siu and E. F. Hayes [Chem. Phys. Lett., 21, 573 (1973)] published semiempirical HF calculations on the open ($1\,^1A_1$) and ring ($2\,^1A_1$) states of ozone, in which they reported that the CNDO/2, INDO, and MINDO approximations all favored the ring state by 5 to 10 eV over the open state, in agreement with our results. Siu and Hayes also reported ab initio Hartree Fock calculations, leading to the ring state about 0.36 eV above the open ground state. However as shown earlier from ab initio GVB and CI calculations, HF wavefunctiong (which exclude electron correlations) are biased in favor of the ring state by 1 eV or more, so that the ab initio relative energy (0.39 eV), of the ring and open states obtained by Siu and Hayes is much smaller than the real spacing between these states. Extensive DZ CI calculations[9c] indicate that the ring state is 1.57 eV above the open ground state.

PART FOUR:

Comparison of INDO and Ab Initio Methods for Correlated

Wavefunctions of the Ground and Excited States of Methylene and Ethylen

# I. INTRODUCTION

In recent years, great progress has been made in developing sufficiently rapid ab initio techniques, so that high quality calculations can be performed on moderate size molecules, e.g., $O_3^1$, $CO_2^2$, $C_4H_6^3$, $C_6H_6^4$, and simple reactive surfaces.[5] Nevertheless, ab initio techniques are still too slow to treat the reactive surfaces and electronic states of larger molecules at the numerous geometries required to delineate reaction or energy transfer mechanisms. As a result, it would appear necessary to use semi-empirical techniques for studying the chemical dynamics of large molecules.

Numerous ab initio investigations[6] have shown the simple wavefunctions obtained from Hartree-Fock calculations to lead to improper descriptions of electronic excitation energies and of processes involving bond dissociation (or formation). In studying reactions, the basic form of the wavefunction should be inherently capable of correctly describing the reactive potential surface and, hence, a properly correlated wavefunction should be used.

Since approximate integral methods have generally been based on and used with Hartree-Fock (HF) wavefunctions, it is quite possible that the semi-empirical parameterizations are inappropriate for correlated wavefunctions. We have tested this by comparing the results of ab initio and approximate integral methods for correlated wavefunctions. Specifically, the INDO approximate integral method[7] was used, since it is parameterized to fit ab initio Hartree-Fock calculations (rather than experiment), and hence, is more likely to involve parameters that would also be appropriate for correlated wavefunctions.

Recently, we compared the results of extensive configuration inter-
action calculations on the excited states of ozone using INDO and ab initio
integrals.[8] There were significant errors (20-30%) in the vertical excitation
energies, but more important was the result that INDO is strongly biased
toward short bond lengths and small bond angles. In fact, the triangular
state of ozone was calculated to be 6-7 eV below the true open ground state!

Ab initio studies of ozone have shown the crucial importance of
correlated wavefunctions for obtaining even qualitatively correct results.
For example, HF wavefunctions lead to a triplet ground state, while experiment
and configuration interaction calculations both indicate that ozone has a
singlet ground state.[1b] Consequently, ozone is a very stiff test on the
efficacy of approximate methods. Herein we test the use of INDO for
describing the potential surfaces of the first three states of methylene as a
function of bond angle and the first three states of ethylene as a function of
dihedral twist angle. These systems provide the simplest prototypes for
$n \to \pi^*$ and $\pi \to \pi^*$ transitions.

Ab initio calculations on methylene[9] and ethylene[10] have shown that
the generalized valence bond (GVB) method[11] leads to a good description of
the potential surfaces. Consequently, we will use the GVB type of
correlated wavefunction for these comparisons.

## II.  METHYLENE

Pople and Beveridge[12] reported INDO HF potential curves for the ground and lowest excited states of methylene, [$^3B_1$ and $^1A_1$, respectively], using a fixed CH bond distance.  Their results are compared with ab initio HF and GVB-CI calculations [9] in Table I.  Somewhat surprisingly, the INDO HF numbers are in better agreement with the ab initio GVB-CI calculations than with the ab initio HF calculations, which the INDO integral approximation was parameterized to reproduce.  Therefore, one might suspect that using INDO with an appropriately correlated wavefunction would lead to worse agreement with the ab initio GVB-CI results.  We will see below that this is indeed the case.

In the HF description of methylene the $^3B_1$ and $^1A_1$ states are described as

$$^3B_1: \quad (3a_1)(1b_1)$$
$$^1A_1: \quad (3a_1)^2 \tag{1}$$

where we have ignored the

$$(1a_1)^2(2a_1)^2(1b_2)^2 \tag{2}$$

configuration common to both states.  The CI calculations show that the correlation energy of the $^1A_1$ state is much larger than that of the $^3B_1$ state, so that HF calculations lead to an adiabatic excitation energy of 1.03 eV whereas the CI calculations lead to 0.50 eV.[9]  The simplest wavefunction treating the $^3B_1$ and $^1A_1$ states consistently is the GVB (1) wavefunction[13] in which the paired orbital of (1) is described as

Table I.  Methylene energies (eV):  $R_{CH} = 2.1a^\circ$

| | INDO | | Ab Initio[a] | | Exp't |
|---|---|---|---|---|---|
| | HF | GVB(1) | HF | GVB-CI | |
| $^3B_1 \rightarrow {}^1A_1(0,0)$ | 0.57 | 0.32 | 1.03 | 0.50 | <1.0[b] |
| $^1A_1 \rightarrow {}^1B_1(0,0)$ | 1.05 | 1.30 | 0.75 | 1.40 | 1.34[c] |
| $^1A_1 \rightarrow {}^1B_1$(vert) | 1.81 | 2.06 | 1.32 | 1.88 | 2.06[d] |
| $^3B_1 \rightarrow {}^1B_1(135^\circ)$ | 1.62 | 1.62 | - | 1.90 | - |
| $^3B_1 \rightarrow {}^1B_1(180^\circ)$ | 1.14 | 1.14 | - | 1.80 | - |
| $^3B_1$ | 0.62 | 0.62 | - | 0.40 | - |
| $^1A_1$ | 1.73 | 1.41 | - | 1.69 | - |
| $^1B_1$ | 0.13 | 0.13 | - | 0.28 | - |
| $^3B_1$ | 129° | 129° | - | 128° | 136°[f] |
| $^1A_1$ | 107° | 106° | - | 103° | 102.4°[g] |
| $^1B_1$ | 144° | 144° | - | 134° | ~140°[h] |

Excitation Energies

Inversion Barriers

Calculated Bond Angles[e]

a Employed a double zeta basis set with d functions on carbon.[9]

b Estimated upper limit.[20]

c Lowest observed transitions.[20] Extrapolation of isotope shifts indicated a 0.88 eV adiabatic excitation energy.[21]

d Obtained assuming the vertical transition to correspond to the middle of the observed $^1B_1$ (0 $\nu$ 0) $\leftarrow$ $^1A_1$ (000) spectrum and adding 0.08 eV to correct for the zero-point energy of the $^1A_1$ state.[20]

e The bond angles were determined using cubic splines with the points $\sphericalangle$HCH = 90°, 105°, 135°, 180°, 225°, 255°, and 270°. More extensive geometry optimization of ab initio CI calculations (Ref. 24) using a DZ basis leads to the following bond angles: ($^3B_1$) 133°, ($^1A_1$) 104°, and ($^1B_1$) 144°.

f Reference 25.

g Reference 21.

h Reference 26.

$$\Psi^{GVB} = \phi_a(1)\phi_b(2) + \phi_b(1)\phi_a(2) = \sqrt{1-\lambda^2}\ \phi_{3a_1}(1)\phi_{3a_1}(2) - \lambda\phi_{1b_1}(1)\phi_{1b_1}(2) \quad (3)$$

rather than as

$$\Psi^{HF} = \phi_{3a_1}(1)\phi_{3a_1}(2) \quad (4)$$

[In the GVB method the orbitals of (2) and (3) are solved for self-consistently.] Since the nonbonding orbitals of the $^3B_1$ state are not paired, the HF and GVB(1) descriptions of this state are the same.[13] The higher-lying $^1B_1$ state is also described consistently with a GVB (1) wavefunction and so will be included in our calculations.

The potential curves as a function of HCH bond angle (using a bond length of 2.1 $a_0$) are shown in Fig. 1. The ab initio results of Fig. 1 are based on an extensive basis set (double zeta plus d polarization functions).[9] Use of the HF wavefunction with INDO leads to slightly better agreement with ab initio calculations than does the GVB-INDO wavefunction, indicating some fortunate cancellation of errors. As shown in Table I, GVB-INDO does lead to significant errors in the rotational barriers for the $^3B_1$ (too large by 50%) and $^1B_1$ (too small by 50%) states. The flatness of the $^1B_1$ INDO potential curve is also manifest in a significantly larger equilibrium bond angle (144° for INDO versus 134° for ab initio). Nevertheless, the overall shape of the GVB-INDO potential surfaces is good, differing by ~ 0.2 eV from the ab initio results.

The worst error in the INDO calculations is the description of the separation between the $^3B_1$ and $^1B_1$ states, especially for large bond angles. For linear methylene the $^3B_1$ - $^1B_1$ energy separation is just $2K_{xy}$ where $K_{xy}$ is the exchange integral between $p_x$ and $p_y$ orbitals on the carbon (taking z as the HCH axis). In the INDO approximation, $K_{xy}$ is set equal to the Slater-Condon parameter,
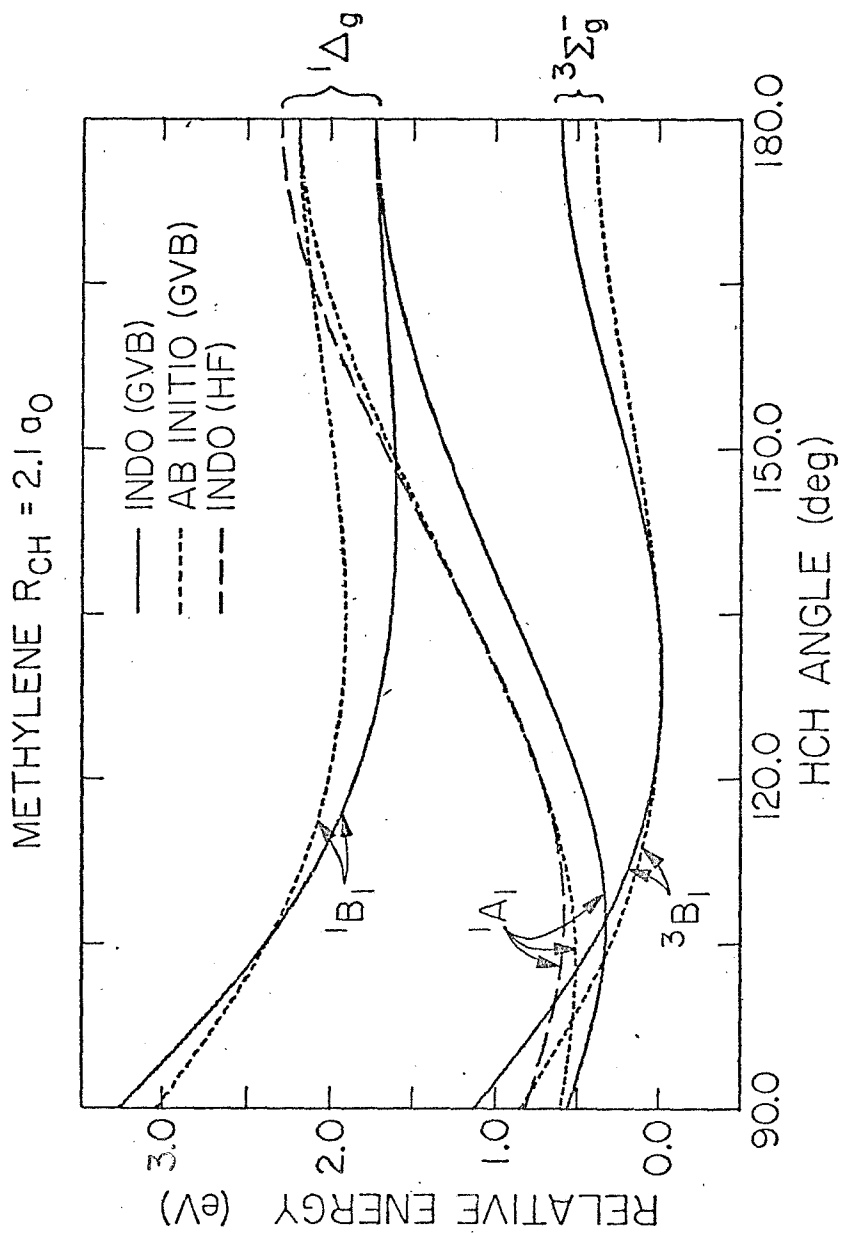
Figure 1. Comparison of ab initio and INDO potential energy curves for the low-lying states of methylene as a function of HCH angle ($R_{CH} = 2.1\ a_0 = 1.11\ Å$).

$$\left(\frac{3}{25}\right) F^2 = 0.57 \text{ eV,}$$

which was obtained by fitting the atomic spectrum. The non-empirical value of $K_{xy}$ for Slater 2p orbitals is 0.98 eV. For carbon the atomic $^3P$-$^1D$ splitting (1.26 eV) used to fit the Slater-Condon parameter, $(3/25)F^2$, is small relative to the comparable molecular singlet-triplet splitting ($\sim$1.80 eV), which is more in line with the non-empirical value for the exchange integral. Using the non-empirical value for $K_{xy}$ instead of the empirical result would improve the approximate integral potential curves, indicating that empirical evaluation of approximate integrals need not be beneficial.

For linear methylene the $^1B_1$ and $^1A_1$ states coalesce into the $^1\Delta_g$ state, so that the $^1A_1$-$^3B_1$ and $^1B_1$-$^3B_1$, splitting energies are the same. The open shell HF wavefunctions for the $^1\Delta_g$ state are

$$^1\Delta_g = \begin{cases} \frac{1}{\sqrt{2}} (xy + yx) \\ \frac{1}{\sqrt{2}} (x^2 - y^2) \end{cases}$$

ignoring the doubly-occupied core part of the wavefunction. However, Pople and Beveridge[12] employed a closed shell HF wavefunction for the $^1A_1$ state at 180°, i.e.,

$$^1A_1 = x^2 \text{ or } y^2.$$

This amounts to mixing in equal portions of the higher energy $^1\Sigma_g^+$ state

$$^1\Sigma_g^+ = \frac{1}{\sqrt{2}} (x^2 + y^2)$$

The energy of the closed shell $^1A_1$ wavefunction is higher by just $K_{xy}$ relative to the energy of the correct open shell wavefunction. As a result, Pople and Beveridge obtained a $^1A_1$ - $^3B_1$ splitting energy of 1.71 eV. for linear $CH_2$, which is in much better agreement with the ab initio CI value of 1.80 eV.

## III.  ETHYLENE

Few results of INDO calculations have been reported on the excited states of hydrocarbons with isolated or conjugated ethylenic groups.  The explanation for the paucity of calculations is that the INDO approximation treats ethylenic $\pi \rightarrow \pi^*$ transitions very poorly, as will be shown for ethylene.

The MO description for the $\pi$ system of ground state (denoted as N) ethylene is

$$N(^1A_{1g}):\ (\pi)^2$$

while for the $\pi \rightarrow \pi^*$ excited states (denoted as T and V) it is

$$T(^3B_{1u}):\ (\pi)(\pi^*)$$
$$V(^1B_{1u}):\ (\pi)(\pi^*)$$

To obtain a comparable description of these three states we allow the N state to be described by a GVB pair

$$\phi_{a\pi}(1)\phi_{b\pi}(2) + \phi_{b\pi}(1)\phi_{a\pi}(2)$$

(solving for all orbitals self-consistently) so that each state has two singly-occupied orbitals.

Calculations on the three states of ethylene were carried out as a function of the dihedral twist angle.  The results are shown in Table II and compared with ab initio calculations.  All the INDO energy separations involving the N, T, and V states are too large by 2-4 eV!

Table II. Energies for Ethylene (eV), using the GVB(1) Wavefunction[a]

| | | INDO | Ab initio | | Exper[d] |
| | | | MBS[b] | DZ[c] | |
|---|---|---|---|---|---|
| Vertical | N ($^1A_{1g}$) | 0.0 | 0.0 | 0.0 | 0.0 |
| Excitation | T ($^3B_{1u}$) | 8.48 | 4.70 | 4.24 | 4.4 |
| Energies | V ($^1B_{1u}$) | 15.25 | 13.28 | 9.99 | 7.65 |
| | N state | 5.23 | --- | 2.91 | 2.82 |
| Rotational | T state | 3.27 | --- | 1.39 | |
| Barriers | V state | 7.27 | --- | 1.84 | |
| Adiabatic | T $\leftarrow$ N | 5.23 | --- | 2.85 | |
| Excitation | | | | | |
| Energies | V $\leftarrow$ N | 7.98 | --- | 6.42 | |
| N—T Separation at $\theta = 90°$ | | 0.0 | --- | 0.06 | |

[a] The experimental ground state geometry of ethylene[22] with $R_{CH}$ = 1.086 Å, $R_{CC}$ = 1.338 Å, $\sphericalangle$ HCH = 117.4° was used for the planar states, while the CC bond was lengthened to $R_{CC}$ = 1.41 Å for the perpendicular states ($\theta = 90°$).

[b] This work using a MBS of Slater orbitals with Slater exponents.

[c] Reference 10b. Used $R_{CC}$ = 1.35 Å for the planar states.

[d] Reference 22.

Ab initio calculations have shown that the V state involves a very diffuse $\pi^*$ orbital[14], and hence, a method such as INDO based on a minimal basis would be expected to yield poor results (with a minimal basis, ab initio calculations lead to a V ← N excitation energy too high by 5.5 eV). However, even minimal basis ab initio calculations lead to a T ← N excitation energy within 1/4 eV of the experimental value, whereas the INDO value is too high by a factor of two.

Using a HF wavefunction for the planar N state would have raised the energy of the ground state by ~ 1 eV,[10] leading to an apparent improvement in the $\pi\pi^*$ excitation energies. This results from a fortuitous partial cancellation of I NDO errors with correlation effects. However, use of the closed shell HF wavefunction for describing the rotational barrier of ethylene would have increased the barrier from the bad value of 5.3 eV obtained with GVB-INDO to a far worse value of 7.27 eV for HF-INDO, 2.6 times the correct value of 2.8 eV. This indicates that one should not rely on fortuitous cancellations; one should base approximations on suitably correlated wavefunctions in order to obtain reliable approximations.

Naively, one might believe that introduction of configuration interaction (CI) will always help overcome the deficiencies of an approximate method. However, INDO calculations on ozone showed that CI actually led to worse excitation energies.[8] For ethylene, we performed a full CI in the spaced spanned by the four GVB orbitals obtained by splitting the $\pi$ and CC $\sigma$ bonding orbitals in the planar N state. The vertical excitation energies to the T and V states were hardly changed by the CI.

The origin of the error in the excitation energies may be readily found by breaking down the excitation energy into one- and two-electron contributions. INDO provides a relatively good approximation for the two-electron part, differing from the exact value by 0.35 eV. However, the one-electron part of the $\pi \rightarrow \pi^*$ excitation energy (for both N $\rightarrow$T and N$\rightarrow$V), which may be written as (having transformed to orthogonal atomic orbitals)

$$\langle \pi | t+v+(2J-K)_\sigma | \pi \rangle - \langle \pi^* | t+v+(2J-K)_\sigma | \pi^* \rangle = 2 \langle 2p_x^\ell | t+v+(2J-K)_\sigma | 2p_x^r \rangle ,$$

is off by 3.43 eV. In INDO, the one-electron part is just $2\beta_{xx} = 2\beta_c^0 S_{xx}$, or -11.38 eV compared to the exact value of -7.95 eV. Thus, the large excitation energies in INDO, arise from the use of a $\beta$ parameter that is too large for the $\pi$ orbitals. The problem is that in INDO there is only one $\beta$ per atom, instead of a separate $\beta$ for each set of orbital interactions, e.g., s-s, s-$p_\sigma$, $p_\sigma$-$p_\sigma$, and $p_\pi$-$p_\pi$. Using a single $\beta$ is fine for relatively isotropic systems, e.g., alkanes, but not for anisotropic systems, e.g., alkenes. Del Bene and Jaffe[15] encountered this problem in using CNDO/2 to describe the excited states of aromatic molecules. They reparametrized CNDO using two $\beta$'s per atom ($\beta\sigma$ and $\beta\pi$) and obtained reasonable results for excitation energies to singlet excited states of various $\pi$ electron systems.

The use of a single isotropic $\beta$ in INDO favors $\pi$ orbitals relative to $\sigma$ orbitals. For example, with INDO the highest occupied orbital of ground state ethylene is not $1b_{3u}(\pi)$ but $1b_{3g}(\sigma)$ and Koopmans' theorem ionization potentials for the $\pi$ orbitals in ground state methylene and ethylene are high by 3 and $4\frac{1}{2}$ eV, respectively. One would expect that INDO would treat n$\rightarrow\pi^*$ and $\sigma \rightarrow \pi^*$ transition energies better than $\pi \rightarrow \pi^*$, since

n and $\sigma$ orbitals are treated more correctly than $\pi$ orbitals. [16,17] Tables I and III show that this is indeed the case. The ethylene $\sigma \rightarrow \pi^*$ vertical excitations are high by 2 eV or less, which is nearly half the error present in the $\pi \rightarrow \pi^*$ energies. Recalling that the use of HF wavefunctions for both the ground and excited states effectively raises the energy of the former by 1 eV, it is clear how INDO HF calculations have in the past produced reasonable vertical excitation energies for some $n \rightarrow \pi^*$ and $\sigma \rightarrow \pi^*$ transitions. [17] Such agreements should not lead one to put too much confidence in INDO results.

TABLE III. $\sigma \to \pi^*$ Vertical Excitation Energies (eV) for Ethylene

| | INDO GVB(1) | ab initio[a] DZ-CI |
|---|---|---|
| $2\ ^1B_{1g}$ | 11.6 | 9.89 |
| $2\ ^3B_{1g}$ | 11.4 | 9.52 |
| $3\ ^1B_{2g}$ | 13.6 | 11.34 |
| $3\ ^3B_{2g}$ | 13.2 | 10.79 |

[a] Reference 23.

## IV. CONCLUSION

The calculations reported here were intended to test the validity of the INDO integral approximation for correlated wavefunctions. On the surface the results were mixed. Using INDO with simple GVB(1) wavefunctions led to HCH bending potential curves(for the three lowest states of methylene) that were in good agreement (~ 0.2 eV) with ab initio calculations. Similar INDO GVB(1) calculations on the rotation barriers for the three lowest states of ethylene produced errors of 2 to 4 eV relative to ab initio results. However, in both cases the INDO approximation frequently led to worse discrepancies when properly correlated wavefunctions were employed in lieu of closed shell HF wavefunctions. The errors inherent in the INDO method were often partially cancelled by correlation effects not properly taken into account by a closed shell HF wavefunction. Moreover, the discrepancies encountered in the INDO treatment of ethylene indicate that the failures of the integral approximation are not limited to systems for which HF fails to give a qualitatively correct description, e.g., ozone. In other words, although INDO was parameterized to reproduce MBS HF results, it is not reliable even for calculating HF wavefunctions for simple systems such as ethylene.

Comparison of the approximate calculations with ab initio results for methylene and ethylene uncovered two major trouble spots in the INDO method. The use of empirical rather than non-empirical values for the one-center exchange integrals led to a small $^3B_1$-$^1B_1$ splitting energy in methylene. This result points out the problem of empiricising approximate methods. One must be careful when fitting parameters to experiment

that (i) the system is representative of a broad class of interesting systems and (ii) the experimental result is inherently describable, i.e., an ab initio calculation with the same wavefunction and basis set, would give a good result. The first condition was not met in this case as the atomic singlet-triplet splitting was much smaller than the comparable molecular splittings. An example of violating the second condition would be to adjust parameters in the INDO approximation so as to reproduce the experimental $N \to V$ vertical excitation energy, which cannot be properly described with a MBS. This principle was violated, for example, in developing the PPP approximation[18].

The large vertical excitation energies and rotational barriers for the N, T and V states in INDO arise from using one $\beta$ parameter per atom. As a result, the $\beta$'s for $\pi$ orbitals are too large, while those for $\sigma$ orbitals are slightly too small.

We investigated ways of solving this problem and came up with the following modification of INDO. For each diatomic pair, one takes the integrals over a valence set of Slater atomic orbitals and transforms to orthogonal atomic orbitals. The transformed integrals, which correspond to

$$\beta_{\mu\nu} = \langle \mu | t+v | \nu \rangle ,$$ are determined. By doing this at various internuclear separations, one can obtain the distance dependence of $\beta_{\mu\nu}$, which turns out to be nearly exponential. Exponential fits to the non-empirical $\beta_{\mu\nu}$ integrals are used to replace the INDO values for these integrals. We have found that for ethylene and benzene the introduction of the non-empirical $\beta$'s leads to reasonable $\pi \to \pi^*$ transition energies for the $\pi\pi^*$ states that are well described by a minimal basis set[19]. To obtain good vertical excitation energies to diffuse excited states, such as the V state in ethylene, one must modify the integral approximation to allow more flexible basis sets.

For an approximate integral method to be useful in describing interesting chemical processes, it must provide good results in conjunction with correlated wavefunctions. Since the available approximations have been based on the HF wavefunction and are not always reliable, even when used with HF wavefunctions,the results with correlated wavefunctions cannot be expected to be very good. This appears to be the case. It is clear, that new approximate integral methods must be developed in the context of suitably correlated wavefunctions. If the initial wavefunction cannot correctly describe the system, how can the integral approximations be expected to be properly balanced? We are presently developing and analyzing integral approximations with correlated wavefunctions.

# REFERENCES

1a. P.J. Hay and W.A. Goddard III, Chem. Phys. Lett., 14, 46 (1972); P.J. Hay, T.H. Dunning Jr. and W.A. Goddard III, Chem. Phys. Lett. 23, 457 (1973).

1b. W.A. Goddard III, P.J. Hay and T.H. Dunning Jr., J. Amer. Chem. Soc. (to be published)

2. N.W. Winter, C.F. Bender and W.A. Goddard III, Chem. Phys. Lett. 20, 489 (1973).

3a. T.H. Dunning Jr., R.P. Hosteny and I. Shavitt, J. Amer. Chem. Soc. 95, 5067 (1973).

3b. G.B. Levin and W.A. Goddard III (to be published).

4a. W.C. Ermler and C.W. Kern, J. Chem. Phys. 58, 3458 (1973).

4b. P.J. Hay and I. Shavitt, Chem. Phys. Lett. 22, 33 (1973)

5a. C.F. Bender, P.K. Pearson, S.V. O'Neill and H.F. Schaefer III, J. Chem. Phys. 56, 4626 (1972).

5b. S.V. O'Neill, P.K. Pearson, H.F. Schaefer III, J. Chem. Phys. 58, 1126 (1973).

5c. P.K. Pearson, W.J. Hunt, C.F. Bender and H.F. Schaefer III, J. Chem. Phys. 58, 5358 (1973).

5d. C.W. Wilson Jr., and W.A. Goddard III, J. Chem. Phys. 56, 5913 (1972).

5e. S. Shih, R.J. Buenker, S.D. Peyerimhoff and C.J. Michejda, J. Amer. Chem. Soc. 94, 7620 (1972).

6. H.F. Schaefer III, "The Electronic Structure of Atoms and Molecules: A Survey of Rigorous Quantum Mechanical Results", (Addison-Wesley, Reading, Ma., 1972)

7. J.A. Pople, D. L. Beveridge and P.A. Dobosh, J. Chem. Phys. $\underline{47}$, 2026 (1967).

8. W. R. Wadt and W. A. Goddard III, J. Amer. Chem. Soc. (In Press)

9. P. J. Hay, W. J. Hunt, and W. A. Goddard, III, Chem. Phys. Lett. $\underline{13}$, 30 (1972).

10a. W. J. Hunt, W. A. Goddard III, and T. H. Dunning, Jr., (to be published)

10b. W. J. Hunt, Ph.D. Thesis, California Institute of Technology, (1971).

10c. U. Kaldor and I. Shavitt, J. Chem. Phys. $\underline{48}$, 191 (1968). Reported MBS configuration interaction calculations which were equivalent to the simplest GVB description of ethylene.

11. P. J. Hay, W. J. Hunt and W. A. Goddard III, J. Amer. Chem. Soc. $\underline{94}$, 8293 (1972).

12. J. A. Pople and D. L. Beveridge, "Approximate Molecular Orbital Theory, " (McGraw-Hill, New York, 1970).

13. We are able to obtain consistent descriptions of the methylene states with the simplest GVB wavefunction, in which all the pairs but one are doubly-occupied, for two reasons. First, the remaining pairs involve the C 1s core orbital or the CH bond orbitals, so that introducing a GVB pair description does not lead to a large effect.[11] Second, and more important, the correlation energy of these pairs is nearly the same in both states ($^{3}B_1$, $^{1}A_1$) and does not change much as the molecule is bent.

14a. T. H. Dunning, Jr., W. J. Hunt and W. A. Goddard III, Chem. Phys. Lett. $\underline{4}$, 147 (1969).

14b. C. F. Bender, T. H. Dunning, Jr., H. F. Schaefer III, W. A. Goddard III and W. J. Hunt, Chem. Phys. Lett. $\underline{15}$, 171 (1972).

15. J. Del Bene and H. H. Jaffe, J. Chem. Phys. $\underline{48}$, 1807, 4050 (1968).

16. Segal[17] previously used the INDO method to describe the low-lying excited states for various small molecules. He also found that the $\pi \rightarrow \pi^*$ transitions were treated much worse than $\sigma \rightarrow \pi^*$, $\pi \rightarrow \sigma^*$ and $\sigma \rightarrow \sigma^*$ transitions. However, only transitions to $^1\pi\pi^*$ states, which require diffuse functions for proper description, were examined. Segal realized that the gross errors were not just due to the INDO method, but no comparison was made to the available ab initio results,[10,14a] which would have indicated problems in the INDO approximation itself.

17. G. A. Segal, J. Chem. Phys. $\underline{53}$, 360 (1970).

18. R. Pariser and R. G. Parr, J. Chem. Phys. $\underline{21}$, 466 (1953).

19. W. R. Wadt and W. A. Goddard III, (unpublished results).

20. G. Herzberg and J. W. C. Jones, Proc. Roy. Soc. $\underline{A295}$, 107 (1966).

21. G. Herzberg, "Electronic Structure of Polyatomic Molecules," (Van Nostrand, Princeton, 1966).

22. A. J. Merer and R. S. Mulliken, Chem. Rev. $\underline{69}$, 639 (1969).

23. R. J. Buenker, S. D. Peyerimhoff and W. E. Kammer, J. Chem. Phys. $\underline{55}$, 814 (1971).

24. S. V. O'Neill, H. F. Schaefer III and C. F. Bender, J. Chem. Phys. 55, 162 (1971).

25. E. Wasserman, W. A. Yager and V. Kuck, J. Am. Chem. Soc. 92, 749 (1970).

26. G. Herzberg and J. W. C. Johns, Proc. Roy. Soc. (London) A295, 107 (1966).

PART FIVE:

Approximate Integral Methods and Correlated Wavefunctions

# I. INTRODUCTION

The concomitant development of faster computers and more efficient programming of <u>ab initio</u> methods has allowed chemists to perform high quality calculations on molecules as large as benzene [1] and pyrazine. [2] However, <u>ab initio</u> techniques are still too slow to properly treat anything other than simple reactive surfaces. [3] The bottleneck here is the large number of geometries required to delineate the reaction or energy transfer mechanism. Therefore, approximate methods would appear necessary to study the chemical dynamics of large molecules.

Much effort has already gone into producing a reliable approximate method, leading to a broad spectrum of techniques. Nearly all of these methods have been based upon closed-shell Hartree-Fock (HF) wavefunctions, including (i) extended Hückel theory, [4] (ii) CNDO, [5] (iii) INDO, [6] (iv) MINDO, [7] (v) NDDO, [8] (vi) PRDDO, [9] (vii) ESE-MO [10] and (viii) Xα-type approaches. [11] It is well known that simple HF wavefunctions (even when carried out exactly) usually provide very poor descriptions of potential surfaces involving bond formation or breakage. [12,13] Moreover, simple HF wavefunctions generally lead to poor descriptions of the relative ordering of molecular excited states. In fact, HF wavefunctions sometimes lead to incorrect ground states. [14] It is disturbing that all the major approximate methods have been based on a wavefunction which, in general, cannot properly describe (even when carried out exactly) the very processes for which the

approximate methods are needed.

In order to test the validity of the available approximate methods for correlated wavefunctions, we recently carried out calculations on $O_3$,[14] $CH_2$ and $C_2H_4$[15] using the INDO[6] approximation with wavefunctions correlated so as to provide a consistent description of the low-lying excited states. The results were mixed. For ozone, INDO led to vertical excitation energies with average errors of ± 0.5 eV relative to comparable ab initio calculations. Bond angles for the low-lying states were found to be in good agreement with both experimental and ab initio results, while the bond lengths were too short by 0.16 Å relative to the comparable ab initio results. Finally, we found that INDO grossly favors closed geometries as opposed to open geometries, predicting the ground state of ozone to be an equilateral triangle state with an energy 6.75 eV below the correct open state. For methylene, INDO led to CH bending curves for the three lowest states in good agreement (0.2 eV errors) with ab initio results, while for ethylene, the dihedral twist curves for the three lowest states were very poor (2 to 4 eV errors).

The origin of the errors in these INDO calculations is not, in general, easy to determine. It is not clear whether the problems arise from the parameterization of INDO to reproduce ab initio minimal basis set HF wavefunctions or from the nature of the truncated set of integrals employed in INDO. However, it is clear that if one wants to deal with problems in chemical dynamics, then the approximate method should be developed in conjunction with the correlated wavefunctions that are required to describe reactions

and energy transfer processes correctly.

In this paper, we report our efforts to develope efficient approximate methods that provide reliable results when used with appropriately correlated wavefunctions. Our investigations are divided into two basic lines of approach. (1) Since some of the results from the INDO calculations were quite reasonable,[14,15] attempts were made to reparameterize the method so as to remedy the major deficiencies. (2) More general studies were carried out to determine the errors that are introduced when the full set of ab initio integrals are truncated in various ways. The first set of calculations are reported in Section II and the second set in Section III.

## II. INDO-TYPE METHODS

### A. Review of the Original INDO Method

INDO [6] was designed to reproduce the results of minimal basis set (MBS) ab initio HF calculations. In the HF method one solves for the optimal wavefunction of the form

$$\Psi^{HF} = \alpha[\phi_1^2 \ \phi_2^2 \ \ldots \phi_n^2 \ \alpha\beta\alpha\beta\ldots\alpha\beta] \tag{1}$$

where $\alpha$ is the antisymmetrizer, which ensures that the wavefunction has the proper permutational symmetry. Note that all the orbitals are constrained to be doubly-occupied and orthogonal. Application of the variational principle leads to the familiar HF equations [in atomic units (a.u.)]

$$F\phi_i = [h + \sum_j (2J_j - K_j)]\phi_i = \varepsilon_i \phi_i \tag{2}$$

where F is the Fock operator, h is the one-electron operator [electronic kinetic energy (t) plus nuclear attraction (v)] and $J_j$ and $K_j$ are the coulomb and exchange operators, respectively. Following Roothaan,[16] each molecular orbital is expanded in terms of a finite set of basis functions

$$\phi_i = \sum_\mu c_{\mu i} \ \chi_\mu \tag{3}$$

so that the (2) becomes a matrix equation

$$\sum_{\nu} (F_{\mu\nu} - \varepsilon_i S_{\mu\nu}) c_{\nu i} = 0 \tag{4a}$$

or

$$\underset{\sim}{F}\,\underset{\sim}{C} = \underset{\sim}{S}\,\underset{\sim}{C}\,\underset{\sim}{E} \tag{4b}$$

where

$$F_{\mu\nu} \equiv h_{\mu\nu} + \sum_{\lambda\sigma} P_{\lambda\sigma} [\langle \mu\nu|\lambda\sigma\rangle - \tfrac{1}{2} \langle \mu\lambda|\nu\sigma\rangle] \tag{5}$$

$$h_{\mu\nu} \equiv \langle \mu|h|\nu\rangle = \int \chi_\mu(1) h \chi_\nu(1) d\tau_1 \tag{6}$$

$$\langle \mu\nu|\lambda\sigma\rangle \equiv \int \left[ \int \chi_\mu(1)\chi_\nu(1)\frac{1}{r_{12}}d\tau_1 \right] \chi_\lambda(2)\chi_\sigma(2) d\tau_2 \tag{7}$$

$$P_{\lambda\sigma} \equiv 2 \sum_i c_{\mu i} c_{\nu i} \tag{8}$$

$$S_{\mu\nu} = \langle \mu|\nu\rangle \tag{9}$$

(We have assumed that all our basis functions are real.)

From (5), the number of one-electron integrals increases as $N^2$ where N is the number of basis functions, while the number of two-electron integrals increases as $N^4$. Consequently, it is the calculation and manipulation of the two-electron integrals which limit ab initio calculations to 50-100 basis functions. The limitations are even more evident when it is recalled that the HF equations are solved iteratively, so that the $N^4$ two-electron integrals must be transformed over molecular orbitals every iteration. Thus, the goal of all approximate methods is to reduce the number of integrals.

In general, the basis functions are centered at the various nuclei, possessing exponential (Slater), $e^{-\zeta r}$, or gaussian, $e^{-\zeta r^2}$, radial dependence and atomic angular momentum symmetries, i.e.,s,p,d,etc. Therefore, most of the two-electron integrals involve basis functions on three or four centers and are expected to be much smaller than the one- and two-center integrals. In addition, the two-electron integral, $\langle \mu\nu|\lambda\sigma\rangle$, is expected to be much larger if $\mu = \nu$ and $\lambda = \sigma$. These ideas are combined into the zero differential overlap (ZDO) approximation, initially proposed by Parr [17], i.e.,

$$\langle \mu\nu|\lambda\sigma\rangle = \delta_{\mu\nu}\delta_{\lambda\sigma} \langle \mu\mu|\lambda\lambda\rangle \tag{10}$$

Equation (10) will be exact if all the basis functions are non-overlapping. However, non-overlapping basis sets are not feasible since the basis functions are either exponentials or gaussians. It has been found that transformation from the standard non-orthogonal basis set to an orthogonal one does improve the validity of the ZDO approximation. This will be considered in more detail in Section III.

In INDO the ZDO approximation is invoked for the two-electron integrals. However, it was found that retention of the one-center exchange integrals $\langle \mu_A\nu_A|\mu_A\nu_A\rangle$ (A denotes the atomic center) was necessary for proper description of singlet and triplet states.[6] Therefore, in INDO one retains only the one- and two-center coulomb integrals, $\langle \mu\mu|\lambda\lambda\rangle$, plus the one-center exchange, leading to an $N^2$ set of two-electron integrals. The reduction in two-electron integrals is tremendous, e.g., for planar ethylene the 3190 two-electron

integrals in an ab initio MBS are reduced to 90 in INDO!

To be consistent, all three-center potential integrals $\langle \mu_A | v_c | v_B \rangle$ are neglected as well as integrals of the form $\langle \mu_A | h | v_A \rangle$ where $\mu_A \neq v_A$. Although application of the ZDO approximation would indicate that the two-center $\langle \mu_A | h | v_B \rangle$ integrals should be neglected, they are retained since they are crucial for describing chemical bonds. Finally, all integrals of the form $\langle \mu_A | h | \mu_A \rangle$ are kept.

In addition to the drastic truncation of the integral set, two additional approximations are made in INDO. (1) The overlap matrix $\underset{\sim}{S}$ in equation (4) is assumed to be the unit matrix, i.e., the basis functions are assumed to be orthogonal. (2) Only the valence electrons are treated explicitly. The inner core electrons are assumed to completely screen the nucleus, i.e., they are represented by a $(C/r)$ potential where C is the number of core electrons.

The integrals retained in INDO are evaluated or parameterized as follows: [6]

(a) $\alpha_\mu \equiv \langle \mu_A | t + v_A | \mu_A \rangle$: Set equal to the difference of the experimental ionization potential and electron affinity for atom A. [18]

(b) $V_{AB} \equiv \langle \mu_A | v_B | \mu_A \rangle$: Set equal to $-Z_B \gamma_{AB}$ where $Z_B$ is the charge on atom B (total charge minus the core electrons) and $\gamma_{AB} \equiv \langle s_A s_A | s_B s_B \rangle$ is the two-center coulomb integral over the appropriate valence Slater s functions.

(c) $\beta_{\mu v} \equiv \langle \mu_A | t + v_A + v_B | v_B \rangle$: Set equal to $(1/2)S_{\mu v}(\beta_A^0 + \beta_B^0)$ where $\beta_A^0$ and $\beta_B^0$ are parameters. The $\beta_A^0$ parameters were adjusted to obtain the best overall fit with ab initio MBS orbital coefficients for ground state diatomic hydrides. The ab initio

coefficients were transformed to an orthogonal basis, i.e.,
a basis with unit overlap matrix, prior to comparison with
the INDO results.

(d) $\langle \mu_A \mu_A | \nu_A \nu_A \rangle$ and $\langle \mu_A \nu_A | \mu_A \nu_A \rangle$: Set equal to the Slater-Condon
parameters, which were obtained by fitting atomic spectra.

(e) $\langle \mu_A \mu_A | \nu_B \nu_B \rangle$: Set equal to $\gamma_{AB} \equiv \langle s_A s_A | s_B s_B \rangle$.


B. Reparameterization of the $\beta$ Integrals

Analysis of our INDO calculations on methylene and ethyl-
ene [15] revealed two major problems in the parameterization of INDO.
(1) The use of empirical values (the Slater-Condon parameters) for
the one-center exchange integrals leads to a small $^3B_1 - {}^1B_1$ splitting
energy in methylene. (2) The use of one $\beta$ parameter per atom leads
to vertical excitation energies and rotational barriers that are too
large for the N,T and V states of ethylene. (N denotes the ground
state, while T and V denote the $^3\pi\pi^*$ and $^1\pi\pi^*$ states, respectively.)
The $\beta$'s for $\pi$ orbitals are too large, while those for $\sigma$ orbitals are
slightly small.

The first deficiency may be easily remedied by calculating
the one-center two-electron integrals over the appropriate valence
Slater orbitals. [19,20] To be consistent, the one-center one-electron
integrals should also be evaluated over Slater orbitals. In both
cases, 2s Slater orbitals are orthogonalized to the 1s Slater orbital
on the same center to ensure the validity of the core-valence electron
separation. [21]

Since the $\beta$ parameters are supposed to represent two-center

one-electron integrals over orthogonal atomic orbitals (OAO),[6] we decided to evaluate them non-empirically using diatomic fragments, e.g., the $\beta$'s involving the two carbons in ethylene are determined from $C_2$. Since there are an infinity of ways to orthogonalize the set of Slater atomic orbitals (AO) for the diatom, we use the criterion that the resultant set of OAO's should be as similar as possible to the original AO's. Löwdin or symmetric orthogonalization [22] satisfies this criterion in a least squares sense. [23] The trans-formation to Löwdin $(\bar{\chi}_i)$ is given by

$$\bar{\chi}_i = \sum_j \chi_j (S^{-1/2})_{ji} \tag{11}$$

where $\underset{\sim}{S}$ is the overlap matrix over AO's $(\chi_j)$. Prior to Löwdin orthogonalization, the 2s Slater orbitals are Schmidt orthogonalized to the 1s on the same center.

Using the above procedure non-empirical $\beta$ integrals were calculated for $C_2$ at internuclear separations (R) of 1.2, 1.4 and 1.6 Å. [24] From the results shown in Table I, it is clear why using a single $\beta$ parameter per atom causes problems. The $\beta$ parameter for the $\pi$ orbitals is ~ 50% the size of the $\beta$ parameters for the $\sigma$ orbitals. Using only two $\beta$ parameters per atom ($\beta_\sigma$ and $\beta_\pi$) over-comes most of the errors inherent with employing one $\beta$ per atom, since the parameters for the $\sigma$ orbitals ($\beta_{ss}$, $\beta_{sp_\sigma}$ and $\beta_{p_\sigma p_\sigma}$) are relatively similar. This explains why DelBene and Jaffe [25] met with reasonable success in describing aromatic $\pi$ systems by reparameterizing CNDO [5] with two $\beta$'s per atom. From Table I we also note that the proportionality

TABLE I.  $\beta_{\mu\nu}$ integrals for $C_2$ (in a.u.)

| | R=1.2Å | R=1.4Å | R=1.6Å | $<\beta_{\mu\nu}^\circ>$AVG |
|---|---|---|---|---|
| $\beta_{ss}$ | -0.545 | -0.358 | -0.223 | |
| $\beta_{ss}^\circ = \beta_{ss}/S_{ss}$ | -1.066 | -0.883 | -0.707 | -0.885 = -24.1 eV |
| $\beta_{sp_\sigma}$ | 0.464 | 0.379 | 0.266 | |
| $\beta_{sp_\sigma}^\circ = \beta_{sp_\sigma}/S_{sp_\sigma}$ | -0.983 | -0.920 | -0.772 | -0.892 = -24.3 eV |
| $\beta_{p_\sigma p_\sigma}$ | 0.353 | 0.346 | 0.268 | |
| $\beta_{p_\sigma p_\sigma}^\circ = \beta_{p_\sigma p_\sigma}/S_{p_\sigma p_\sigma}$ | -1.214 | -1.044 | -0.830 | -1.030 = - 28.0 eV |
| $\beta_{p_\pi p_\pi}$ | -0.174 | -0.119 | -0.079 | |
| $\beta_{p_\pi p_\pi}^\circ = \beta_{p_\pi p_\pi}/S_{p_\pi p_\pi}$ | -0.518 | -0.487 | -0.458 | -0.488 = - 13.3 eV |
| INDO | | | | - 21 eV |

between $\beta_{\mu\nu}$ and $S_{\mu\nu}$ assumed in INDO is roughly obeyed.

Previous *ab initio* calculations on ethylene [26] have shown that the generalized valence bond (GVB) correlated wavefunction [27] leads to a good description of the dihedral twist potential curves for the N and T states. Therefore, we tested the introduction into INDO of non-empirical carbon $\beta$ parameters (shown in Table I) and non-empirical. values for the one-center integrals by performing GVB calculations on the N and T states of ethylene at two geometries: (1) the planar ($\theta = 0°$) experimental ground state geometry [28] with $R_{CH} = 1.086Å$, $R_{CC} = 1.338Å$.<HCH = 117.4° and (2) a perpendicular ($\theta = 90°$) geometry with $R_{CC} = 1.41 Å$. The specific GVB wavefunction employed in the calculations is designated GVB(2/PP) and has the form

$$\Psi = \alpha[\phi_1^2...\phi_n^2(\phi_{\sigma_\ell}\phi_{\sigma_r}+\phi_{\sigma_r}\phi_{\sigma_\ell})(\phi_{\pi_\ell}\phi_{\pi_r}+\phi_{\pi_r}\phi_{\pi_\ell})\alpha\beta...\alpha\beta] \qquad (12)$$

$$\underbrace{\qquad\qquad}_{\sigma_{CC}\text{ pair}} \qquad \underbrace{\qquad\qquad}_{\pi\text{ pair}}$$

where the $\sigma_{CC}$ and $\pi$ bonds are described by a pair of singlet-coupled non-orthogonal orbitals as opposed to the HF wavefunction, in which they are forced to be doubly-occupied. Splitting the $\pi$ pair affords a consistent description of the planar and perpendicular N and T states. The results of the calculations are shown in Table II. For convenience of discussion, our modifications of INDO will be designated Approximate Integrals - zeroth level or AI/0.

Since the proportionality between $\beta_{\mu\nu}$ and $S_{\mu\nu}$ is not exact, one can either use the $\beta_{\mu\nu}$ from $C_2$ calculated at the appropriate internuclear separation or choose an average $\beta_{\mu\nu}^o$ and employ $\beta_{\mu\nu} = \beta_{\mu\nu}^o S_{\mu\nu}$.

TABLE II. Ethylene GVB(2/PP) energies for the N and T states (in eV).

| | AI/O[a] | AI/O[b] | INDO | Ab initio[c] |
|---|---|---|---|---|
| N → T (vert.) | 4.54 | 4.43 | 8.48 | 4.69 |
| N → V (vert.) | 11.8 | 11.7 | 15.2 | 13.3 |
| N → T (0,0) | 4.41 | 2.46 | 5.05 | 2.73 |
| N rotation barrier | 4.41 | 2.46 | 5.05 | 2.78 |
| T rotation barrier | 0.13 | 1.97 | 3.43 | -1.97 |
| N → $^2B_{3u}$ (KT)[d] | 9.87 | 9.81 | 15.9 | 11.2 |

[a]Employs the appropriate $\beta_{\mu\nu}$ for $C_2$ (interpolated from the results in Table I).

[b]Employs $\beta_{\mu\nu} = \beta^{\circ}_{\mu\nu} S_{\mu\nu}$ with $\beta^{\circ}_{\mu\nu}$ for $C_2$ at R = 1.4 Å.

[c]Slater MBS.

[d]Koopmans' Theorem.[40]

The results in Table II show that the latter procedure leads to better agreement with ab initio calculations. Both procedures lead to reasonable vertical excitation energies. However, forcing $\beta_{\mu\nu}$ to be proportional to the overlap leads to better rotational barriers. The explanation for the improved rotational barriers is not manifest and probably represents a fortuitous cancellation of errors.

Since the N and T states are well described (errors $\leq$ 0.3 eV) by the AI/O scheme in which the values for $\beta_{\mu\nu}$ from $C_2$ at R = 1.4 Å are used, the same scheme was tested on the ground state potential curves for $C_2$ and $O_2$ using HF wavefunctions. The resulting bond lengths were 0.03 to 0.05 Å longer than for comparable INDO calculations, in much better agreement with ab initio results (cf. Table III).

We appear to have overcome some of the major problems of INDO, namely, tightly bound $\pi$ orbitals and short bond lengths. [14,15] However, when the AI/O scheme was tested on ozone, we found, to our dismay, that the $2^1A_1(6\pi)$ ring state of ozone was calculated to be 8.0 eV lower than the $1^1A_1(4\pi)$ open state, the true ground state. [29] The AI/O scheme is more strongly biased in favor of closed geometries than INDO! Consequently, one cannot ascribe the bias toward closed geometries of the INDO approximation to the use of one $\beta$ parameter per atom. Therefore, further modifications are warranted to remove this bias.

TABLE III. HF Bond Lengths for $C_2$ and $O_2$ using INDO and AI/O (in Å)

| | AI/O[a] | INDO | Ab initio[b] |
|---|---|---|---|
| $C_2(^1\Sigma_g^+)$ | 1.194 | 1.148 | 1.233 |
| $O_2(^3\Sigma_g^-)$ | 1.172 | 1.140 | 1.217 |

[a]Employs $\beta_{\mu\nu} = \beta_{\mu\nu}^\circ S_{\mu\nu}$ with $\beta_{\mu\nu}^\circ$ for $C_2$ at 1.4Å and for $O_2$ at 1.278Å.

[b]STO-3G calculations. M. D. Newton, W. A. Lathan, W. J. Hehre, and J.A. Pople, <u>J. Chem. Phys.</u>, 52, 4064 (1970).

## C. Proper Core Orthogonalization and Parametric Integral Fits

Prior to transforming the two-center $\beta$ integrals over

OAO's, the 2s AO's were orthogonalized to the 1s AO on the same center

to ensure the validity of the core-valence electron separation.[21]

However, the 2s and $2p_\sigma$ AO's are not orthogonal to the 1s AO on the

other center and, hence, the separation into core and valence electrons

breaks down. A consequence of the non-orthogonality is that the

electrons in 2s or $2p_\sigma$ orbitals will not be properly shielded from the

other nuclei. To correct this problem, the 2s and $2p_\sigma$ AO's are

orthogonalized to the 1s AO's on both centers prior to transformation

to OAO's. In addition, the repulsion of the paired 1s electrons is

represented by 2J-K potential rather than the simple point charge

2/r potential. The 2J-K potential is more accurate as it allows the

valence orbitals to penetrate the 1s core electrons, leading to more

negative nuclear attraction integrals.

The set of integrals (transformed over OAO's) that are

normally kept in INDO are shown in Table IV for $C_2$ at R = 1.2, 1.4 and

1.6 Å. Comparison of the $\beta$ integrals from Tables I and IV indicates

a significant effect arising from orthogonalization to both 1s AO's.

Not only are the values  different,  but the $\beta$ integrals are no

longer proportional to the overlap integrals. Instead, all the $\beta$

integrals have an exponential dependence on R. This is very con-

venient, since the $\beta$ integrals may be evaluated at several inter-

nuclear separations and the resulting integrals fit with a simple

exponential, $Be^{-AR}$, in a least-squares manner. The two parameters,

A and B, may then be used in the integral generation program to

TABLE IV. $C_2$ integrals over Löwdin OAO's orthogonalized to the 1s core (in a.u.).

| | | R=1.2Å | R=1.4Å | R=1.6Å |
|---|---|---|---|---|
| **I. One-electron** | **A. One-center ($\alpha$)** | | | |
| | $\langle s_L | t+v_L | s_L \rangle^a$ | -1.945 | -2.106 | -2.187 |
| | $\langle z_L | t+v_L | z_L \rangle^b$ | -1.850 | -1.890 | -1.911 |
| | $\langle x_L | t+v_L | x_L \rangle^c$ | -1.928 | -1.942 | -1.950 |
| | $\langle s_L | t+v_L | z_L \rangle$ | 0.170 | 0.105 | 0.063 |
| | **B. Two-center ($V_{AB}$)** | | | |
| | $\langle s_L | v_R | s_L \rangle$ | -1.723 | -1.493 | -1.317 |
| | $\langle z_L | v_R | z_L \rangle$ | -1.665 | -1.483 | -1.342 |
| | $\langle x_L | v_R | x_L \rangle$ | -1.546 | -1.376 | -1.237 |
| | $\langle s_L | v_R | z_L \rangle$ | -0.395 | -0.359 | -0.317 |
| | **C. Two-center ($\beta$)** | | | |
| | $\langle s_L | t+v_L+v_R | s_R \rangle$ | -0.235 | -0.138 | -0.086 |
| | $\langle z_L | t+v_L+v_R | z_R \rangle$ | 0.457 | 0.346 | 0.254 |
| | $\langle x_L | t+v_L+v_R | x_R \rangle$ | -0.167 | -0.113 | -0.075 |
| | $\langle s_L | t+v_L+v_R | z_R \rangle$ | 0.378 | 0.261 | 0.180 |
| **II. Two-electron** | **A. One-center Coulomb** | | | |
| | $\langle s_L s_L | s_L s_L \rangle$ | 0.617 | 0.609 | 0.600 |
| | $\langle s_L s_L | z_L z_L \rangle$ | 0.621 | 0.618 | 0.611 |
| | $\langle s_L s_L | x_L x_L \rangle$ | 0.613 | 0.606 | 0.599 |
| | $\langle z_L z_L | z_L z_L \rangle$ | 0.719 | 0.701 | 0.685 |
| | $\langle z_L z_L | x_L x_L \rangle$ | 0.609 | 0.600 | 0.592 |
| | $\langle x_L x_L | x_L x_L \rangle$ | 0.654 | 0.647 | 0.643 |
| | $\langle x_L x_L | y_L y_L \rangle$ | 0.582 | 0.577 | 0.573 |
| | **B. One-center Exchange** | | | |
| | $\langle s_L z_L | s_L z_L \rangle$ | 0.103 | 0.115 | 0.121 |
| | $\langle s_L x_L | s_L x_L \rangle$ | 0.140 | 0.137 | 0.134 |
| | $\langle z_L x_L | z_L x_L \rangle$ | 0.037 | 0.037 | 0.037 |
| | $\langle x_L y_L | x_L y_L \rangle$ | 0.036 | 0.035 | 0.035 |
| | **C. Two-Center Coulomb** | | | |
| | $\langle s_L s_L | s_R s_R \rangle$ | 0.390 | 0.348 | 0.313 |
| | $\langle s_L s_L | z_R z_R \rangle$ | 0.385 | 0.350 | 0.321 |
| | $\langle s_L s_L | x_R x_R \rangle$ | 0.370 | 0.333 | 0.302 |
| | $\langle z_L z_L | z_R z_R \rangle$ | 0.382 | 0.357 | 0.333 |
| | $\langle z_L z_L | x_R x_R \rangle$ | 0.358 | 0.331 | 0.307 |
| | $\langle x_L x_L | x_R x_R \rangle$ | 0.356 | 0.324 | 0.295 |
| | $\langle x_L x_L | y_R y_R \rangle$ | 0.347 | 0.317 | 0.290 |

[a] $s_L$ indicates a 2s OAO centered on the left carbon.

[b] $z_L$ indicates a $2p_z$ OAO centered on the left carbon.

[c] $x_L$ indicates a $2p_x$ OAO centered on the left carbon.

calculate the β integrals for all R. The β integrals obtained in this manner are appropriate for a diatomic coordinate system, in which the nuclei are on the z-axis. The diatomic coordinate system must be rotated, so that it coincides with the molecular coordinate system being used. The rotated integrals are then used in the SCF calculations.

The above procedure for evaluating the β integrals is very useful in that it can be extended in a straightforward manner to include more atoms, e.g., H, O, S, Fe, etc., by fitting the appropriate diatomic integrals, e.g., $H_2$, CH, $O_2$, CO, OH, etc.. Since the fits to the β integrals should be most accurate for internuclear separations characteristic of bond lengths, we have always fit the integrals at values of R that span the range of bond lengths normally encountered in molecules. For example, fitting the β integrals for $C_2$ at R = 1.2, 1.4 and 1.6 Å with a non-linear least-squares program led to errors less than 3 mh = 0.08 eV, [30] which is well within the limits of the other approximations being made. Similar results were obtained fitting the β integrals for $H_2$, CH and $O_2$.

Although implementation of the exponential fits to the β integrals may improve the results, the bias toward closed geometries will still be present. However, examination of Table IV appears to reveal how the bias arises. All the one-center integrals over OAO's increase algebraically as the R decreases, except for the relatively small one-center exchange integrals. The increase in the α integrals is expected, since the additional kinetic energy arising from orthogonalization increases as R decreases. The increase in the one-center coulomb integrals is not readily explained but occurs in general.

This destabilization of the one-center integrals over OAO's, which occurs for closed geometries or short bond lengths, is ignored when the atomic values are used as in INDO.

Since the destabilization of the $\alpha$ integrals is significantly greater than that of the one-center coulomb integrals, we will initially consider only the former. Moreover, transformation to OAO's decreases the size of the two-center coulomb integrals, so that the errors in using AO values for the coulomb integrals tend to cancel. The change in the $\alpha$ integrals arising from orthogonalization, $\Delta\alpha$, has an exponential dependence on R and may be fit to 1 mh = 0.03 eV with $Be^{-AR}$. In a polyatomic molecule, the $\Delta\alpha$ corrections are evaluated for each diatomic fragment, rotated and summed to give the total correction. The validity of this procedure will be considered in Section III.B.

For consistency the $V_{AB}$ integrals should also be evaluated in a manner analogous to the $\alpha$ and $\beta$ integrals. The long range dependence of $V_{AB}$ will, of course, be -Z/R, where Z is the nuclear charge minus the number of core electrons. We found that the function $-Z/R + e^{-AR}(B + Z/R)$, which has the proper limits as $R \rightarrow \infty$ [-Z/R] and as $R \rightarrow 0$ [B], fits the $V_{AB}$ integrals to 2 mh = 0.05 eV.[31] Finally, the one-electron integrals, $<s|t + v_L|z_L>$ and $<s|v_R|z_L>$, which are neglected in INDO, are retained, since they are comparable in size to the other integrals that are kept (cf. Table IV).

Using the new AI/O scheme with fitted one-electron integrals over OAO's and two-electron integrals over AO's, GVB(2/PP) calculations were carried out on the planar N, T and V states of ethylene. The results in Table V show that,although the vertical excitation energies

TABLE V.  Ethylene GVB(2/PP) energies for the planar N and T
state (in eV).

| | AI/O | | | |
|---|---|---|---|---|
| | $\alpha,\beta,V_{AB}$ [a] | $\beta,V_{AB}$ [b] | $\beta$ [c] | Ab initio |
| N → T (vert) | 4.21 | 4.21 | 4.21 | 4.69 |
| N → V (vert) | 11.47 | 11.47 | 11.47 | 13.27 |
| N → $^2B_{3u}$ (KT) [d] | 5.15 | 7.15 | 9.52 | 11.21 |

[a] Parametric fits used for the $\alpha$, $\beta$ and $V_{AB}$ integrals.

[b] Parametric fits used for the $\beta$ and $V_{AB}$ integrals; $\alpha$ integrals over
AO's.

[c] Parametric fits used for the $\beta$ integrals; $\alpha$ integrals over AO's;
$V_{AB} = - Z_B \gamma_{AB}$ (as in INDO).

[d] Koopmans' Theorem. [40]

to the T and V states are reasonably well described, the $\pi$ orbital is too weakly bound by > 6 eV. In fact, nearly all the orbitals are too weakly bound by 5 eV. If one neglects the destabilization corrections to $\alpha$ integral arising from orthogonalization, all the orbital energies decrease significantly. However, the $\pi$ orbital is still too weakly bound by 4 eV (cf.Table V). Re-introducing $V_{AB} = -Z_B\gamma_{AB}$ leads to results very similar to those obtained in Table II. The $\pi$ ionization potential is now too small by less than 2 eV. The only difference between this AI/O scheme and that reported in Table II is the manner in which the $\beta$ integrals are calculated. Consequently, using only fitted $\beta$ integrals again leads to poor results for the N and T rotational barriers, namely 4.44 eV and -0.23 eV.

Inclusion of the $\Delta\alpha$ corrections are expected to be necessary to obtain reasonable potential curves, but our calculations show that other alterations in the approximation scheme (probably in the treatment of two-electron integrals) are required to describe ionization correctly.

Prior to rethinking our modifications of INDO, we decided to test whether the reasonable results obtained for the $\pi \rightarrow \pi^*$ vertical excitation energies in ethylene would carry over to benzene. Toward this end, we used the following AI/O scheme: $\alpha$ and two-electron integrals evaluated non-empirically over AO's, $\beta$ integrals evaluated using parametric fits to the OAO's integrals and $V_{AB}$ integrals set equal to $-Z_B\gamma_{AB}$ as in INDO. The ground state HF wavefunction was calculated and a full configuration interaction (CI) calculation was performed among the six $\pi$ orbitals, freezing the $\sigma$ orbitals as

in the ground state. The vertical excitation energies from the $\pi$ CI are shown in Table VI. The AI/O results are in much better agreement (0.27 to 1.19 eV errors) with comparable ab initio calculations than INDO (1.75 to 3.44 eV errors). Therefore, we may conclude that the large $\pi \rightarrow \pi^*$ excitation energies produced by INDO may be overcome by merely calculating the $\beta$ integrals correctly over OAO's.

D.  Introduction of Local Potentials and Corrections to the Two-Electron Integrals

The poor values obtained in Section II.C for the rotational barriers of the ethylene N and T states are expected to arise from the neglect of the $\Delta\alpha$ corrections and the evaluation of the $V_{AB}$ integrals as in INDO. Therefore, calculations should be made on the rotational barriers using parametric fits for all the one-electron integrals. Before carrying out these calculations, we decided to replace the 2J-K potential for 1s electrons with a local potential,[32] to be described in the next section. The reasons for introducing the local potential will be made clear in Section III.D.

1. Local Potentials

In approximate methods one generally wants to consider only the valence electrons, since the wavefunction for the core electrons is basically unchanged for low-lying excited states or simple chemical reactions. Two methods for neglecting the core electrons have been considered previously, namely, replacement of the core electrons with either a point charge potential, C/r, or a 2J-K potential. Both methods require orthogonalization of the valence orbitals to the core

TABLE VI.   Benzene $\pi \to \pi$ vertical excitation energies from a full
$\pi$ CI (in eV).

|                | AI/O | Ab initio[a] | INDO  |
|----------------|------|----------|-------|
| $^1A_{1g}$     | 0.0  | 0.0      | 0.0   |
| $^3B_{2u}$     | 3.21 | 3.98     | 7.28  |
| $^1B_{2u}$     | 4.27 | 5.26     | 8.70  |
| $^3E_{1u}$     | 4.58 | 5.39     | 8.77  |
| $^3B_{2u}$     | 8.03 | 7.76     | 11.04 |
| $^1B_{1u}$     | 8.27 | 9.48     | 11.23 |
| $^1E_{1u}$     | 9.85 | 10.61    | 13.51 |

[a]MBS full $\pi$ CI.  R.J. Buenker, J.L. Whitten and J.D. Petke,

J. Chem. Phys., 49, 2261 (1973).

orbitals. An alternative procedure, which does not require orthog-
onalization to the core, is to replace the core electrons with a
local or effective potential. Detailed discussions of local potentials
have been presented elsewhere, [32] so that only a brief outline of the
method will be given here.

The local potential is constructed so that the lowest solutions
obtained with it are valence-like orbitals. The major difference be-
tween the valence orbitals obtained with the local potential and those
obtained with the core electrons present is the absence of any radial
(spherical) nodes, which are required in the latter case for orthogonality
to the core orbitals. For example, using a local potential for the 1s
electrons of the first row atoms, leads to 2s orbitals which have the
same shape as Slater 2s functions, i.e., $re^{-\zeta r}$. The valence orbitals,
such as the 2s, are prevented from collapsing into the core by the
presence of a very repulsive potential, which effectively projects out
any core character.

The actual procedure for obtaining a local potential will be
illustrated for carbon atom. First, we solve for the ab initio HF
ground state $^3P$ wavefunction leading to the following HF equations for
the 2s and 2p orbitals.

$$\langle\mu|(h + V_{core} + V^s_{val})|2s\rangle = \epsilon_{2s}\langle\mu|2s\rangle \qquad (13)$$

$$\langle\mu|(h + V_{core} + V^p_{val})|2p\rangle = \epsilon_{2p}\langle\mu|2p\rangle \qquad (14)$$

where $\mu$ is any basis function, $V_{core}$ represents the 2J-K potential of

the core electrons and $V_{val}^s$ and $V_{val}^p$ represent the electron repulsion from the other valence electrons for the 2s and 2p orbitals, respectively. Next, a valence s orbital without radial nodes [designated the coreless HF (CHF) 2s orbital] is formed by adding the proper amount of the 1s HF orbital to the 2s HF orbital so that the resultant orbital goes to zero as $r \to 0$. Using the CHF 2s orbital and the HF equations, we have

$$\langle \mu | V_{loc} | 2s_{CHF} \rangle \equiv \langle \mu | \epsilon_{2s} - h - V_{val}^{s\,CHF} | 2s_{CHF} \rangle \tag{15}$$

$$\langle \mu | V_{loc} | 2p \rangle = \langle \mu | \epsilon_{2p} - h - V_{val}^p | 2p \rangle \tag{16}$$

where $V_{loc}$ is the desired local potential. Note that by definition the lowest solutions of $V_{loc}$ are just the valence 2s and 2p orbitals without radial nodes, but with the same orbital energies as the HF orbitals.

Previous work has shown that the local potential can be expanded in terms of spherical haromics $Y_{\ell m}$ (denoted by $|\ell m\rangle$) [32a,b]

$$V_{loc} = \sum_{\ell=0}^{\infty} V_{\ell}(r) \, |\ell m\rangle\langle\ell m| \tag{17}$$

where $V_{\ell}(r)$ is a radial function, $|\ell m\rangle\langle\ell m|$ is a projection operator onto states of angular momentum $\ell m$ and a sum over m is assumed. Moreover, the $V_{\ell}(r)$ are approximately equal for all angular momenta $\ell$ greater than the maximum angular momentum $\lambda$ involved in the core (e.g., $\lambda = 1$ for C). [32a,b] Therefore, (17) becomes (using $\sum_{\ell m} |\ell m\rangle\langle\ell m| = 1$)

$$V_{loc} = V_{\lambda+1}(r) + \sum_{\ell=0}^{\lambda} \Delta V_\ell(r) |\ell m><\ell m| \qquad (18)$$

where $\Delta V_\ell \equiv V_\ell - V_{\lambda+1}$. For carbon, we have

$$V^C_{loc} = V_p(r) + V_{s-p}(r)|s><s| \qquad (19)$$

and

$$<\mu|V^C_{loc}|2s_{CHF}> = <\mu|V_p + V_{s-p}|2s_{CHF}> = <\mu|V_s|2s_{CHF}> \qquad (20)$$

$$<\mu|V^C_{loc}|2p> = <\mu|V_p|2p> \qquad (21)$$

so that the local potential depends upon the angular momentum of the valence electron.

Explicit forms for $V_s$ and $V_p$ are found by expanding them in terms of gaussian functions [32c]

$$V_\ell(r) = \sum_k c_k r^{n_k} e^{-\zeta_k r^2} \qquad (22)$$

and fitting the matrix elements calculated in (15) and (16) in a least-squares sense. In general, values for $n_k$ are restricted to $0, -1$ and $-2$. [32c]

## 2. Local Potential for Carbon 1s Electrons

The matrix elements shown in (15) and (16) were calculated using an (11s,7p) set of uncontracted gaussians consisting of Huzinaga's [33] (9s,5p) set augmented with two diffuse s primitives (exponents 0.051 and 0.017) and two diffuse p primitives (exponents 0.039 and 0.013). The extra diffuse functions are necessary to ensure

that the local potential has the correct long range dependence. The $V_p$ and $V_{s-p}$ potentials were fit with four gaussians each. The parameters are given in Table VII. The local potential was tested by performing open shell HF calculations on the $^3P$ and $^5S$ states of carbon atom [using the (11s, 7p) basis] and GVB(1) calculations [34] on the $^1\Sigma_g^+$ and $^3\Sigma_u^+$ states of $C_2$ at R = 1.2 Å (using an STO-6G basis [35]). The results in Table VIII show that the local potential underestimates the $^3P$ - $^5S$ splitting by 0.35 eV and overestimates the $^1\Sigma_g^+$ - $^3\Sigma_u^+$ splitting by 0.08 eV. The origin of these significant errors may be ascribed to changes in the valence region of the CHF 2s orbital relative to the 2s HF orbital. These differences in the CHF 2s orbital lead to changes in $V_{val}^{s\,CHF}$ relative to $V_{val}^s$ and, hence, in $V_{loc}$ via (15).

To minimize the difference between the 2s HF orbital and the coreless 2s orbital, a new method for constructing coreless orbitals was developed[36] The HF 2s orbital coefficients for the s basis functions, which describe the valence region (namely the four most diffuse), are fixed and the coefficient of the next most diffuse function is varied, so that the orbital goes to zero at the origin[37] The resulting coreless valence orbital (CVO) leads to a $V_{val}^s$ that is significantly closer to the HF $V_{val}^s$ than the CHF $V_{val}^s$ was.

As expected the CVO local potential leads to better results for the $^3P$ - $^5S$ splitting (cf. Table VIII), reducing the error by 60%. However, the results for $C_2$ are horrendous. The $^1\Sigma_g^+$ - $^3\Sigma_u^+$ splitting is calculated to be 0.01 eV. In addition, the energies of the orbitals are too high by 0.03 to 0.25 a.u. The explanation for these poor results is that the 2s CVO drops off much faster than a 2s Slater function as r → 0. As a result, the repulsive potential determined by

TABLE VII.  Carbon 1s local potential using $^3P$ state orbitals and a CHF 2s.

|     | $k$ | $n_k$ | $c_k$ | $\zeta_k$ |
|-----|-----|-------|-------|-----------|
| $V_p$ | 1 | 0 | 2.4069 | 9.8782 |
|     | 2 | 0 | 0.4061 | 0.8591 |
|     | 3 | -1 | -1.2080 | 10.5732 |
|     | 4 | -1 | -0.3311 | 0.5199 |
| $V_{s-p}$ | 1 | 0 | 23.3711 | 7.6985 |
|     | 2 | 0 | 0.8237 | 1.4383 |
|     | 3 | -2 | 0.2959 | 7.7448 |
|     | 4 | -2 | 0.2196 | 0.5397 |

215

TABLE VIII. Test of carbon 1s local potentials (in eV)

| | Exact | CHF($^3$P) | CHF($^5$S) | CVO($^3$P) | CVO-6G$^c$ Exact | CVO($^3$P) |
|---|---|---|---|---|---|---|
| $E[C(^3P)] - E[C(^5S)]^a$ | 2.45 | 2.10 | 1.89 | 2.31 | 2.30 | 2.30 |
| $E[C_2(^1\Sigma_g^+)] - E[C_2(^3\Sigma_u^+)]^b$ | 0.88 | 0.96 | 0.89 | 0.01 | 0.63 | 1.57 |

[a]Open shell HF wavefunction with (11s, 7p) basis.

[b]GVB(1) wavefunction with STO-6G basis at R = 1.2 Å.

[c]STO-6G basis recontracted for the C($^3$P) state using the CVO($^3$P) local potential.

the 2s CVO,which prevents the 2s orbital from collapsing into core, extends into regions where a 2s Slater function has significant character. Consequently, the 2s Slater function is destabilized. Since the 2s CHF orbital behaves like a 2s Slater function as $r \to 0$, the repulsive potential determined by the 2s CHF is tighter and no problems arise. We tried to overcome this problem by recontracting the STO-6G expansion of the 2s orbital to accomodate the repulsive part of the CVO local potential. An HF calculation on the carbon $^3P$ state with the CVO local potential was carried out using an uncontracted STO-6G basis. The resulting 2s and 2p orbital coefficients were fixed to give a new contraction, denoted CVO-6G. However, the results on $C_2$ were still terrible, as shown in Table VIII, with errors of 0.9 eV in the splitting energy. Therefore, we decided to abandon the 2s CVO orbitals and return to the 2s CHF which, at least, provided better results for the $C_2$ molecule.

Analysis of the differences between HF $V_{val}^S$ and CHF $V_{val}^S$ showed that they would be much smaller for the $^5S$ state than for the $^3P$. Moreover, the coupling of the valence electrons in the $^5S$ state is closer to the coupling normally found in molecular carbon. Therefore, we decided to calculate a local potential using the orbitals from the $^5S$ state. The 2s CHF orbital for the $^5S$ state was constructed in a manner analogous to that for the $^3P$. The $V_p$ and $V_{s-p}$ potentials were again fit with four gaussians each. The parameters are shown in Table IX. The results for the $^3P$ - $^5S$ splitting are actually worse with $^5S$ local potential, while they are excellent for the $^1\Sigma_g^+$ - $^3\Sigma_u^+$ splitting (cf. Table VIII). In Table X, more de-

TABLE IX.   Carbon 1s local potential using $^5S$ state orbitals and a
CHF 2s.

|  | k | $n_k$ | $c_k$ | $\zeta_k$ |
|---|---|---|---|---|
| $V_p$ | 1 | 0 | 1.0221 | 9.8903 |
|  | 2 | 0 | 0.1221 | 0.6088 |
|  | 3 | -1 | -1.1563 | 10.6134 |
|  | 4 | -1 | -0.1137 | 0.3265 |
| $V_{s-p}$ | 1 | 0 | 23.7940 | 7.6985 |
|  | 2 | 0 | 0.9983 | 1.5383 |
|  | 3 | -2 | 0.3293 | 7.7448 |
|  | 4 | -2 | 0.1580 | 0.2397 |

TABLE X.  $C_2(^1\Sigma_g^+)$ GVB(1) results using the $^5$S local potential (in a.u.)

|  | R = 1.2 Å | | R = 1.4 Å | | R = 1.6 Å | |
|---|---|---|---|---|---|---|
|  | Ab initio | Loc Pot | Ab initio | Loc Pot | Ab initio | Loc Pot |
| Total E | -10.5920[a] | -10.5805 | -10.5581[a] | -10.5454 | -10.4646[a] | -10.4488 |
| $1\sigma_g$ O.E. | - 1.030 | - 0.998 | - 0.943 | - 0.913 | - 0.875 | - 0.848 |
| $2\sigma_g$ O.E. | - 0.690 | - 0.688 | - 0.731 | - 0.723 | - 0.783 | - 0.769 |
| $1\sigma_u$ O.E. | - 0.571 | - 0.565 | - 0.567 | - 0.561 | - 0.572 | - 0.563 |
| $1\pi_{ux}$ O.E. | - 0.435 | - 0.430 | - 0.369 | - 0.363 | - 0.320 | - 0.314 |
| $1\pi_{uy}$ O.E. | - 0.435 | - 0.430 | - 0.369 | - 0.363 | - 0.320 | - 0.314 |
| $E(^3\Sigma_u^+)-E(^1\Sigma_g^+)$[b] | 0.88 | 0.89 | 1.70 | 1.59 | 2.79 | 2.57 |

[a]The energy of the 1s core orbitals is not included.

[b]in eV.

tailed results for $C_2$ using the $^5S$ local potential are presented. The quality of the results degrade as the internuclear separation increases, which is to be expected in light of the poor results for carbon atom. Nevertheless, except for the most lightly bound orbital (the $1\sigma_g$), the orbital energies are reproduced to within 10 mh = 0.3 eV.

The $^5S$ local potential was also tested with GVB(2/PP) wavefunctions for the ethylene N and T states in the planar and perpendicular geometries. The results, shown in Table XI, are better than expected. [38,39] The vertical excitation energies and rotational barriers are reproduced to within 0.03 eV, while the orbital energies are in very good agreement with <u>ab initio</u> results except for the most tightly bound orbitals. Therefore, we may conclude that the $^5S$ local potential is good enough for use with our approximate integral methods.

### 3. AI/O Calculations Using Local Potentials

Introducing local potentials into AI/O requires a few changes. To begin with, the valence 2s and 2p are not orthogonalized to the 1s orbitals prior to Löwdin orthogonalization. As a consequence, the kinetic energy of the OAO's, especially the 2s, decreases significantly. Next, evaluation of the gaussian local potential integrals over Slater orbitals is quite cumbersome. To avoid this problem, an STO-6G basis,[35] which entails a least-squares fit of six gaussian primitives to each Slater-type orbital (STO), is used. The STO-6G basis reproduces the results of a Slater MBS very well.[35] The resulting integrals over OAO's for diatomic fragments, e.g., $C_2$, CH, $O_2$, are fit with analytic functions as in Section II.C.

Using the parametric fits for the one-electron integrals

TABLE XI. $C_2H_4$ N state GVB(2/PP) results using the $^5S$ local potential (in a.u.).

| | | | Planar[a] | | Perpendicular[b] | |
|---|---|---|---|---|---|---|
| | | | ab initio | Loc Pot | ab initio | Loc Pot |
| | Total E | | $-13.1899^c$ | $-13.1681$ | $-13.0879^c$ | $-13.0656$ |
| | $1a_g(1a_1)^d$ | O.E. | $-0.855$ | $-0.824$ | $-0.847$ | $-0.816$ |
| | $2a_g(2a_1)$ | O.E. | $-0.730$ | $-0.732$ | $-0.690$ | $-0.694$ |
| | $1b_{1u}(1b_2)$ | O.E. | $-0.776$ | $-0.766$ | $-0.777$ | $-0.767$ |
| | $2b_{1u}(2b_2)$ | O.E. | $-1.824$ | $-1.839$ | $-1.659$ | $-1.665$ |
| | $1b_{2u}(1e_1)$ | O.E. | $-0.634$ | $-0.634$ | $-0.571$ | $-0.571$ |
| | $1b_{3g}(1e_2)$ | O.E. | $-0.494$ | $-0.495$ | $-0.571$ | $-0.571$ |
| | $1b_{3u}(2e_1)$ | O.E. | $-0.412$ | $-0.412$ | $-0.366$ | $-0.366$ |
| | $1b_{2g}(2e_2)$ | O.E. | $-0.704$ | $-0.705$ | $-0.366$ | $-0.366$ |
| $\sigma_{CC}$ pair | $c(2a_g)$ | | $0.998$ | $0.998$ | $0.998$ | $0.997$ |
| | $c(2b_{1u})$ | | $-0.059$ | $-0.062$ | $-0.069$ | $-0.072$ |
| | $S$ | | $-0.888$ | $-0.883$ | $-0.871$ | $-0.865$ |
| | $\Delta E(eV)$ | | $0.21$ | $0.23$ | $0.25$ | $0.27$ |
| $\pi$ pair | $c(1b_{3u})$ | | $0.971$ | $0.971$ | | |
| | $c(1b_{2g})$ | | $-0.240$ | $-0.229$ | | |
| | $S$ | | $-0.603$ | $-0.618$ | | |
| | $\Delta E(eV)$ | | $1.06$ | $1.01$ | | |
| $N \rightarrow T(0°)^e$ | | | $4.69$ | $4.72$ | | |
| $T \rightarrow N(90°)^e$ | | | $0.05$ | $0.05$ | | |
| N rotational barrier[e] | | | $2.78$ | $2.79$ | | |
| T rotational barrier[e] | | | $-1.97$ | $-1.98$ | | |

[a] $R_{CC} = 1.338$ Å

[b] $R_{CC} = 1.41$ Å

[c] The energy of the 1s core orbitals is not included.

[d] Orbital designation for the perpendicular geometry.

[e] in eV.

$(\alpha, \beta$ and $V_{AB})$ and the two-electron integrals evaluated over AO's, the N and T states of ethylene were calculated as before. (As in Section II.C all three-center potential integrals are neglected and only coulomb and one-center exchange integrals are retained from the two-electron integrals.) The results in Table XII are very similar to those obtained using the 2J-K potential for the 1s orbitals (cf. Table V). This is not unexpected. The orbital energies (except for the $2a_g$) are all too high by $\sim 0.2$ a.u., so that the ionization potentials will be too small. As a test, we performed a GVB(2/PP) calculation on the $^2B_{3u}$ $\pi$ cation. The calculated ionization potential was 4.60 eV, while Koopmans' theorem[40] gave 5.17 eV compared to the ab initio value of 11.21 eV. The calculated rotational barriers for the N and T state are in error by $\sim 1$ eV. The results for the rotational barriers are better than when the $\alpha$ integrals are evaluated over AO's and the $V_{AB}$ integrals are set equal to $-Z_B\gamma_{AB}$ (cf. Table V). However, they are still quite poor and indicate further modifications in AI/O are warranted.

Other than neglecting three-center potential terms, the only approximation being made for the one-electron integrals is evaluation of the OAO integrals for diatomic fragments rather than for the molecule as a whole. Assuming for the moment that this approximation is valid (It will be considered in Section III.), attention should be focused on the two-electron integrals. Since we do not want to retain any three- or four-center two-electron integrals, only the one- and two-center terms will be considered. Previously, two approximations have been invoked for the two-electron integrals: (1) only

TABLE XII. $C_2H_4$ N state GVB(2/PP) AI/O-local potential results (in a.u.)

| | | Planar[a] | | | Perpendicular[b] | |
|---|---|---|---|---|---|---|
| | | LocPot | AI/O[c] | AI/O[d] | LocPot | AI/O[c] |
| | Total E | -13.1681 | -12.5507 | -12.5377 | -13.0656 | -12.5045 |
| | $1a_g(1a_1)$[e] O.E. | - 0.824 | - 0.596 | - 0.604 | - 0.816 | - 0.632 |
| | $2a_g(2a_1)$ O.E. | - 0.732 | - 0.937 | - 1.015 | - 0.694 | - 0.842 |
| | $1b_{1u}(1b_2)$ O.E. | - 0.766 | - 0.519 | - 0.558 | - 0.767 | - 0.541 |
| | $2b_{1u}(2b_2)$ O.E. | - 1.839 | - 2.004 | - 2.140 | - 1.665 | - 1.739 |
| | $1b_{2u}(1e_1)$ O.E. | - 0.634 | - 0.524 | - 0.597 | - 0.571 | - 0.413 |
| | $1b_{3g}(1e_2)$ O.E. | - 0.495 | - 0.269 | - 0.354 | - 0.571 | - 0.413 |
| | $1b_{3u}(2e_1)$ O.E. | - 0.412 | - 0.190 | - 0.259 | - 0.366 | - 0.136 |
| | $1b_{2g}(2e_2)$ O.E. | - 0.705 | - 0.446 | - 0.515 | - 0.366 | - 0.136 |
| $\sigma_{CC}$ pair | $c(2a_g)$ | 0.998 | 0.997 | 0.995 | 0.997 | 0.996 |
| | $c(2b_{1u})$ | - 0.062 | - 0.078 | - 0.101 | - 0.072 | - 0.093 |
| | S | - 0.883 | - 0.855 | - 0.816 | - 0.865 | - 0.829 |
| | $\Delta E$(eV) | 0.23 | 0.36 | 0.64 | 0.27 | 0.43 |
| $\pi$ pair | $c(1b_{3u})$ | 0.971 | 0.971 | 0.952 | | |
| | $c(1b_{2g})$ | - 0.229 | - 0.238 | - 0.307 | | |
| | S | - 0.618 | - 0.606 | - 0.512 | | |
| | $\Delta E$ (eV) | 1.01 | 0.89 | 1.62 | | |
| N → T (0°)[f] | | 4.72 | 4.22 | 3.57 | | |
| T → N (90°)[f] | | 0.05 | 0.02 | | | |
| N rotational barrier[f] | | 2.79 | 1.26 | | | |
| T rotational barrier[f] | | - 1.98 | - 2.99 | | | |

[a] $R_{CC}$ = 1.338 Å

[b] $R_{CC}$ = 1.41 Å

[c] Two-electron integrals evaluated over AO's.

[d] Two-electron integrals include fitted correction to account for transformation to OAO's.

[e] Orbital designation for the perpendicular geometry.

[f] in eV.

coulomb and one-center exchange integrals are retained and (2) these integrals are evaluated over AO's rather than OAO's. We will consider the latter approximation first.

As discussed in Section II.C the coulomb integrals do change significantly when evaluated over OAO's, the one-center terms increasing relative to the AO value and the two-center terms decreasing. The two trends appear to cancel one another, so that evaluation over AO's will not introduce significant errors. In Section III.A, this argument is shown to have some validity for doubly-occupied HF orbitals, but not for GVB or open shell HF orbitals. For example, analysis of the energy expression for GVB pairs that describe bonds reveals terms involving the difference of one- and two-center coulomb integrals. It is clear that evaluation of the coulomb integrals over AO's will greatly underestimate the value of this difference and may lead to a poor description of the GVB pair.

Therefore, we decided to evaluate the two-electron integrals over OAO's in a manner analogous to that used for the $\alpha$ integrals. The differences between the values of the two-electron integrals over AO's and over OAO's were determined for diatomic fragments at various internuclear separations. These differences were then fit with simple exponentials. There is an additional problem for the two-electron integrals with regard to rotational invariance. For example, the integrals <ss|zz> and <ss|xx> (either one- or two-center) over OAO's are not equal (cf. Table IV). Consequently, when the diatomic coordinate system is rotated to coincide with the molecular system, the transformed integral, <s's'|x'z'>, in the molecular system will be non-zero.

For example, consider a rotation of 45° about the y-axis so that

$$s' = s$$

$$x' = (x-z)/\sqrt{2}$$

$$z' = (x+z)/\sqrt{2}$$

and

$$\langle s's'|x'z'\rangle = \frac{1}{2}\langle ss|(x-z)(x+z)\rangle$$

$$= \frac{1}{2}(\langle ss|xx\rangle - \langle ss|zz\rangle) \neq 0$$

This problem may be overcome by spherically averaging the OAO integrals in the diatomic coordinate system, e.g., we replace $\langle ss|xx\rangle$, $\langle ss|yy\rangle$ and $\langle ss|zz\rangle$ with $\frac{1}{3}(\langle ss|xx\rangle + \langle ss|yy\rangle + \langle ss|zz\rangle)$ so that $\langle s's'|x'z'\rangle = 0$ as desired.

The results on the planar N and T states of ethylene are shown in Table XII for introducing the spherically averaged OAO corrections to the two-electron integrals. If anything, the results are worse than when the two-electron integrals are evaluated over AO's. Note that the descriptions of the GVB $\pi$ and $\sigma_{CC}$ pairs change drastically, as expected. However, the descriptions are now worse than before. Apparently we have disrupted a favorable cancellation of errors.

The only conclusion that can be drawn is that additional two-electron integrals need to be retained, if better results are to be achieved. The largest two-electron integrals that are being neglected have the form $\langle \mu_A \nu_A | \rho_A \rho_A \rangle$, $\langle \mu_A \nu_A | \rho_B \rho_B \rangle$ and $\langle \mu_A \nu_B | \rho_A \rho_A \rangle$, ranging in size from 4 to 40 mh. Motivation to retain these "hybrid"

integrals may be found in the fact that they serve to balance the potential integrals $\langle \mu_A | v_A | v_A \rangle$, $\langle \mu_A | v_B | v_A \rangle$ and $\langle \mu_A | v_A | v_A \rangle$ which are present in AI/0. Inclusion of these integrals implies going beyond INDO and AI/0 to a higher level of approximation (AI/1). Therefore, it seems appropriate to start from scratch in order to determine which integrals must be retained and which may be neglected. Further modifications of AI/0 are gropings in the dark, since the validity of each of the approximations made in AI/0 are not really known.

### D. Summary

Previous calculations on $O_3$,[14] $CH_2$ and $C_2H_4$[15] using INDO in conjunction with correlated wavefunctions revealed four major weaknesses in the INDO integral approximation: (1) calculated bond lengths too short by 0.1 to 0.2 Å, (2) closed or ring-like geometries artificially favored over open geometries by as much as 6 eV, (3) the empirical parameterization of one-center exchange integrals, and (4) the employment of only one $\beta$ parameter operation. Nevertheless, some of the results, such as calculated bond angles, were quite reasonable. Therefore, we tried to correct the deficiencies of INDO, retaining the basic truncated set of integrals.

Non-empirical evaluation of the one-center integrals over AO's and reparameterization of the $\beta$'s, so that they corresponded to actual diatomic integrals over OAO's, greatly improved the description of the $\pi \to \pi^*$ transitions in $C_2H_4$ and led to more reasonable calculated bond lengths for $C_2$ and $O_2$. However, the N and T state rotational barriers were poorly described and the bias toward the ring

state of ozone was enhanced rather than diminished.

When the $\beta$ integrals were calculated for diatoms, the valence Slater AO's were orthogonalized only to the core orbitals (1s) on the same center prior to transformation over OAO's. Orthogonalization to the core orbitals on both centers is required to ensure proper core-valence electron separation. In addition, the core electrons should be represented by a 2J-K potential rather than a C/r potential. When the correct core orthogonalization is carried out with a 2J-K potential, the resulting integrals over valence OAO's are significantly different. The $\beta$ integrals are no longer proportional to the overlap integrals as assumed in INDO. Instead the $\beta$ integrals have an exponential dependence on R. This led us to institute a new procedure for evaluating the $\beta$ integrals.

The integrals for a diatomic fragment, e.g., $C_2$, CH, $H_2$, were transformed over OAO's at a set of selected internuclear separations, chosen to span the range of bond lengths normally encountered in molecules, e.g., for $C_2$, R = 1.2, 1.4, 1.6 Å were used. The OAO integrals were then least-squared fit with a simple exponential $Be^{-AR}$. The parameters A and B, stored in our integral program, were then used to generate the $\beta$ integrals. The least-squares fits led to standard deviations of < 3mh = 0.01 eV.

Similar procedures were used for the $\alpha$ and $V_{AB}$ integrals. The $\alpha$ integrals over OAO's increase algebraically as R decreases because of the additional kinetic energy arising from orthogonalization. This destabilization ($\Delta\alpha$) of the $\alpha$ integrals relative to their AO values, neglected in INDO, may explain the bias toward closed geometries

found with INDO. The $\Delta\alpha$ corrections are again easily fit with a simple exponential $Be^{-AR}$, while the $V_{AB}$ integrals may be fit with $-Z/R + e^{-AR}(B + Z/R)$.

Implementation of the parametric fits for the one-electron integrals (the two-electron integrals still being evaluated over AO's) led to good vertical excitation energies, but poor rotational barriers and ionization potentials for ethylene. Basically the same results were obtained, when the 2J-K potential for the core electrons was replaced with a local potential, obviating the need to orthogonalize the valence orbitals to the core. Finally, the effects of trans- forming the coulomb and one-center exchange integrals to OAO's were taken into account via parametric fits with simple exponentials. Inclusion of these two-electron corrections did not improve the results for ethylene.

In conclusion, the AI/O schemes that we have developed lead to much better descriptions of vertical $\pi \to \pi^*$ transitions in ethylene and benzene than INDO. However, the description of the rotational barriers in ethylene are less satisfactory, while the ionization po- tentials are quite poor. Nevertheless, further tests on other systems such as $O_3$ and $CH_2$ are warranted to determine whether AI/O provides a significantly better alternative to INDO for determining potential curves. It is expected that the inclusion of the $\Delta\alpha$ destabilization corrections will alleviate the bias toward closed geometries. Finally, the origin of the poor orbital energies in ethylene is not understood. This problem will be pursued in Section III.

## III. APPROXIMATE INTEGRAL METHODS: A GENERAL INVESTIGATION

In this section we consider the effect of truncating ab initio integral sets in various ways in order to design a fast, reliable approximate integral method. The simplest molecular system, $H_2$, is investigated first. Then progressively more complex systems $H_3$, $C_2$ and $O_2$ and finally $C_2H_4$ and $O_3$ are studied. This graduated approach will, hopefully, serve to delineate not only the deficiencies of the approximations, but also the source of the deficiencies.

### A. $H_2$

#### 1. Wavefunctions and Energy Expressions

The great advantage of studying the $H_2$ molecule is that the number of integrals is so small and the energy expressions so simple that one can follow exactly the effect of each approximation. Three different states will be considered, namely, the ground state $^1\Sigma_g^+$, lowest triplet $^3\Sigma_u^+$ and lowest cation $^2\Sigma_g^+$. For the ground state, both the HF and GVB wavefunctions will be used

$$\psi^{HF}(^1\Sigma_g^+) = \frac{1}{\sqrt{2}} \phi_g\phi_g(\alpha\beta - \beta\alpha) \tag{23}$$

$$\psi^{GVB}(^1\Sigma_g^+) = \frac{1}{\sqrt{2}} (c_g\phi_g\phi_g - c_u\phi_u\phi_u)(\alpha\beta-\beta\alpha) \tag{24a}$$

$$= \frac{1}{2\sqrt{1+S_{ab}^2}}(\phi_a\phi_b-\phi_b\phi_a)(\alpha\beta-\beta\alpha) \tag{24b}$$

where

$$\phi_g = (\chi_a + \chi_b)/\sqrt{1 + S}$$

$$\phi_u = (\chi_a - \chi_b)/\sqrt{1 - S}$$

$$\phi_a = (\sqrt{c_g}\phi_g + \sqrt{c_u}\phi_u)/\sqrt{c_g + c_u}$$

$$\phi_b = (\sqrt{c_g}\phi_g - \sqrt{c_u}\phi_u)/\sqrt{c_g + c_u}$$

$$S_{ab} \equiv \langle\phi_a|\phi_b\rangle = (c_g - c_u)/(c_g + c_u)$$

$$S \equiv \langle\chi_a|\chi_b\rangle$$

and $\chi_a$ and $\chi_b$ are 1s Slater orbitals (orbital exponent = 1.2), centered on the left and right hydrogens, respectively. The triplet state wavefunction is

$$\Psi(^3\Sigma_u^+) = \tfrac{1}{2}(\phi_g\phi_u - \phi_u\phi_g)(\alpha\beta+\beta\alpha) \tag{25a}$$

$$= \frac{1}{2\sqrt{1-S_{ab}^2}}(\phi_b\phi_a - \phi_a\phi_b)(\alpha\beta+\beta\alpha) \tag{25b}$$

and the cation wavefunction is

$$\Psi(^2\Sigma_g^+) = \phi_g\alpha \tag{26}$$

Using these wavefunctions, the energy expressions are as follows:

$$E^{HF}(^1\Sigma_g^+) = (t_{aa} + 2t_{ab} + t_{bb} + v_{aa} + 2v_{ab} + v_{bb})/(1 + S)^2$$

$$+ (J_{aa} + 2J_{ab} + J_{bb} + 4L_{ab} + 4K_{ab} + 4L_{ba})/4(1 + S)^4 + \frac{1}{R} \tag{27}$$

where $\quad t_{ab} \equiv <a|t|b>$

$$v_{ab} \equiv <a|v|b>$$

$$J_{ab} \equiv <aa|bb>$$

$$K_{ab} \equiv <ab|ab>$$

$$L_{ab} \equiv <aa|ab>$$

$$E^{GVB}(^1\Sigma_g^+) = c_g^2 E_{gg} - 2c_g c_u K_{gu} + c_u^2 E_{uu} \quad , \tag{28}$$

where $\quad E_{gg} = E^{HF}(^1\Sigma_g^+)$ ,

$$E_{uu} = (t_{aa} - 2t_{ab} + t_{bb} + v_{aa} - 2v_{ab} + v_{bb})/(1 - S)^2$$

$$+ (J_{aa} + 2J_{ab} + J_{bb} - 4L_{ab} + 4K_{ab} - 4L_{ba})/4(1-S)^4 + \frac{1}{R} \quad , \tag{29}$$

$$K_{gu} = \langle \phi_g \phi_u | \phi_u \phi_g \rangle = (J_{aa} - 2J_{ab} + J_{bb})/4[(1+S)^2(1-S)^2] \qquad (30)$$

$$E(^3\Sigma_u^+) = (t_{aa} - 2St_{ab} + t_{bb} + v_{aa} - 2Sv_{ab} + v_{bb} + J_{ab} - K_{ab})/(1-S^2) + \frac{1}{R} \; , \qquad (31)$$

$$E(^2\Sigma_g^+) = (t_{aa} + 2t_{ab} + t_{bb} + v_{aa} + 2v_{ab} + v_{bb})/2(1+S) + \frac{1}{R} \; . \qquad (32)$$

## 2. Transformation to Löwdin OAO's

In Section II, the integrals were transformed over OAO's under the premise that the validity of the ZDO approximation improved in the transformed basis. The foundation for this idea may be seen as follows. The expectation value of the unit operator, I, is just the overlap, so that in the orthogonal basis we have,

$$\langle \mu | I | \nu \rangle = \langle \mu | \nu \rangle = \delta_{\mu\nu} \qquad (33)$$

Replacing the unit operator with the nuclear attraction $[v = \sum_A (Z_A/r_A)]$ or electron repulsion operator $(1/r_{12})$ is expected to alter (33) but not drastically, so that

$$\langle \mu | v | \nu \rangle \cong \delta_{\mu\nu} \langle \mu | v | \mu \rangle \qquad (34a)$$

and

$$\langle \mu\nu | \lambda\sigma \rangle \cong \delta_{\mu\nu}\delta_{\lambda\sigma} \langle \mu\mu | \nu\nu \rangle \qquad (34b)$$

In Table XIII, the integrals for $H_2$ over AO's and OAO's are presented for various internuclear separations. The $v_{ab}^A$ ($\equiv \langle a | v_A | b \rangle$), $K_{ab}$ and

TABLE XIII. $H_2$ integrals over AO's and OAO's (in a.u.).

| $R(a_o)$ | | $t_{aa}$ | $t_{ab}$ | $v_{aa}^A$ | $v_{aa}^B$ | $v_{ab}^A$ | $J_{aa}$ | $J_{ab}$· | $K_{ab}$ | $L_{ab}$ |
|------|-----|--------|--------|--------|--------|--------|--------|--------|--------|--------|
| 1.2 | AO | 0.720 | 0.298 | -1.200 | -0.719 | -0.694 | 0.750 | 0.598 | 0.375 | 0.501 |
|     | OAO | 1.109 | -0.525 | -1.348 | -0.631 | 0.040 | 0.846 | 0.507 | 0.012 | -0.006 |
| 1.4 | AO | 0.720 | 0.233 | -1.200 | -0.648 | -0.599 | 0.750 | 0.560 | 0.303 | 0.443 |
|     | OAO | 1.033 | -0.464 | -1.328 | -0.580 | 0.044 | 0.832 | 0.484 | 0.011 | -0.006 |
| 1.6 | AO | 0.720 | 0.179 | -1.200 | -0.586 | -0.514 | 0.750 | 0.523 | 0.240 | 0.387 |
|     | OAO | 0.970 | -0.412 | -1.308 | -0.534 | 0.047 | 0.820 | 0.460 | 0.010 | -0.006 |
| 1.8 | AO | 0.720 | 0.133 | -1.200 | -0.532 | -0.437 | 0.750 | 0.488 | 0.187 | 0.336 |
|     | OAO | 0.919 | -0.367 | -1.290 | -0.494 | 0.048 | 0.809 | 0.437 | 0.009 | -0.006 |
| 2.5 | AO | 0.720 | 0.036 | -1.200 | -0.396 | -0.239 | 0.750 | 0.384 | 0.070 | 0.193 |
|     | OAO | 0.805 | -0.245 | -1.242 | -0.385 | 0.045 | 0.780 | 0.363 | 0.006 | -0.007 |

$L_{ab}$ integrals decrease dramatically (by factors of 10 to 100) when transformed over OAO's. On the other hand, the $v_{aa}$, $J_{aa}$ and $J_{ab}$ integrals change by less than 15%. Therefore, transformation to OAO's does indeed improve the validity of the ZDO approximation.

Examination of Table XIII reveals that the off-diagonal kinetic energy integrals decrease algebraically, but increase in magnitude when transformed over OAO's. This behavior is diametrically opposed to that of the potential integrals and has its origin in the nature of the kinetic energy operator. Using the explicit form for the kinetic energy operator, namely, $-(1/2)\nabla^2$, we have

$$\langle \bar{a}|t|\bar{b}\rangle = -\frac{1}{2}\langle\bar{a}|\nabla^2|\bar{b}\rangle = \frac{1}{2}\langle\nabla\bar{a}\cdot\nabla\bar{b}\rangle \tag{35}$$

where the bars, e.g., $\bar{a}$, denote OAO's. For $H_2$ the relationship between the OAO's and AO's is given by

$$\bar{a} = (a - \lambda b)/\sqrt{1 + \lambda^2} \tag{36a}$$

$$\bar{b} = (b - \lambda a)/\sqrt{1 + \lambda^2} \tag{36b}$$

where $\lambda = (1- \sqrt{1-S^2})/S$ and $S = \langle a|b\rangle$. Substituting (36) into (35) leads to (using $\langle a|t|a\rangle = \langle b|t|b\rangle$)

$$\langle\bar{a}|t|\bar{b}\rangle = [(1+\lambda^2)\langle a|t|b\rangle - 2\lambda\langle a|t|a\rangle]/(1+\lambda^2) \tag{37}$$

But $S = 2\lambda/(1 + \lambda^2)$, so that (37) becomes

$$\langle \bar{a}|t|\bar{b}\rangle = \langle a|t|b\rangle - S\langle a|t|a\rangle$$

$$=(\langle \nabla a \cdot \nabla b\rangle - S\langle \nabla a \cdot \nabla a\rangle)/2 \qquad (38)$$

Previous work on $H_2$ [41] has shown that $S\langle a|t|a\rangle$ dominates $\langle a|t|b\rangle$. Since $S\langle a|t|a\rangle$ is positive, (38) indicates that $\langle \bar{a}|t|\bar{b}\rangle$ is negative (as shown in Table XIII). The reason why $S\langle a|t|a\rangle$ dominates is that $\nabla a \cdot \nabla a$ is, of course, positive everywhere, while $\nabla a \cdot \nabla b$ may be negative or positive depending on the relative phase of the gradients of a and b. In fact, it has been shown that the contragradience of a and b, i.e., the region where $\nabla a \cdot \nabla b < 0$, is directly correlated with the strength of the chemical bond in $H_2$. [41] Consequently, the off-diagonal kinetic energy integrals, $t_{ab}$, should not be neglected in any approximate integral scheme. [42]

### 3. Integral Approximations

From Table XIII it is clear that neglecting the two-electron exchange and hybrid integrals ($K_{ab}$ and $L_{ab}$) should be a good approximation. The results in Tables XV - XVII bear this expectation out for the singlet and triplet states of $H_2$. Note that the errors increase for the singlet from 1 to 6 mh as R increases from 1.2 to $2.5a_0$, while those for the triplet decrease from 11 to 6 mh. Invoking the ZDO approximation for the $v_{ab}$ integrals is expected to lead to worse results, since the neglected integrals are larger. In fact, neglecting $v_{ab}$ leads to 80 - 90 mh (2 to 2½ eV) errors in the $H_2^+$ potential curve (cf. Table XIV). The errors double for singlet $H_2$, since $v_{ab}$ appears twice in the

TABLE XIV.   $H_2^+(^2\Sigma_g^+)$ energies (in a.u.).

| | R($a_0$) | | | | |
|---|---|---|---|---|---|
| | 1.2 | 1.4 | 1.6 | 1.8 | 2.5 |
| Ab initio | -0.480 | -0.536 | -0.566 | -0.580 | -0.578 |
| Neglect $v_{ab}$ | -0.558 | -0.623 | -0.659 | -0.676 | -0.667 |

TABLE XV.    $H_2$ ($^1\Sigma_g^+$) HF energies (in a.u.)·

|  | $R(a_0)$ | | | | |
|---|---|---|---|---|---|
|  | 1.2 | 1.4 | 1.6 | 1.8 | 2.5 |
| Ab initio · | -1.118 | -1.128 | -1.118 | -1.096 | -0.993 |
| Neglect $K_{ab}$, $L_{ab}$ | -1.120 | -1.128 | -1.116 | -1.093 | -0.984 |
| Neglect $v_{av}$, $K_{ab}$, $L_{ab}$ | -1.276 | -1.303 | -1.302 | -1.284 | -1.162 |
| J's over AO's | -1.120 | -1.131 | -1.121 | -1.101 | -0.997 |
| Neglect $K_{ab}$, $L_{ab}$; J's over AO's | -1.122 | -1.131 | -1.120 | -1.098 | -0.988 |

TABLE XVI.  $H_2$ $(^1\Sigma_g^+)$ GVB energies (in a.u.).

| | R(a$_0$) | | | | |
|---|---|---|---|---|---|
| | 1.2 | 1.4 | 1.6 | 1.8 | 2.5 |
| Ab initio | -1.134 | -1.148 | -1.142 | -1.127 | -1.053 |
| Neglect $K_{ab}$, $L_{ab}$ | -1.135 | -1.148 | -1.141 | -1.124 | -1.047 |
| Neglect $V_{ab}$, $K_{ab}$, $L_{ab}$ | -1.289 | -1.319 | -1.322 | -1.308 | -1.204 |
| J's over AO's | -1.124 | -1.137 | -1.131 | -1.116 | -1.045 |
| Neglect $K_{ab}$, $L_{ab}$; J's over AO's | -1.125 | -1.137 | -1.130 | -1.113 | -1.038 |

TABLE XVII.  $H_2$ $(^3\Sigma_u^+)$ energies (in a.u.).

| | R($a_0$) | | | | |
|---|---|---|---|---|---|
| | 1.2 | 1.4 | 1.6 | 1.8 | 2.5 |
| Ab initio | -0.411 | -0.563 | -0.669 | -0.746 | -0.887 |
| Neglect $K_{ab}$, $L_{ab}$ | -0.400 | -0.551 | -0.659 | -0.737 | -0.881 |
| Neglect $v_{ab}$, $K_{ab}$, $L_{ab}$ | -0.400 | -0.551 | -0.659 | -0.737 | -0.881 |
| J's over AO's | -0.321 | -0.486 | -0.606 | -0.695 | -0.866 |
| Neglect $K_{ab}$, $L_{ab}$; J's over AO's | -0.309 | -0.474 | -0.596 | -0.686 | -0.860 |

energy expression (28). However, for triplet $H_2$, $v_{ab}$ may be rigorously neglected, since it appears as $Sv_{ab}$ (and $S = 0$) in the energy expression (31). As a result, neglecting $v_{ab}$ leads to 4 - 4½ eV errors in the $H_2$ singlet-triplet excitation energy. We conclude that the $v_{ab}$ integrals should be retained in our approximate integral scheme.

In many of the available approximate integral methods, e.g., CNDO,[5] INDO,[6] MINDO,[7] NDDO[8] and ESE-MO,[10] the two-electron integrals are evaluated empirically or over AO's rather than over OAO's. From Table XIII, the values of $J_{aa}$ increase upon transformation to OAO's, while those of $J_{ab}$ decrease. In Section II we argued that these effects tended to cancel one another. In fact, we note that the sum $J_{aa} + J_{ab}$, remains relatively unchanged (within 5 to 9 mh) upon transformation to OAO's. This is very convenient, since for the HF singlet $H_2$ wavefunction the J's appear in the energy expression [(27) and (29)] as $J_{aa} + J_{ab}$. Therefore, we performed calculations on $H_2$ using the AO values for J's in conjunction with the full set of OAO one-electron integrals (the $K_{ab}$ and $L_{ab}$ integrals being neglected).

The results in Tables XV - XVII show that using AO values for the coulomb integrals leads to 2 to 4 mh errors for the HF $^1\Sigma_g^+$ energy and 8 to 11 mh errors for the GVB $^1\Sigma_g^+$ energy. The poorer results for the GVB wavefunction may be directly ascribed to errors in $K_{gu}$. From (30) we see that $K_{gu}$ is proportional to the difference of coulomb integrals, which will be significantly underestimated (by as much as 5 eV at 1.2 $a_0$) when atomic values for the J's are used. As a result, the GVB energy calculated from (28) is too high.

Even worse errors (20 to 90 mh) are obtained for the $^3\Sigma_u^+$ state. Again, examination of the energy expression in (31) shows why.

For the $^3\Sigma_u^+$ only the $J_{ab}$ integral appears in (31) and, hence, the discrepancy between the AO and OAO values is manifested directly in the energy.

We conclude that using atomic values for the two-electron integrals may be a good approximation for closed shell HF wavefunctions, but leads to significant errors for GVB and open shell HF wavefunctions. This result illustrates the need to develop approximate methods in conjunction with correlated wavefunctions.

### 4. Invariance of $J_{aa} + J_{ab}$

At this point one might wonder whether the apparent invariance of $J_{aa} + J_{ab}$ under Löwdin orthogonalization was fortuitous or not. In fact, if one expands the transformed coulomb ($J_{\overline{aa}}$, $J_{\overline{ab}}$) integrals in terms of the atomic two-electron integrals and invokes the Mulliken approximation [43]

$$ab = \frac{S}{2}(aa + bb)$$

to express the exchange and hybrid integrals in terms of the atomic coulomb integrals, one finds that $J_{\overline{aa}} + J_{\overline{ab}} = J_{aa} + J_{ab}$ to second order in the overlap integral S. In other words, the invariance is well-founded.

### 5. Importance of Using $t_{aa}$ over OAO's

Before moving on to $H_3$, a few words concerning the bias of previous approximate methods toward closed geometries are warranted.

Table XIII shows that the one-center kinetic energy terms increase significantly (100 to 400 mh!) when transformed to OAO's. The increase is reasonable in that orthogonalization introduces nodes into the orbitals, making them less smooth and, hence, increasing the kinetic energy (recall $<a|t|a> = <\nabla a \cdot \nabla a>$). In addition, the value of $t_{aa}$ increases as R decreases.

Previous approximate integral methods (CNDO,[5] INDO [6] and MINDO [7]) have employed atomic values for $t_{aa}$ (and $v_{aa}$) in conjunction with parametric values for $t_{ab}$ (and $v_{ab}$), which correspond more closely to the OAO integrals. It is not surprising, therefore, that these methods are grossly biased in favor of closed goemetries, since the destabilizing increase in the $t_{aa}$ integrals over OAO's is neglected.

The same problem arose in CNDO/1 calculations by Pople [44] on the $H_2(^3\Sigma_u^+)$ potential curve, which is well known to be strictly repulsive. However, the CNDO/1 calculations led to a bound state with a minimum of -0.637 eV at 0.85 Å! In CNDO/1 the binding energy (BE) of the $^3\Sigma_u^+$ is

$$BE = J_{ab} + 2v_{aa}^B + 1/R \qquad (39)$$

where the atomic values are used for $J_{ab}$ and $v_{aa}^B$. To circumvent this problem, Pople [44] set $v_{aa}^B = - J_{ab}$ (or in his notation $V_{AB} = -\gamma_{AB}$), which amounts to neglecting the penetration of the electron on A through the electron on B to the nucleus, so that (39) becomes

$$BE = 1/R - J_{ab} > 0 \quad \text{for all R} \qquad (40)$$

Thus, the desired repulsive curve was obtained. In Table XVIII we show the calculated BE for $H_2$ ($^3\Sigma_u^+$) using CNDO/1, CNDO/2 ($v_{aa}^B = - J_{ab}$), our scheme, in which the $K_{ab}$ and $L_{ab}$ OAO integrals are neglected and atomic J's are used, and finally the exact results. We see that although CNDO/2 does not lead to a bound $^3\Sigma_u^+$ state, the potential curve is still much too attractive. As a result, CNDO/2 as well as INDO and MINDO are still biased toward closed geometries.

## B. $H_3$

### 1. Truncation of the Ab Initio Integral Set

The $H_3$ molecule provides the simplest test for the approximation of neglecting all three-center integrals. Moreover, the problem of treating open and closed geometries equivalently may be investigated. Towards this end, we considered the $^2\Sigma_u^+$ state of $H_3$ using a GVB(1) wavefunction

$$\Psi(^2\Sigma_u^+) = \alpha\{[c_1(1a_1)^2 - c_2(2a_1)^2]1b_2 \ \alpha\beta\alpha\} \tag{41}$$

Symmetrical geometries were employed with $R_{HH} = 1.883$ a.u., the MBS ab initio saddle point geometry for the linear configuration,[45] and $\theta \equiv < HHH = 180°, 120°, 60°$.

As before, the integrals were transformed over Löwdin OAO's prior to any approximation. Neglecting all three-center OAO integrals leads to ± 15 mh errors as shown in Table XIX. However, if the integrals are not transformed to OAO's and three-center AO integrals are neglected, 70 to 300 mh errors are introduced (cf. Table XIX). Moreover, the

TABLE XVIII.  $H_2(^3\Sigma_u^+)$ binding energies (in a.u.)

|  | $R(a_0)$ | | | | |
| --- | --- | --- | --- | --- | --- |
|  | 1.2 | 1.4 | 1.6 | 1.8 | 2.5 |
| Ab initio | 0.589 | 0.437 | 0.331 | 0.254 | 0.113 |
| CNDO/1 | -0.007 | -0.021 | -0.024 | -0.021 | -0.008 |
| CNDO/2 | 0.235 | 0.154 | 0.102 | 0.068 | 0.016 |
| Neglect $K_{ab}, L_{ab}$; J's over AO's | -0.691 | 0.526 | 0.404 | 0.314 | 0.140 |

TABLE XIX.  $H_3$ $(^2\Sigma_u^+)$ GVB energies for R = $1.883a_0$ (in a.u.).

| | $\theta=180°$ | $\theta=120°$ | $\theta=60°$ |
|---|---|---|---|
| 1.  Ab initio | -1.562 | -1.545 | -1.370 |
| 2.  Neglect 3-ctr. ints. over OAO's | -1.578 | -1.549 | -1.356 |
| 3.  Neglect 3-ctr. ints. over AO's | -1.630 | -1.632 | -1.671 |
| 4.  (3)+ neglect 2-ctr. $K_{ab}$ ints. over OAO's | -1.583 | -1.554 | -1.353 |
| 5.  (4)+neglect 2-ctr. $L_{ab}$ ints. over OAO's | -1.556 | -1.536 | -1.355 |
| 6.  (5) except J's over AO's | -1.549 | -1.510 | -1.290 |
| 7.  (6) + neglect 2-ctr. $V_{ab}$ ints. over AO's | -1.619 | -1.579 | -1.294 |
| 8.  AI/O (fitted 1e⁻ ints.) | -1.470 | -1.460 | -1.297 |
| 9.  AI/O (fitted 1e⁻ and 2e⁻ ints.) | -1.497 | -1.489 | -1.343 |
| 10. (8) except $\alpha$'s over AO's | -1.868 | -1.872 | -1.884 |

calculations are now strongly biased toward the $\theta = 60°$ geometry. The need to transform the integrals over OAO's prior to truncation of the integral set is manifest.

Next we considered disgarding the two-center exchange integrals $(K_{ab})$ while retaining the two-center hybrid integrals $(L_{ab})$. This truncation scheme is identical with that proposed by Brown and Burton [46] and used in their ESE-MO [10] method. However, they employ integrals over AO's, which will cause problems as we have already seen. The results in Tabel XIX indicate that neglecting only $K_{ab}$ integrals leads to slightly larger errors ($\pm$ 20 mh).

Neglecting both the two-center exchange and hybrid integrals gives an integral set comparable to that employed in the AI/O methods developed in Section II, but now the integrals are evaluated exactly over OAO's. The overall errors (6 to 15 mh) are actually less than when the $L_{ab}$ and $K_{ab}$ integrals are retained (cf. Table XIX). This is very encouraging. In addition, the bias of CNDO, INDO and MINDO toward ring states has apparently been overcome.

The next logical step was to test the effect of using atomic J's rather than OAO values. Table XIX shows that using atomic J's increases the errors significantly (13 to 80 mh), the results being worse for $\theta = 60°$. As in the case of the $H_2$ $^1\Sigma_g^+$ state, these errors arise from the poor description of the GVB pair. It is becoming increasingly clear that the coulomb integrals should be evaluated over OAO's in order to provide good GVB and open shell HF wavefunctions.

Although poor results were expected, the $v_{ab}$ integrals were also neglected with the $v_{aa}$ and J integrals evaluated over AO's. The

resulting errors of ± 70 mh in Table XIX confirm our expectations.

## 2. AI/O Methods

Finally, the AI/O schemes developed in Section II.C.3 were applied to $H_3$ in order to test the validity of breaking the molecule into diatomic fragments for evaluation of the integrals over OAO's. Two versions of AI/O were employed, one with parametric fits for the one-electron OAO integrals using two-electron integrals over AO's and the other with parametric fits for both the one- and two-electron OAO integrals. In Table XIX comparison should be made between rows 6 and 8 and between rows 5 and 9. We see that introduction of the parametric fits for the coulomb integrals (row 9 vs 8) leads to approximately the same effect as using coulomb integrals over OAO's instead of AO's (row 5 vs 6). In both cases, deficiencies in the description of the GVB pair are being corrected.

Comparing rows 6 and 8, we see that the method of evaluating the one-electron OAO integrals used in AI/O does introduce significant errors. Moreover, these errors vary drastically with θ, being -7 mh at 60° and + 79 mh at 180°. These errors are disturbing and warrant further analysis.

In Table XX, the exact OAO integrals are compared with the values used in AI/O. Errors of 100 - 200 mh are encountered in the kinetic energy integrals. Smaller errors (40 - 80 mh) in the nuclear attraction integrals tend to compensate those in the kinetic energy, so that the errors in the total one-electron integrals are smaller (10 - 50 mh), except for $\langle \ell | h | r \rangle$ (50 - 100 mh errors). The results for

TABLE XX.  $H_3$ ($R = 1.883a_0$): comparison of <u>ab initio</u> and AI/O OAO integrals (in a.u.).

| | θ = 180° | | θ = 120° | | θ = 60° | |
|---|---|---|---|---|---|---|
| | ab initio | AI/O | ab initio | AI/O | ab initio | AI/O |
| **A. Kinetic energy** | | | | | | |
| $\langle c\|t\|c\rangle^a$ | 1.171 | 1.078 | 1.125 | 1.078 | 0.990 | 1.078 |
| $\langle \ell\|t\|c\rangle$ | 0.910 | 0.920 | 0.898 | 0.936 | 0.990 | 1.078 |
| $\langle c\|t\|\ell\rangle$ | -0.409 | -0.350 | -0.366 | -0.350 | -0.261 | -0.350 |
| $\langle \ell\|t\|r\rangle$ | 0.067 | -0.115 | -0.005 | -0.155 | -0.261 | -0.350 |
| **B. Nuclear attraction** | | | | | | |
| $\langle c\|v_c\|c\rangle$ | -1.401 | -1.362 | -1.384 | -1.362 | -1.327 | -1.362 |
| $\langle \ell\|v_c^\ell\|\ell\rangle$ | -1.287 | -1.296 | -1.283 | -1.305 | -1.327 | -1.362 |
| $\langle c\|v_\ell\|c\rangle$ | -0.511 | -0.479 | -0.498 | -0.479 | -0.476 | -0.479 |
| $\langle \ell\|v_c^\ell\|\ell\rangle$ | -0.479 | -0.479 | -0.479 | -0.479 | -0.476 | -0.479 |
| $\langle \ell\|v_c^r\|\ell\rangle$ | -0.254 | -0.264 | -0.292 | -0.302 | -0.476 | -0.479 |
| $\langle c\|v_c^r+v_\ell\|\ell\rangle$ | 0.122 | 0.096 | 0.100 | 0.096 | 0.056 | 0.096 |
| $\langle \ell\|v_c+v_\ell^r\|r\rangle$ | -0.014 | 0.059 | 0.014 | 0.071 | 0.056 | 0.096 |
| **C. Electron repulsion** | | | | | | |
| $\langle cc\|cc\rangle$ | 0.880 | 0.858 | 0.872 | 0.858 | 0.834 | 0.858 |
| $\langle \ell\ell\|\ell\ell\rangle$ | 0.808 | 0.815 | 0.805 | 0.821 | 0.834 | 0.858 |
| $\langle cc\|\ell\ell\rangle$ | 0.451 | 0.428 | 0.442 | 0.428 | 0.428 | 0.428 |
| $\langle \ell\ell\|rr\rangle$ | 0.242 | 0.258 | 0.279 | 0.292 | 0.428 | 0.428 |
| **D. Total one-electron integrals** | | | | | | |
| $\langle c\|h\|c\rangle$ | -1.253 | -1.242 | -1.256 | -1.242 | -1.288 | -1.242 |
| $\langle \ell\|h\|\ell\rangle$ | -1.109 | -1.117 | -1.155 | -1.148 | -1.288 | -1.242 |
| $\langle c\|h\|\ell\rangle$ | -0.288 | -0.254 | -0.266 | -0.254 | -0.205 | -0.254 |
| $\langle \ell\|h\|r\rangle$ | 0.053 | -0.055 | 0.008 | -0.083 | -0.205 | -0.254 |

[a] c, ℓ, r denote the OAO on the center, left and right hydrogens, respectively.

$\beta_{\ell r} \equiv <\ell|h|r>$ point out a very serious problem in AI/O. Since exponential fits were used to evaluate the $\beta$ integrals, they will never change sign as a function of R. However, for Table XX, $<\ell|h|r>$ is negative at 60°, but positive at 120° and 180° (i.e., at larger R). Consequently, AI/O leads to signficiant errors (90 - 110 mh) at these geometries. This result is a very serious blow against the possible usefulness of the AI/O schemes. (We note in passing, that the best agreement between AI/O and ab initio OAO integrals occurs for the $v_{aa}^B$ and J integrals.)

The results for $H_3$ indicate that the truncated integral set utilized in AI/O may afford a reliable approximate method as long as the integrals are evaluated exactly over OAO's. The only difficulty with this scheme is that when the truncated OAO integral set is expanded in terms of AO's, the full set of AO integrals is involved. Not only must the complete set of AO integrals be calculated, but the transformation to OAO's (especially for the two-electron integrals) is extremely time consuming for large basis sets (50 - 200 functions), vitiating any savings derived from the truncated integral set in the SCF calculations. Procedures for alleviating this problem will be presented in the next section.

## C.  $C_2$ and $O_2$

### 1. Wavefunctions

From the point of view of approximate methods, the key difference between $C_2$ or $O_2$ and $H_2$ is the presence of more than one basis function per atom. Consequently, the question of which integrals should be retained becomes more complex. In addition, the problem of

the core electrons must be dealt with. At least for the moment, the 1s orbitals are disposed of by representing them with a 2J-K potential and orthogonalizing the valence basis functions to the 1s orbitals on both centers. These core-orthogonalized valence orbitals are then transformed to Löwdin OAO's.

Initially, we consider the ground $^1\Sigma_g^+$ and excited $^3\Sigma_u^+$ states of $C_2$. The $^3\Sigma_u^+$ state may be considered as arising from the $1\sigma_u \rightarrow 2\sigma_g$ electron promotion. To obtain a consistent description of this excitation process, the ground state $1\sigma_u$ orbital, doubly-occupied in the HF wavefunction, is split with the $2\sigma_g$ orbital into a GVB pair, i.e.

$$(1\sigma_u)^2 \rightarrow c_1(1\sigma_u)^2 - c_2(2\sigma_g)^2$$

## 2. INDO-like Approximations

The results on $H_2$ indicated that two-center exchange and hybrid integrals may be safely neglected. Therefore, we tried truncating the OAO integral set as it is in INDO,[6] i.e., retaining only coulomb and one-center exchange integrals and neglecting one-electron integrals of the form $\langle\mu_A|h|\nu_A\rangle$. The results in Tables XXI and XXII reveal 0.4 to 0.8 eV errors in the $^1\Sigma_g^+ \rightarrow {}^3\Sigma_u^+$ excitation energy as well as 200 mh errors in the total energy for the ground state. Moreover, there are 60 to 130 mh errors in the orbital energies for the ground state at 1.2 Å (cf. Table XXIV). Needless to say, these results are not satisfactory.

TABLE XXI. $C_2$ $(^1\Sigma_g^+)$ GVB(1) energies (in a.u.)

|  | | R(Å) | |
|---|---|---|---|
|  | 1.2 | 1.4 | 1.6 |
| 1. Ab initio | -75.289 | -75.256 | -75.163 |
| 2. INDO over OAO's | -75.073 | -75.045 | -74.968 |
| 3. (2) except 2e⁻ ints. over AO's | -75.065 | -75.021 | -74.914 |
| 4. (2) + all t ints. | -75.728 | -75.462 | -75.214 |
| 5. (2) + all 1-ctr. 1e⁻ ints. | -75.046 | -75.015 | -74.952 |
| 6. (5) except 2e⁻ ints. over AO's | -75.039 | -74.990 | -74.896 |
| 7. (2) + all 1e⁻ ints. | -75.170 | -75.294 | -75.290 |
| 8. Brown's scheme over OAO's | -75.316 | -75.282 | -75.181 |
| 9. Brown's scheme over AO's | -76.093 | -75.760 | -75.436 |
| 10. Ruedenberg approx. for OAO's | -75.317 | -75.278 | -75.178 |
| 11. Brown-Ruedenberg scheme over OAO's | -75.312 | -75.240 | -75.158 |
| 12. NDDO over OAO's | -75.162 | | |

TABLE XXII. $C_2$ $^1\Sigma_g^+ \to {}^3\Sigma_u^+$ GVB(1) vertical excitation energies (in eV).

|  | | R(Å) | | |
|---|---|---|---|---|
|  | | 1.2 | 1.4 | 1.6 |
| 1. | Ab initio | 0.90 | 1.75 | 2.85 |
| 2. | INDO over OAO's | 1.32 | 2.25 | 3.66 |
| 3. | (2) + all t ints. | 10.67 | 8.51 | 7.59 |
| 4. | (2) + all 1-ctr. 1e⁻ ints. | 0.97 | 1.84 | 3.51 |
| 5. | (4) except 2e⁻ ints. over AO's | 0.96 | 1.39 | 2.36 |
| 6. | Brown's scheme over OAO's | 0.85 | 1.62 | 2.65 |
| 7. | Brown's scheme over AO's | 1.83 | 1.08 | 1.08 |
| 8. | Ruedenberg approx. for OAO's | 1.05 | 1.85 | 2.86 |
| 9. | Brown-Ruedenberg scheme over OAO's | 2.16 | 2.02 | 2.90 |

TABLE XXIII. $O_2$ ($^3\Sigma_g^-$) HF energies (in a.u.)

|  | | R(Å) | |
|---|---|---|---|
|  | 1.2 | 1.4 | 1.6 |
| 1. Ab initio | -149.090 | -149.026 | -148.904 |
| 2. Brown's scheme over OAO's | -149.094 | -149.031 | -148.906 |
| 3. Brown's scheme over AO's | -149.099 | -149.025 | -148.900 |
| 4. Ruedenberg approx. for OAO's | -149.097 | -149.032 | -148.907 |
| 5. Brown-Ruedenberg scheme over OAO's | -149.047 | -149.014 | -148.900 |

TABLE XXIV. $C_2$ ($^1\Sigma_g^+$) GVB(1) orbital energies for R = 1.2Å (in a.u.).

| | Ab initio | (1)[a] | (2)[a] | (3)[a] | (4)[a] | (5)[a] | (6)[a] |
|---|---|---|---|---|---|---|---|
| $1\sigma_g$ O.E. | -1.033 | -0.977 | -0.808 | -0.863 | -1.032 | -1.133 | -0.952 |
| $2\sigma_g$ O.E. | -0.692 | -0.568 | -0.710 | -0.747 | -0.675 | -0.761 | -0.630 |
| $1\sigma_u$ O.E. | -0.572 | -0.441 | -0.600 | -0.643 | -0.561 | -0.554 | -0.538 |
| $1\pi_{ux}$ O.E. | -0.435 | -0.373 | -0.371 | -0.318 | -0.445 | -0.463 | -0.383 |
| $1\pi_{uy}$ O.E. | -0.435 | -0.373 | -0.371 | -0.318 | -0.445 | -0.463 | -0.383 |
| n pair $c(2\sigma_g)$ | -0.463 | -0.417 | -0.460 | -0.454 | -0.476 | -0.352 | -0.534 |
| $c(1\sigma_u)$ | 0.886 | 0.909 | 0.888 | 0.891 | 0.879 | 0.936 | 0.845 |
| S | 0.314 | 0.372 | 0.317 | 0.325 | 0.298 | 0.453 | 0.226 |
| $\Delta E$(eV) | 2.75 | 2.01 | 2.37 | 2.12 | 2.86 | 2.04 | 3.67 |

[a](1) INDO over OAOs; (2) INDO + 1-ctr. 1e⁻ ints. over OAO's; (3) INDO + 1-ctr. 1e⁻ ints. over OAO's, 2e⁻ ints. over AO's; (4) Brown's scheme over OAO's; (5) Brown-Ruedenberg scheme over OAO's and (6) NDDO over OAO's.

The largest integrals that are being neglected are the $\langle \mu_A |h| \nu_A \rangle$ integrals. Therefore, we tried three schemes in which portions of the $\langle \mu_A |h| \nu_A \rangle$ integrals were included in the integral set, namely, (1) retaining $\langle \mu_A |t| \nu_A \rangle$, (2) retaining $\langle \mu_A |t+v_A| \nu_A \rangle$, and (3) retaining $\langle \mu_A |h| \nu_A \rangle$. The results are shown in Tables XXI, XXII and XXIV. Although it is clear from our previous results on $H_2$ and $H_3$ that no kinetic energy integrals should be neglected, retaining just $\langle \mu_A |t| \nu_A \rangle$ leads to horrendous results (errors of 5 to 10 eV in the excitation energy and 50 to 500 mh in the ground state energy). Retaining $\langle \mu_A |t + v_A| \nu_A \rangle$ leads to much better results indicating that one-center t and v integrals must be considered together when truncating. Compared to the INDO OAO results, the calculated excitation energies are significantly improved, while the ground state total and orbital energies are not much better. When all the one-electron integrals are retained, i.e., inclusion of $\langle \mu_A |h| \nu_A \rangle$, the ground state potential curve becomes biased toward longer bond lengths. Since the AI/O schemes developed in Section II were based on this particular truncated set of integrals, the poor results of $C_2$ obtained here, indicate that further calculations with AI/O should be carried out neglecting the $\langle \mu_A |v_B| \nu_A \rangle$ integrals and, perhaps, the $\langle \mu_A |t + v_A| \nu_A \rangle$ integrals.

The effect of not transforming the two-electron integrals was again tested with INDO and INDO + $\langle \mu_A |t+v_A| \nu_A \rangle$ OAO integrals. Using atomic values for the two-electron integrals leads to significantly different excitation energies which are in slightly worse agreement with the ab initio calculations (cf. Table XXII). In

addition, the agreement of the orbital energies with ab initio values deteriorates significantly (cf. Table XXIV).

### 3. Higher-Order Approximations

The results obtained with an INDO set of two-electron integrals are not very satisfactory. Therefore, we decided to investigate two higher-order approximations. The first, proposed by Pople,[8] is called NDDO in which the ZDO approximation is relaxed so that integrals involving monocentric differential overlap are retained, i.e.,

$$\langle \mu_A \nu_B | \lambda_C \sigma_D \rangle = \delta_{AB} \delta_{CD} \langle \mu_A \nu_A | \lambda_B \sigma_B \rangle \tag{42}$$

Accordingly, one-electron integrals of the form $\langle \mu_A | h | \nu_A \rangle$ are retained, i.e., all one- and two-center one-electron integrals are retained. Using the NDDO scheme over OAO's for ground state $C_2$ at $R = 1.2$ Å, we find that the calculated total energy and orbital energies are significantly improved. The errors are now 120 mh for the total energy and 50 mh for the orbital energies. However, the description of the GVB pair is actually much worse (cf. Table XXIV).

An even higher-order approximation has been proposed by Brown,[46] in which one also retains hybrid integrals of the form $\langle \mu_A \nu_B | \lambda_A \sigma_A \rangle$. These integrals tend to balance the $\langle \mu_A | \nu_A | \nu_B \rangle$ integrals. Using Brown's scheme over OAO's, the results are quite good as they should be, since only the small two-center exchange integrals are neglected. The errors have been reduced to 20 mh or less for the total and orbital energies and 0.2 eV or less for the excitation energies.

Brown [46] obtained good results on the ground state of FCN using this truncated integral set over AO's rather OAO's. Therefore, we tried Brown's scheme over AO's for $C_2$. The results were terrible (cf. Tables XXI and XXII). The ground state potential curve displayed 800 mh errors and was strongly biased toward short bond lengths. These results are not unexpected in light of similar findings for $H_3$. It appears as if fortuitous cancellations occurred in the case of FCN.[46] This possibility is supported by open shell HF calculations on the $O_2$ ground state $(^3\Sigma_g^-)$. The agreement with ab initio results is good for calculations using Brown's truncation scheme over both OAO and AO integrals (cf. Table XXIII). However, use of AO integrals does lead to 100 mh errors in the $O_2$ $^3\Sigma_g^-$ orbital energies.

### 4. The Ruedenberg Approximation

It is clear that Brown's scheme will be reliable only for OAO integrals. As mentioned earlier, the entire set of AO integrals must be calculated and transformed in order to obtain the truncated set of OAO integrals. However, Brown [47] has developed a means to avoid calculation of the full set of AO integrals by invoking the Ruedenberg approximation.[48]

The Ruedenberg approximation involves expanding a function on one-center in terms of the functions on another center, i.e.,

$$\mu_A = \sum_\nu \langle \mu_A | \nu_B \rangle \nu_B \qquad (43)$$

Equation (43) is exact if the set $\{\nu_B\}$ is complete. For normal basis

sets this, of course, will not be true, so that (43) is only approximately correct.  Using (43), we may write the bicentric product $\mu_A \nu_B$ as

$$\mu_A \nu_B \cong \frac{1}{2} \left[ \sum_{\rho_B} \langle \mu_A | \rho_B \rangle \rho_B \nu_B + \sum_{\sigma_A} \langle \sigma_A | \nu_B \rangle \mu_A \sigma_A \right] \tag{44}$$

Now (44) provides a means whereby the two-center exchange integrals, $\langle AB | A'B' \rangle$, which we do not want to evaluate in the AO basis, may be expressed in terms of hybrid $\langle AB | A'A'' \rangle$ or NDDO-type integrals $\langle A'A'' | B'B'' \rangle$, which are calculated.  Using the Ruedenberg approximation one can express all the integrals in terms of NDDO-type integrals.  However, we have found that using the exact values for the two-center hybrid integrals, rather than approximate Ruedenberg values, leads to better results for the two-center exchange integrals.

In general, the Ruedenberg approximation leads to values for the $\langle AB | A'B' \rangle$ integrals that are within 5 to 10% of the true values, except for a few small integrals (<10 mh) for which the values may be off by as much as 35%.  Using the Ruedenberg values for $\langle AB | A'B' \rangle$ when transforming the OAO's leads to significant errors.  The results are worse for small integrals (< 10 mh), but a few integrals larger than 10 mh are off by as much as a factor of four!  Moreover, there is a systematic error such that integrals involving s functions are too large, while those involving $p_\sigma$ functions are too small.  As a consequence, calculations may lead to a large shift of electrons from the s to the $p_\sigma$ orbitals.

As a test, calculations using the complete set of Ruedenberg OAO integrals were made.  The results in Tables XXI-XXIII were better

than expected. The expected electron shift from s to $p_\sigma$ orbitals did

not materialize, while the errors introduced were comparable to those

of Brown's scheme over OAO's. Therefore, we went ahead to try Brown's

scheme with the Ruedenberg OAO integrals. The results of the Brown-

Ruedenberg scheme were nearly not as good. The $^1\Sigma_g^+ \to {}^3\Sigma_u^+$ excitation

energies were very poor (errors as large as 1.25 eV). Similarly,

large errors were found for the $\sigma_g$ orbital energies, while the de-

scription of the GVB pair was poor. Therefore, it seems that more

work needs to be done on finding an efficient, reliable scheme for

expanding a truncated set of OAO integrals in terms of a comparably

truncated set of AO integrals.

## D. $C_2H_4$ and $O_3$

### 1. Calculations Using 2J-K Potentials for the 1s Core Electrons

The relative success of Brown's scheme over OAO's for $C_2$

and $O_3$ led us to try it on ethylene and ozone. As usual, the basis

set consists of valence Slater OAO's which have been orthogonalized

to 1s core orbitals. A 2J-K potential is used to represent the 1s

electrons.

For ethylene we consider the N and T state at the planar

and perpendicular geometries using GVB(2/PP) wavefunctions described

previously. For ozone, we consider the ground, $1^1A_1(4\pi)$, and lowest

triplet, $1^3B_2(4\pi)$, states at the experimental equilibrium geometry,

R = 1.278 Å, $\theta$ = 116.8°,[49] and the ring state, $2^1A_1(6\pi)$, at R = 1.278Å,

$\theta$ = 60°. A GVB(1) wavefunction which provides a consistent description

of the three states is employed.[14]

For polyatomic molecules Brown's scheme for truncation amounts to neglecting all three- and four-center integrals as well as the two-center exchange integrals. As a check, we also performed calculations (denoted by No 3-ctr. in the tables) in which the two-center exchange integrals were retained. The results presented in Tables XXV - XXVIII, are surprisingly poor. Errors as large as 1.5 h are made in the total energies. while the orbital energies are in error by as much as 0.5 h. More important, the ring state in ozone is predicted to be 12 eV below the open ground state! This result is even worse than that for INDO.[14] Even the simple singlet-triplet excitations of ozone and ethylene are in error by 0.5 to 10 eV. Retention of the two-center exchange integrals improves the singlet-triplet energies, but the overall results are quite similar to Brown's scheme.

The calculations on ozone tend to indicate that the bias toward the ring state arises from neglecting the three-center integrals. This, of course, would not be unreasonable, since the three-center integrals are expected to be more important for the ring state. On the other hand, there is a possibility that some of these problems arise from the core orthogonalization. Orthogonalizing the valence orbitals to the 1s core leads to more delocalized basis functions. The increased delocalization of the resulting OAO's may lead to deterioration in the ZDO approximation. To determine whether or not this is the case, we decided to replace the 2J-K core potential with a local potential, which does not require orthogonalization of the valence orbitals to the core (cf. Section II.C.1 for more details on

TABLE XXV. $O_3$ $[1^1A_1(4\pi)]$ GVB(1) energies: R = 1.278Å, θ = 116.8° (in a.u.)

|  | Ab initio | No 3-ctr.[a] | Brown[a] |
|---|---|---|---|
| Total E | -223.6156 | -224.5921 | -224.5917 |
| $1a_1$ O.E. | - 1.595 | - 1.943 | - 1.948 |
| $2a_1$ O.E. | - 0.955 | - 0.922 | - 0.926 |
| $3a_1$ O.E. | - 0.640 | - 0.689 | - 0.691 |
| $4a_1$ O.E. | - 0.380 | - 0.373 | - 0.364 |
| $1b_2$ O.E. | - 1.294 | - 1.576 | - 1.584 |
| $2b_2$ O.E. | - 0.627 | - 0.617 | - 0.620 |
| $3b_2$ O.E. | - 0.428 | - 0.382 | - 0.376 |
| $1a_2$ O.E. | - 0.459 | - 0.406 | - 0.396 |
| $1b_1$ O.E. | - 0.608 | - 0.760 | - 0.769 |
| $2b_1$ O.E. | - 0.605 | - 0.629 | - 0.631 |
| π pair  $c(1a_2)$ | 0.843 | 0.898 | 0.905 |
| $c(2b_1)$ | - 0.538 | - 0.440 | - 0.426 |
| S | - 0.221 | - 0.342 | - 0.360 |
| ΔE(eV) | 4.86 | 3.52 | 3.34 |

[a]Employs a 2J-K potential for oxygen 1s orbitals.

TABLE XXVI.  $O_3[2^1A_1(6\pi)]$ GVB(1) energies: R = 1.278Å, θ = 60°

(in a.u.)

| | Ab initio | No 3-ctr.[a] | Brown[a] |
|---|---|---|---|
| Total E | -223.5385 | -225.0414 | -225.0218 |
| $1a_1$ O.E. | - 1.772 | - 2.257 | - 2.254 |
| $2a_1$ O.E. | - 1.110 | - 1.057 | - 1.051 |
| $3a_1$ O.E. | - 0.636 | - 0.762 | - 0.764 |
| $4a_1$ O.E. | - 0.679 | - 0.996 | - 1.008 |
| $1b_2$ O.E. | - 1.149 | - 1.241 | - 1.244 |
| $2b_2$ O.E. | - 0.560 | - 0.529 | - 0.525 |
| $3b_2$ O.E. | - 1.330 | - 2.286 | - 2.312 |
| $1a_2$ O.E. | - 0.404 | - 0.288 | - 0.277 |
| $1b_1$ O.E. | - 0.768 | - 0.965 | - 0.972 |
| $2b_1$ O.E. | - 0.404 | - 0.408 | - 0.397 |
| $\sigma_{cc}$ pair  $c(4a_1)$ | 0.987 | 0.997 | 0.997 |
| $c(3b_2)$ | - 0.159 | - 0.081 | - 0.080 |
| S | - 0.723 | - 0.851 | - 0.851 |
| ΔE (eV) | 0.98 | 0.47 | 0.47 |

[a]Employs 2J-K potential for oxygen 1s orbitals

TABLE XXVII.  $O_3$ GVB(1) and $C_2H_4$ GVB(2) excitation energies (in eV).

| | Ab initio | No 3-ctr.[a] | Brown[a] |
|---|---|---|---|
| A)  Ozone | | | |
| $1\,^1A_1(4\pi) \rightarrow 1\,^3B_2(4\pi)$ | 0.48 | 1.36 | 1.52 |
| $1\,^1A_1(4\pi) \rightarrow 2\,^1A_1(6\pi)$ | 2.10 | - 12.23 | - 11.70 |
| B)  Ethylene | | | |
| $N \rightarrow T(0°)$ | 4.69 | 5.14 | 5.81 |

[a]Employs 2J-K potential for oxygen and carbon 1s orbitals.

TABLE XXVIII.  $C_2H_4$ N state energies: R = 1.338Å, θ = 0° (in a.u.)

| | Ab initio | No 3-ctr.[a] | Brown[a] |
|---|---|---|---|
| Total E | -77.8849 | -78.0768 | -78.0754 |
| $1a_g$ O.E. | - 0.855 | - 0.778 | - 0.771 |
| $2a_g$ O.E. | - 0.730 | - 0.794 | - 0.795 |
| $1b_{1u}$ O.E. | - 0.776 | - 0.699 | - 0.693 |
| $2b_{1u}$ O.E. | - 1.824 | - 2.005 | - 2.029 |
| $1b_{2u}$ O.E. | - 0.634 | - 0.661 | - 0.676 |
| $1b_{3g}$ O.E. | - 0.494 | - 0.513 | - 0.510 |
| $1b_{3u}$ O.E. | - 0.412 | - 0.402 | - 0.407 |
| $1b_{2g}$ O.E. | - 0.704 | - 0.713 | - 0.736 |
| π Pair:  c$(1b_{3u})$ | 0.971 | 0.974 | 0.976 |
| c$(1b_{2g})$ | - 0.240 | - 0.228 | - 0.217 |
| S | - 0.603 | - 0.620 | - 0.636 |
| ΔE (eV) | 1.06 | 1.01 | 0.95 |
| $\sigma_{cc}$ Pair: c$(2a_g)$ | 0.998 | 0.998 | 0.999 |
| c$(2b_{1u})$ | - 0.059 | - 0.055 | - 0.054 |
| S | - 0.888 | - 0.896 | - 0.898 |
| ΔE (eV) | 0.21 | 0.20 | 0.19 |

[a]Employs 2J-K potential for carbon 1s orbitals.

local potentials).

### 2. Calculations Using Local Potentials for the 1s Core Electrons

In section II.C.2 a local potential for the carbon 1s electrons was constructed. The local potential led to good agreement with the ab initio calculations on ethylene (cf. Table XI). Using similar methods a local potential for the oxygen 1s electrons was constructed.[50] The local potential parameters are shown in Table XXIX. In Tables XXX, XXXI and XXXIV the calculations on ozone using the local potential are compared to the ab initio results.[51] As for ethylene, only the lowest orbital energies disagree by more than 10 mh and these by less than 30 mh. The GVB pairs are well-described as is the $1\,^1A_1(4\pi) \rightarrow 1\,^3B_2(4\pi)$. However, the energy of the ring state is lowered by 0.73 eV relative to the ground state. Nevertheless, the quality of the local potential is certainly adequate for testing the various approximate integral methods.

Calculations using the truncation schemes of the previous section were repeated, i.e., neglecting all three- and four-center integrals and Brown's scheme. The only difference is that the valence basis functions were not orthogonalized to the core functions prior to Löwdin orthogonalization. The results in Tables XXX-XXXIV show that core orthogonalization leads to significant effects when the OAO integral sets are truncated.

For ozone, the agreement with ab initio values for the total and orbital energies is approximately twice as good for the local

TABLE XXIX.  Oxygen 1s local potential using $^3P$ state orbitals and a CHF 2s.

| | $k$ | $n_k$ | $c_k$ | $\zeta_k$ |
|---|---|---|---|---|
| $V_p$ | 1 | 0 | 1.0221 | 9.8903 |
| | 2 | 0 | 0.1211 | 0.6088 |
| | 3 | -1 | -1.1563 | 10.6134 |
| | 4 | -1 | -0.1137 | 0.3265 |
| $V_{s-p}$ | 1 | 0 | 23.7940 | 7.6985 |
| | 2 | 0 | 0.9983 | 1.5383 |
| | 3 | -2 | 0.3293 | 7.7448 |
| | 4 | -2 | 0.1580 | 0.2397 |

TABLE XXX. $O_3$ $1^1A_1(4\pi)$ GVB(1) energies: R = 1.278Å, θ = 116.8° (in a.u.)

| | Ab initio[a] | Loc Pot | No 3-ctr | Brown | NDDO | INDO (OAO) | INDO (AO) |
|---|---|---|---|---|---|---|---|
| Total E | -223.6156 | -46.6211 | -47.3426 | -47.3353 | -46.9872 | | -46.8088 |
| $1a_1$ O.E. | - 1.595 | - 1.575 | - 1.784 | - 1.788 | - 1.551 | | - 1.985 |
| $2a_1$ O.E. | - 0.955 | - 0.969 | - 0.929 | - 0.927 | - 0.958 | | - 0.961 |
| $3a_1$ O.E. | - 0.640 | - 0.638 | - 0.657 | - 0.665 | - 0.569 | | - 0.301 |
| $4a_1$ O.E. | - 0.380 | - 0.380 | - 0.382 | - 0.373 | - 0.383 | | - 0.008 |
| $1b_2$ O.E. | - 1.294 | - 1.288 | - 1.450 | - 1.455 | - 1.348 | | - 1.739 |
| $2b_2$ O.E. | - 0.627 | - 0.629 | - 0.688 | - 0.691 | - 0.690 | | - 0.420 |
| $3b_2$ O.E. | - 0.428 | - 0.426 | - 0.448 | - 0.442 | - 0.444 | | - 0.177 |
| $1a_2$ O.E. | - 0.459 | - 0.457 | - 0.463 | - 0.450 | - 0.481 | | - 0.219 |
| $1b_1$ O.E. | - 0.608 | - 0.605 | - 0.625 | - 0.635 | - 0.520 | | - 0.301 |
| $2b_1$ O.E. | - 0.605 | - 0.605 | - 0.615 | - 0.614 | - 0.578 | | - 0.576 |
| π pair: | | | | | | | |
| $c(1a_2)$ | 0.843 | 0.844 | 0.847 | 0.857 | 0.795 | | 0.995 |
| $c(2b_1)$ | - 0.538 | - 0.537 | - 0.531 | - 0.516 | - 0.607 | | - 0.097 |
| S | - 0.221 | - 0.222 | - 0.229 | - 0.248 | - 0.134 | | - 0.822 |
| ΔE(eV) | 4.86 | 4.83 | 4.78 | 4.53 | 6.21 | | 0.22 |

[a]Includes 1s core energy.

TABLE XXXI. $O_3$ $2^1A_1(6\pi)$ GVB(1) energies: R = 1.278Å, θ = 60° (in a.u.)

| | Ab initio[a] | LocPot | No 3-ctr | Brown | NDDO | INDO (OAO) | INDO (AO) |
|---|---|---|---|---|---|---|---|
| Total E | -223.5385 | -46.5706 | -46.8754 | -46.8495 | -46.6013 | -47.6074 | |
| $1a_1$ O.E. | - 1.772 | - 1.744 | - 1.818 | - 1.817 | - 1.582 | - 2.187 | |
| $2a_1$ O.E. | - 1.110 | - 1.118 | - 1.102 | - 1.096 | - 1.075 | - 1.298 | |
| $3a_1$ O.E. | - 0.636 | - 0.633 | - 0.637 | - 0.639 | - 0.624 | - 0.336 | |
| $4a_1$ O.E. | - 0.679 | - 0.676 | - 0.692 | - 0.701 | - 0.658 | - 0.326 | |
| $1b_2$ O.E. | - 1.149 | - 1.155 | - 1.228 | - 1.228 | - 1.194 | - 1.458 | |
| $2b_2$ O.E. | - 0.560 | - 0.560 | - 0.635 | - 0.634 | - 0.607 | - 0.275 | |
| $3b_2$ O.E. | - 1.330 | - 1.321 | - 1.329 | - 1.352 | - 1.287 | - 0.653 | |
| $1a_2$ O.E. | - 0.404 | - 0.402 | - 0.416 | - 0.405 | - 0.407 | - 0.327 | |
| $1b_1$ O.E. | - 0.768 | - 0.764 | - 0.769 | - 0.777 | - 0.658 | - 0.555 | |
| $2b_1$ O.E. | - 0.404 | - 0.401 | - 0.417 | - 0.407 | - 0.409 | - 0.312 | |
| | | | | | | | |
| σ Pair: | | | | | | | |
| $c(4a_1)$ | 0.987 | 0.987 | 0.986 | 0.987 | 0.985 | 0.098 | |
| $c(3b_2)$ | - 0.159 | - 0.161 | - 0.164 | - 0.162 | - 0.170 | - 0.995 | |
| S | - 0.723 | - 0.719 | - 0.715 | - 0.718 | - 0.705 | - 0.820 | |
| ΔE(eV) | 0.98 | 1.00 | 1.03 | 1.02 | 1.08 | 0.16 | |

[a]Includes 1s core energy.

TABLE XXXII.   $C_2H_4$ N state GVB(2/PP) energies: R = 1.338Å,
θ = 0° (in a.u.)

| | Ab initio[a] | LocPot | No 3-ctr | Brown | NDDO | INDO (OAO) | INDO (AO) |
|---|---|---|---|---|---|---|---|
| Total E | -77.8849 | -13.1681 | -14.1658 | -14.1571 | -13.8774 | -13.6478 | -13.8687 |
| $1a_g$ O.E. | - 0.855 | - 0.824 | - 0.903 | - 0.891 | - 0.847 | - 0.726 | - 0.642 |
| $2a_g$ O.E. | - 0.730 | - 0.732 | - 0.745 | - 0.747 | - 0.748 | - 0.925 | - 0.974 |
| $1b_{1u}$ O.E. | - 0.776 | - 0.766 | - 0.821 | - 0.814 | - 0.788 | - 0.638 | - 0.576 |
| $2b_{1u}$ O.E. | - 1.824 | - 1.839 | - 1.933 | - 1.958 | - 1.936 | - 2.028 | - 2.079 |
| $1b_{2u}$ O.E. | - 0.634 | - 0.634 | - 0.739 | - 0.752 | - 0.661 | - 0.648 | - 0.648 |
| $1b_{3g}$ O.E. | - 0.494 | - 0.495 | - 0.613 | - 0.607 | - 0.582 | - 0.582 | - 0.540 |
| $1b_{3u}$ O.E. | - 0.412 | - 0.412 | - 0.402 | - 0.407 | - 0.360 | - 0.392 | - 0.169 |
| $1b_{2g}$ O.E. | - 0.704 | - 0.705 | - 0.711 | - 0.735 | - 0.641 | - 0.650 | - 0.426 |
| **π Pair:** | | | | | | | |
| $c(1b_{3u})$ | 0.971 | 0.971 | 0.973 | 0.976 | 0.967 | 0.963 | 0.972 |
| $c(1b_{2g})$ | - 0.240 | - 0.240 | - 0.229 | - 0.218 | - 0.253 | - 0.271 | - 0.236 |
| S | - 0.603 | - 0.604 | - 0.618 | - 0.635 | - 0.585 | - 0.561 | - 0.609 |
| ΔE(eV) | 1.06 | 1.06 | 1.01 | 0.96 | 1.12 | 1.21 | 0.88 |
| **σ Pair:** | | | | | | | |
| $c(2a_g)$ | 0.998 | 0.998 | 0.998 | 0.998 | 0.999 | 0.995 | 0.997 |
| $c(2b_{1u})$ | - 0.059 | - 0.062 | - 0.059 | - 0.058 | - 0.053 | - 0.095 | - 0.078 |
| S | - 0.888 | - 0.883 | - 0.888 | - 0.891 | - 0.899 | - 0.825 | - 0.855 |
| ΔE(eV) | 0.21 | 0.23 | 0.22 | 0.21 | 0.18 | 0.56 | 0.37 |

[a]Includes 1s core energy.

TABLE XXXIII. $C_2H_4$ N state GVB(2/PP) energies: R = 1.41Å, θ = 90°
(in a.u.)

|  | Ab Initio[a] | LocPot | No3-ctr. | Brown | NDDO | INDO (OAO) | INDO (AO) |
|---|---|---|---|---|---|---|---|
| Total E | -77.7829 | -13.0656 | -14.0246 | -14.0115 | -13.7946 | -13.6220 | -13.7712 |
| $1a_1$ O.E. | - 0.847 | - 0.816 | - 0.901 | - 0.893 | - 0.853 | - 0.728 | - 0.669 |
| $2a_1$ O.E. | - 0.690 | - 0.694 | - 0.710 | - 0.707 | - 0.696 | - 0.839 | - 0.898 |
| $1b_2$ O.E. | - 0.777 | - 0.767 | - 0.826 | - 0.822 | - 0.808 | - 0.650 | - 0.603 |
| $2b_2$ O.E. | - 1.659 | - 1.665 | - 1.754 | - 1.761 | - 1.713 | - 1.789 | - 1.847 |
| $1e_1$ O.E. | - 0.571 | - 0.571 | - 0.683 | - 0.689 | - 0.636 | - 0.688 | - 0.597 |
| $1e_2$ O.E. | - 0.571 | - 0.571 | - 0.683 | - 0.689 | - 0.636 | - 0.688 | - 0.597 |
| $2e_1$ O.E. | - 0.366 | - 0.366 | - 0.362 | - 0.352 | - 0.337 | - 0.228 | - 0.152 |
| $2e_2$ O.E. | - 0.366 | - 0.366 | - 0.362 | - 0.352 | - 0.337 | - 0.228 | - 0.152 |
| σ pair: |  |  |  |  |  |  |  |
| $c(2a_1)$ | 0.998 | 0.997 | 0.998 | 0.998 | 0.998 | 0.994 | 0.996 |
| $c(2b_2)$ | - 0.069 | - 0.072 | - 0.068 | - 0.067 | - 0.065 | - 0.113 | - 0.092 |
| S | - 0.871 | - 0.865 | - 0.872 | - 0.873 | - 0.878 | - 0.796 | - 0.831 |
| ΔE(eV) | 0.25 | 0.27 | 0.26 | 0.26 | 0.23 | 0.67 | 0.45 |

[a]Includes 1s core energy.

TABLE XXXIV.   $O_3$ GVB(1) and $C_2H_4$ GVB(2/PP) excitation energies (in a.u.)

| | Ab initio | LocPot | No 3-ctr. | Brown | NDDO | INDO (OAO) | INDO (AO) |
|---|---|---|---|---|---|---|---|
| **A. Ozone** | | | | | | | |
| $1^1A_1(4\pi)\to1^3B_2(4\pi)$ | 0.48 | 0.48 | 0.55 | 0.66 | 0.20 | | 4.51[a] |
| $1^1A_1(4\pi)\to2^1A_1(6\pi)$ | 2.10 | 1.37 | 12.71 | 13.22 | 10.50 | | |
| **B. Ethylene** | | | | | | | |
| N → T (0°) | 4.69 | 4.72 | 5.10 | 5.78 | 4.46 | 3.93 | 4.27 |
| T → N (90°) | 0.05 | 0.05 | 0.04 | 0.00 | 0.00 | 0.00 | 0.00 |
| N rotational barrier | 2.78 | 2.79 | 3.84 | 3.96 | 2.25 | 0.70 | 2.65 |
| T rotational barrier | -1.97 | -1.98 | -1.30 | -1.82 | -2.21 | -3.24 | -1.62 |

[a]Using $1^1A_1(4\pi)$ orbitals for the $1^3B_2(4\pi)$ state.

potential calculations as for the 2J-K calculations. Moreover, the description of the ozone $\pi$ system for the open geometry is greatly improved as manifest in the GVB pair information and the $1\,^1A_1(4\pi) \rightarrow 1\,^3B_2(4\pi)$ excitation energy (errors of 0.1 to 0.2 eV instead of 0.5 to 1.0 eV). More striking is the fact that the ring state is now calculated to be 13 eV <u>above</u> the open ground state. Comparison of the electronic energies reveals that nearly all of the 25 eV change relative to the 2J-K potential results arises from the description of the ring state, which is 23.77 eV higher in the local potential calculation.

Comparison of the integrals used in the 2J-K and local potential calculations does not reveal any significant differences. The largest of these (10 to 50 mh) involve integrals with the 2s functions, as expected, since they are most affected by core orthogonalization. However, the changes in the one- and two-electron terms appear to cancel. Consequently, the origin of the 23.77 eV difference in the ring state electronic energies is not understood. Analysis of the electronic energies does, however, show that 80% of the difference arises from the two-electron integrals.

Since the description of the ozone wavefunctions is significantly better for the local potential calculations than for the 2J-K, the former procedure for replacing the core electrons is considered preferrable for approximate integral methods. The results on ethylene, which do not display as significant differences between the two procedures, support this conclusion. The errors in the orbital energies for ethylene are smaller in the local potential calculations.

Since the results on ozone and ethylene (apart from the bias

against the ozone ring state) for Brown's scheme are reasonable, calculations with smaller two-electron integral sets were made. The next logical approximation is to neglect the two-center hybrid integrals, leading to an NDDO set of two-electron integrals. The results are shown in Tables XXX - XXXIV.

For ozone, NDDO leads to an improved description of the $\sigma$ system, but a worse description of the $\pi$ system. The $1\,^1A_1(4\pi) \rightarrow 1\,^3B_2(4\pi)$ excitation energy is significantly underestimated, while the ring state is still calculated to be 10 eV above the ground state. The results for ethylene are similar in that the calculated $N \rightarrow T(0°)$ excitation energy drops significantly relative to Brown's scheme and is in better agreement with the ab initio results. The rotational barriers are not well described, however, as the N state barrier is too small by 1/2 eV while the T state barrier is too large by 1/4 eV.

Since the results of the NDDO calculations were not unreasonable, the two-electron integral set was reduced even further to the level of INDO. That is, only coulomb and one-center exchange integrals were retained. As a further test, calculations were performed in which AO values were used for the two-electron integrals. The results are shown in Tables XXX - XXXIV.

For ozone, we encountered convergence problems. This was not expected, since similar problems had not arisen in earlier INDO calculations.[14] Nevertheless, the two calculations that did converge required many more iterations (20 to 40) than the other calculations in Tables XXX to XXXIV (5 to 7 iterations). Moreover, the converged INDO (OAO) and INDO (AO) vectors are drastically different from the

higher-order approximate calculations. The description of the $\pi$ pair in the ground state and the $\sigma_{00}$ pair in the ring state have changed radically. Errors of 300 to 500 mh in the orbital energies are common. Moreover, the total energy of the ring state has decreased by nearly one Hartree! The results are not even similar to earlier INDO calculations.[14] The origin of the drastic change observed between the NDDO and INDO (OAO) calculations is not apparent.

On the other hand, no convergence problems were encountered for ethylene. The orbital energies in both calculations deteriorated significantly relative to NDDO. Moreover, the descriptions of all the GVB pairs were very poor in INDO (OAO), the splitting energies being overestimated by 0.2 to 0.4 eV. These errors are diminished in INDO (AO), since the exchange integrals, $K_{gu}$, are systematically underestimated (cf. Section III.A.3). Similarly, INDO (AO) leads to much better results for the $N \rightarrow T(0°)$ excitation energy as well as for the rotational barriers. The chief deficiency of INDO (AO) is the poor orbital energies, especially the 250 mh underestimation of the $\pi$ ($1b_{3u}$) orbital energy.

The INDO (AO) approximation is identical to the AI/O method developed in Section II.C.3, except that the one-electron integrals over evaluated exactly over OAO's. (The INDO (OAO) approximation corresponds to the AI/O method in which OAO corrections to the two-electron integrals were taken into account.) Comparison of the results in Tables XXXII - XXXIV with those in Table XII provides a test of evaluating the OAO integrals over diatomic fragments. The total energies increase by more than a hartree in AI/O. This increase is

most evident in the $1b_{2u}$ and $1b_{3g}$ orbital energies, indicating signif-
icant errors in the treatment of the carbon $p_y$ OAO's. Although the
$N \rightarrow T(0°)$ excitation energy is well reproduced in AI/0, the rotational
barriers deteriorate greatly. These results together with those on
$H_3$ indicate that the one-electron integrals over OAO's must be evaluated
exactly. Since the number of one-electron integrals increases as $N^2$,
transformation to exact OAO integrals is feasible even for large basis
sets (100 - 200 functions).

### D. Conclusions

The goal of the present investigation was to determine the
validity of various truncated sets of integrals for performing molecular
quantum mechanical calculations. Towards this end, increasingly complex
molecular systems [(1) $H_2$, (2) $H_3$, (3) $C_2$ and $O_2$, (4) $C_2H_4$ and $O_3$] were
studied, so that the deficiencies of the various truncations might be
explicitly delineated. Our conclusions are summarized below.

In all the calculations, it was evident that for integral
set truncation to have any validity whatsoever, the integrals must be
transformed to OAO's. Calculations on $H_3$ showed that truncated AO
integral sets are strongly biased toward closed geometries (cf. Table
XIX), while calculations on $C_2$ showed that they may lead to short
calculated bond lengths and poor excitation energies (cf. Tables XXI
and XXII).

Next, our calculations indicated that the problem of core-
valence separation is best handled by using local potentials rather
than 2J-K potentials for the core. The problem with 2J-K potentials is

that the valence OAO's must be orthogonal to the core orbitals. The core orthogonalization (unnecessary for local potentials) leads to further delocalization of the OAO's, which appears to present problems when the integral set is truncated. Various approximate integral calculations on $C_2H_4$ and $O_3$ clearly demonstrated that replacement of the core electrons with local potentials rather than 2J-K potentials leads to better results (compare Tables XXV - XXVIII with Tables XXX - XXXIV).

Having transformed to OAO's (in particular Löwdin [22] OAO's) with the core electrons represented by local potentials, the results of our calculations using different truncated sets of integrals are not clear cut. For $H_2$ neglecting two-center hybrid and exchange integrals led to good results (errors $\leq$ 10 mh), while no one-electron integrals (in particular, $v_{ab}$) could be disgarded without significant errors.

Similarly, for $H_3$ all three-center and two-center hybrid and exchange integrals could be neglected without seriously affecting the results (errors < 15 mh). In addition, we found that evaluating the OAO integrals over diatomic fragments as in AI/O (cf Section II.B and II.C) led to significant errors (as large as 100 mh). The errors were worse for the one-electron integrals (cf. Table XX). Therefore, the one-electron OAO integrals should be evaluated exactly. This conclusion was supported by results on $C_2H_4$ and $O_3$ (compare Table XII and Tables XXXII - XXXIV).

Calculations on $C_2$ and $O_2$ indicated that the two-center exchange integrals can still be neglected without detriment, but disgarding the one- and two-center hybrid integrals leads to significant errors. If only the coulomb and one-center exchange integrals are

retained (as in INDO), the best results on $C_2$ were obtained when the $\langle\mu_A|v_B|v_A\rangle$ integrals were neglected. Retention of all the one-electron integrals led to long calculated bond lengths for the ground state (cf. Table XXI).

Attempts were also made to use the Ruedenberg [48] approximation to express the truncated set of OAO integrals in terms of a truncated set of AO integrals. This procedure has been previously proposed by Brown.[47] The Brown-Ruedenberg scheme led to a poor description of the $C_2$ potential curves, but a good description of the $O_2$ ground state curve (cf. Table XXI - XXIV).

Calculations on ozone, neglecting all three-center integrals, led to a poor description of the ring state relative to the open ground state, with the former predicted to be 13 eV higher instead of 2 eV as in the ab initio calculations. This result tends to indicate that truncated sets involving only one- and two-center integrals cannot consistently describe states at closed and open geometries. In addition, calculations employing an INDO-like set of two-electron integrals led to wavefunctions completely different from the ab initio results. Moreover, some of the wavefunctions would not even converge!

The results for ethylene are not as discouraging. In fact, using an INDO-like set of two-electron integrals evaluated over AO's in conjunction with the full set of one- and two-center one-electron integrals over OAO's, led to good results for the N $\rightarrow$ T(0°) excitation energy as well as the N and T state rotational barriers (cf. Table XXXIV). The major deficiency of this method is that the orbital energies are, in general, too high (200 mh errors).

In Table XXXV the size of the various truncated two-electron integral sets employed for $O_3$ and $C_2H_4$ are shown. It is clear from size considerations why an approximate method involving an INDO-like set of two-electron integrals is so desirable. Our results on ozone indicate that even Brown's scheme is not a reliable approximation of ab initio MBS calculations, and that three-center integrals must be retained to describe ring states consistently. Retention of three-center integrals implies the number of integrals increases as $N^3$, rather than $N^2$, which leads to significant limitations on the size of the calculations that are feasible. At present there are two available approximate methods, PRDDO[9] and ESE-MO,[10] which retain the most important three-center integrals, namely, $\langle \mu_A | v_C | v_B \rangle$ and $\langle \mu_A v_B | \rho_C \rho_C \rangle$. Neither of these methods have been tested with correlated wavefunctions. Tests on molecules such as ozone, which have many low-lying valence excited states, are clearly warranted.

On the other hand, our results on ethylene indicate there may still be hope for INDO-like methods. Further calculations are warranted on ethylene in which the $\langle \mu_A | v_B | v_A \rangle$ or $\langle \mu_A | h | v_B \rangle$ integrals are neglected. Finally, in light of the poor results on ozone, calculations on different molecular systems, e.g. $CH_2$ and $C_6H_6$, are needed to ascertain the breadth of applicability of the INDO-like approximate method developed herein.

TABLE XXXV. Relative size of the truncated-integral sets.

| Number of Integrals for: | Ab initio | Loc Pot | No 3-ctr. | Brown | NDDO | INDO |
|---|---|---|---|---|---|---|
| $O_3$: R=1.278Å, θ=116.8° | 3451 | 1504 | 1020 | 792 | 264 | 96 |
| $O_3$: R=1.278Å, θ=60° | 3531 | 1504 | 1020 | 792 | 264 | 96 |
| $C_2H_4$: R=1.338Å, θ=0° | 3190 | 1733 | 574 | 468 | 144 | 90 |
| $C_2H_4$: R=1.41Å, θ=90° | 4468 | 2581 | 874 | 724 | 200 | 90 |

REFERENCES

1. (a) W.C. Ermler and C.W. Kern, <u>J. Chem. Phys.</u>, 58, 3458 (1973);

   (b) P.J. Hay and I. Shavitt, <u>Chem. Phys. Lett.</u>, 22, 23 (1973);

   <u>J. Chem. Phys.</u>, 60, 2865 (1974).

2. (a) W.R. Wadt and W.A. Goddard III (submitted for publication);

   (b) W.R. Wadt, W.A. Goddard III and T.H. Dunning Jr. (submitted for publication).

3. (a) C.F. Bender, P.K. Pearson, S.V. O'Neill and H.F. Schaefer III, <u>J. Chem. Phys.</u>, 56, 4626 (1972); (b) S.V. O'Neill, P.K. Pearson and H.F. Schaefer III, <u>ibid.</u>, 58, 1126 (1973); (c) P.K. Pearson, W.J. Hunt, C.F. Bender and H.F. Schaefer III, <u>ibid.</u>, 58, 5358 (1973); C.W. Wilson Jr. and W.A. Goddard III, <u>ibid.</u>, 56, 5913 (1972); (e) S. Shih, R.J. Buenker, S.D. Peyerimhoff and C.J. Michejda, <u>J. Amer. Chem. Soc.</u>, 94, 7620 (1972).

4. R. Hoffmann, <u>J. Chem. Phys.</u>, 39, 1397 (1963).

5. (a) J.A. Pople and G.A. Segal, <u>J. Chem. Phys.</u>, 43, 5136 (1965); (b) <u>ibid.</u>, 44, 3289 (1966).

6. J.A. Pople, D.L. Beveridge and P.A. Dobosh, <u>J. Chem. Phys.</u>, 47, 2026 (1967).

7. (a) N.C. Baird and M.J.S. Dewar, <u>J. Chem. Phys.</u>, 50, 1262 (1969); (b) M.J.S. Dewar and E. Haselbach, <u>J. Amer. Chem. Soc.</u>, 92, 590 (1970).

8. J.A. Pople, D.P. Santry and G.A. Segal, <u>J. Chem. Phys.</u>, 43, 5129 (1965).

9. (a) T.A. Halgren and W.N. Lipscomb, <u>Proc. Nat. Acad. Sci. USA</u>, 69, 652 (1972); (b) <u>J. Chem. Phys.</u>, 58, 1569 (1973).

10. (a) P.G. Burton and R.D. Brown, Chem. Phys., 4, 220 (1974);

    (b) P.G. Burton, ibid., 4, 226 (1974).

11. J.C. Slater and J.H. Wood, Int. J. Quantum Chem., 45, 3 (1971).

12. W.A. Goddard II, Phys. Rev., 157, 81 (1967).

13. These problems of the HF wavefunction do not depend on whether

    an ab initio or an approximate method is employed.

14. W.R. Wadt and W.A. Goddard III, J. Amer. Chem. Soc., 96, 1689

    (1974) and references cited therein.

15. W.R. Wadt and W.A. Goddard III, J. Amer. Chem. Soc., 96,

    0000 (1974).

16. C.C.J. Roothaan, Rev. Mod. Phys., 23, 69 (1951).

17. R.G. Parr, J. Chem. Phys., 20, 239 (1952).

18. The experimental values for the ionization potential and elec-

    tron affinity are multiplicity-weighted averages over all the

    states arising from the ground atomic configuration.

19. Throughout this work, we use Slater's rules [20] to determine

    the exponents for the Slater orbitals.

20. J.C. Slater, Phys. Rev., 36, 57 (1930).

21. P.G. Lykos and R.G. Parr, J. Chem. Phys., 24, 1166 (1956).

22. P.O. Löwdin, J. Chem. Phys., 18, 365 (1950).

23. B.C. Carlson and J.M. Keller, Phys. Rev., 105, 102 (1957).

24. The internuclear axis is always chosen to be the z-axis.

25. J. DelBene and H.H. Jaffe, J. Chem. Phys., 48, 1807, 4050

    (1968).

26. (a) W.J. Hunt, W.A. Goddard III and T.H. Dunning, Jr., (to be

    submitted for publication); (b) W.J. Hunt, Ph.D. thesis,

---

California Institute of Technology, 1971.

27. P.J. Hay, W.J. Hunt and W.A. Goddard III, J. Amer. Chem. Soc., 94, 8293 (1972).

28. A.J. Merer and R.S. Mulliken, Chem. Rev., 69, 639 (1969).

29. GVB(1) wavefunctions, described in reference 14, which provide a consistent description of the open and ring states, were used in the ozone calculations.

30. mh denotes millihartrees = $10^{-3}$ a.u., 1 hartree = 27.2117 eV.

31. The $\langle p_\sigma|V_{AB}|p_\sigma\rangle$ and $\langle p_\pi|V_{AB}|p_\pi\rangle$ integrals were actually evaluated by fitting the spherical part, $(\langle p_\sigma|V_{AB}|p_\sigma\rangle + 2\langle p_\pi|V_{AB}|p_\pi\rangle)/3$, with $-Z/R + e^{-AR}(B + Z/R)$ and the quadrupole part, $(\langle p_\pi|V_{AB}|p_\pi\rangle - \langle p_\sigma|V_{AB}|p_\sigma\rangle)/2$, with a simple exponential, $Be^{-AR}$.

32. (a) L.R. Kahn and W.A. Goddard III, J. Chem. Phys., 56, 2685 (1972); (b) C.F. Melius, W.A. Goddard III and L.R. Kahn, ibid., 3342 (1972); (c) C.F. Melius, Ph.D. thesis, California Institute of Technology, 1973; (d) C.F. Melius, B.D. Olafson and W.A. Goddard III (submitted for publication).

33. S. Huzinaga, J. Chem. Phys., 42, 1293 (1965).

34. The non-bonding lobe orbitals in $C_2$ were described with a GVB pair.

35. W.J. Hehre, R.J. Stewart and J.A. Pople, J. Chem. Phys., 51, 2657 (1969).

36. B.D. Olafson, W.A. Goddard III, W.R. Wadt, A. Redondo-Muiño, (unpublished results).

37. One may vary more than one of the tighter basis functions to construct a coreless valence orbital (CVO). However,

the resulting CVO is not as smooth in the core region (even
if one imposes a minimum kinetic energy criterion on the
orbital) and, as a consequence, the resulting local potential
is "wiggly."

38. In Table XI and subsequent tables information concerning the
GVB pairs is presented. Each GVB pair may be represented in
terms of two non-orthogonal singlet-coupled orbitals as in
reference 12, or equivalently as a two term expansion in
orthogonal natural orbitals,[39] i.e.,

$$(\phi_a\phi_b + \phi_b\phi_a) = c_1^2\phi_1^2 - c_2^2\phi_2^2$$

The expansion coefficients $c_1$ and $c_2$ as well as the overlap
$(S = <\phi_a|\phi_b>)$ of the non-orthogonal orbitals are presented in
the tables. Finally, the energy lowering ($\Delta E$) arising from
splitting the HF doubly-occupied orbital into a GVB pair is
also shown.

39. A.C. Hurley, J.E. Lennard-Jones and J.A. Pople, Proc. Roy. Soc.,
Ser. A, 220, 446 (1953).

40. T. Koopmans, Physica, 1, 104 (1933).

41. C.W. Wilson, Jr. and W.A. Goddard III, Chem. Phys. Lett., 5,
45 (1970); Theor. Chim. Acta, 26, 195, 211 (1972).

42. The β integrals were retained in INDO for just this reason.

43. R.S. Mulliken, J. Chim. Phys., 46, 500, 521 (1949).

44. J.A. Pople and D.L. Beveridge, "Approximate Molecular Orbital
Theory," (McGraw-Hill, New York, N.Y., 1970).

45. I. Shavitt, R.M. Stevens, F.L. Minn and M. Karplus, J. Chem. Phys.,
48, 2700 (1968).

46. R.D. Brown and P.G. Burton, <u>Chem. Phys. Lett.</u>, 20, 45 (1973).

47. R.D. Brown, F.R. Burden and G.R. Williams, <u>Theor. Chim. Acta</u>, 18, 98 (1970).

48. K. Ruedenberg, <u>J. Chem. Phys.</u>, 19, 1433 (1951).

49. G. Herzberg, "Molecular Spectra and Molecular Structures," (Van Nostrand, Princeton, N.J., 1967) Vol. 3.

50. Ground state $O(^3P)$ HF orbitals over an (11s, 7p) basis were used to determine the local potential. A singly-occupied HF 2p orbital was used for the $V_p$ potential.

51. For all the ozone local potential calculations, an STO-4G [35] basis set scaled to Slater [20] exponents was employed. The <u>ab initio</u> calculations employed a Slater MBS.